

**Development of cuprous ion-responsive protein
labeling reagents applicable *in vitro* and in live cells**

Rong Cheng

2024

Preface and Acknowledgements

The research presented in this PhD thesis was conducted under the guidance of Professor Itaru Hamachi at the Department of Synthetic and Biological Chemistry, Graduate School of Engineering, Kyoto University, from April 2020 to June 2024. The research focused on developing protein labeling reagents responsive to cuprous ions and applicable *in vitro* and live cells.

I would like to express my gratitude to several individuals for their invaluable support and guidance during my PhD journey. Foremost, I am deeply grateful to my research supervisor, Prof. Itaru Hamachi, for his unwavering support and inspiration throughout these past years. I also extend my thanks to my advisor, Junior Associate Prof. Tomonori Tamura, for his invaluable instructions and encouragement. My heartfelt thanks also go to Dr. Yuki Nishikawa for synthesizing DiaR used in Chapter 1 and conducting the *in vitro* metal selectivity test of DiaR. I am additionally grateful to Assistant Prof. Hao Zhu for providing the synthesized TcatR for analysis in Chapter 1. I am also thankful to Dr. Keiichirou Uchida for assisting with synthesizing one synthetic intermediate used in Chapter 2. I also want to express my gratitude to Dr. Muneo Tsujikawa for constructing and providing the CTR1-expression plasmid that was used in both Chapters 1 and 2. Many thanks to Mr. Wagatsuma Takumi and Associate Prof. Kambe Taiho for their assistance in providing ATP7A knockout cell lines used in Chapter 3. I am also thankful to Assistant Prof. Tanaka Yu-ki and Prof. Ogra Yasumitsu for the ICP-MS test of the samples involved in the study in Chapter 3. I am also grateful to Associate Prof. Seji Sakamoto, Junior Associate Prof. Ryou Kubota, Associate Prof. Hiroshi Nonaka, Associate Prof. Hideki Nakamura, and Assistant Prof. Masaki Tsuchiya for their invaluable assistance, advice, and technical support during my time in Hamachi Lab. Additionally, I very much appreciate the anonymous referee whose review of our submitted manuscript offered valuable insights and specialized knowledge about copper, inspiring me to consider additional experiments to strengthen the research further.

I also want to thank the members of the Hamachi lab, past and present, who have provided valuable support and inspiration. I extend my heartfelt thanks to Drs. Vikram Thimaradka, Yuki Nishikawa, Keisuke Nakamura, Wataru Tanaka, Mikiko Takato, Ms. Yuna Matsuda, Mr. Kazuki Shiraiwa, Shogo Torigoe, Takeharu Mino, and Masaharu Kawano for their invaluable insights and comments during lab meetings, their technical assistance, and the uplifting conversations we've shared. I would like to express my gratitude to Drs. Kyoichi Matsuba and Yuka Nabeta for their indispensable support in biochemical experiments. Many thanks to Ms. Yuri Tanimura, Ms.

Mengchu Wang, Mrs. Youying Shen, Ziyang Li, Kazutoshi Nagao, Yuchong Liu, Chengli Qiu, Hiroaki Uno, and Yuriki Ikuta for the wonderful scientific and non-scientific conversations at lab parties. I am thankful to Ms. Asami Ozaki for her invaluable assistance with official matters. To all other members of the Hamachi lab, thank you for making the lab a memorable and enjoyable place.

Additionally, I am very grateful to Kyoto University for the Kyoto University Graduate Division Fellowship (DC2) and to the Japan Society for the Promotion of Science (JSPS) for a Research Fellowship (DC3 - DC4) for the financial support that enabled me to complete this research.

I am immensely grateful to my friends for their support during challenging times. Their comforting presence and emotional guidance have been invaluable to me. I would like to express special thanks to my mentors for their exceptional wisdom and profound influence on my growth. I also want to express my deepest appreciation to my parents, who have supported my journey with love and granted me the freedom to carve my path. Although I may have yet to have the opportunity to meet with you as frequently as I would have liked, please know that you are always in my thoughts.

Lastly, I am deeply thankful to all whose work forms the foundation of this research. Their contributions are duly acknowledged in the references section of each chapter. I also want to express my sincere gratitude to all whose labor work has molded and continues to shape the world in which we reside.

Rong Cheng

June 2024

Table of content

General introduction

Chapter 1

Design and study of the chemical labeling reagents for protein labeling in response to copper ions in living cells

Chapter 2

Development of cuprous ion-selective quinone-methide-based chemical labeling reagent for imaging and proteome profiling in living cells

Chapter 3

Imaging and profiling of proteome in response to intracellular cuprous ions in the living ATP7A knockout cells

List of publications and presentations

General introduction

Introduction

Copper, one of the 20 essential elements in the human body, exhibits potent redox activities and plays crucial roles in various biological processes, including aerobic respiration, epigenetic modification, neurotransmission, and aging. Bound copper ions serve as cofactors for numerous enzymes, while loosely bound copper ions are involved in mediating signaling processes. Any imbalance in copper levels, whether surplus or deficiency, can lead to various cellular damages and diseases, underscoring the importance of maintaining systemic and cellular copper levels for normal biochemical processes. Recent studies have also demonstrated that copper surplus can lead to a type of cell death known as cuproptosis, caused by the aggregation of copper with a few lipoylated proteins in mitochondria. The absorption, distribution, and excretion of copper in mammalian animals are strictly regulated to maintain systemic and cellular copper levels within a narrow homeostatic range, which is crucial for ensuring normal biochemical processes.

Understanding the biological functions of copper ions is crucial for comprehending both the physiological and pathological processes in which copper is involved. Techniques such as isotope detection, ICP-MS, and fluorescence microscopy using fluorescent sensors are utilized to investigate copper ions, providing valuable information on their speciation, quantification, distribution, and dynamics within biological systems. However, these methods also have their inherent limitations when studying copper in living biological systems. Despite the contributions of these conventional methods to our understanding of copper's roles in living organisms, our knowledge of copper homeostasis and dyshomeostasis is still constrained by the lack of methodologies for identifying the involved proteins. To address this knowledge gap, a covalent protein bioconjugation strategy has been developed. This strategy leverages a carefully designed chemical tool to respond to the target biomolecule or biometal and labels proteins *in situ* as immobilized target signals. Coupled with downstream analytical techniques such as fluorescence microscopy and proteomics studies, this approach enables the profiling of proteins in the target biomolecule or biometal-rich sites.

The current chemical tools designed to respond to copper ions using the covalent protein bioconjugation strategy have certain limitations. These limitations include high background signals and a lack of selectivity for the most common form of intracellular copper ions, cuprous ions (Cu^+). To overcome these limitations, the research in this thesis introduces the development

of an efficient and selective Cu^+ -responsive protein labeling reagent. This reagent can serve as a valuable chemical tool for the strategy and can be integrated with common protein profiling techniques, bio-imaging, and proteomics studies.

The thesis comprises three main chapters. Chapter 1 explores four distinct chemical tools for labeling proteins in response to copper ions, and ultimately has found that the quinone methide-based reagent (QmCuR) stands out for its high selectivity for Cu^+ and biocompatibility. Chapter 2 focuses on optimizing the chemical structures of QmCuR to enhance its response to intracellular Cu^+ , resulting in the identification of the optimal Cu^+ -responsive protein labeling reagent (CuR). Chapter 3 applies the optimal CuR to analyze intracellular Cu^+ levels in various cell models, particularly emphasizing a model with impaired ATP7A function. The findings underscore the versatility and specificity of the CuR tool across diverse cell models and provide valuable insights into Cu^+ regulation, trafficking, and export within living cells.

1. Biometals in biology

In the evolution of life, such as in human beings, 20 essential elements have become necessary for the human body. Ten of these are biometal elements, including sodium (Na), potassium (K), magnesium (Mg), calcium (Ca), iron (Fe), manganese (Mn), cobalt (Co), copper (Cu), zinc (Zn), and molybdenum (Mo), each of which has developed biological functions in biological systems.^{1,2} All life forms require metals as they are essential constituents of life and play critical roles in biological processes such as biomineralization, osmotic regulation, metabolism, signaling, and catalysis.^{1,3} Biometals can be roughly classified into two groups based on their abundance in life: alkali and alkaline earth metals and transition metals. Alkali and alkaline earth metals, including Na, K, Mg, and Ca, are abundant in most organisms and are well-known for their roles in osmotic regulation, signaling, and potential energy regulation.^{1,4,5,6,7} Transition metals, including mainly Mn, Co, Cu, Zn, and Mo, are trace elements since they are generally present at much lower levels than alkali and alkaline earth metals, but still play critical biological roles such as catalysis, gene expression, and signaling in life.^{8,9,10,11} The regulation of biometals is crucial for maintaining cellular function.^{1,2} When these biometals are properly regulated, they play essential roles. However, both deficiency and excess of biometals can lead to cytotoxicity and even diseases in life.^{12,13} In biological systems, biometals exist in various forms, including tightly bound forms (such as protein- or nucleic-bound forms), loosely bound forms (i.e., labile) ready to

associate with the environment, labile forms that can easily transform, and free forms (biometal pools) that can act in signaling.^{14,11} The diverse forms of biometals add complexity to their study. While some of their important biological functions have been discovered and characterized,^{1,15,16} much fundamental information remains unknown. This includes the amount and speciation, localization, dynamics, and functions of biometals in cells and organisms, as well as the mechanisms by which cells precisely recruit and regulate biometals. Therefore, a comprehensive understanding of the intricate biological chemistry of biometals is still a long way off.

2. Copper in biology

2.1 Biological roles of copper

Copper (Cu) is an essential biometal and the third most abundant transition metal for human beings.¹ It plays a crucial role in various biological processes, including aerobic respiration, epigenetic modification, neurotransmitter synthesis, signaling, pigmentation of hair, retina, and skin, and catecholamine biosynthesis.^{11,17,18,19,20} In a healthy human adult (70 kg) body, there are about 112 mg of copper, mainly found in the liver (9.9 mg), brain (8.8 mg), blood (6.2 mg), muscle (26.2 mg), and skeleton (45.5 mg).²¹ Copper ions, with two oxidation states- cupric ion (Cu(II)/Cu²⁺) and cuprous ion (Cu(I)/Cu⁺)-as either a recipient or a donor of electrons, show potent redox activities and participate in various biological processes.²² Bound copper ions act as cofactors for multiple enzymes, such as dopamine β -hydroxylase (DBH) (**Figure 1d**), cytochrome c oxidase, tyrosinase (**Figure 1e**), and Cu/Zn superoxide dismutase (SOD1) (**Figure 1f**), influencing neuronal activity, energy generation, aerobic respiration, melanin synthesis, and epigenetic modifications.^{8,19,23,24} Loosely bound (i.e., labile) copper ions mediate signaling processes, including immune response and neurotransmission.^{16,20,25} Imbalances in copper levels, both excess and deficiency, are associated with cellular malfunctions and various disorders, such as neurodegenerative diseases like Alzheimer's and Parkinson's diseases, cancer, amyotrophic lateral sclerosis (ALS), and genetic disorders including occipital horn syndrome (OHS), isolated distal motor neuropathy, Wilson's disease, and Menkes's disease.^{26,27} Therefore, maintaining systemic and cellular copper levels within a narrow homeostatic range is crucial to ensure normal biochemical processes.²⁸

Labile copper ions exist in the reductive cellular environment as reduced speciation (Cu⁺). By using genetic engineering methods including knockdown or knockout of essential copper

transporters in a combination of the physiological and biochemical study of the proteins of interest, researchers have revealed several copper ions-required signaling pathways on the basis of binding between copper ions with specific proteins^{29,30,31}. Tursi et al. reported the novel role of copper ions in Ras/mitogen-activated protein kinase (MAPK) signaling that copper influx enhances mitogen-activated protein kinase kinase 1 (MEK1) phosphorylation of extracellular signal-regulated protein kinases 1 and 2 (ERK1/2) through Cu-MEK1 interaction.²⁹ Based on this finding, Brady et al. found that copper ion is also required for oncogenic signaling and suggested the usage of Cu-chelators in the therapy of cancers containing (B-Raf proto-oncogene, serine/threonine kinase) BRAF^{V600E} mutation.³¹ Moreover, by performing an alignment of Cu-binding sequence in MEK1 against other kinase domains, Brady et al. have identified autophagic kinases ULK1 and ULK2 as potential candidates that involve Cu in signaling pathway and have proved that copper ions could act as an essential regulator of ULK1/2 (Unc-51-like autophagy-activating kinases 1 and 2), for example, the increased copper levels enhance the reactivity of ULK1 through direct interaction with it and are required for autophagosome complex formation.³⁰

Cuproptosis is a copper-induced cell death distinct from other known cell death mechanisms (ferroptosis, necroptosis, apoptosis, and oxidative stress).³² It is characterized by intracellular copper accumulation, which induces the aggregation of mitochondrial lipoylated proteins and destabilizes iron–sulfur cluster proteins, leading to cell death (**Figure 2**). Seven proteins that are essential in regulating cuproptosis have been identified by genome-wide CRISPR-Cas9 (clustered regularly interspaced short palindromic repeats and CRISPR-associated protein 9) loss-of-function and knockout screens. These proteins include the key upstream regulator of protein lipoylation (Adrenodoxin (FDX1)), three proteins in lipoic acid pathway (Lipoyltransferase 1(LIPT1), Lipoyl synthase (LIAS), Dihydrolipoamide dehydrogenase (DLD), and the protein targets of lipoylation (the pyruvate dehydrogenase complex (PDH complex) that includes Dihydrolipoamide acetyltransferase (DLAT), Pyruvate dehydrogenase E1 component subunit beta (PDHB), and Pyruvate dehydrogenase E1 component subunit alpha 1(PDHA1))). Thus, the dynamics and trafficking of Cu⁺ are precisely controlled in cells to regulate copper homeostasis and signaling. The current Cuproptosis mechanism suggests that the binding between lipoylated DLAT and Cu⁺ leads to the aggregation of the proteins, thus causing cuproptosis. The report indicated that lipoylated DLAT bound “directly” with Cu⁺ to lead to the aggregation of lipoylated DLAT via disulfide bonds, acting as the key cause of cuproptosis.³² However, the

binding between copper ions and lipoylated DLAT was only elucidated *in vitro* using CuCl₂-preloaded resin. Hence, its interaction with Cu⁺ was not confirmed *in situ*, possibly due to the lack of methods that could detect possible interactions between Cu⁺ and proteins in cells. It was also reported copper ions interact with Dihydropolipoamide S-succinyltransferase (DLST), another protein target of lipoylation, but the binding between lipoylated proteins and copper ions (Cu²⁺ rather than Cu⁺) was only proven by the *in vitro* study.³²

Therefore, elucidating the mechanisms of the cellular regulation of labile copper ions (Cu⁺) is significant for understanding copper homeostasis, the associated physiological functions, pathological processes, and related diseases.

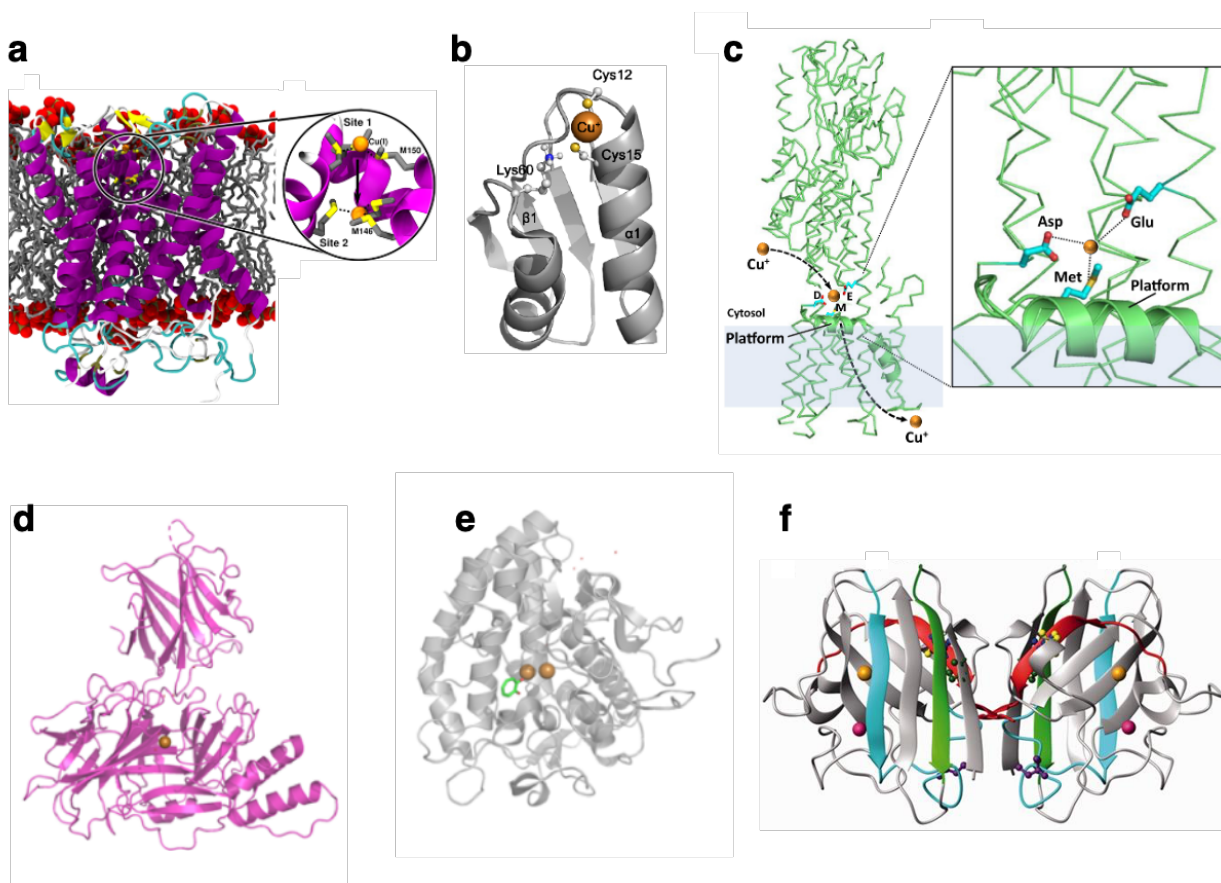


Figure 1. **Structure of copper proteins.** (a) Structure of CTR1 transporter and the close-up of the Met triads occupied with copper ions.³³ (b) Structure of Atox1.^{34,35} (c) Homology-derived structure of human ATP7A/B.³⁶ Structures of (d) dopamine β -hydroxylase (DBH),³⁷ (e) tyrosinase,³⁷ and (f) SOD1.³⁸ The copper ions are shown as orange in color.

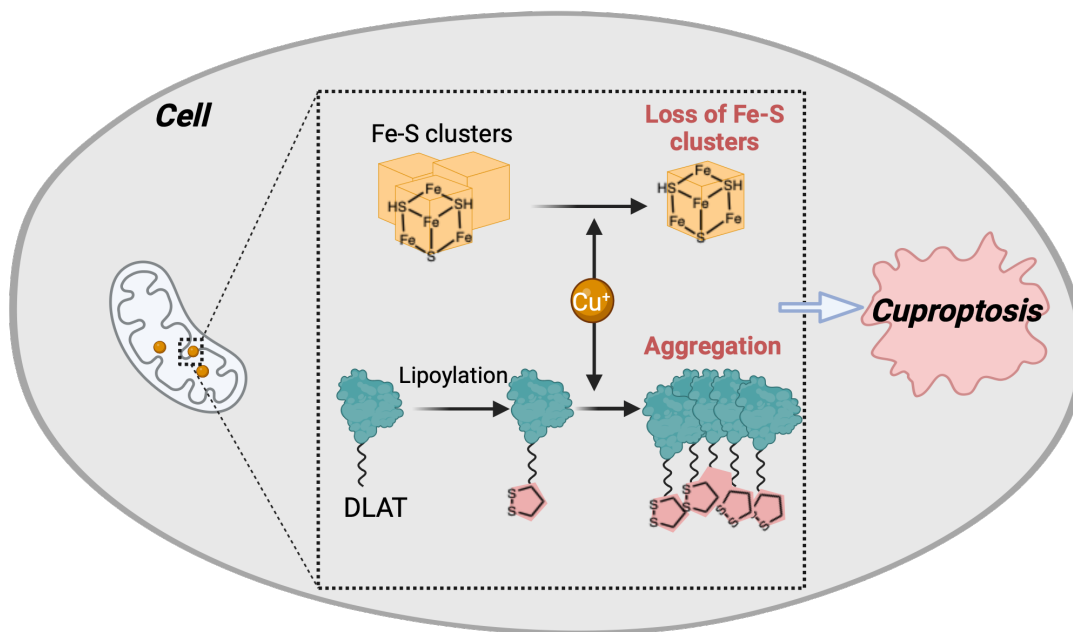


Figure 2. **Illustration of Cuproptosis: a recently discovered copper-induced cell death pathway.**³²

2.2 Copper metabolism

Copper ions are absorbed, distributed, and excreted in mammalian animals.¹⁸ Copper is found in various foods, including liver, crustaceans, whole grains, beans, nuts, chocolate, shrimp, milk, mushrooms, and red meat.^{39,40} The recommended dietary allowance (RDI) for copper is 0.9 mg per day for adult humans, while the tolerable upper intake level (UL) is 10 mg per day.⁴¹ The median dietary intake of copper for adults is approximately 1.0-1.6 mg per day.⁴¹ Therefore, a sufficient amount of copper for humans can be obtained from a balanced daily diet. Ingested copper from food is primarily absorbed in the small intestine.^{42,43,44} Cupric ion (Cu^{2+}) is the form of extracellular copper ions present in the small intestine.⁴⁵ Though it can be incorporated into divalent metal transporter 1 (DMT1), it cannot be directly transported for use by cells via DMT1 in the intestine.⁴⁶ Prior to absorption, cupric ions are reduced to cuprous ions (Cu^+) by cytochrome b reductase 1 (CYBRD1)⁴⁷ or members of the six-transmembrane epithelial antigen of the prostate (STEAP) reductase family.^{48,49} Subsequently, cuprous ion is absorbed into the lumen of enterocytes across the apical membranes of enterocytes in a high-affinity manner by copper transporter 1 (CTR1) (**Figure 1a**).^{50,51,52} Cu^+ is then delivered to intracellular copper proteins for copper buffering and directed to cuproenzymes or intracellular compartments.^{53,54,55} Specifically, CTR1 interacts with the antioxidant 1 copper chaperone (ATOX1) (**Figure 1b**) via its carboxyl

terminus and intracellular loops to deliver Cu^+ .⁵⁶ ATOX1 delivers Cu^+ to copper-transporting ATPase 1 (ATP7A) (**Figure 1c**) located in the *trans*-Golgi network, where ATP7A metallates cuproenzymes or translocates to the basolateral membrane to efflux copper from the enterocyte into the blood for portal circulation in response to cellular copper levels (**Figure 3a**).^{57,58} The latter process occurs classically in enterocytes, as intracellular copper levels are elevated through transport by CTR1 via the apical membrane from dietary copper, allowing for the secretion of a large proportion of absorbed cuprous ions from enterocytes into circulation. Once in the portal circulation, copper ions predominantly bind to serum proteins such as albumin⁵⁹ and α 2-macroglobulin (transcuprein),⁶⁰ forming complexes that are mainly conveyed to the liver.^{61,62} In the liver, copper ions are imported into hepatocytes via CTR1 through the basolateral membrane.^{63,64} The intracellular copper ions can then bind to intracellular copper-binding components such as metallothioneins and GSH for copper storage, or to copper transporters for delivery to target proteins or compartments.^{53,54,55} They can also be shuttled by ATOX1 to deliver to ATP7B, a copper-transporting P-type ATPase 2 that localizes in the *trans*-Golgi network.^{53,57} Copper ions complexed by ATP7B can be incorporated into cuproenzymes for secretion of metallated enzymes,⁶⁵ or to *apo*-ceruloplasmin for secretion into the blood for circulation,⁶⁵ or it can be excreted into the bile by translocating ATP7B from the *trans*-Golgi network to the apical membrane.^{53,66,67} This intracellular metabolism of copper is regulated to maintain copper homeostasis in the liver and other tissues.^{48,68,69} Ceruloplasmin-bound copper ions enter the blood and are then conveyed to other organs and tissues via circulation (**Figure 3b**).⁷⁰

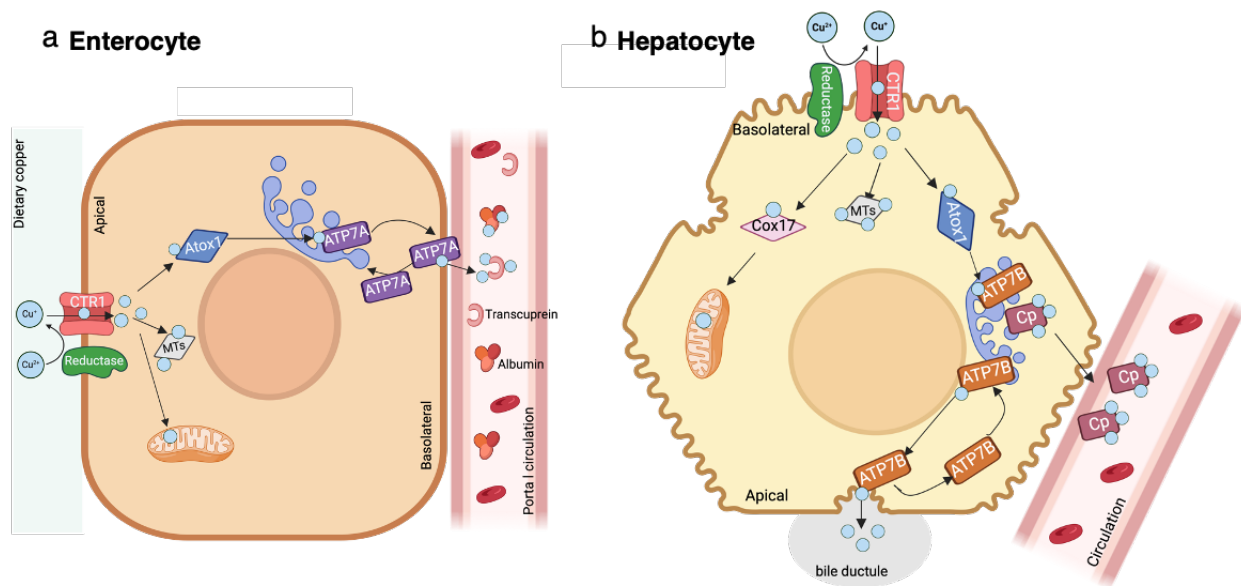


Figure 3. Copper metabolism in (a) enterocytes and (b) hepatocytes.

3. Methods for studying copper ions in biology

Understanding the functions of copper ions is essential for comprehending biological and pathological processes. To achieve this, it is crucial to investigate copper absorption, transport, distribution, storage, excretion, Cu-binding, and utilization. Several powerful and widely used techniques can be employed for studying copper ions, including isotope detection, inductively coupled plasma mass spectrometry (ICP-MS), and fluorescence microscopy using fluorescent sensors. The choice of analytical technique depends mainly on the specific information the researcher aims to obtain. The techniques above have proven valuable in providing insights into the speciation, quantification, distribution, and dynamics of copper ions *in vitro*, in intact cells, fixed tissues, or *in vivo*. They have significantly contributed to our understanding of the biological roles of copper ions in various biological systems.

3.1 Isotope detection

Copper isotopes, both radioactive and stable, have been utilized for trace analysis of copper in cells, tissues, and living organisms to explore the dynamics of copper metabolism (Figure 4a). This method has also been expanded to yield more comprehensive insights into copper metabolism, copper biological functions, copper-associated biological pathways, and diseases through

integration with other techniques such as purification and mass spectrometry. The use of copper radioactive isotopes as tracers, particularly ^{64}Cu and ^{67}Cu , has been common in studying the biological processes of copper ions, encompassing their biological roles and metabolism in living systems.^{62,71} This method is highly sensitive and enables accurate quantification with a strong signal-to-noise ratio. It has been employed to track copper absorption in the intestine,^{42,46} copper transport in circulation,^{59,60} and copper influx and efflux within cells,^{72,73,74} thus facilitating the identification of copper-binding components, quantification of copper transport rates based on cell numbers, and comprehension of copper metabolism under homeostasis and dyshomeostasis. For example, it has identified albumin,⁵⁹ transcuprein,⁶⁰ and ceruloplasmin⁷⁵ as copper transporters in circulation and as the source of copper for cells and quantified copper uptake rate while characterizing the biochemical properties of CTR1^{52,72} to gain better insights into its copper transport mechanism in cells. However, concerns regarding safety, availability, short half-life, and potential disruption to biological systems have imposed significant limitations on experimental design and the accuracy of obtained information. The stable isotopes ^{63}Cu and ^{65}Cu have gained attention as a non-radioactive alternative to radioactive isotopes for detecting and studying copper ions. This approach is cost-effective and eliminates the need for stringent safety measures associated with radioactive isotopes. Researchers have applied this method to study copper homeostasis in living organisms or at the cellular level, particularly in the context of health and diseases. For example, it has been used to study and diagnose copper-associated diseases such as Wilson disease and ALS,^{76,77,78} as well as to gain insights into copper-involved pathways and biological processes such as the erythropoietic pathway and aging.^{78,79,80} Additionally, this approach has facilitated the elucidation of copper metabolism, including its binding, absorption, distribution, and excretion.^{43,81,82,83} It is important to note that while this isotope detection method has its advantages, it does have limitations, as it cannot provide any information about the binding or labile state, oxidative state, or *in-situ* Cu-protein interactions.

3.2 Inductively coupled plasma mass spectrometry (ICP-MS)

Inductively coupled plasma mass spectrometry (ICP-MS) has emerged as a versatile and reliable analytical technique for detecting and quantifying copper (**Figure 4b**). Integrating multiple techniques and methods allows for analyzing copper concentration, distribution, and isotope compositions in a wide range of biological samples, thus aiding the study of the biological

processes and mechanisms related to copper in both health and diseases. ICP-MS utilizes inductively coupled plasma (ICP) to ionize the sample, decomposing it into its elemental components and generating ions for mass spectrometry detection.⁸⁴ It demonstrates high sensitivity (with a limit of detection (LOD) of $< 10 \text{ pg mL}^{-1}$), precision, statistical power, and the capability for multi-element analysis.^{85,86} ICP-MS was originally designed for analyzing liquid samples and has since been utilized to quantify total copper levels in serum, whole blood, and urine samples from patients.^{87,88} This allows for monitoring systemic copper fluctuations related to various physiological or pathological conditions, such as sclerosis,⁸⁹ and supports the early detection of diseases like Wilson's disease.^{27,90,91} Additionally, it can be employed to analyze the average total copper concentrations in whole cells or in subcellular compartments that have been separated before ICP-MS analysis, offering supplementary insights into copper overload or deficiency in specific biological processes, or to investigate the intricacies of cellular copper metabolism.^{92,93} Notably, ICP-MS can be combined with other techniques and methods to broaden its applications in studying copper in biology. Its integration with purification techniques such as chromatography allows for the separation and identification of various copper-binding components involved in copper metabolism under different health or disease conditions.^{81,94,95,96} This aids in comprehending systemic and molecular copper metabolism mechanisms. For instance, this combined approach enables the measurement of changes in copper content during copper transport between domains within copper transporters like ATP7B.⁹⁷ LC-ICP-MS (liquid chromatography-ICP-MS) has been employed to separate and identify different copper species, including ceruloplasmin (CP)-bound, non-CP bound, albumin-bound, and "loosely bound or exchangeable" copper in serum samples from animal models or clinical patients with Wilson's disease, contributing to a deeper understanding of copper metabolism mechanisms related to this disease.^{95,96,98} ICP-MS, combined with isotope detection, has been used to simultaneously detect and map copper and its isotopes within the same biological sample, allowing for the tracking of copper metabolism and exploration of isotope variations in different copper-related biological processes.^{73,81,99} For example, the concurrent detection of copper isotopes in serum samples from patients with liver cirrhosis has yielded valuable insights into isotope compositions and variations associated with the disease, thereby aiding in diagnosis and prognosis.⁹⁹ Laser ablation (LA) combined with LA-ICP-MS enables the visualization of copper distribution and concentration in solid tissue samples such as the brain, heart, kidney, and liver tissues (**Figure 4c**).^{86,100,101,102,103}

This technology contributes to a better understanding of copper's biological roles and metabolism in living organisms in health and disease states. For example, LA-ICP-MS has been utilized to study copper levels and distribution in healthy and fibrotic/cirrhotic human liver tissues,¹⁰¹ in liver tissues from animal models with Wilson's disease,¹⁰⁰ in tumor-containing brain tissues^{104,105} thus facilitating understanding of the roles of copper in various diseases and the different stage of the diseases. It is also important to acknowledge the limitations of ICP-MS while recognizing its diverse applications in the study of biological copper. ICP-MS requires bulk samples and ionizes samples for atomic mass detection, which means it cannot provide information about *in-situ* copper states, including binding or labile state, oxidative state, and dynamic protein interactions. While the hyphenation of LA to ICP-MS incorporates high spatial resolution (10–100 μm for nanosecond lasers),⁸⁶ it still limits the application for studying cellular and subcellular copper as evidence continues to suggest that copper ions are distributed heterogeneously within cells and in multicellular systems, thus shows less competitive spatial resolution compared to other bio-imaging techniques, such as fluorescence microscopy (nm scale). In addition, ICP-MS faces inherent limitations such as physical interferences stemming from differences in sample surface tension and viscosity compared to standards,¹⁰⁶ as well as spectral interferences from overlapping mass-to-charge (m/z) ratios with other ions (such as isobaric and polyatomic species).¹⁰⁷ Although efforts to address these limitations have been made through the use of internal standards and the development of ICP-tandem mass spectrometry (ICP-MS/MS),^{106,107} these challenges still need to be considered when interpreting and validating results.

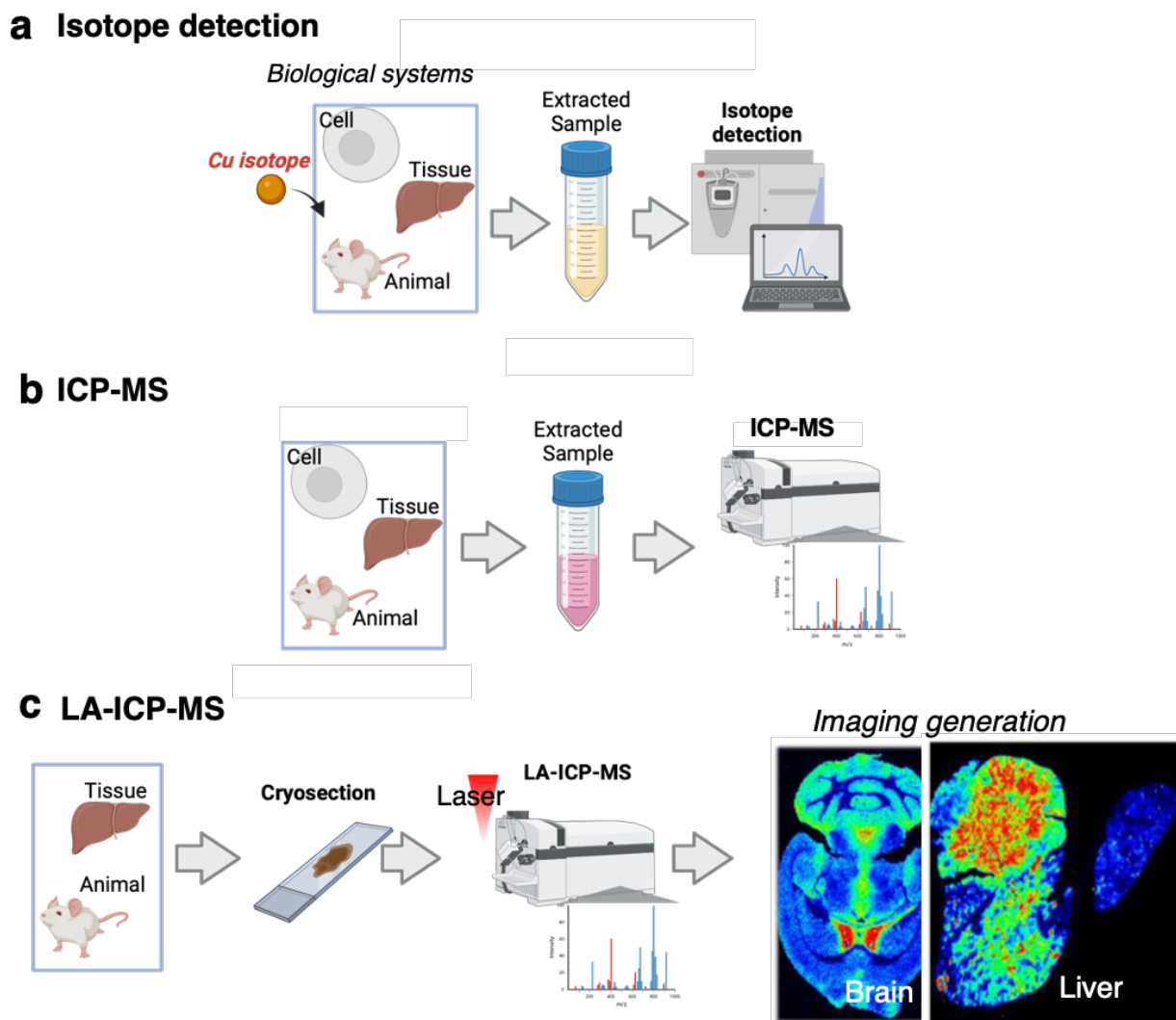


Figure 4. **Illustration of the workflow of several conventional methods for studying biological copper ions.** Workflow of (a) isotope detection method, (b) inductively coupled plasma mass spectrometry (ICP-MS) method, and (c) laser ablation (LA)-ICP-MS method ¹⁰².

3.3 Fluorescent microscopy using copper sensors

Fluorescence microscopy, using carefully crafted copper-responsive fluorescence sensors, has become a powerful method for studying the distribution, dynamics, and oxidation states of copper ions within live cells at both cellular and subcellular levels (**Figure 5**).^{108,109,110,111} Recent advancements in super-resolution microscopy have significantly improved spatial resolution, overcoming limitations posed by light interference and revolutionizing the field of fluorescent microscopy.¹¹² These advances have also facilitated the development of copper-responsive

fluorescent sensors, furthering their application in studying the biological roles of copper within living systems. Integrated with fluorescence microscopy, fluorescent sensors have become indispensable for visualizing copper ions and analyzing their dynamics in a wide range of biological systems, including living cells, tissues, and entire organisms such as fish and mice.^{111,113,114,115} Fluorescent sensors typically adhere to fundamental design principles involving the conversion of binding events into modified fluorescent signals, either through enhancement or quenching, via electron-transfer or charge-transfer processes. Various mechanisms, including excited-state intracellular proton (ESIPT),^{116,117} photoinduced electron transfer (PET),^{118,113} Förster resonance energy transfer (FRET),¹¹⁹ and chemical reaction-based fluorophore's structural conversion,^{120,121} have been widely employed in the development of a diverse array of fluorescent sensors for detecting copper ions *in vitro* and in live biological systems.^{108,111} In recent advancements, specialized fluorescent sensors for copper have been devised to explore the functions of copper ions in various cellular components, such as the mitochondria,^{122,123} lysosome,¹²⁴ endoplasmic reticulum (ER),^{125,126} Golgi,¹²⁷ and others. These sensors are typically engineered with precise subcellular targeting capabilities, achieved by attaching an organelle-localizing group, such as a chemical group or signal peptides, to the general fluorescent sensor.¹²⁸ It is also important to acknowledge the limitations of using copper fluorescent sensors in conjunction with fluorescence microscopy. The inherent probe diffusion feature reduces the spatial resolution after the target response, leading to increased inaccuracy in the distribution of original copper signals within live cells and limiting downstream analysis. Furthermore, the compatibility with other downstream analytical methods is restricted, making it impossible to identify the proteins likely involved in copper biological roles or metabolism *in situ*, which is essential for understanding their functions.

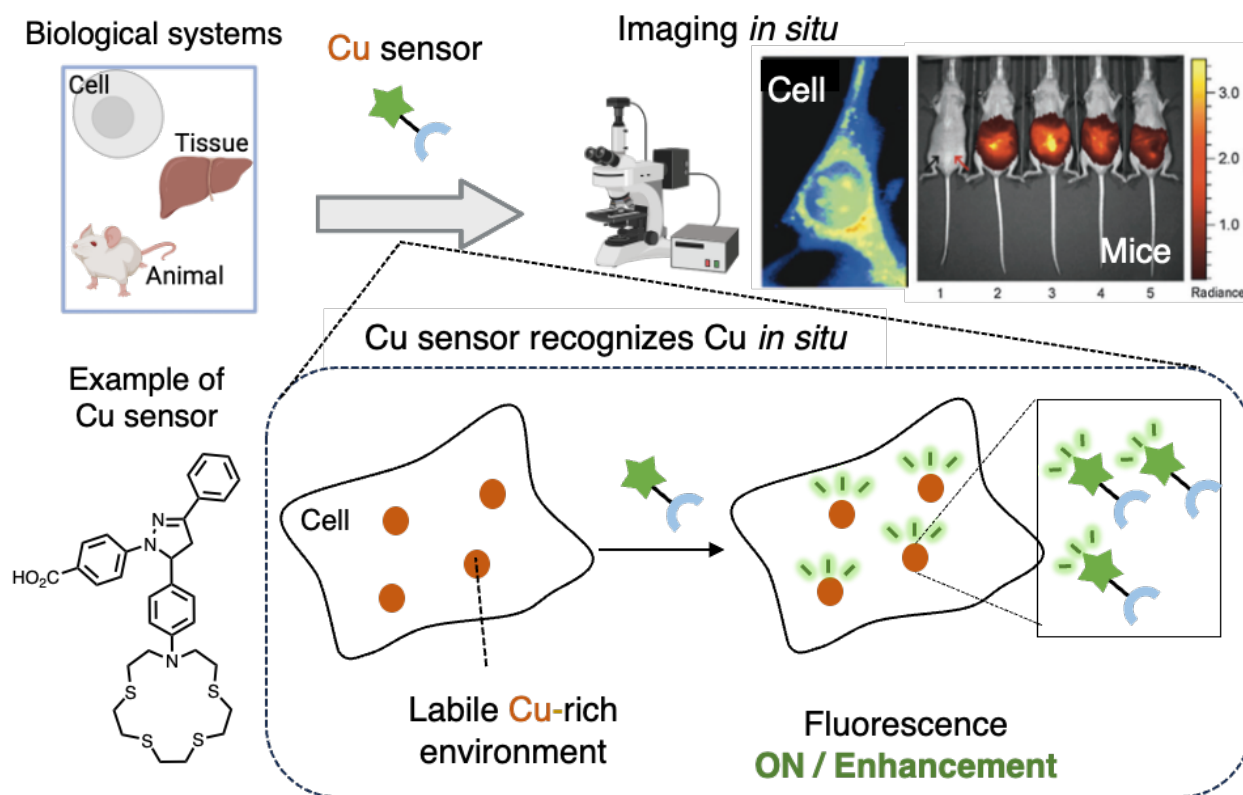


Figure 5. **Illustration of the workflow and applications of conventional Cu-responsive fluorescence sensors.** ^{113,118}

3.4 Combination of fluorescent microscopy with chemoproteomics

The covalent protein bioconjugation strategy involves the use of a carefully designed chemical tool that can react to a specific biometal ion or biomolecule in live cells, allowing for the labeling of proteins located in target-rich areas. When combined with fluorescence microscopy and chemoproteomics analysis, this approach can provide valuable information about the distribution of target biometal ions or biomolecules and the proteins close to these target-rich areas (**Figure 6**). ^{129,130,131,132,133,134} For instance, a zinc ion (Zn^{2+})-responsive protein labeling reagent called AIZin, consisting of a Zn^{2+} -binding dipicolylamine chelator and a reporter fluorescent dye connected by an acyl imidazole moiety, has been developed.¹³¹ This reagent shows low reactivity in the absence of Zn^{2+} , but its reactivity increases upon complexation with Zn^{2+} , enabling the covalent labeling of proteins. AIZin has been used to identify proteins localized in Zn^{2+} -rich

vesicles produced in glioma cells stimulated with nitric oxide, revealing their association with the endoplasmic reticulum (ER) and Golgi apparatus. In recent studies, the Copper-Directed Acyl Imidazole (CDAI) strategy has been used to detect copper ions within living cells by developing the copper ion-responsive protein labeling reagent through a copper-mediated enhancement of acyl imidazole electrophile activity.^{129,130} This strategy allows for labeling proximal proteins located in areas with elevated copper levels. With the CDAI strategy, reagents that respond comparably to Cu^+ and Cu^{2+} without selectivity or exhibit higher reactivity to Cu^{2+} than Cu^+ have been developed.^{129,130} Unlike traditional target-selective fluorescence chemosensors, the CDAI strategy offers several advantages, including reduced probe diffusion, the immobilized signal of the target, and the potential for proteomic study to identify labeled proteins. This approach enhances spatial resolution and enables downstream analysis within target-rich microenvironments, such as immunostaining and proteomic studies. However, the inherent activity of acyl imidazole electrophiles tends to produce high background signals, which limits the usability of these probes. Additionally, the CDAI strategy-based copper probes have primarily been combined with fluorescence microscopy but have not been integrated with proteomics studies. Consequently, there is still a lack of proteomics information regarding the proteins labeled by the copper probes in intracellular copper-rich sites using this approach. Furthermore, a probe that operates on covalent protein modification and selectively responds to Cu^+ , the most prevalent oxidation state of intracellular copper ions,⁴⁵ has not yet been reported.

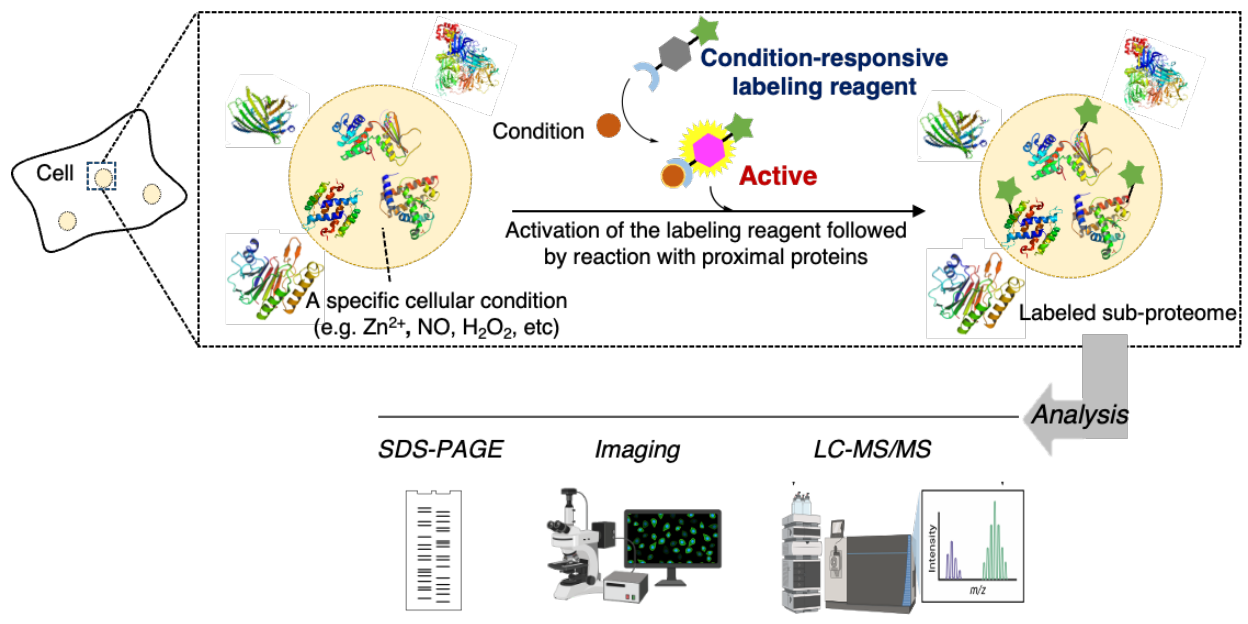


Figure 6 **Emerging conditional proteomics approach that combines fluorescence microscopy with chemoproteomics.**

4. Summary of this thesis

As introduced above, copper is crucial for the functioning of living organisms. However, disruptions in copper homeostasis are associated with diseases such as cancer and Alzheimer's. Understanding how copper is regulated within cells is increasingly important for comprehending its roles in normal biology and disease. A covalent protein bioconjugation strategy has been developed to study biological molecules and metal ions, including detecting copper ions within live cells. However, the current methods based on the strategy have limitations, including high background signals and a lack of selectivity for the most common form of intracellular copper ions, cuprous ions (Cu^+). To address these limitations, I developed an efficient Cu^+ -responsive protein labeling reagent, which responds to Cu^+ by generating reactive electrophiles that react with and tag the proximal proteins, thus enabling the immobilization of Cu^+ signals *in situ* and the identification of proteins located in Cu^+ -rich sites within cells.

In Chapter 1, I demonstrated a copper ion-responsive protein labeling method and explored four distinct chemical tools to develop an effective Cu^+ -responsive protein labeling reagent (CuR). Among these, the TPA-cage-masked quinone methide-based reagent (QmCuR) showed superior

performance due to its high selectivity for Cu^+ and its effectiveness in detecting elevated Cu^+ levels within various cell models.

In Chapter 2, I continued to optimize the chemical structures of QmCuR to address its limited response to intracellular Cu^+ . I focused on developing and synthesizing various copper ion-ligand-appended quinone methide-based reagents to optimize the molecular design. Through assessments and comparisons *in vitro* and in live cells, I identified the most effective Cu^+ -responsive protein labeling reagent (CuR) and elucidated the Cu^+ -responsive reaction mechanisms. The optimal CuR shows remarkable selectivity for Cu^+ over other bio-metal ions and ROS and its superior Cu^+ -responsive efficacy both *in vitro* and in live cells compared to the QmCuR developed in Chapter 1.

In Chapter 3, I further investigated the applications of the optimal CuR in various cell models, focusing particularly on a model with impaired ATP7A function. This exploration aimed to evaluate the reliability of CuR and utilize it to examine the intracellular regulation of labile Cu^+ accumulation, in conjunction with subsequent analyses such as imaging and proteomics. The results underscored the versatility of the CuR tool across diverse cell models and its specificity in Cu^+ -concentrated cells. Furthermore, the findings indicated potential *in situ* interactions of Cuproptosis proteins with Cu^+ and highlighted the potential significance of the MXXXM motif in proteins in responding to toxic intracellular Cu^+ levels, offering valuable insights into Cu^+ regulation, trafficking, and export within living cells.

Reference

- 1 Zoroddu, M. A. *et al.* The essential metals for humans: a brief overview. *J Inorg Biochem* **195**, 120-129 (2019). <https://doi.org:10.1016/j.jinorgbio.2019.03.013>
- 2 Lippard, S. J. B., J. M. *Principles of Bioinorganic Chemistry*. (University Science Books, 1994).
- 3 Andreini, C., Bertini, I., Cavallaro, G., Holliday, G. L. & Thornton, J. M. Metal ions in biological catalysis: from enzyme databases to general principles. *J. Biol. Inorg. Chem.* **13**, 1205-1218 (2008). <https://doi.org:10.1007/s00775-008-0404-5>
- 4 Strazzullo, P. & Leclercq, C. Sodium. *Adv Nutr* **5**, 188-190 (2014). <https://doi.org:10.3945/an.113.005215>
- 5 Jaiswal, J. K. Calcium - how and why? *J Biosci* **26**, 357-363 (2001). <https://doi.org:10.1007/BF02703745>
- 6 Vormann, J. Magnesium: nutrition and metabolism. *Mol Aspects Med* **24**, 27-37 (2003). [https://doi.org:10.1016/s0098-2997\(02\)00089-4](https://doi.org:10.1016/s0098-2997(02)00089-4)
- 7 Weaver, C. M. Potassium and health. *Adv Nutr* **4**, 368S-377S (2013). <https://doi.org:10.3945/an.112.003533>
- 8 Turski, M. L. & Thiele, D. J. New roles for copper metabolism in cell proliferation, signaling, and disease. *J Biol Chem* **284**, 717-721 (2009). <https://doi.org:10.1074/jbc.R800055200>
- 9 Finney, L. A. & O'Halloran, T. V. Transition metal speciation in the cell: insights from the chemistry of metal ion receptors. *Science* **300**, 931-936 (2003). <https://doi.org:10.1126/science.1085049>
- 10 O'Halloran, T. V. Transition metals in control of gene expression. *Science* **261**, 715-725 (1993). <https://doi.org:10.1126/science.8342038>
- 11 Chang, C. J. Searching for harmony in transition-metal signaling. *Nat Chem Biol* **11**, 744-747 (2015). <https://doi.org:10.1038/nchembio.1913>
- 12 Jomova, K. & Valko, M. Advances in metal-induced oxidative stress and human disease. *Toxicology* **283**, 65-87 (2011). <https://doi.org:10.1016/j.tox.2011.03.001>
- 13 Harris, E. D. Basic and clinical aspects of copper. *Crit Rev Clin Lab Sci* **40**, 547-586 (2003). <https://doi.org:10.1080/10408360390250649>
- 14 Rosenzweig, A. C. Metallochaperones: bind and deliver. *Chem Biol* **9**, 673-677 (2002). [https://doi.org:10.1016/s1074-5521\(02\)00156-4](https://doi.org:10.1016/s1074-5521(02)00156-4)
- 15 Kambe, T., Tsuji, T., Hashimoto, A. & Itsumura, N. The Physiological, Biochemical, and Molecular Roles of Zinc Transporters in Zinc Homeostasis and Metabolism. *Physiol Rev* **95**, 749-784 (2015). <https://doi.org:10.1152/physrev.00035.2014>
- 16 Ackerman, C. M. & Chang, C. J. Copper signaling in the brain and beyond. *J Biol Chem* **293**, 4628-4635 (2018). <https://doi.org:10.1074/jbc.R117.000176>
- 17 Tsang, T., Davis, C. I. & Brady, D. C. Copper biology. *Current Biology* **31**, R421-R427 (2021). <https://doi.org:10.1016/j.cub.2021.03.054>
- 18 Kim, B.-E. *et al.* Mechanisms for copper acquisition, distribution and regulation. *Nat Chem Biol* **4**, 176-185 (2008). <https://doi.org:10.1038/nchembio.72>
- 19 Festa, R. A. & Thiele, D. J. Copper: an essential metal in biology. *Curr Biol* **21**, R877-883 (2011). <https://doi.org:10.1016/j.cub.2011.09.040>
- 20 Grubman, A. & White, A. R. Copper as a key regulator of cell signalling pathways. *Expert Rev Mol Med* **16**, e11 (2014). <https://doi.org:10.1017/erm.2014.11>
- 21 Linder, M. C. *Biochemistry of Copper*. (Springer New York, NY, 1991).

- 22 Kardos, J. *et al.* Copper signalling: causes and consequences. *Cell Commun Signal* **16**, 71 (2018). <https://doi.org:10.1186/s12964-018-0277-3>
- 23 Ruiz, L. M., Libedinsky, A. & Elorza, A. A. Role of Copper on Mitochondrial Function and Metabolism. *Front Mol Biosci* **8**, 711227 (2021). <https://doi.org:10.3389/fmolb.2021.711227>
- 24 Linder, M. C. & Hazegh-Azam, M. Copper biochemistry and molecular biology. *Am J Clin Nutr* **63**, 797S-811S (1996). <https://doi.org:10.1093/ajcn/63.5.797>
- 25 Achard, M. E. *et al.* Copper redistribution in murine macrophages in response to Salmonella infection. *Biochem J* **444**, 51-57 (2012). <https://doi.org:10.1042/BJ20112180>
- 26 Tisato, F., Marzano, C., Porchia, M., Pellei, M. & Santini, C. Copper in diseases and treatments, and copper-based anticancer strategies. *Med Res Rev* **30**, 708-749 (2010). <https://doi.org:10.1002/med.20174>
- 27 Czlonkowska, A. *et al.* Wilson disease. *Nat Rev Dis Primers* **4**, 21 (2018). <https://doi.org:10.1038/s41572-018-0018-3>
- 28 Davis, A. V. & O'Halloran, T. V. A place for thioether chemistry in cellular copper ion recognition and trafficking. *Nat Chem Biol* **4**, 148-151 (2008). <https://doi.org:10.1038/nchembio0308-148>
- 29 Turski, M. L. *et al.* A novel role for copper in Ras/mitogen-activated protein kinase signaling. *Mol Cell Biol* **32**, 1284-1295 (2012). <https://doi.org:10.1128/MCB.05722-11>
- 30 Tsang, T. *et al.* Copper is an essential regulator of the autophagic kinases ULK1/2 to drive lung adenocarcinoma. *Nat Cell Biol* **22**, 412-424 (2020). <https://doi.org:10.1038/s41556-020-0481-4>
- 31 Brady, D. C. *et al.* Copper is required for oncogenic BRAF signalling and tumorigenesis. *Nature* **509**, 492-496 (2014). <https://doi.org:10.1038/nature13180>
- 32 Tsvetkov, P. *et al.* Copper induces cell death by targeting lipoylated TCA cycle proteins. *Science* **375**, 1254-1261 (2022). <https://doi.org:10.1126/science.abf0529>
- 33 Janos, P., Aupic, J., Ruthstein, S. & Magistrato, A. The conformational plasticity of the selectivity filter methionines controls the in-cell Cu(I) uptake through the CTR1 transporter. *QRB Discov* **3**, e3 (2022). <https://doi.org:10.1017/qrd.2022.2>
- 34 Anastassopoulou, I. *et al.* Solution structure of the apo and copper(I)-loaded human metallochaperone HAH1. *Biochemistry* **43**, 13046-13053 (2004). <https://doi.org:10.1021/bi0487591>
- 35 Hatori, Y. & Lutsenko, S. The Role of Copper Chaperone Atox1 in Coupling Redox Homeostasis to Intracellular Copper Distribution. *Antioxidants (Basel)* **5** (2016). <https://doi.org:10.3390/antiox5030025>
- 36 Shanbhag, V. C. *et al.* Copper metabolism as a unique vulnerability in cancer. *Biochimica Et Biophysica Acta-Molecular Cell Research* **1868**, 16 (2021). <https://doi.org:10.1016/j.bbamcr.2020.118893>
- 37 Chaudhary, D., Chong, F., Neupane, T., Choi, J. & Jee, J. G. New Inhibitors of Laccase and Tyrosinase by Examination of Cross-Inhibition between Copper-Containing Enzymes. *Int J Mol Sci* **22** (2021). <https://doi.org:10.3390/ijms222413661>
- 38 Ida, M. *et al.* Structural basis of Cu, Zn-superoxide dismutase amyloid fibril formation involves interaction of multiple peptide core regions. *J Biochem* **159**, 247-260 (2016). <https://doi.org:10.1093/jb/mvv091>

- 39 Pennington, J. A. T. *et al.* Composition of Core Foods of the U.S. Food Supply, 1982-1991. *Journal of Food Composition and Analysis* **8**, 171-217 (1995). <https://doi.org/10.1006/jfca.1995.1014>
- 40 Myint, Z. W., Oo, T. H., Thein, K. Z., Tun, A. M. & Saeed, H. Copper deficiency anemia: review article. *Ann Hematol* **97**, 1527-1534 (2018). <https://doi.org/10.1007/s00277-018-3407-5>
- 41 Micronutrients, I. o. M. U. P. o. *Dietary Reference Intakes for Vitamin A, Vitamin K, Arsenic, Boron, Chromium, Copper, Iodine, Iron, Manganese, Molybdenum, Nickel, Silicon, Vanadium, and Zinc.*, (Washington (DC): National Academies Press (US);, 2001).
- 42 Crampton, R. F., Matthews, D. M. & Poisner, R. Observations on the Mechanism of Absorption of Copper by the Small Intestine. *J Physiol* **178**, 111-126 (1965). <https://doi.org/10.1113/jphysiol.1965.sp007618>
- 43 Turnlund, J. R., Keyes, W. R., Anderson, H. L. & Acord, L. L. Copper absorption and retention in young men at three levels of dietary copper by use of the stable isotope ⁶⁵Cu. *Am J Clin Nutr* **49**, 870-878 (1989). <https://doi.org/10.1093/ajcn/49.5.870>
- 44 Markowitz, H., Gubler, C. J., Mahoney, J. P., Cartwright, G. E. & Wintrobe, M. M. Studies on copper metabolism. XIV. Copper, ceruloplasmin and oxidase activity in sera of normal human subjects, pregnant women, and patients with infection, hepatolenticular degeneration and the nephrotic syndrome. *J Clin Invest* **34**, 1498-1508 (1955). <https://doi.org/10.1172/JCI103201>
- 45 Falcone, E. *et al.* Extracellular Cu²⁺ pools and their detection: From current knowledge to next-generation probes. *Coordination Chemistry Reviews* **433** (2021). <https://doi.org/10.1016/j.ccr.2020.213727>
- 46 Shawki, A. *et al.* Intestinal DMT1 is critical for iron absorption in the mouse but is not required for the absorption of copper or manganese. *Am J Physiol Gastrointest Liver Physiol* **309**, G635-647 (2015). <https://doi.org/10.1152/ajpgi.00160.2015>
- 47 Wyman, S., Simpson, R. J., McKie, A. T. & Sharp, P. A. Dcytb (Cybrd1) functions as both a ferric and a cupric reductase in vitro. *FEBS Lett* **582**, 1901-1906 (2008). <https://doi.org/10.1016/j.febslet.2008.05.010>
- 48 Gulec, S. & Collins, J. F. Molecular mediators governing iron-copper interactions. *Annu Rev Nutr* **34**, 95-116 (2014). <https://doi.org/10.1146/annurev-nutr-071812-161215>
- 49 Ohgami, R. S., Campagna, D. R., McDonald, A. & Fleming, M. D. The Steap proteins are metalloreductases. *Blood* **108**, 1388-1394 (2006). <https://doi.org/10.1182/blood-2006-02-003681>
- 50 Gupta, A. & Lutsenko, S. Human copper transporters: mechanism, role in human diseases and therapeutic potential. *Future Med Chem* **1**, 1125-1142 (2009). <https://doi.org/10.4155/fmc.09.84>
- 51 Nose, Y. *et al.* Ctrl is an apical copper transporter in mammalian intestinal epithelial cells in vivo that is controlled at the level of protein stability. *J Biol Chem* **285**, 32385-32392 (2010). <https://doi.org/10.1074/jbc.M110.143826>
- 52 Lee, J., Pena, M. M., Nose, Y. & Thiele, D. J. Biochemical characterization of the human copper transporter Ctrl. *J Biol Chem* **277**, 4380-4387 (2002). <https://doi.org/10.1074/jbc.M104728200>
- 53 Rodriguez-Granillo, A., Crespo, A., Estrin, D. A. & Wittung-Stafshede, P. Copper-transfer mechanism from the human chaperone Atox1 to a metal-binding domain of Wilson disease protein. *J Phys Chem B* **114**, 3698-3706 (2010). <https://doi.org/10.1021/jp911208z>

- 54 Banci, L. *et al.* Copper(I)-mediated protein-protein interactions result from suboptimal interaction surfaces. *Biochem J* **422**, 37-42 (2009). <https://doi.org:10.1042/BJ20090422>
- 55 Morgan, M. T., Nguyen, L. A. H., Hancock, H. L. & Fahrni, C. J. Glutathione limits aquacopper(I) to sub-femtomolar concentrations through cooperative assembly of a tetranuclear cluster. *J Biol Chem* **292**, 21558-21567 (2017). <https://doi.org:10.1074/jbc.M117.817452>
- 56 Levy, A. R., Nissim, M., Mendelman, N., Chill, J. & Ruthstein, S. Ctr1 Intracellular Loop Is Involved in the Copper Transfer Mechanism to the Atox1 Metallochaperone. *J Phys Chem B* **120**, 12334-12345 (2016). <https://doi.org:10.1021/acs.jpcc.6b10222>
- 57 Wernimont, A. K., Huffman, D. L., Lamb, A. L., O'Halloran, T. V. & Rosenzweig, A. C. Structural basis for copper transfer by the metallochaperone for the Menkes/Wilson disease proteins. *Nat Struct Biol* **7**, 766-771 (2000). <https://doi.org:10.1038/78999>
- 58 Nyasae, L., Bustos, R., Braiterman, L., Eipper, B. & Hubbard, A. Dynamics of endogenous ATP7A (Menkes protein) in intestinal epithelial cells: copper-dependent redistribution between two intracellular sites. *American Journal of Physiology-Gastrointestinal and Liver Physiology* **292**, G1181-G1194 (2007). <https://doi.org:10.1152/ajpgi.00472.2006>
- 59 Gordon, D. T., Leinart, A. S. & Cousins, R. J. Portal copper transport in rats by albumin. *Am J Physiol* **252**, E327-333 (1987). <https://doi.org:10.1152/ajpendo.1987.252.3.E327>
- 60 Weiss, K. C. & Linder, M. C. Copper transport in rats involving a new plasma protein. *Am J Physiol* **249**, E77-88 (1985). <https://doi.org:10.1152/ajpendo.1985.249.1.E77>
- 61 Abou Zeid, C. & Kaler, S. G. in *Wilson Disease* 17-22 (2019).
- 62 Linder, M. C. *et al.* Copper transport. *Am J Clin Nutr* **67**, 965S-971S (1998). <https://doi.org:10.1093/ajcn/67.5.965S>
- 63 Kim, H., Son, H. Y., Bailey, S. M. & Lee, J. Deletion of hepatic Ctr1 reveals its function in copper acquisition and compensatory mechanisms for copper homeostasis. *Am J Physiol Gastrointest Liver Physiol* **296**, G356-364 (2009). <https://doi.org:10.1152/ajpgi.90632.2008>
- 64 Zhou, B. & Gitschier, J. hCTR1: a human gene for copper uptake identified by complementation in yeast. *Proc Natl Acad Sci U S A* **94**, 7481-7486 (1997). <https://doi.org:10.1073/pnas.94.14.7481>
- 65 Terada, K. *et al.* Restoration of Holoceruloplasmin Synthesis in LEC Rat after Infusion of Recombinant Adenovirus Bearing WND cDNA. *Journal of Biological Chemistry* **273**, 1815-1820 (1998). <https://doi.org:10.1074/jbc.273.3.1815>
- 66 Terada, K. *et al.* Biliary excretion of copper in LEC rat after introduction of copper transporting P-type ATPase, ATP7B. *FEBS Lett* **448**, 53-56 (1999). [https://doi.org:10.1016/s0014-5793\(99\)00319-1](https://doi.org:10.1016/s0014-5793(99)00319-1)
- 67 Forbes, J. R. & Cox, D. W. Copper-dependent trafficking of Wilson disease mutant ATP7B proteins. *Hum Mol Genet* **9**, 1927-1935 (2000). <https://doi.org:10.1093/hmg/9.13.1927>
- 68 Nyasae, L. K., Schell, M. J. & Hubbard, A. L. Copper directs ATP7B to the apical domain of hepatic cells via basolateral endosomes. *Traffic* **15**, 1344-1365 (2014). <https://doi.org:10.1111/tra.12229>
- 69 Gupta, A. *et al.* Cellular copper levels determine the phenotype of the Arg875 variant of ATP7B/Wilson disease protein. *Proc Natl Acad Sci U S A* **108**, 5390-5395 (2011). <https://doi.org:10.1073/pnas.1014959108>
- 70 Roberts, E. A. & Sarkar, B. Liver as a key organ in the supply, storage, and excretion of copper. *Am J Clin Nutr* **88**, 851S-854S (2008). <https://doi.org:10.1093/ajcn/88.3.851S>

- 71 Oeser, E. A. & Tuck, J. L. Radioactive Isotopes of Copper. *Nature* **139**, 1110-1110 (1937).
<https://doi.org:10.1038/1391110a0>
- 72 Maryon, E. B., Molloy, S. A. & Kaplan, J. H. Cellular glutathione plays a key role in copper uptake mediated by human copper transporter 1. *Am J Physiol Cell Physiol* **304**, C768-779 (2013). <https://doi.org:10.1152/ajpcell.00417.2012>
- 73 Leary, S. C. *et al.* The human cytochrome c oxidase assembly factors SCO1 and SCO2 have regulatory roles in the maintenance of cellular copper homeostasis. *Cell Metab* **5**, 9-20 (2007). <https://doi.org:10.1016/j.cmet.2006.12.001>
- 74 Herd, S. M., Camakaris, J., Christofferson, R., Wookey, P. & Danks, D. M. Uptake and efflux of copper-64 in Menkes'-disease and normal continuous lymphoid cell lines. *Biochem J* **247**, 341-347 (1987). <https://doi.org:10.1042/bj2470341>
- 75 Lee, S. H., Lancey, R., Montaser, A., Madani, N. & Linder, M. C. Ceruloplasmin and copper transport during the latter part of gestation in the rat. *Proc Soc Exp Biol Med* **203**, 428-439 (1993). <https://doi.org:10.3181/00379727-203-43619>
- 76 Sauzeat, L. *et al.* Isotopic Evidence for Disrupted Copper Metabolism in Amyotrophic Lateral Sclerosis. *iScience* **6**, 264-271 (2018). <https://doi.org:10.1016/j.isci.2018.07.023>
- 77 Lyon, T. D. *et al.* Use of a stable copper isotope (⁶⁵Cu) in the differential diagnosis of Wilson's disease. *Clin Sci (Lond)* **88**, 727-732 (1995). <https://doi.org:10.1042/cs0880727>
- 78 Morel, J. D. *et al.* The mouse metallomic landscape of aging and metabolism. *Nat Commun* **13**, 607 (2022). <https://doi.org:10.1038/s41467-022-28060-x>
- 79 Speisky, H., Navarro, P., Cherian, M. G. & Jimenez, I. Copper-binding proteins in human erythrocytes: searching for potential biomarkers of copper over-exposure. *Biometals* **16**, 113-123 (2003). <https://doi.org:10.1023/a:1020724331271>
- 80 Albarede, F., Telouk, P., Lamboux, A., Jaouen, K. & Balter, V. Isotopic evidence of unaccounted for Fe and Cu erythropoietic pathways. *Metallomics* **3**, 926-933 (2011). <https://doi.org:10.1039/c1mt00025j>
- 81 Cabrera, A. *et al.* Copper binding components of blood plasma and organs, and their responses to influx of large doses of (⁶⁵)Cu, in the mouse. *Biometals* **21**, 525-543 (2008). <https://doi.org:10.1007/s10534-008-9139-6>
- 82 Linder, M. C. Ceruloplasmin and other copper binding components of blood plasma and their functions: an update. *Metallomics* **8**, 887-905 (2016). <https://doi.org:10.1039/c6mt00103c>
- 83 Turnlund, J. R., Keyes, W. R., Peiffer, G. L. & Scott, K. C. Copper absorption, excretion, and retention by young men consuming low dietary copper determined by using the stable isotope ⁶⁵Cu. *Am J Clin Nutr* **67**, 1219-1225 (1998). <https://doi.org:10.1093/ajcn/67.6.1219>
- 84 Houk, R. S. *et al.* Inductively Coupled Argon Plasma as an Ion-Source for Mass-Spectrometric Determination of Trace-Elements. *Analytical Chemistry* **52**, 2283-2289 (1980). <https://doi.org:DOI 10.1021/ac50064a012>
- 85 Wilschefska, S. C. & Baxter, M. R. Inductively Coupled Plasma Mass Spectrometry: Introduction to Analytical Aspects. *Clin Biochem Rev* **40**, 115-133 (2019). <https://doi.org:10.33176/AACB-19-00024>
- 86 Pozebon, D., Scheffler, G. L., Dressler, V. L. & Nunes, M. A. G. Review of the applications of laser ablation inductively coupled plasma mass spectrometry (LA-ICP-MS) to the analysis of biological samples. *J. Anal. At. Spectrom.* **29**, 2204-2228 (2014). <https://doi.org:10.1039/c4ja00250d>

- 87 Harrington, J. M., Young, D. J., Essader, A. S., Sumner, S. J. & Levine, K. E. Analysis of human serum and whole blood for mineral content by ICP-MS and ICP-OES: development of a mineralomics method. *Biol Trace Elem Res* **160**, 132-142 (2014). <https://doi.org/10.1007/s12011-014-0033-5>
- 88 Townsend, A. T., Miller, K. A., McLean, S. & Aldous, S. The determination of copper, zinc, cadmium and lead in urine by high resolution ICP-MS. *Journal of Analytical Atomic Spectrometry* **13**, 1213-1219 (1998). <https://doi.org/DOI> 10.1039/a805021j
- 89 de Oliveira, M., Gianeti, T. M. R., da Rocha, F. C. G., Lisboa-Filho, P. N. & Piacenti-Silva, M. A preliminary study of the concentration of metallic elements in the blood of patients with multiple sclerosis as measured by ICP-MS. *Sci Rep* **10**, 13112 (2020). <https://doi.org/10.1038/s41598-020-69979-9>
- 90 Favier, R. P. *et al.* Aberrant expression of copper associated genes after copper accumulation in COMMD1-deficient dogs. *Journal of Trace Elements in Medicine and Biology* **29**, 347-353 (2015). <https://doi.org/10.1016/j.jtemb.2014.06.007>
- 91 Direct Analysis of Ceruloplasmin in Human Blood Serum by HPLC/Inductively Coupled Plasma-Mass Spectrometry for the Diagnosis of Wilson Disease.
- 92 Gudekar, N. *et al.* Metallothioneins regulate ATP7A trafficking and control cell viability during copper deficiency and excess. *Sci Rep* **10**, 11 (2020). <https://doi.org/10.1038/s41598-020-64521-3>
- 93 Bhattacharjee, A. *et al.* The Activity of Menkes Disease Protein ATP7A Is Essential for Redox Balance in Mitochondria. *J Biol Chem* **291**, 16644-16658 (2016). <https://doi.org/10.1074/jbc.M116.727248>
- 94 Solovyev, N. *et al.* Biomedical copper speciation in relation to Wilson's disease using strong anion exchange chromatography coupled to triple quadrupole inductively coupled plasma mass spectrometry. *Anal Chim Acta* **1098**, 27-36 (2020). <https://doi.org/10.1016/j.aca.2019.11.033>
- 95 Quarles, C. D., Jr. *et al.* LC-ICP-MS method for the determination of "extractable copper" in serum. *Metallomics* **12**, 1348-1355 (2020). <https://doi.org/10.1039/d0mt00132e>
- 96 Gromadzka, G., Grycan, M. & Przybylkowski, A. M. Monitoring of Copper in Wilson Disease. *Diagnostics (Basel)* **13** (2023). <https://doi.org/10.3390/diagnostics13111830>
- 97 Bunce, J., Achila, D., Hetrick, E., Lesley, L. & Huffman, D. L. Copper transfer studies between the N-terminal copper binding domains one and four of human Wilson protein. *Biochimica Et Biophysica Acta-General Subjects* **1760**, 907-912 (2006). <https://doi.org/10.1016/j.bbagen.2006.02.005>
- 98 Marković, K., Cemazar, M., Sersa, G., Milačič, R. & Ščančar, J. Speciation of copper in human serum using conjoint liquid chromatography on short-bed monolithic disks with UV and post column ID-ICP-MS detection. *Journal of Analytical Atomic Spectrometry* **37**, 1675-1686 (2022). <https://doi.org/10.1039/d2ja00161f>
- 99 Costas-Rodriguez, M. *et al.* Isotopic analysis of Cu in blood serum by multi-collector ICP-mass spectrometry: a new approach for the diagnosis and prognosis of liver cirrhosis? *Metallomics* **7**, 491-498 (2015). <https://doi.org/10.1039/c4mt00319e>
- 100 Kim, P. *et al.* Accurate Measurement of Copper Overload in an Experimental Model of Wilson Disease by Laser Ablation Inductively Coupled Plasma Mass Spectrometry. *Biomedicines* **8** (2020). <https://doi.org/10.3390/biomedicines8090356>
- 101 M-M, P., Weiskirchen, R., Gassler, N., Bosserhoff, A. K. & Becker, J. S. Novel bioimaging techniques of metals by laser ablation inductively coupled plasma mass spectrometry for

- diagnosis of fibrotic and cirrhotic liver disorders. *PLoS One* **8**, e58702 (2013).
<https://doi.org/10.1371/journal.pone.0058702>
- 102 Weiskirchen, S., Kim, P. & Weiskirchen, R. Determination of copper poisoning in Wilson's
disease using laser ablation inductively coupled plasma mass spectrometry. *Ann Transl
Med* **7**, S72 (2019). <https://doi.org/10.21037/atm.2018.10.67>
- 103 M-M, P., Merle, U., Weiskirchen, R. & Becker, J. S. Bioimaging of copper deposition in
Wilson's diseases mouse liver by laser ablation inductively coupled plasma mass
spectrometry imaging (LA-ICP-MSI). *International Journal of Mass Spectrometry* **354-
355**, 281-287 (2013). <https://doi.org/10.1016/j.ijms.2013.07.006>
- 104 Zoriy, M. V., Dehnhardt, M., Matusch, A. & Becker, J. S. Comparative imaging of P, S, Fe,
Cu, Zn and C in thin sections of rat brain tumor as well as control tissues by laser ablation
inductively coupled plasma mass spectrometry. *Spectrochimica Acta Part B: Atomic
Spectroscopy* **63**, 375-382 (2008). <https://doi.org/10.1016/j.sab.2007.11.030>
- 105 Zoriy, M. V., Dehnhardt, M., Reifenberger, G., Zilles, K. & Becker, J. S. Imaging of Cu,
Zn, Pb and U in human brain tumor resections by laser ablation inductively coupled plasma
mass spectrometry. *International Journal of Mass Spectrometry* **257**, 27-33 (2006).
<https://doi.org/10.1016/j.ijms.2006.06.005>
- 106 Grochowski, C. *et al.* Analysis of Trace Elements in Human Brain: Its Aim, Methods, and
Concentration Levels. *Front Chem* **7**, 115 (2019).
<https://doi.org/10.3389/fchem.2019.00115>
- 107 Lum, T.-S. & Sze-Yin Leung, K. Strategies to overcome spectral interference in ICP-MS
detection. *Journal of Analytical Atomic Spectrometry* **31**, 1078-1088 (2016).
<https://doi.org/10.1039/c5ja00497g>
- 108 Carter, K. P., Young, A. M. & Palmer, A. E. Fluorescent Sensors for Measuring Metal Ions
in Living Systems. *Chemical Reviews* **114**, 4564-4601 (2014).
<https://doi.org/10.1021/cr400546e>
- 109 Que, E. L., Domaille, D. W. & Chang, C. J. Metals in neurobiology: Probing their chemistry
and biology with molecular imaging. *Chemical Reviews* **108**, 1517-1549 (2008).
<https://doi.org/10.1021/cr078203u>
- 110 Sivaraman, G. *et al.* Chemically diverse small molecule fluorescent chemosensors for
copper ion. *Coordination Chemistry Reviews* **357**, 50-104 (2018).
<https://doi.org/10.1016/j.ccr.2017.11.020>
- 111 Cotruvo, J. A., Jr., Aron, A. T., Ramos-Torres, K. M. & Chang, C. J. Synthetic fluorescent
probes for studying copper in biological systems. *Chem Soc Rev* **44**, 4400-4414 (2015).
<https://doi.org/10.1039/c4cs00346b>
- 112 Huang, B., Bates, M. & Zhuang, X. Super-resolution fluorescence microscopy. *Annu Rev
Biochem* **78**, 993-1016 (2009).
<https://doi.org/10.1146/annurev.biochem.77.061906.092014>
- 113 Hirayama, T., Van de Bittner, G. C., Gray, L. W., Lutsenko, S. & Chang, C. J. Near-infrared
fluorescent sensor for in vivo copper imaging in a murine Wilson disease model. *Proc. Natl.
Acad. Sci. U. S. A.* **109**, 2228-2233 (2012). <https://doi.org/10.1073/pnas.1113729109>
- 114 Swamy, K. M. *et al.* Boronic acid-linked fluorescent and colorimetric probes for copper
ions. *Chem Commun (Camb)*, 5915-5917 (2008). <https://doi.org/10.1039/b814167c>
- 115 Xiao, T. *et al.* Copper regulates rest-activity cycles through the locus coeruleus-
norepinephrine system. *Nat Chem Biol* **14**, 655-663 (2018).
<https://doi.org/10.1038/s41589-018-0062-z>

- 116 Jiang, J. *et al.* AIE + ESIPT activity-based NIR Cu(2+) sensor with dye participated binding strategy. *Chem Commun (Camb)* **57**, 7685-7688 (2021). <https://doi.org/10.1039/d1cc02233d>
- 117 Devasia, J., Joy, F. & Nizam, A. A Selective Excited-State Intramolecular-Proton-Transfer (ESIPT) Sensor for Copper(II) Based on Chelation-Enhanced Quenching and "Off-On" Detection of Amino Acids. *Chemistry* **29**, e202203652 (2023). <https://doi.org/10.1002/chem.202203652>
- 118 Yang, L. C. *et al.* Imaging of the intracellular topography of copper with a fluorescent sensor and by synchrotron x-ray fluorescence microscopy. *Proc. Natl. Acad. Sci. U. S. A.* **102**, 11179-11184 (2005). <https://doi.org/10.1073/pnas.0406547102>
- 119 Chung, C. Y. *et al.* Activity-based ratiometric FRET probe reveals oncogene-driven changes in labile copper pools induced by altered glutathione metabolism. *Proc Natl Acad Sci U S A* **116**, 18285-18294 (2019). <https://doi.org/10.1073/pnas.1904610116>
- 120 Yu, K. K., Li, K., Hou, J. T. & Yu, X. Q. Coumarin-TPA derivative: a reaction-based ratiometric fluorescent probe for Cu(I). *Tetrahedron Letters* **54**, 5771-5774 (2013). <https://doi.org/10.1016/j.tetlet.2013.08.046>
- 121 Taki, M., Iyoshi, S., Ojida, A., Hamachi, I. & Yamamoto, Y. Development of highly sensitive fluorescent probes for detection of intracellular copper(I) in living systems. *J Am Chem Soc* **132**, 5938-5939 (2010). <https://doi.org/10.1021/ja100714p>
- 122 Dodani, S. C., Leary, S. C., Cobine, P. A., Winge, D. R. & Chang, C. J. A targetable fluorescent sensor reveals that copper-deficient SCO1 and SCO2 patient cells prioritize mitochondrial copper homeostasis. *J Am Chem Soc* **133**, 8606-8616 (2011). <https://doi.org/10.1021/ja2004158>
- 123 Taki, M., Akaoka, K., Mitsui, K. & Yamamoto, Y. A mitochondria-targeted turn-on fluorescent probe based on a rhodol platform for the detection of copper(I). *Org Biomol Chem* **12**, 4999-5005 (2014). <https://doi.org/10.1039/c4ob00527a>
- 124 Tian, R. *et al.* NIR fluorescent probe with variable lipophilicity for imaging lysosomal copper during cuproptosis in HCC cells. *Dyes and Pigments* **219** (2023). <https://doi.org/10.1016/j.dyepig.2023.111590>
- 125 Lee, Y. H. *et al.* Organelle-selective fluorescent Cu²⁺ ion probes: revealing the endoplasmic reticulum as a reservoir for Cu-overloading. *Chem Commun (Camb)* **50**, 3197-3200 (2014). <https://doi.org/10.1039/c4cc00091a>
- 126 Park, S. Y. *et al.* An endoplasmic reticulum-selective ratiometric fluorescent probe for imaging a copper pool. *Chem Commun (Camb)* **53**, 4457-4460 (2017). <https://doi.org/10.1039/c7cc01430a>
- 127 Jung, K. H., Oh, E. T., Park, H. J. & Lee, K. H. Development of new peptide-based receptor of fluorescent probe with femtomolar affinity for Cu(+) and detection of Cu(+) in Golgi apparatus. *Biosens Bioelectron* **85**, 437-444 (2016). <https://doi.org/10.1016/j.bios.2016.04.101>
- 128 Goshisht, M. K., Tripathi, N., Patra, G. K. & Chaskar, M. Organelle-targeting ratiometric fluorescent probes: design principles, detection mechanisms, bio-applications, and challenges. *Chem Sci* **14**, 5842-5871 (2023). <https://doi.org/10.1039/d3sc01036h>
- 129 Lee, S. *et al.* Activity-Based Sensing with a Metal-Directed Acyl Imidazole Strategy Reveals Cell Type-Dependent Pools of Labile Brain Copper. *J Am Chem Soc* **142**, 14993-15003 (2020). <https://doi.org/10.1021/jacs.0c05727>

- 130 Pezacki, A. T. *et al.* Oxidation state-specific fluorescent copper sensors reveal oncogene-driven redox changes that regulate labile copper(II) pools. *Proc Natl Acad Sci U S A* **119**, e2202736119 (2022). <https://doi.org:10.1073/pnas.2202736119>
- 131 Miki, T. *et al.* A conditional proteomics approach to identify proteins involved in zinc homeostasis. *Nat Methods* **13**, 931-937 (2016). <https://doi.org:10.1038/nmeth.3998>
- 132 Zhu, H. *et al.* Imaging and Profiling of Proteins under Oxidative Conditions in Cells and Tissues by Hydrogen-Peroxide-Responsive Labeling. *Journal of the American Chemical Society* **142**, 15711-15721 (2020). <https://doi.org:10.1021/jacs.0c02547>
- 133 Noguchi, K. *et al.* β -Galactosidase-Catalyzed Fluorescent Reporter Labeling of Living Cells for Sensitive Detection of Cell Surface Antigens. *Bioconjugate Chemistry* **31**, 1740-1744 (2020). <https://doi.org:10.1021/acs.bioconjchem.0c00180>
- 134 Nishikawa, Y. *et al.* Development of a Nitric Oxide-Responsive Labeling Reagent for Proteome Analysis of Live Cells. *Acs Chem Biol* **14**, 397-404 (2019). <https://doi.org:10.1021/acscchembio.8b01021>

Chapter 1

Design and study of the chemical labeling reagents for protein labeling in response to copper ions in living cells

Abstract

Copper is essential for living organisms, acting as a cofactor for various biological processes, and recent research has revealed labile copper ion pools that regulate signal transduction and influence cell activities. Disruptions in copper homeostasis can lead to the shortage and accumulation of copper ions, which are associated with diseases such as cancer, Alzheimer's, Parkinson's, and genetic disorders. Understanding intracellular copper pool dynamics is increasingly important. The covalent protein bioconjugation strategy is a valuable tool for studying biological molecules and bio-metal ions through protein labeling, offering advantages over conventional chemosensors such as reduced probe diffusion, compatibility with cell fixation, and potential for proteomic analysis of intracellular microenvironments. The strategy has been employed to detect copper ions within living cells. However, the current reagents utilizing this approach are limited by high background signals and a lack of a tool that selectively responds to the prevalent form of intracellular copper ions, Cu^+ . To tackle these challenges, I have explored various chemical strategies to develop an efficient Cu^+ -responsive covalent protein tagging method for use in biology, particularly in living cells. We have designed and synthesized four distinct copper ion-responsive chemical tools utilizing various chemical reactions. I then conducted tests *in vitro* and in live cells to evaluate and compare the copper-responsiveness properties of these reagents. The analytical results revealed that all four types of reagents demonstrated copper ion-responsive protein labeling capabilities. Notably, the TPA-cage-masked quinone methide-based reagent exhibited superior performance due to its high selectivity for Cu^+ and its effectiveness in detecting elevated Cu^+ levels within various cell models.

Introduction

Copper plays a vital role in the functioning of living organisms, with its redox-active property (the interconversion of Cu^+ and Cu^{2+}) serving as a cofactor for metalloenzymes involved in various biological processes, including aerobic respiration, epigenetic modification, and metabolism.^{1,2,3} Recent research has also revealed the presence of loosely bound, labile copper ion pools, which are thought to be involved in regulating signal transduction by reversibly binding to protein targets and influencing their activities and structural properties.^{4,5,6} Under normal conditions, the concentration of intracellular labile copper ions is kept low.⁷ However, when there is a disruption in copper homeostasis, these ions accumulate within the cell and lead to reactive oxygen species (ROS) generation through Fenton and Haber–Weiss reactions, resulting in oxidative damage to the cell.^{8,9} Recently, a significant copper-mediated cell death pathway known as cuproptosis has been identified. Cuproptosis is characterized by intracellular copper accumulation, which triggers the aggregation of mitochondrial lipoylated proteins and destabilization of iron-sulfur cluster proteins, ultimately causing proteotoxic stress and cell death.¹⁰ The dysregulation of copper homeostasis has been linked to cellular dysfunction and is associated with a range of diseases, including Alzheimer's and Parkinson's diseases, cancer, as well as genetic disorders like Wilson's and Menke's diseases.^{8,11,12,13} This underscores the growing significance of exploring intracellular copper pool dynamics.

The covalent protein bioconjugation strategy, which responds to the target signaling molecule, has proven to be a valuable and increasingly popular tool for studying target biological molecules or bio-metal ions through protein labeling.^{14,15,16,17,18} In comparison to traditional target-selective chemosensors, this covalent protein modification mechanism offers several advantages: (1) reduced probe diffusion, leading to improved spatial resolution following the target response; (2) immobilized signal compatibility with cell fixation; and (3) the potential for proteomic analysis of intracellular target-rich microenvironments. This strategy has also been utilized in the study of copper ions, and a few fluorescent reagents based on protein labeling in response to copper ions have been reported.^{14,15} The Copper-Directed Acyl Imidazole (CDAI) strategy has been utilized to detect copper ions, preserving spatial information in living cells through a copper-mediated enhancement of acyl imidazole electrophile activity.^{14,15} This allows for subsequent labeling of proximal proteins at sites with elevated copper levels upon binding with copper ions. With the CDAI strategy, reagents that respond comparably to Cu^+ and Cu^{2+} without selectivity or exhibit

higher reactivity to Cu^{2+} than Cu^+ have been developed.^{14,15} However, the inherent activity of acyl imidazole electrophiles results in relatively high background signals, limiting the application of these probes. Furthermore, a covalent protein modification-based probe that selectively responds to Cu^+ , the most prevalent oxidation state of intracellular copper ions,¹⁹ has not yet been reported. To address the limitations of the CDAI strategy and bridge the gap in Cu^+ -selective protein bioconjugation-based probes, I aimed to develop a new cuprous ion (Cu^+)-activated covalent chemical reaction-based protein bioconjugation strategy.

Four copper-activated or copper-catalyzed chemical reactions have come into our interest and are utilized in developing new strategies. The metal-catalyzed heteroatom-hydrogen (X-H) insertion of the diazo compound via the generation of metal-carbenoid is a potent tool in chemical synthesis, utilizing transition metal catalysts such as rhodium (Rh) and copper (Cu).²⁰ The application of Rh-catalyzed X-H insertion of biotin-appended diazo reagent to modify target proteins *in vitro*²¹ has inspired our endeavor to develop a diazo-based protein-labeling reagent to label proteins activated by present copper ions. The copper ions-catalyzed oxidation of catechol produces *o*-quinone, a reactive electrophile capable of undergoing a Michael addition-type reaction with nucleophiles.^{22,23,24} Furthermore, the active *o*-quinone has been utilized to modify target proteins *in vitro*,^{25,26,27} leading us to believe that catechol could serve as a promising copper ion-responsive labeling reagent. Additionally, the Cu^+ -catalyzed oxidative C–O bond cleavage of the benzyl ether upon complexation of tris(2-pyridylmethyl) amine (TPA) ligand with Cu^+ has been employed in developing Cu^+ -selective fluorescent probes for live cell application.^{28,29} Consequently, we sought to apply this chemical strategy to mask a reactive intermediate that can react with the nucleophiles on the surface of proximal proteins, for which quinone methide (QM) - a highly reactive Michael receptor of nucleophiles^{17,28,30,31} - and the potential copper-activatable catechol have been chosen. Therefore, I aim to apply these four chemical strategies in designing copper ion-responsive protein labeling reagents to explore which strategy would be an effective Cu^+ -responsive covalent protein tagging method for application in biology, at least in living cells.

In this chapter, we utilized four chemical strategies introduced earlier to develop and synthesize protein labeling reagents: diazo-based, catechol-based, TPA-cage-masked catechol, and TPA-cage-masked QM-based reagents. We then conducted tests *in vitro* and in live cells to evaluate and compare the copper-responsiveness properties of these reagents. The analytical results revealed that all four types of reagents demonstrated copper ion-responsive protein labeling

capabilities. However, the TPA-cage-masked QM-based reagent exhibited superior performance to the other three types due to its high selectivity for Cu^+ and its effectiveness in detecting elevated Cu^+ levels within various cell models.

Results and Discussion

Design of chemical labeling tools in response to copper ion

Using various chemical reactions, I aimed to develop protein labeling tools that respond to cuprous ions. These tools consist of a copper ion-responsive reactive component and a fluorophore as the label. Fluorescein (FL), tetramethylrhodamine (TMR), 7-(diethylamino)coumarin (Dc), and diacetate fluorescein (AcFL) are the typical fluorophores used for applications *in vitro* and in living cells. The copper ion-responsive reactive component is designed based on different chemical reactions. For instance, the diazo reagent, in the presence of transition metal catalysts such as rhodium (Rh) and copper (Cu), is used to generate heteroatom-hydrogen insertion products.^{20,21} Inspired by this, we aimed to develop a diazo-based protein-labeling reagent that labels proteins when activated by copper ions. Additionally, copper ions can catalyze the oxidation of catechol reagents to generate *o*-quinone, a reactive electrophile capable of undergoing Michael addition-type reactions with nucleophilic residues on proteins.^{22,23,24} making it a promising novel chemical tool for protein labeling. Furthermore, the *ortho*-hydroxyl groups also act as metal binding groups, showing a good binding affinity for various metal ions, including Cu ($K_d = 26.3$ fM for Cu^{2+}),³² which may enhance the response to Cu. Considering that cuprous ions can catalyze the cleavage of the C-O bond of the benzyl ether upon Cu-binding, we also incorporated a copper ligand, tris(2-pyridylmethyl) amine (TPA) ($K_d = 126$ fM for Cu^+),^{28,29,33} into the catechol reagent to design TPA-caged catechol reagent in hopes of improving the affinity for Cu^+ and enabling the selection for Cu^+ . Additionally, we utilized quinone methide (QM) precursor as the reactive component^{17,28,30,31} and incorporated it with the cuprous ion recognition moiety to design a quinone methide-based Cu-responsive reagent. As a result, we designed and synthesized a diazo-based reagent (DiaR), catechol-based reagent (CatR), TPA-ligand-caged catechol reagent (TCatR), and quinone-methide-based reagent (QmCuR) (**Figure. 1.1**).

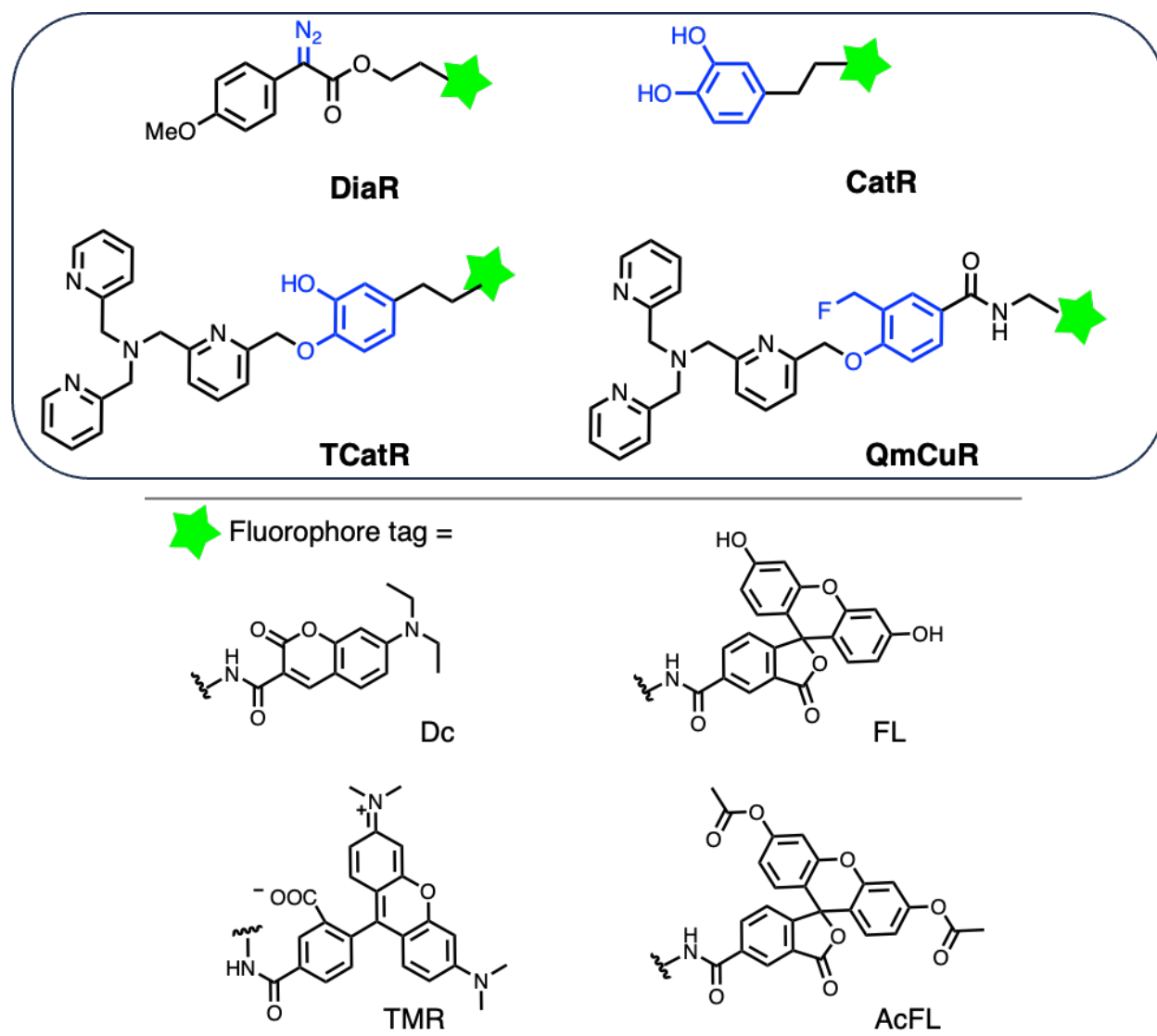


Figure 1.1 **Molecular design of the chemical tools.** Molecular structures of the designed copper ion-responsive protein labeling reagents. TMR, tetramethylrhodamine; FL, fluorescein; AcFL, diacetylated fluorescein; Dc, 7-(diethylamino)coumarin. The FL and Dc fluorophore tags are utilized for *in vitro* studies. The TMR fluorophore tag can be used for both *in vitro* and in live cell studies, while the AcFL fluorophore tag is only applied for live cell studies.

Evaluation of DiaR in vitro and in living cells

Initially, we conducted a study on the Cu-responsiveness properties of DiaR through *in vitro* tests using BSA as the model protein or the HeLa cell lysate as the proteome model, as well

as in living Hela cells. Our findings indicated that DiaR exhibits a higher protein labeling intensity in response to Cu^+ and Cu^{2+} ions than other bio-metals, such as redox-active Fe^{2+} and Fe^{3+} ions (**Figure 1.2a**). This demonstrates its capability for protein labeling in response to copper ions and suggests its strong selectivity for copper ions ($\text{Cu}^{+/2+}$). I also observed that Cu-responsive protein labeling can be quenched by the copper ions chelator- bathocuproine disulfonate (BCS) - thus confirming that the labeling originates from Cu-response (**Figure 1.2b**). Additionally, our *in vitro* dose dependency analysis revealed that the protein labeling is Cu-concentration dependent, with the half maximal effective concentration (EC_{50}) at approximately 100 μM (**Figure 1.2b, 1.2c**). This concentration may be too low to detect the intracellular labile copper ions. DiaR was then applied to living cells to assess its effectiveness in labeling proteins in response to intracellular copper ions. DiaR rapidly entered the cells and spread evenly within 5 minutes (**Figure 1.2d**). In cells treated with extracellular CuCl_2 and the copper ions ligand-neocuproine (Neo), DiaR exhibited a significantly enhanced protein labeling intensity (**Figure 1.2e, 1.2f**), demonstrating its capability for intracellular Cu-responsive protein labeling. However, DiaR displayed minimal intracellular protein labeling in response to extracellularly administered copper ions in the absence of the copper ion carrier - Neo (**Figure 1.2f**). In contrast, the commercially available cuprous ion probe, CopperGREEN, indicated a detectable elevation in the level of labile Cu^+ ions within the cell under this condition (**Figure 1.3**). This suggests that the copper sensitivity of DiaR is relatively low, potentially limiting its utility in studying typical physiological or pathological labile copper ions within living systems, such as living cells. Therefore, while DiaR is an effective tool for copper ion-responsive protein labeling, its lack of selectivity for Cu^+ and Cu^{2+} , as well as its low sensitivity for copper ions ($\text{Cu}^{+/2+}$), restricts its application in studying copper ions in living systems. As a result, we proceeded to investigate alternative chemical tools with higher sensitivity to copper ions.

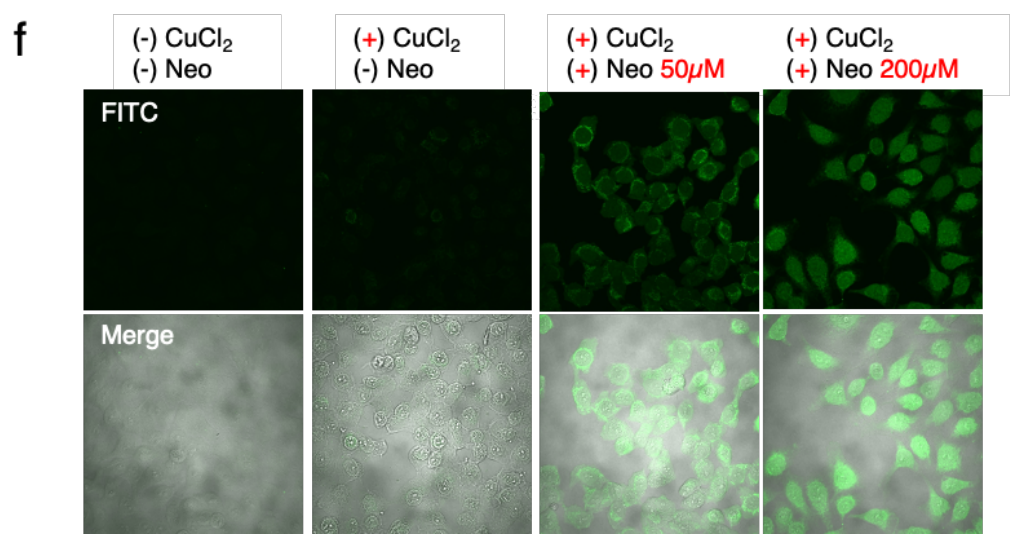
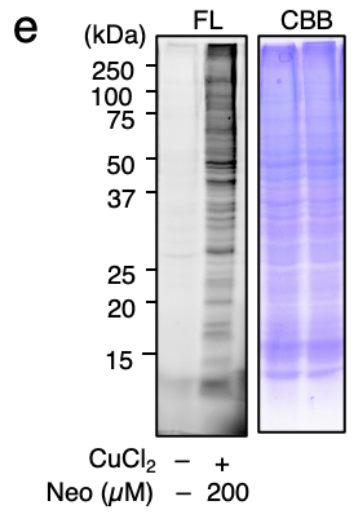
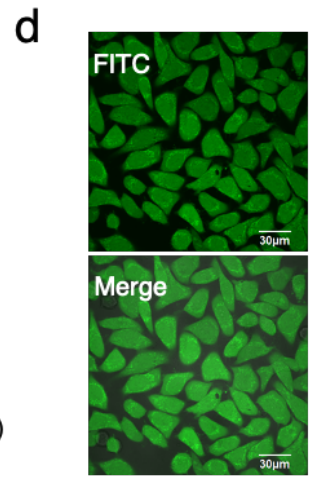
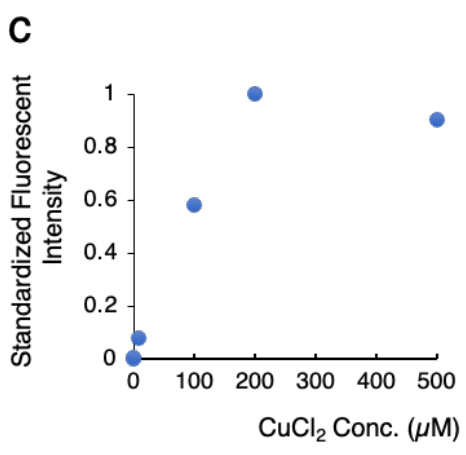
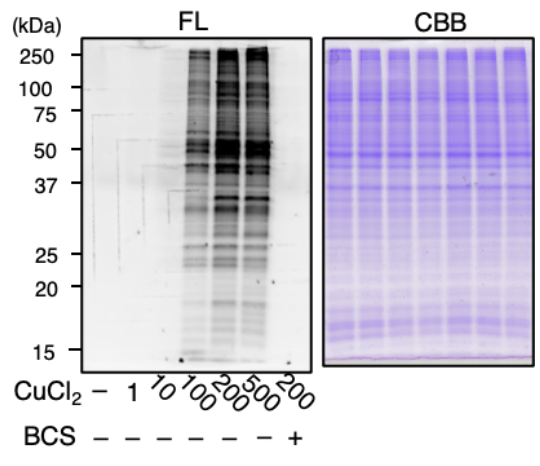
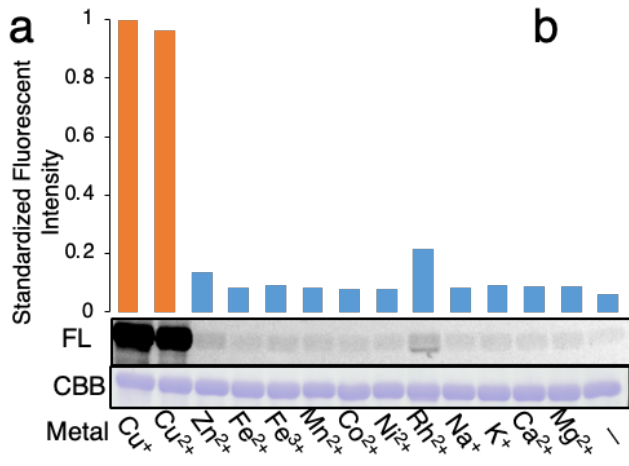


Figure 1.2 **Copper ion-responsive protein labeling by DiaR *in vitro* and in live HeLa cells.** (a) Selectivity of DiaR for several metal ions. A mixture of DiaR (50 μM) and BSA (10 μM) in 50 mM HEPES buffer (pH 7.4) was incubated at 37°C for 1 h in the presence of various metal ions (50 μM for Cu^+ , Cu^{2+} , Zn^{2+} , Co^{2+} , Fe^{2+} , Fe^{3+} , Ni^{2+} , Mn^{2+} , and Rh^{2+} , and 5 mM for Na^+ , K^+ , Ca^{2+} , and Mg^{2+}). (b) SDS-PAGE and in-gel fluorescence analysis and (c) quantitative analysis of the Cu-concentration dependencies of protein labeling by DiaR in HeLa lysate. A mixture of DiaR (1 μM) and HeLa lysate (3.5 mg/mL) in 100 mM HEPES (pH 7.4) was incubated at 37°C for 1 h with CuCl_2 (1 μM , 10 μM , 100 μM , 200 μM , or 500 μM) in the presence and absence of bathocuproine disulfonate (BCS) (500 μM). (d) Fluorescence imaging showing the cell permeability and uniform distribution of DiaR in HeLa cells. (e) In-gel fluorescence analysis and (f) CLSM imaging analysis of protein labeling in live HeLa cells. DiaR (10 μM) was loaded into HeLa cells at 37°C for 5 minutes, after removing the extracellular DiaR by washing, the cells were incubated with and without CuCl_2 (100 μM) together with neocuproine (Neo; 50 or 200 μM) at 37°C for 1h. FL, in-gel fluorescence; CBB, coomassie brilliant blue; BSA, bovine serum albumin; CLSM, confocal laser scanning microscopy; Fluorescein fluorescence images (FITC, green); Merge: FITC images were overlaid with differential interference contrast (DIC) to give Merge images.

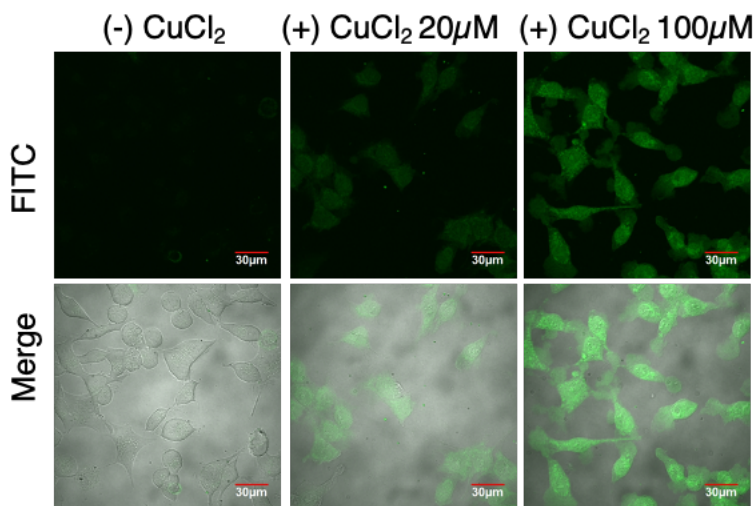


Figure 1.3 **CLSM images of fluorescent intensity of HeLa cells stained by CopperGREEN with and without CuCl_2 -treatment.** The HeLa cells were treated with or without CuCl_2 (20 μM , 100 μM) for 1 h followed by incubation with CopperGREEN at 37°C for 2 h, followed by imaging. CLSM, confocal laser scanning microscopy; Fluorescein fluorescence images (FITC, green);

Merge: FITC images were overlaid with differential interference contrast (DIC) to give Merge images.

Evaluation of CatR in vitro and in living cells

I then developed and synthesized CatR and assessed its Cu-responsive protein labeling capabilities both *in vitro* and in living cells. *In vitro* experiments using BSA as the model protein demonstrated that CatR exhibits Cu-responsive protein labeling ability and displays a stronger response to $\text{Cu}^{+/2+}$ compared to other biometal ions (**Figure 1.4a**). Moreover, HPLC analysis revealed the Cu-responsive reaction mechanism, indicating that copper ions catalyze the production of active quinone from CatR, which then reacts with nucleophilic amino acids such as Cys (**Figure 1.4d, 1.4e**). The dose-dependency test illustrated that CatR responds to both Cu^+ and Cu^{2+} in a concentration-dependent manner (**Figure 1.4b**), with an EC_{50} of approximately 15 μM (**Figure 1.4c**), demonstrating its higher affinity for Cu compared to DiaR (**Figure 1.2c**). Furthermore, CatR exhibits excellent permeability in living cells, evenly distributing within the cells within 5 minutes (**Figure 1.4h**). Subsequent application of CatR to living HeLa cells, both with and without CuCl_2 treatment, revealed increased intracellular protein labeling intensities in response to elevated exogenous Cu treatment (**Figure 1.4f, 1.4g, 1.4i**). This provides evidence that CatR can respond to elevated intracellular labile Cu ions and exhibits greater sensitivity to intracellular labile Cu ions compared to DiaR.

Next, I applied CatR to HeLa cells transiently transfected with a plasmid that expresses copper transporter 1 (CTR1) - a membrane protein that selectively imports extracellular cuprous ions into cells³⁴ - to compare the intracellular Cu^+ -responsiveness of CatR with CopperGREEN. The results showed that the intracellular labile Cu^+ levels were elevated in the Cu-pretreated CTR1-overexpressed cells compared to the Cu-pretreated CTR1-WT cells (**Figure 1.5a**). However, CatR did not detect such elevation in labile Cu^+ levels (**Figure 1.5b**). This suggests that while the sensitivity of CatR for Cu ions was increased compared to DiaR, it cannot rival CopperGREEN, possibly due to its lower affinity for $\text{Cu}^{+/2+}$ and unselectivity between Cu^+ and Cu^{2+} . The failure of CatR's application in CTR1-overexpressed cells also indicates that a ligand with a higher affinity for Cu ions is probably necessary for the design.

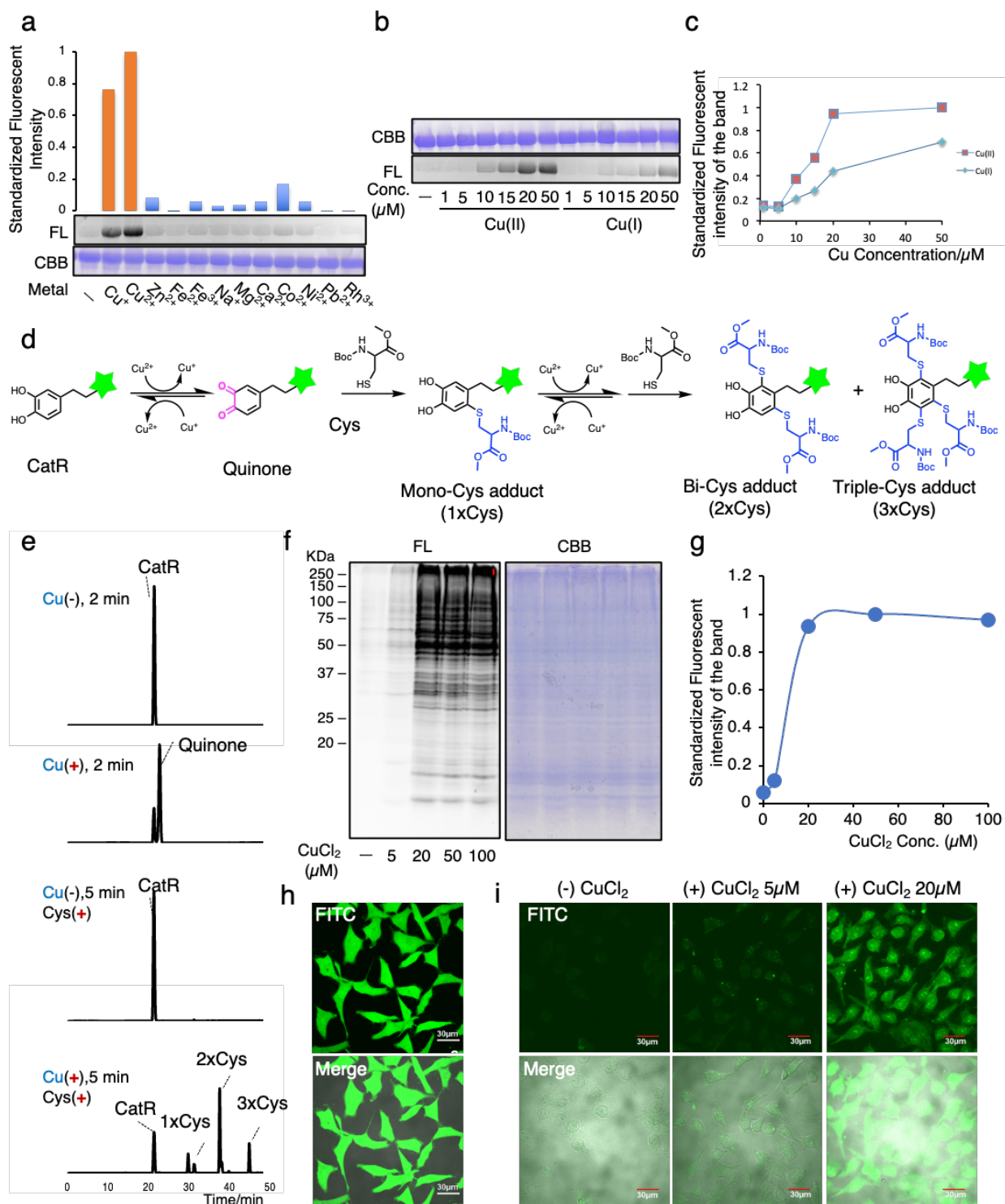


Figure 1.4 Copper ion-responsive protein labeling by CatR *in vitro* and in live HeLa cells. (a) Selectivity of CatR for several metal ions. A mixture of CatR (50 μM) and BSA (10 μM) in 50 mM HEPES buffer (pH7.2) was incubated at 37°C for 1 h in the presence of various metal ions (50 μM for Cu^+ , Cu^{2+} , Zn^{2+} , Co^{2+} , Fe^{2+} , Fe^{3+} , Ni^{2+} , Pb^{2+} , and Rh^{3+} , and 5 mM for Na^+ , Ca^{2+} , and

Mg²⁺). (b) SDS-PAGE and in-gel fluorescence analysis and (c) quantitative analysis of the Cu-concentration dependencies of protein labeling by CatR. A mixture of CatR (50 μM) and BSA (10 μM) in 50 mM HEPES buffer (pH 7.2) with CuCl₂ or Cu(MeCN)₄PF₆ (1, 5, 10, 15, 20, 50 μM) at 37°C for 1 h. (d) The presumed reaction mechanism of the Cu-responsive reaction of CatR. (e) Confirmation of Cu-catalyzed quinone formation and the reaction with amino acids such as cysteine by HPLC analysis. (h) Fluorescence imaging showing the cell permeability and uniform distribution of CatR in HeLa cells. (f) SDS-PAGE and in-gel fluorescence analysis, (g) quantitative analysis, and (i) CLSM imaging analysis of protein labeling in live HeLa cells. CatR was loaded into HeLa cells at 37°C for 5 minutes; after removing extracellular CatR by washing, the cells were incubated with CuCl₂ (0-100 μM) for 1h at 37°C. After labeling, the cells were lysed for SDS-PAGE analysis or fixed for CLSM imaging. HPLC, High-performance liquid chromatography; FL, in-gel fluorescence; CBB, coomassie brilliant blue; BSA, bovine serum albumin; CLSM, confocal laser scanning microscopy; Fluorescein fluorescence images (FITC, green); Merge: FITC images were overlaid with differential interference contrast (DIC) to give Merge images.

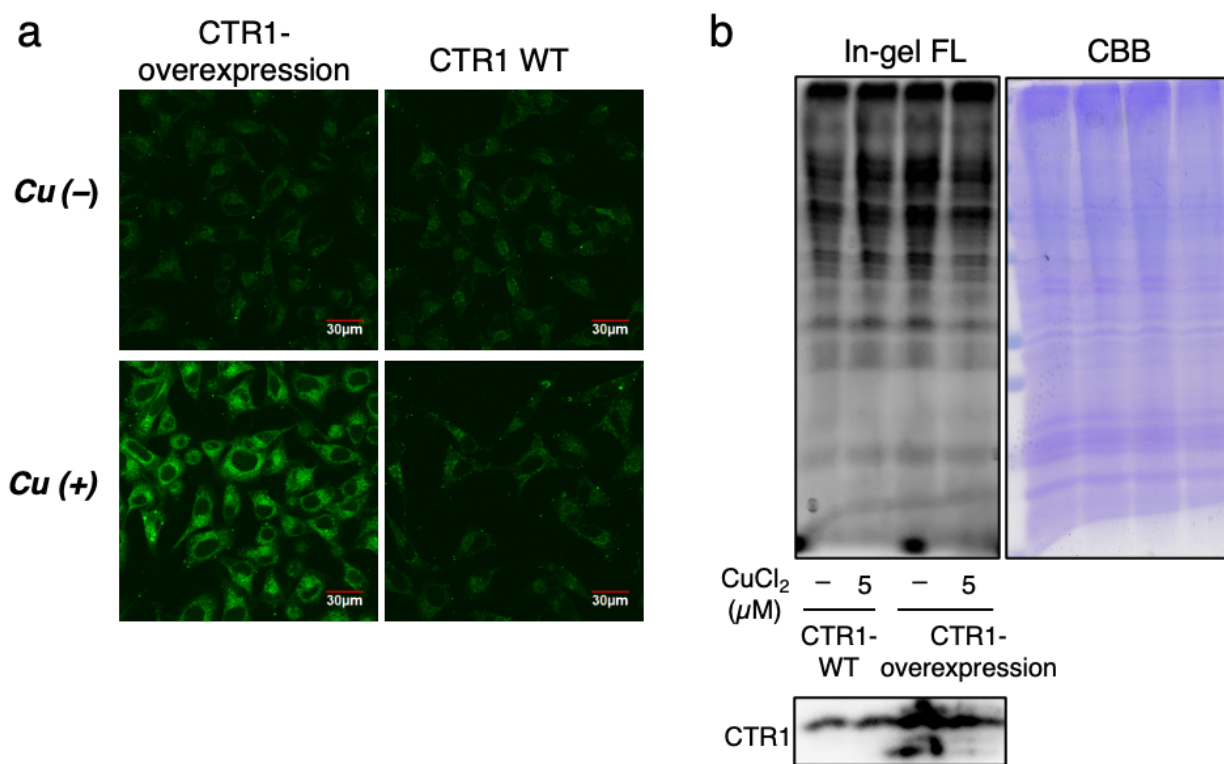


Figure 1.5 Compare intracellular Cu⁺-responsive capability of CopperGREEN and CatR in CTR1-overexpressed HeLa cells. (a) CLSM images of fluorescent intensity of CopperGREEN -

stained live CTR1-WT and CTR1-overexpressed HeLa cells. (b) SDS-PAGE and in-gel fluorescence analysis of protein labeling by CatR in live CTR1 - WT and CTR1-overexpressed HeLa cells. HeLa cells transfected with a CTR1-expression plasmid were pretreated with CuCl_2 (5 μM) for 8.5 h, then incubated with CopperGREEN (5 μM) for 2.5 h or CatR (5 μM) for 0.5 h. CTR1, copper transporter 1; WT, wild type; CLSM, confocal laser scanning microscopy

Evaluation of TCatR in vitro and in living cells

Subsequently, we developed TCatR with the aim of enhancing its affinity for Cu^+ and its selectivity for Cu^+ , and I assessed its ability to respond to cuprous ions both *in vitro* and in living cells. The findings indicate that TCatR indeed exhibits Cu^+ -responsive protein labeling capability, demonstrating selectivity for Cu^+ over Cu^{2+} (**Figure 1.6a**), as anticipated. Furthermore, the Cu^+ -responsive protein labeling is contingent on the concentration of Cu^+ , with an EC_{50} of approximately 1 μM (**Figure 1.6b**), confirming its heightened Cu^+ affinity compared to the original CatR, achieved by incorporating the TPA ligand. Upon application to living cells, TCatR demonstrates rapid intracellular penetration and uniform distribution within 5 minutes (**Figure 1.6c**). However, while TCatR is capable of responding to increased intracellular labile Cu^+ ions in CuCl_2 -treated cells (**Figure 1.6d**), this response is considerably lower than that of CatR (**Figure 1.6e**), possibly due to its slower kinetics involving a three-step reaction: Cu^+ -catalyzed C-O bond cleavage, Cu-binding with the released catechol reagent, and Cu-catalyzed generation of quinone, followed by the reaction of active quinone with proteins. Moreover, TCatR fails to respond to the elevated Cu^+ transported by overexpressed CTR1 in living cells (**Figure 1.6f**).

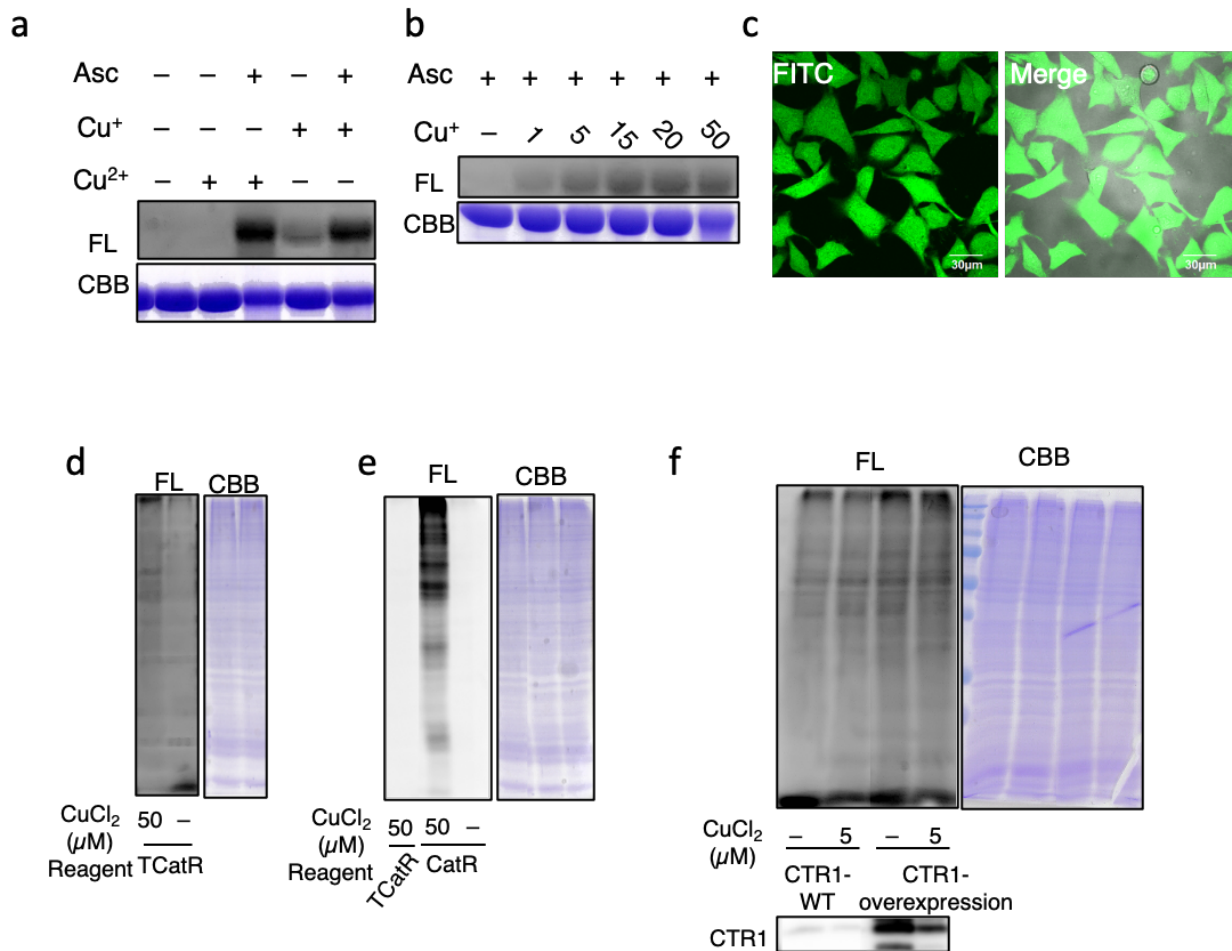


Figure 1.6 Copper ion-responsive protein labeling by TCatR *in vitro* and in live HeLa cells.

(a) Selectivity of TCatR for Cu⁺ compared to Cu²⁺. A mixture of TCatR (50 µM) and BSA (10 µM) in 50 mM HEPES buffer (pH7.2) was incubated at 37°C for 1 h in the presence of Cu⁺ (Cu(MeCN)₄PF₆) or Cu²⁺ (CuCl₂) (50 µM) with and without sodium-*L*-ascorbate (Asc; 1 mM). (b) SDS-PAGE and in-gel fluorescence analysis of the Cu-concentration dependencies of protein labeling by TCatR. A mixture of TCatR (50 µM) and BSA (10 µM) in 50 mM HEPES buffer (pH 7.2) with and without Cu(MeCN)₄PF₆ (1, 5, 15, 20, 50 µM) in the presence of sodium-*L*-ascorbate (Asc; 1 mM) at 37°C for 1 h. (c) Fluorescence imaging showing the cell permeability and uniform distribution of TCatR in HeLa cells. (d) SDS-PAGE and in-gel fluorescence analysis of protein labeling by TCatR in live HeLa cells. (e) Compare the intracellular Cu-responsive protein labeling by TCatR and CatR in live cells. TCatR or CatR was loaded into HeLa cells at 37°C for 5 minutes; after removing the extracellular reagent by washing, the cells were incubated with CuCl₂ (50 µM)

for 1h at 37°C. Note that even though the labeling conditions for (d) and (e) are the same, the labeling efficiency of TCatR is significantly weaker than that of CatR. As a result, the fluorescence of the labeled proteins by TCatR was almost indiscernible in (e) but discernible in (d) due to the differing contrast of the two images. (f) SDS-PAGE and in-gel fluorescence analysis of protein labeling by TCatR in live CTR1-WT and CTR1-overexpressed HeLa cells. HeLa cells transfected with a CTR1-expression plasmid were pretreated with CuCl₂ (5 μM) for 8.5 h, then incubated with TCatR (5 μM) for 2.5 h. Note that the expression level of CTR1 in copper-treated transfected cells decreased due to the negative feedback of CTR1 in response to intracellular copper accumulation.³⁵ CTR1, copper transporter 1; WT, wild type.

Evaluation of QmCuR in vitro and in living cells

I then developed the TPA-caged quinone methide precursor-based Cu-responsive reagent (QmCuR), intending to enhance its affinity for Cu⁺, selectivity for Cu⁺, and Cu⁺-responsive protein labeling efficiency. The Cu⁺-responsive properties of QmCuR were assessed through *in vitro* and in-live cell tests. QmCuR exhibited the highest protein labeling intensity in response to Cu⁺ compared to other biometal ions and reactive oxygen species (ROS) (**Figure 1.7a, 1.7b**), demonstrating its capability for Cu⁺-responsive protein labeling and high selectivity for Cu⁺. Additionally, the Cu⁺-responsive protein labeling was dose-dependent on Cu⁺, with an EC₅₀ of approximately 10 μM according to this *in vitro* test (**Figure 1.7c**), while its affinity for Cu⁺ was measured at 126 fM.³³ Subsequently, QmCuR was applied to living cells following exogenous CuCl₂ treatment or transient transfection of overexpressed CTR1-expression plasmid. The results indicated that QmCuR could respond to intracellular elevated labile Cu⁺ levels resulting from exogenous Cu treatment and the excessive import of extracellular Cu⁺ due to overexpressed CTR1 (**Figure 1.7d, 1.7e, 1.7f**).

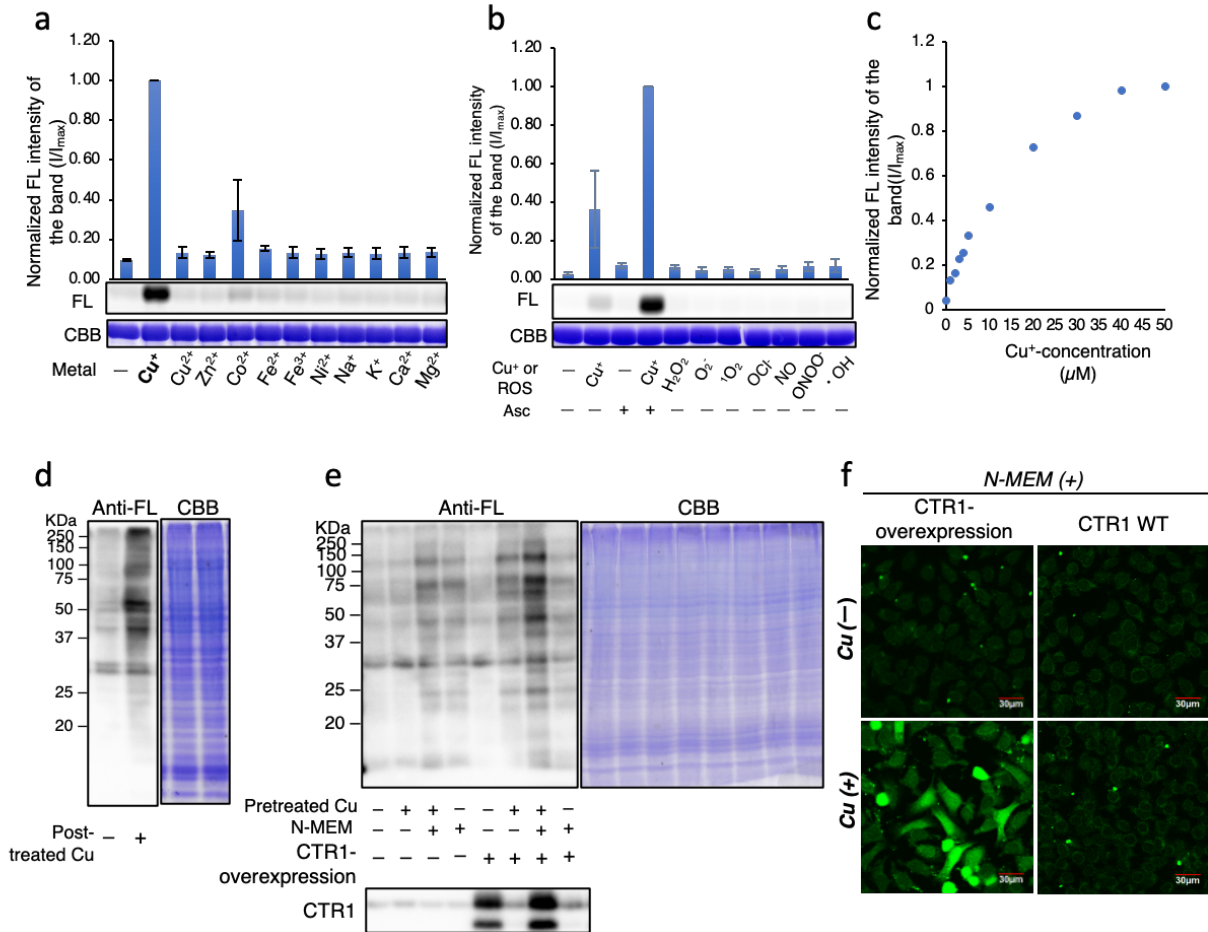


Figure 1.7 Cu^+ ion-responsive protein labeling by QmCuR *in vitro* and in live HeLa cells. (a, b) Selectivity of QmCuR for (a) several metal ions and (b) ROS. A mixture of QmCuR (50 μM) and BSA (10 μM) in 50 mM HEPES buffer (pH7.2) was incubated at 37°C for 1 h in the presence of various metal ions (50 μM for Cu^+ , Cu^{2+} , Zn^{2+} , Co^{2+} , Fe^{2+} , Fe^{3+} , and Ni^{2+} , and 5 mM for Na^+ , K^+ , Ca^{2+} , and Mg^{2+}) or ROS/ROS generating reagent (50 μM). $n = 3$ biological replicates. (c) Quantitative analysis of the Cu^+ -concentration dependencies of protein labeling by QmCuR. A mixture of QmCuR (50 μM) and BSA (10 μM) in 50 mM HEPES buffer (pH 7.2) with varying concentrations of Cu^+ in the presence of sodium-*L*-ascorbate (100 μM) at 37°C for 1 h. (d) SDS-PAGE and western-blotting analysis of protein labeling by QmCuR in live HeLa cells. QmCuR (5 μM) was loaded into HeLa cells at 37°C for 25 minutes; after removing the extracellular reagent by washing, the cells were incubated with $CuCl_2$ (5 μM) for 30 min at 37°C. (e) SDS-PAGE and western-blotting analysis, and (f) CLSM imaging analysis of protein labeling by QmCuR in live CTR1-WT and CTR1-overexpressed HeLa cells. HeLa cells transfected with a CTR1-expression

plasmid were pretreated with CuCl_2 (5 μM) for 8.5 h, then incubated with QmCuR (5 μM) for 25 min, followed by 10 min of N-MEM (100 μM) treatment. CTR1, copper transporter 1; WT, wild type; N-MEM, *N*-methylmaleimide; CLSM, confocal laser scanning microscopy.

Conclusion

In this chapter, I have examined four distinct Cu-responsive tools that rely on various chemical reactions: DiaR, CatR, TcatR, and QmCuR. DiaR and CatR exhibit selectivity for $\text{Cu}^+/\text{Cu}^{2+}$ over other bio metals, but they do not differentiate between Cu^+ and Cu^{2+} . CatR demonstrates higher sensitivity for $\text{Cu}^{+/2+}$ than DiaR, but its sensitivity is insufficient to detect elevated Cu^+ transported by overexpressed CTR1 in HeLa cells, unlike the current commercially available Cu^+ probe, CopperGREEN, which can. TcatR is selective for Cu^+ over Cu^{2+} and more sensitive to Cu^+ than CatR, but it also fails to respond to elevated Cu^+ transported by overexpressed CTR1 in HeLa cells. Based on these findings, although DiaR, CatR, and TcatR are effective copper ion-responsive protein labeling reagents, their design is suboptimal and limits their application in studying intracellular copper ions in living cells. In contrast, QmCuR exhibits high selectivity and sensitivity for Cu^+ and can detect elevated Cu^+ levels under Cu-supplementation and transported by overexpressed CTR1 in live HeLa cells. Therefore, among these four candidates based on different chemical reactions, the Cu-recognition moiety-appended QmCuR is the most promising. Consequently, I will focus on optimizing and characterizing QmCuRs in the following chapter 2.

Experimental section

General materials and methods for the biochemical/biological experiments

Unless otherwise noted, all proteins/enzymes and reagents were obtained from commercial suppliers (Sigma-Aldrich, Tokyo Chemical Industry (TCI), Fujifilm Wako Pure Chemical Corporation, Sasaki Chemical, Bio-Rad, Thermo Fisher Scientific, Dojindo, or Watanabe Chemical Industries) and used without further purification. SDS- polyacrylamide gel electrophoresis (SDS-PAGE) and western blotting were carried out using a Bio-Rad Mini-Protean III electrophoresis apparatus. Fluorescence gel images were acquired with a FUSION FX (Vilber) equipped with a SPECTRA-Capsule BLUE (480) and a fluorescence filter (F535-Y2). Proteins were stained by Instant Blue Coomassie Protein Stain (Abcam) or Imperial Protein Stain (Thermo Fisher Scientific). Cell imaging was performed with a confocal laser scanning microscope (CLSM) (Carl Zeiss LSM800 or Olympus FV1000) equipped with a 20 × or a 63 × oil immersion objective lens. Reversed-phase HPLC (RP-HPLC) was carried out on a Hitachi Chromaster HPLC system equipped with a Chromaster 5410 UV detector (detection at 420 nm). All runs used linear gradients of acetonitrile containing 0.1% TFA (solvent A) and 0.1% aqueous TFA (solvent B) unless otherwise noted. High-resolution mass spectra were measured on an Exactive (Thermo Scientific) equipped with electron spray ionization (ESI).

Cu⁺-responsive labeling with BSA or proteins in Hela lysate

10 μM purified bovine serum albumin (BSA) in 50 mM HEPES buffer (pH 7.2 or pH 7.4) was incubated with 50 μM Cu-responsive protein labeling reagent (DiaR, CatR, TeatR, or QmCuR) in the presence or absence of 50 μM Cu(MeCN)₄PF₆ at 37°C for 1 h. For metal selectivity assay, various metal salts (5 mM of NaCl, KCl, MgCl₂ or MgSO₄, CaCl₂, or 50 μM of CuCl₂ or CuSO₄, ZnCl₂ or ZnSO₄, FeCl₂, FeCl₃, CoSO₄ or CoCl₂, NiCl₂ or NiSO₄, MnSO₄, Rh(CH₃COO)₂), and Pb(NO₃)₂ were used instead of Cu(MeCN)₄PF₆. For evaluating responsiveness to ROS, 50 μM of H₂O₂, O₂⁻, ¹O₂, OCl⁻, NO, ONOO⁻, or •OH was added. The ROS solutions were prepared freshly: KO₂ for O₂⁻, 4-Methyl-1,4-etheno-2,3-benzodioxin-1(4H)-propanoic acid for ¹O₂, Fenton reaction with FeCl₂ and H₂O₂ for •OH, NaOCl for OCl⁻, NOC-7 for NO, and SIN-1 (Cayman Chemical, 82220) for ONOO⁻. For the studies that used Sodium-*L*-ascorbate as a reducing agent to prevent oxidation of Cu⁺ in the aqueous solution, 100 μM or 1 mM Sodium-*L*-ascorbate was added. For evaluating the copper-concentration dependency, varying concentrations of Cu(MeCN)₄PF₆ and

CuCl₂ were applied in the reaction. For evaluating Cu-responsive protein labeling in HeLa lysate, home-made HeLa lysate (3.0-3.5 mg/mL) in 100 mM HEPES buffer (pH 7.4) was incubated with CuCl₂ (1 μM -500 μM) and 1 μM DiaR with and without 500 μM bathocuproine disulfonate (BCS) at 37°C for 1 h. After the reaction, each sample was mixed with an equal volume of 2 × SDS sample buffer (130 mM Tris-HCl, 6% SDS, 8% sucrose, 0.01% bromophenol blue) containing 10% 2-mercaptoethanol (2-ME) and 1 mM EDTA and boiled at 95°C for 5 min. The samples were then resolved by 12.5 % homemade polyacrylamide gel and analyzed by in-gel fluorescence imaging. The loaded protein was visualized by CBB stains. The fluorescence intensity of the labeled BSA's or lysate proteins' bands was quantitated by Image J.

HPLC test of the reactions for CatR

CatR (Dc-appended type; 50 μM) was dissolved in a mixing solvent of PBS and CH₃CN (4:6 v/v), followed by the addition of CuCl₂ (500 μM) and BocNH-Cys-COOMe (300 μM). The mixture was then incubated at 37°C. At each time point, 1.2 mL of the reacting mixture was taken and subjected to RP-HPLC (Column: YMC-pack ODS-A, 250 × 10 mm; CH₃CN (0.1 % TFA)/ H₂O (0.1 % TFA) = 40/60 to 80/20 (linear gradient over 40 min); flow rate, 3.0 mL/min; UV-Vis detector at 420 nm). The eluates were then collected and identified by HR-ESI MS.

Cell lines and culture conditions

HeLa cells were cultured in high glucose Dulbecco's Modified Eagle Medium (DMEM, 043-30085) supplemented with 10% fetal bovine serum (FBS; NICHIREI) and 1% Antibiotic-Antimycotic (Anti-Anti, Gibco) under a humidified atmosphere of 5% CO₂ in air at 37°C. These cells were harvested from subconfluent cultures using a trypsin-EDTA solution (Gibco) or cell scraper and then resuspended in a fresh medium. Subculture was performed every 2–3 days.

Observation of intracellular Cu⁺ in CuCl₂-supplemented HeLa cells by CopperGreen

The HeLa cells (3.0 × 10⁵ cells per dish) were cultured on 35mm-dish in DMEM supplemented with 10 % v/v FBS and 1% anti-anti at 37 °C under 5% CO₂ for 24 h. The cells were washed twice with HEPES-buffered saline (HBS) buffer (20 mM HEPES, 107 mM NaCl, 6 mM KCl, 2 mM CaCl₂, 1.2 mM MgSO₄, 11.5 mM Glucose, pH 7.4) and incubated in the medium with and without CuCl₂ (20 μM, 100 μM) at 37 °C under 5% CO₂ for 1 h. After washing cells twice with phosphate-

buffered saline (PBS) buffer containing 1mM EDTA and once with serum-free DMEM (no phenol-red, 25mM HEPES), the cells were incubated in serum-free DMEM (no phenol-red, 25mM HEPES) containing 5 μ M CopperGREEN™ at 37°C for 2 h. The fluorescent images were obtained by excitation at 488 nm and simultaneous detection with a FITC emission filter (510-560 nm).

Cu-responsive protein labeling in HeLa cells

The HeLa cells (3.0×10^5 cells per dish) were cultured on 35mm-dishes in DMEM supplemented with 10 % v/v FBS and 1% anti-anti at 37 °C under 5% CO₂ for 24 h. The cells were washed twice with phenol red-free Dubecco phosphate-buffered saline (DPBS; Gibco) containing 0.9 mM CaCl₂ and 0.5 mM MgCl₂, and incubated in the medium containing 10 μ M labeling reagent (DiaR, CatR, TCatR, QmCuR) at 37 °C (5% CO₂) for 5min (for DiaR, CatR, and TCatR) or 25 min (for QmCuR). The cells were then washed twice with DPBS (0.9 mM CaCl₂, 0.5 mM MgCl₂) (used for DiaR and CatR) or Hepes buffered saline (HBS) (used for TCatR and QmCuR) and incubated in the medium with and without CuCl₂ (5 μ M - 100 μ M) together with and without Neocuproine (50 μ M, 200 μ M) at 37 °C (5% CO₂) for 1 h (for DiaR, CatR, and TCatR) or 30 min (for QmCuR). After washing cells twice with phosphate-buffered saline (PBS) and the buffer was removed, 100 μ L of 1 \times laemmli buffer containing 50 mM dithiothreitol (DTT) and 1 mM EDTA were added to the cells. The cells were homogenized by ultrasonic treatment with Branson 450 Sonifier (Output control: 1; Duty cycle:10). The supernatants of each sample were then resolved by 12.5 % homemade polyacrylamide gel and fluorescein-labeled proteins were then detected by in-gel fluorescence imaging.

For imaging analysis, the cells, after the labeling, were fixed with cold methanol (-20 °C) and placed at -20 °C for 15 min, followed by washing twice with PBS buffer. The fluorescent images were obtained by excitation at 488 nm and simultaneous detection with a FITC emission filter (510-560 nm).

Preparation of CTR1 expression plasmid

A cDNA encoding the full-length human copper transporter 1 (CTR1) and NheI/NotI sites was purchased from Eurofins. After digested with NheI and NotI, the fragment was inserted into the same digestion site of the pCAGGS2 plasmid to obtain the pCAGGS2-CTR1 plasmid.³⁶

Intracellular Cu⁺ observation by CopperGreen in the living CTR1-overexpressed HeLa cells

The HeLa cells (2.0×10^5 cells per 35 mm dish) were cultured on 35-mm dishes in DMEM supplemented with 10 % v/v FBS and 1% anti-anti at 37 °C under 5% CO₂ for 24 h. The cells were transfected with pCAGGS2-CTR1 using Lipofectamine 2000 (Invitrogen) according to the manufacturer's instructions. After 18–24 h, the cells were cultured in the medium with and without CuCl₂ (5 μM) for 8.5 h. Subsequently, the cells were washed with FBS-free DMEM-HEPES (Gibco, 1 % anti-anti) twice and incubated in FBS-free DMEM-HEPES (Gibco, 1 % anti-anti) containing 5 μM CopperGREEN at 37 °C under 5% CO₂ for 2.5 h. The fluorescent images were then obtained by excitation at 488 nm and simultaneous detection with a FITC emission filter (510–560 nm).

Cu⁺-responsive labeling in CTR1-overexpressed HeLa cells

The HeLa cells (1.0×10^5 cells per well) were cultured on the 12-well plate in DMEM supplemented with 10 % v/v FBS and 1% anti-anti at 37 °C under 5% CO₂ for 24 h. The cells were transfected with pCAGGS2-CTR1 using Lipofectamine 2000 (Invitrogen) according to the manufacturer's instructions. After 18–24 h, the cells were cultured in the medium with and without CuCl₂ (5 μM) for 8.5 h. Subsequently, the cells were washed with growth medium twice and incubated in FBS-free DMEM-HEPES (Gibco, 1 % anti-anti) containing 5 μM Cu-responsive protein labeling reagents (CatR, TCatR, and QmCuR) at 37 °C under 5% CO₂ for 25 min (for QmCuR), 30 min (for CatR), or 2.5 h (for TCatR). The cells were then washed once with DMEM-HEPES and added with fresh labeling medium with or without 100 μM N-methylmaleimide (N-MEM) and incubated for 10 min at 37 °C (5% CO₂). The cells were washed once with PBS containing 1mM EDTA, and then lysed with 100 μL of 1 × SDS-sample buffer (65 mM Tris-HCl, 3% SDS, 4% sucrose, 0.005% bromophenol blue) containing 1 mM EDTA and 100 mM dithiothreitol (DTT) on ice for 5 min. The lysate was collected into a 1.5 mL tube using a cell scraper and sonicated with Branson 450 Sonifier (Output control: 1; Duty cycle:10; Shots: 10). The obtained protein mixture was then vortexed for 10 min at room temperature and applied to 12.5 % homemade AA gels for protein electrophoresis. The fluorescein-labeled proteins were then detected by in-gel fluorescence imaging or western-blotting analyses. For western blotting analyses, the proteins were then transferred to ImmunBlot PVDF membranes (Bio-Rad). After being blocked with 5% skim milk in TBST (Tris-buffered saline with 0.05% Tween 2036 (Sigma-

Aldrich)) for 1 hour, membranes were incubated with primary antibodies diluted in 1 % skim milk in TBST at 4 °C overnight, followed by two rounds of 5 min wash with TBST and one round of 15 min wash with TBST. Membranes were then incubated with peroxidase (HRP)-conjugated secondary antibodies diluted in 1 % skim milk in TBST for 1 hour, followed by two rounds of 5 min wash with TBST and one round of 15 min wash with TBST. The membrane was immersed in ECL prime blotting substrate (Bio-Rad) for chemiluminescence detection. Antibodies used in this study include rabbit anti-fluorescein (1:3000; ab19491, Abcam), rabbit anti-CTR1 (1:2000; ab129067, Abcam), and rabbit anti-beta tubulin (1:2000; ab15568, Abcam), and HRP-conjugated anti-rabbit IgG (CST, 7074s).

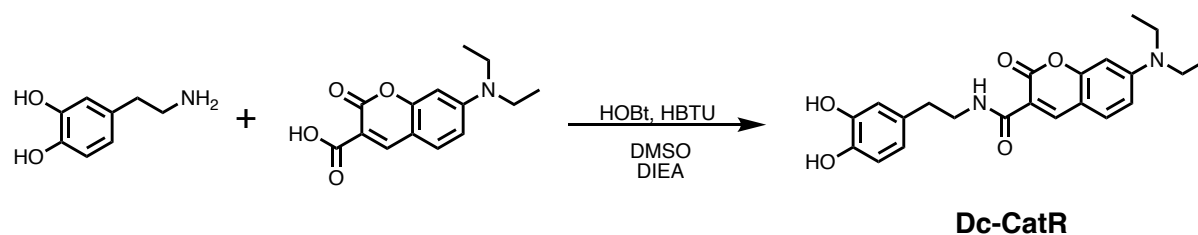
For imaging analysis, the cells, after the labeling, were fixed with cold methanol (-20 °C) and placed at -20 °C for 15 min, followed by washing twice with PBS buffer. The fluorescent images were obtained by excitation at 488 nm and simultaneous detection with a FITC emission filter (510-560 nm).

Synthetic schemes and processes

General materials and methods for organic synthesis

All chemical reagents and solvents were obtained from commercial suppliers (Tokyo Chemical Industry (TCI), Sigma-Aldrich, Fujifilm-Wako Pure Chemical Corporation, Watanabe Chemical Industries, BLD Pharmatech Ltd., or Kanto Chemical Co., Inc.) and used without further purification. Thin layer chromatography (TLC) was performed on silica gel 60 F254 precoated aluminium sheets (Merck) and visualized by fluorescence quenching, fluorescence by 365 nm excitation, or staining with reagents (Ninhydrin, Bromocresol Green Stain, Phosphomolybdic Acid (PMA)). Chromatographic purification was accomplished using flash column chromatography on silica gel 60 N (neutral, 40–50 μm , Kanto Chemical) or Isolera Spektra One (Biotage) by using Sfar Silica HC Duo columns (Biotage) or on the manually packed silica gel 60 N (neutral, 40–50 μm , Kanto Chemical). $^1\text{H-NMR}$ spectra were recorded in deuterated solvents on a Varian Mercury 400 (400 MHz) spectrometer and calibrated to tetramethylsilane (= 0 ppm) or residual solvent peak. Multiplicities are abbreviated as follows: s = singlet, brs = broad singlet, d = doublet, t = triplet, q = quartet, m = multiplet, dd = double doublet, td = triplet of doublets. Matrix-assisted laser desorption/ionization time-of-flight mass spectrometry (MALDI-TOF MS) spectra were recorded on an Autoflex III instrument (Bruker Daltonics) using α -cyano-4-hydroxycinnamic acid (CHCA)

as the matrix. High-resolution mass spectra were measured on an Exactive (Thermo Scientific) equipped with electron spray ionization (ESI). Unless otherwise noted, reversed-phase HPLC (RP-HPLC) was carried out on a Hitachi Chromaster HPLC system equipped with a Chromaster 5410 UV detector, and a YMC-Pack ODS-A column (5 μ m, 250 \times 20 mm) at a flow rate of 9.9 mL/min. UV detection was at 220 nm and 254 nm. All runs used linear gradients of acetonitrile containing 0.1% TFA (solvent A) and 0.1% aqueous TFA (solvent B).



Scheme 1 Synthetic scheme of **Dc-CatR**.

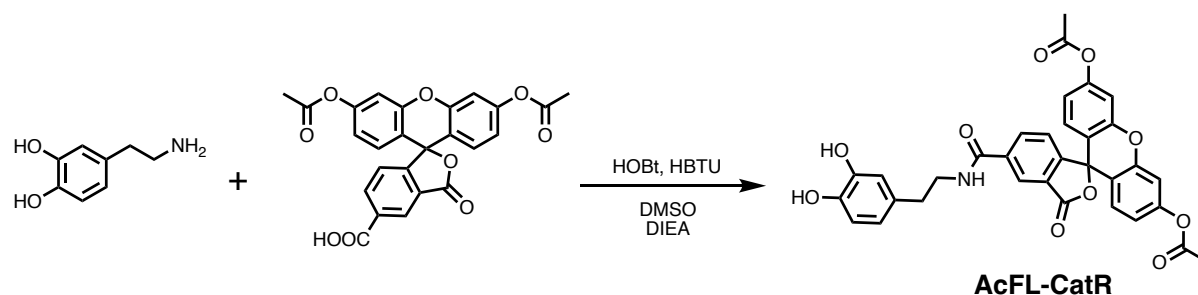
Compound Dc-CatR

To a stirred solution of 3-hydroxytyramine hydrogen chloride (9.0 mg, 0.047 mmol) in dry DMSO (2 mL) was added 7-diethylaminocoumarin-3-carboxylic acid (13.7 mg, 0.052 mmol), HBTU (26.9 mg, 0.071 mmol), HOBt \cdot H₂O (27 mg, 0.176 mmol), and DIEA (42 μ L, 0.141 mmol). The mixture was stirred overnight at room temperature. After the reaction was confirmed completed, the solution was concentrated under reduced pressure. The crude product was dissolved in CHCl₃ and purified by Isolera (gradient was automatically generated based on TLC information; Solvent: CHCl₃-MeOH) to give the product containing impurities, which was further purified by RP-HPLC (C18 column; A: B = 40:60 \rightarrow 60:40 (20 min)) to yield compound **Dc-CatR** (10 mg, 0.025 mmol, yield: 54 %) as yellow solids. The purity of the final product was also confirmed by HPLC. **¹H-NMR** (400 MHz, CD₃OD) δ /ppm 8.521 (s, 1H), 7.801 (s, 1H), 7.446 (d, 1H, J = 4.0 Hz), 7.453 (d, 1H, J = 9.6 Hz), 6.723 (dd, 1H, J = 2.4 Hz, J = 8.8 Hz), 6.602 (s, 1H), 6.586 (d, 1H, J = 2.8 Hz), 6.491-6.471 (m, 1H), 3.491-3.421 (m, 6H), 2.638 (t, 2H, J = 7.2 Hz), 1.131 (t, 6H, J = 7.0 Hz). **ESI-MS**: For [M+Na]⁺ calcd. 419.1577, obsd. 419.1583.

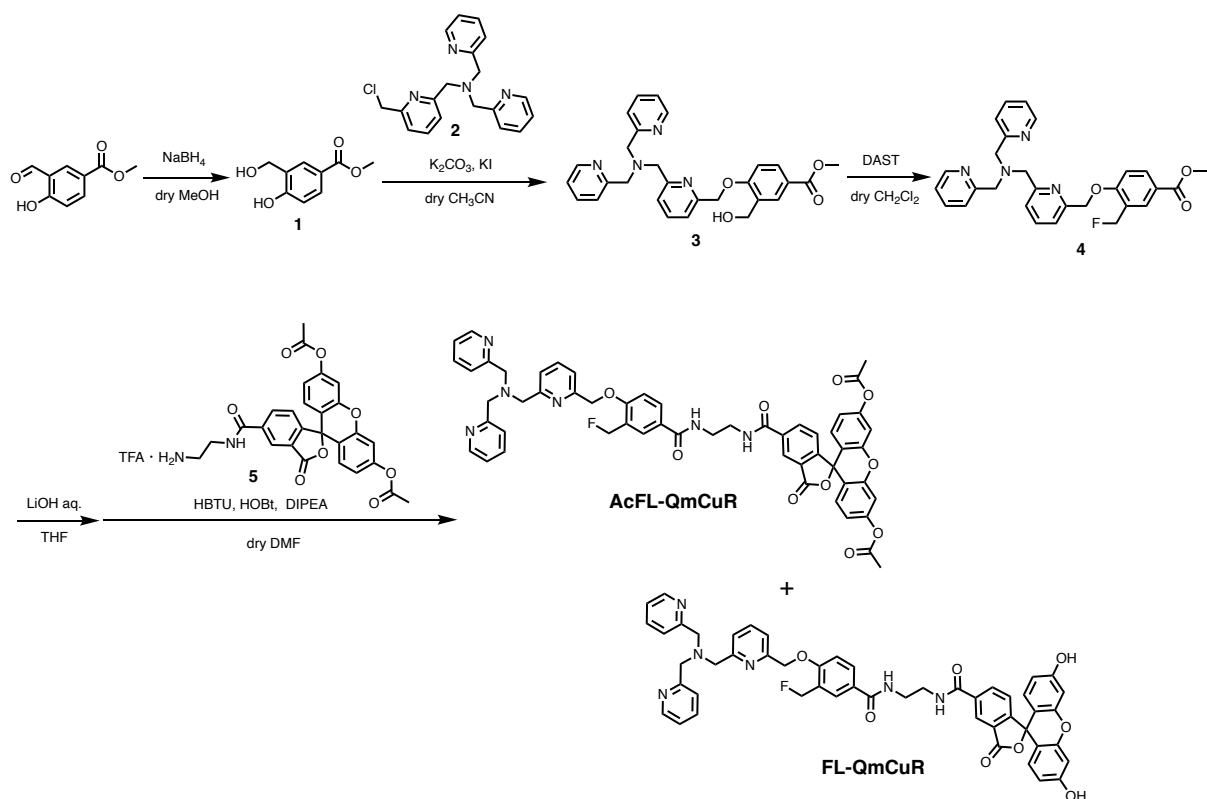
Compound AcFL-CatR

To a stirred solution of 3-hydroxytyramine hydrogen chloride (9.5 mg, 0.050 mmol) in dry DMSO (1 mL) was added fluorescein diacetate (18.0 mg, 0.039 mmol), HBTU (24.8 mg, 0.065 mmol),

HOBt · H₂O (11.8 mg, 0.077 mmol), and DIEA (21 μL, 0.121 mmol). The mixture was stirred overnight at room temperature. After the reaction was confirmed completed, the solution was concentrated under reduced pressure. The crude product was dissolved in CHCl₃ and purified by Isolera (gradient was automatically generated based on TLC information; Solvent: CHCl₃-MeOH), but the purity of the collected product was not good. So, it was further purified by RP-HPLC (C18 column; A: B = 25:75→70:30 (45 min)) to yield compound AcFL-CatR (16 mg, 0.027 mmol, yield: 69 %) as white solids. ¹H-NMR (400 MHz, CDCl₃) δ/ppm 8.197 (s, 1H), 8.085 (d, 1H, *J* = 9.6 Hz), 7.111 (s, 2H), 6.995 (s, 1H), 6.857-6.772 (m, 11H), 6.69 (dd, 2H, *J* = 2.4 Hz, *J* = 8.0 Hz), 3.718 (q, 2H, *J* = 6.4 Hz), 2.860 (t, 2H, *J* = 6.0 Hz) 2.320 (s, 6H). ESI-MS: For [M+Na]⁺ calcd. 618.1371, obsd. 618.1379.



Scheme 2 Synthetic scheme of AcFL-CatR.



Scheme 3 Synthetic scheme of **AcFL-QmCuR** and **FL-QmCuR**.

Compound 1

To a solution of methyl 3-formyl-4-hydroxybenzoate (500 mg, 2.78 mmol, 1.0 Eq) in super dehydrated MeOH (10 mL) was added NaBH₄ (0.161 g, 4.24 mmol, 1.5 eq.) in several portions (portions over 3 min) at 0 °C under Ar atmosphere. The reaction mixture was stirred at room temperature for 1 h and concentrated. The residue was suspended in EtOAc (50 mL) and washed with a saturated aqueous solution of NH₄Cl (2 × 15 mL), water (15 mL), then brine (15 mL). Then the organic part was dried over Na₂SO₄, filtrated, and concentrated to give compound **1** (344 mg, 1.89 mmol, yield: 68%) as a white solid. ¹H-NMR (400 MHz, CD₃OD/CDCl₃): δ/ppm 7.93 (d, *J* = 2.0 Hz, 1H), 7.82 (dd, *J* = 8.4, 2.4 Hz, 1H), 6.82 (d, *J* = 8.0 Hz, 1H), 4.71 (s, 2H), 3.86 (s, 3H).

Compound 3

To a solution of compound **2**³⁷ (477 mg, 1.41 mmol, 1.0 Eq) in super dehydrated CH₃CN (15 mL) was added with compound **1** (293 mg, 1.61 mmol, 1.1 Eq), dry crushed K₂CO₃ (583 mg, 4.23 mmol, 3.0 Eq), and KI (55 mg, 0.33 mmol, 0.2 Eq) under Ar atmosphere. The reaction mixture

was refluxed overnight. After cooling down to room temperature, the residue was filtered, concentrated, and purified by Isolera (Sfar HC Duo 25 g, (MeOH +0.05 % NH₃·H₂O)/ CHCl₃: 0% =>5% => 20%) to give compound **3** (590 mg, 1.21 mmol, yield 86 %) as sticky yellow oil-like solids. **¹H-NMR** (400 MHz, CDCl₃): 8.53 (d, *J* = 3.6 Hz, 2H), 8.02 (d, *J* = 1.6 Hz, 1H), 7.95 (dd, *J* = 8.4, 2.4 Hz, 1H), 7.70–7.62 (m, 3H), 7.56–7.52 (m, 3H), 7.25 (s, 1H), 7.14 (td, *J* = 6.0, 1.2 Hz, 2H), 6.96 (d, *J* = 8.8 Hz, 1H), 5.28 (s, 2H), 4.79 (s, 2 H), 3.92 (s, 2H), 3.88 (s, 3H), 3.87 (s, 4H). **ESI-MS**: cald. For [M+H]⁺ as 485.2183, obsd. 485.2182.

Compound 4

To compound **3** (6 mg, 12.4 μmol, 1.0 Eq) in super dehydrated CH₂Cl₂ (0.5 mL) was slowly added diethylaminosulfur trifluoride (10 μL, 74.4 μmol, 6.0 Eq) at 0 °C under Ar atmosphere. The reaction mixture was stirred at 0 °C for 20 min, then warmed to room temperature and stirred overnight. After quenching the reaction with ddH₂O (10 mL), the solution was extracted with CH₂Cl₂ (15 mL × 2). The organic parts were collected, washed once with brine (15 mL), dried over Na₂SO₄, filtrated, and concentrated. The residue was purified by column chromatography on silica gel (CHCl₃/ MeOH/ NH₃·H₂O: 35/1/0.1) to give compound **4** (3 mg, 6.2 μmol, yield: 50 %) as pale-yellow solids. **¹H-NMR** (400 MHz, CDCl₃): δ/ppm 8.54 (d, *J* = 4.4 Hz, 2H), 8.09 (s, 1H), 8.00 (d, *J* = 8.8 Hz, 1H), 7.72–7.64 (m, 3H), 7.58–7.52 (m, 3H), 7.33 (d, *J* = 7.6 Hz, 1H), 7.16–7.13 (m, 2H), 6.97 (d, *J* = 8.8 Hz, 1H), 5.54 (d, *J* = 47.6 Hz, 2H), 5.27 (s, 2H), 3.92 (s, 3H), 3.89 (s, 4H), 3.88 (d, 2H). **ESI-MS**: cald. For [M+Na]⁺ as 509.1959, obsd. 509.1959.

AcFL-QmCuR and FL-QmCuR

To a solution of compound **4** (37.4 mg, 76.9 μmol, 1.0 Eq) in THF (2 mL) was added dropwise 1M LiOH aq. (461 μL, 461 μmol, 6.0 Eq) at 0 °C. The reaction mixture was stirred at 0 °C for 5 min, then warmed to room temperature and stirred for 3 days. The mixture was neutralized with 1 M HCl until pH reached ~6 and extracted with CHCl₃/MeOH (2/1; 3 mL) The organic layer was concentrated and dried in vacuo to give the desired hydrolyzed product, which was used for the next reaction without further purification. To a solution of the hydrolyzed product (29.5 mg, 35.6 μmol, 1.0 Eq) in super dehydrated DMF (1 mL) was added HOBt (12.6 mg, 82.3 μmol, 2.3 Eq), HBTU (32.0 mg, 84.4 μmol, 2.4 Eq), compound **5**¹⁷ (25.4 mg, 38.0 μmol, 1.1 Eq), and DIPEA (33.4 μL, 192 μmol, 5.4 Eq). The mixture was stirred at room temperature for 14 h. After removing

the solvent via evaporation, the residue was diluted with CH₃CN/H₂O/DMF (5/5/1; 2.2 mL), filtered with 0.45 µm syringe filter, and purified by RP-HPLC (A: B = 20/80 => 70/30 (50 min)). The fractions that contain target compounds were collected respectively and freeze-dried overnight to give **AcFL-QmCuR** (2.6 mg, 2.7 µmol, 7.6%) as pale-yellow solids and **FL-QmCuR** (2.15 mg, 2.5 µmol, 7%) as orange solids.

AcFL-QmCuR: ¹H-NMR (400 MHz, CDOD₃): δ/ppm 8.61 (d, *J* = 4.4 Hz, 2H), 8.40 (d, *J* = 1.2 Hz, 1H), 8.17 (dd, *J* = 8.8, 1.6 Hz, 1H), 7.93 (d, *J* = 1.6 Hz, 1H), 7.91–7.89 (m, 2 H), 7.87–7.81 (m, 2H), 7.52–7.43 (m, 5H), 7.32 (dd, *J* = 7.6, 2.4 Hz, 2H), 7.20 (d, *J* = 2.0 Hz, 2H), 7.12 (d, *J* = 8.8 Hz, 1H), 6.90–6.82 (m, 4H), 5.49 (d, *J* = 47.6 Hz, 2H), 5.31 (s, 2H), 4.48 (s, 4H), 4.40 (s, 2H), 3.66 (s, 4H), 2.29 (s, 6H). **ESI-MS**: cald. For [M+Na]⁺ as 979.3073, obsd. 979.3098.

FL-QmCuR: ¹H-NMR (400 MHz, CD₃OD): δ/ppm 8.62 (d, *J* = 5.6 Hz, 2H), 8.36 (s, 1H), 8.16 (dd, *J* = 8.0, 1.6 Hz, 1H), 7.94 (d, *J* = 1.6 Hz, 1H), 7.92–7.90 (m, 2H), 7.85–7.79 (m, 2H), 7.52–7.44 (m, 5H), 7.32 (d, *J* = 6.8 Hz, 1H), 7.26 (d, *J* = 8.0 Hz, 1H), 7.12 (d, *J* = 8.8 Hz, 1H), 6.69 (d, *J* = 1.6 Hz, 2H), 6.56–6.50 (m, 4H), 5.50 (d, *J* = 48.0 Hz, 2H), 5.31 (s, 2H), 4.48 (s, 4H), 4.40 (s, 2H). 3.66 (s, 4H). **ESI-MS**: cald. For [M+Na]⁺ as 895.2862, obsd. 895.2882.

Other compounds introduced and analyzed in this chapter

Compounds DiaR-TMR and DiaR-AcFL (The TMR and AcFL fluorophore tags-appended DiaR) were synthesized and provided by Dr. Yuki Nishikawa. And compounds TCatR-Dc and TCatR-AcFL (The DC and AcFL fluorophore tags-appended TCatR) were synthesized and provided by Assistant Prof. Hao Zhu.

Reference

- 1 Kim, B.-E. *et al.* Mechanisms for copper acquisition, distribution and regulation. *Nat Chem Biol* **4**, 176-185 (2008). <https://doi.org:10.1038/nchembio.72>
- 2 Festa, R. A. & Thiele, D. J. Copper: an essential metal in biology. *Curr Biol* **21**, R877-883 (2011). <https://doi.org:10.1016/j.cub.2011.09.040>
- 3 Tsang, T., Davis, C. I. & Brady, D. C. Copper biology. *Current Biology* **31**, R421-R427 (2021). <https://doi.org:10.1016/j.cub.2021.03.054>
- 4 Ackerman, C. M., Lee, S. & Chang, C. J. Analytical Methods for Imaging Metals in Biology: From Transition Metal Metabolism to Transition Metal Signaling. *Analytical Chemistry* **89**, 22-41 (2017). <https://doi.org:10.1021/acs.analchem.6b04631>
- 5 Banci, L. *et al.* Affinity gradients drive copper to cellular destinations. *Nature* **465**, 645-648 (2010). <https://doi.org:10.1038/nature09018>

- 6 Grubman, A. & White, A. R. Copper as a key regulator of cell signalling pathways. *Expert Rev Mol Med* **16**, e11 (2014). <https://doi.org:10.1017/erm.2014.11>
- 7 Rae, T. D., Schmidt, P. J., Pufahl, R. A., Culotta, V. C. & O'Halloran, T. V. Undetectable intracellular free copper: The requirement of a copper chaperone for superoxide dismutase. *Science* **284**, 805-808 (1999). <https://doi.org:10.1126/science.284.5415.805>
- 8 Jomova, K. & Valko, M. Advances in metal-induced oxidative stress and human disease. *Toxicology* **283**, 65-87 (2011). <https://doi.org:10.1016/j.tox.2011.03.001>
- 9 Speisky, H. *et al.* Generation of superoxide radicals by copper-glutathione complexes: redox-consequences associated with their interaction with reduced glutathione. *Bioorg Med Chem* **17**, 1803-1810 (2009). <https://doi.org:10.1016/j.bmc.2009.01.069>
- 10 Tsvetkov, P. *et al.* Copper induces cell death by targeting lipoylated TCA cycle proteins. *Science* **375**, 1254-1261 (2022). <https://doi.org:10.1126/science.abf0529>
- 11 Ge, E. J. *et al.* Connecting copper and cancer: from transition metal signalling to metalloplasia. *Nature Reviews Cancer* **22**, 102-113 (2022). <https://doi.org:10.1038/s41568-021-00417-2>
- 12 Czlonkowska, A. *et al.* Wilson disease. *Nat Rev Dis Primers* **4**, 21 (2018). <https://doi.org:10.1038/s41572-018-0018-3>
- 13 Kaler, S. G. ATP7A-related copper transport diseases-emerging concepts and future trends. *Nat Rev Neurol* **7**, 15-29 (2011). <https://doi.org:10.1038/nrneurol.2010.180>
- 14 Lee, S. *et al.* Activity-Based Sensing with a Metal-Directed Acyl Imidazole Strategy Reveals Cell Type-Dependent Pools of Labile Brain Copper. *J Am Chem Soc* **142**, 14993-15003 (2020). <https://doi.org:10.1021/jacs.0c05727>
- 15 Pezacki, A. T. *et al.* Oxidation state-specific fluorescent copper sensors reveal oncogene-driven redox changes that regulate labile copper(II) pools. *Proc Natl Acad Sci U S A* **119**, e2202736119 (2022). <https://doi.org:10.1073/pnas.2202736119>
- 16 Miki, T. *et al.* A conditional proteomics approach to identify proteins involved in zinc homeostasis. *Nat Methods* **13**, 931-937 (2016). <https://doi.org:10.1038/nmeth.3998>
- 17 Zhu, H. *et al.* Imaging and Profiling of Proteins under Oxidative Conditions in Cells and Tissues by Hydrogen-Peroxide-Responsive Labeling. *Journal of the American Chemical Society* **142**, 15711-15721 (2020). <https://doi.org:10.1021/jacs.0c02547>
- 18 Noguchi, K. *et al.* β -Galactosidase-Catalyzed Fluorescent Reporter Labeling of Living Cells for Sensitive Detection of Cell Surface Antigens. *Bioconjugate Chemistry* **31**, 1740-1744 (2020). <https://doi.org:10.1021/acs.bioconjchem.0c00180>
- 19 Falcone, E. *et al.* Extracellular Cu²⁺ pools and their detection: From current knowledge to next-generation probes. *Coordination Chemistry Reviews* **433** (2021). <https://doi.org:10.1016/j.ccr.2020.213727>
- 20 Gillingham, D. & Fei, N. Catalytic X-H insertion reactions based on carbenoids. *Chemical Society Reviews* **42**, 4918 (2013). <https://doi.org:10.1039/c3cs35496b>
- 21 Chen, Z., Popp, B. V., Bovet, C. L. & Ball, Z. T. Site-specific protein modification with a dirhodium metallopeptide catalyst. *Acs Chem Biol* **6**, 920-925 (2011). <https://doi.org:10.1021/cb2001523>
- 22 Sugumaran, M. Reactivities of Quinone Methides versus o-Quinones in Catecholamine Metabolism and Eumelanin Biosynthesis. *Int. J. Mol. Sci.* **17**, 1576 (2016). <https://doi.org:10.3390/ijms17091576>

- 23 Balla, J., Kiss, T. & Jameson, R. F. Copper(I)-Catalyzed Oxidation of Catechol by Molecular-Oxygen in Aqueous-Solution. *Inorganic Chemistry* **31**, 58-62 (1992). <https://doi.org/DOI 10.1021/ic00027a012>
- 24 Li, Y., Jongberg, S., Andersen, M. L., Davies, M. J. & Lund, M. N. Quinone-induced protein modifications: Kinetic preference for reaction of 1,2-benzoquinones with thiol groups in proteins. *Free Radic Biol Med* **97**, 148-157 (2016). <https://doi.org/10.1016/j.freeradbiomed.2016.05.019>
- 25 Fischer, L., Steffens, R. C., Paul, T. J. & Hartmann, L. Catechol-functionalized sequence-defined glycomacromolecules as covalent inhibitors of bacterial adhesion. *Polymer Chemistry* **11**, 6091-6096 (2020). <https://doi.org:10.1039/d0py00975j>
- 26 Chen, S. H. & Li, C. W. Detection and Characterization of Catechol Quinone-Derived Protein Adducts Using Biomolecular Mass Spectrometry. *Front Chem* **7**, 571 (2019). <https://doi.org:10.3389/fchem.2019.00571>
- 27 Weigert Munoz, A., Meighen-Berger, K. M., Hacker, S. M., Feige, M. J. & Sieber, S. A. A chemical probe unravels the reactive proteome of health-associated catechols. *Chem Sci* **14**, 8635-8643 (2023). <https://doi.org:10.1039/d3sc00888f>
- 28 Taki, M., Iyoshi, S., Ojida, A., Hamachi, I. & Yamamoto, Y. Development of highly sensitive fluorescent probes for detection of intracellular copper(I) in living systems. *J Am Chem Soc* **132**, 5938-5939 (2010). <https://doi.org:10.1021/ja100714p>
- 29 Yu, K. K., Li, K., Hou, J. T. & Yu, X. Q. Coumarin-TPA derivative: a reaction-based ratiometric fluorescent probe for Cu(I). *Tetrahedron Letters* **54**, 5771-5774 (2013). <https://doi.org:10.1016/j.tetlet.2013.08.046>
- 30 Guo, F., Qin, S., Liu, Z., Chen, P. R. & Fan, X. Decaging-to-labeling: Development and investigation of quinone methide warhead for protein labeling. *Bioorg Chem* **143**, 107088 (2024). <https://doi.org:10.1016/j.bioorg.2023.107088>
- 31 Zlatic, K. *et al.* Labeling of Proteins by BODIPY-Quinone Methides Utilizing Anti-Kasha Photochemistry. *ACS Appl Mater Interfaces* **12**, 347-351 (2020). <https://doi.org:10.1021/acsami.9b19472>
- 32 Smith, R. M. & Martell, A. E. *Critical Stability Constants*. (1989).
- 33 Ambundo, E. A. *et al.* Influence of coordination geometry upon copper(II/I) redox potentials. Physical parameters for twelve copper tripodal ligand complexes. *Inorganic Chemistry* **38**, 4233-4242 (1999). <https://doi.org:DOI 10.1021/ic990334t>
- 34 Ren, F. *et al.* X-ray structures of the high-affinity copper transporter Ctr1. *Nat Commun* **10**, 1386 (2019). <https://doi.org:10.1038/s41467-019-09376-7>
- 35 Petris, M. J., Smith, K., Lee, J. & Thiele, D. J. Copper-stimulated endocytosis and degradation of the human copper transporter, hCtr1. *J Biol Chem* **278**, 9639-9646 (2003). <https://doi.org:10.1074/jbc.M209455200>
- 36 Wakayama, S. *et al.* Chemical labelling for visualizing native AMPA receptors in live neurons. *Nat Commun* **8**, 14850 (2017). <https://doi.org:10.1038/ncomms14850>
- 37 Jia, J. *et al.* A DPA-based highly selective and sensitive fluorescent probe for mercuric ions and its imaging in living cells. *Dalton Trans* **45**, 9402-9406 (2016). <https://doi.org:10.1039/c6dt01258b>

Chapter 2

Development of cuprous ion-selective quinone-methide-based chemical labeling reagent for imaging and proteome profiling in living cells

Abstract

Copper is an essential trace element that plays a crucial role in various biological processes. It acts as a cofactor for enzymes and is involved in regulating signal transduction. Synthetic fluorescent probes have been developed to detect and visualize labile copper ions in living cells. Covalent protein bioconjugation is another method used to study biological molecules and bio-metal ions through protein labeling, offering advantages over conventional chemosensors. In Chapter 1, four copper ion-responsive tools are introduced, with the TPA-cage-masked quinone methide-based protein labeling reagent (QmCuR) standing out as the most promising due to its high selectivity for Cu^+ and its applicability in detecting Cu^+ in various live cell models. However, its limited response to intracellular Cu^+ suggests a suboptimal chemical structural design and the Cu^+ -responsive reaction mechanisms remain to be elucidated. In this chapter, I focused on developing and synthesizing various copper ion-ligand-appended quinone methide-based reagents to optimize their chemical structures. Through *in vitro* and in-live cell assessments and comparisons of the Cu^+ -responsive protein labeling capabilities of these reagents, I have identified the most effective reagent and elucidated the Cu^+ -responsive reaction mechanisms of the quinone methide-based reagent. The results also demonstrate the remarkable selectivity of the optimal reagent for Cu^+ over other bio-metal ions and ROS, as well as its superior Cu^+ -responsive efficacy both *in vitro* and in live cells compared to the QmCuR developed in Chapter 1.

Introduction

Copper is an essential trace element that is integral to various biological processes. Its redox-active properties, which involve the interconversion of Cu^+ and Cu^{2+} , enable it to act as a cofactor for metalloenzymes that participate in diverse biological functions.^{1,2,3} In addition to the copper ions that are tightly bound to proteins, recent studies have uncovered the existence of loosely bound, labile copper ions, which play a role in regulating signal transduction by reversibly binding to protein targets and influencing their activities and structural characteristics.^{4,5,6} In the reductive intracellular environment, cuprous ions are the primary redox species.⁷ Synthetic fluorescent probes capable of detecting and visualizing labile cuprous ions in living systems are valuable tools for investigating the cellular regulation of labile copper ions and associated biological functions.^{8,9,10,11,12} Several cuprous ion-selective chemosensors have been developed to monitor the dynamic changes in cuprous ions in live cells.^{11,12} Most of these chemosensors are designed to link the fluorophore to a copper-specific chelator, which undergoes reversible or irreversible changes in its spectral properties upon binding to copper. However, traditional target-selective fluorescent chemosensors have limitations due to their low spatial-temporal resolution caused by probe diffusion and mobile recognition signals.

The covalent protein bioconjugation strategy, designed in response to specific target signaling molecules, has emerged as a valuable and increasingly popular tool for studying biological molecules and bio-metal ions through protein labeling.^{13,14,15} This method offers distinct advantages over conventional target-selective chemosensors, including enhanced spatial resolution, compatibility with cell fixation, and the potential for proteomic analysis of intracellular target-rich microenvironments. Currently, two types of copper probes based on covalent protein bioconjugation have been identified: those responsive to both Cu^+ and Cu^{2+} and those selective for Cu^{2+} .^{13,14} Notably, probes that selectively respond to Cu^+ , the most prevalent oxidation state of intracellular copper ions,⁷ have not yet been reported.

Chapter 1 introduces four distinct Cu-responsive tools that have been developed, evaluated, and compared based on different chemical reactions. Among these tools, a TPA-cage-masked QM (quinone methide)-based protein labeling reagent (QmCuR) demonstrates high selectivity for Cu^+ and has been effectively utilized to respond to increased intracellular labile Cu^+ in living cells, showing promise. However, the limited response to intracellular Cu^+ indicates that the chemical

structural design may be suboptimal. Additionally, further elucidation of the Cu⁺-responsive chemical mechanisms is still needed.

In this chapter, I developed and synthesized several Cu-ligand-appended QM-based reagents to modulate Cu⁺ affinity and fine-tune reactivity for optimizing chemical structures. I conducted *in vitro* assessments and comparisons of the Cu⁺-responsive protein labeling capabilities of these reagents, ultimately identifying the most effective reagent. Additionally, I investigated the Cu⁺-responsive reaction mechanisms of these reagents *in vitro* through HPLC testing. I proceeded to explore the Cu⁺-responsive properties of the optimal reagent and applied it to living cells using CTR1-overexpressed Hela cells as a cell model. The findings indicated that the optimal reagent exhibited remarkable selectivity for Cu⁺ over other bio-metal ions and ROS, could detect elevated Cu⁺ levels under varying conditions in live cells and demonstrated superior Cu⁺-responsive efficacy both *in vitro* and in live cells compared to the QmCuR developed in Chapter 1.

Results and Discussion

Design and optimization of CuRs

I aimed to enhance and refine the design of quinone methide-based Cu⁺-responsive protein labeling reagents (CuRs). In the development of CuRs, a fluorophore tag, and a Cu⁺-binding unit were connected with a latent quinone methide (QM) precursor, which is intended to be released through Cu⁺-dependent oxidative cleavage and then reacts with nearby proteins. I developed a range of CuRs to optimize the structure (**Figure 2.1**). To enhance the recognition of Cu⁺, I employed tris[(2-pyridyl)methyl]amine (TPA) unit and 2-pyridylmethylbis(2-ethylthioethyl)amine, which have respective K_d values of 126 fM and 1 fM for Cu⁺.¹⁶ Additionally, I explored 2-fluoromethylphenol (*ortho*-QM type: O2, O3) and 4-fluoromethylphenol (*para*-QM type: P2, P3) derivatives as QM precursors to modify reactivity.^{17,18} Furthermore, I synthesized CuRs without any chelating group (O1, P1) to serve as negative control reagents.

Next, I assessed the protein labeling capabilities of CuRs *in vitro* by testing their response to Cu⁺ using purified bovine serum albumin (BSA) as a model protein. All CuRs with chelator components demonstrated enhanced protein labeling efficiency in the presence of Cu⁺, with minimal fluorescence observed in its absence (**Figure 2.2**). Control compounds O1 and P1 did not exhibit Cu⁺-responsive activation. Among the effective CuRs, TPA-based probes O2 and P2 displayed greater Cu⁺-responsive labeling efficiency compared to thioether-based probes O3 and

P3, respectively. Furthermore, *para*-QM-based CuRs (P2 and P3) exhibited a more robust Cu⁺ response than *ortho*-QM-based CuRs (O2 and O3), respectively. It was also noted that the 2-fluoromethylphenol-based compound O1 displayed intrinsic reactivity toward proteins, resulting in relatively high background labeling. Consequently, the design of P2 is deemed optimal for Cu⁺-responsive protein labeling in terms of achieving the highest efficiency.

Subsequently, I investigated the labeling reaction of CuRs in the presence and absence of Cu⁺ to clarify the labeling mechanism. Initially, I verified the Cu⁺-catalyzed oxidative cleavage of the benzyl ether^{12,19} and the subsequent generation of highly reactive QM, which covalently reacts with nucleophilic amino acids (e.g., Cys, Lys, and His),²⁰ using high-performance liquid chromatography (HPLC). As depicted in **Figure 2.3a**, the addition of Cu⁺ resulted in the consumption of P2' and the appearance of a new peak in the chromatogram. Mass spectrometry analysis revealed the product to be the cysteine adduct of QM generated by the elimination of the TPA moiety, clearly indicating the progression of the expected reaction (**Figure 2.3b, 2.3c**). The reactivity of the active Cu⁺-catalyzed product of P2' with other amino acids, including His and Lys, was also confirmed, validating the broad coverage of amino acids by the reagent (**Figure 2.3d-2.3g**). Furthermore, Cu⁺-mediated reactivity enhancement was observed for O2 (**Figure 2.4a, 2.4d**), while control compounds O1 and P1 exhibited no response to Cu⁺ (**Figure 2.4a, 2.4g, 2.4h**). Notably, O3 and P3 yielded multiple products resulting from the Cu-promoted oxidation of thioether moieties (**Figure 2.4 b-c, 2.4e-f**), suggesting that the lower Cu⁺-responsive labeling activities of O3 and P3 were likely the result of their deactivation by the Cu⁺-mediated oxidation of the thioether moiety prior to C–O bond cleavage.

Taken together, I concluded that the design of P2 is optimal for Cu⁺-responsive protein labeling in terms of the highest signal-to-noise ratio, and I continued to characterize it further.

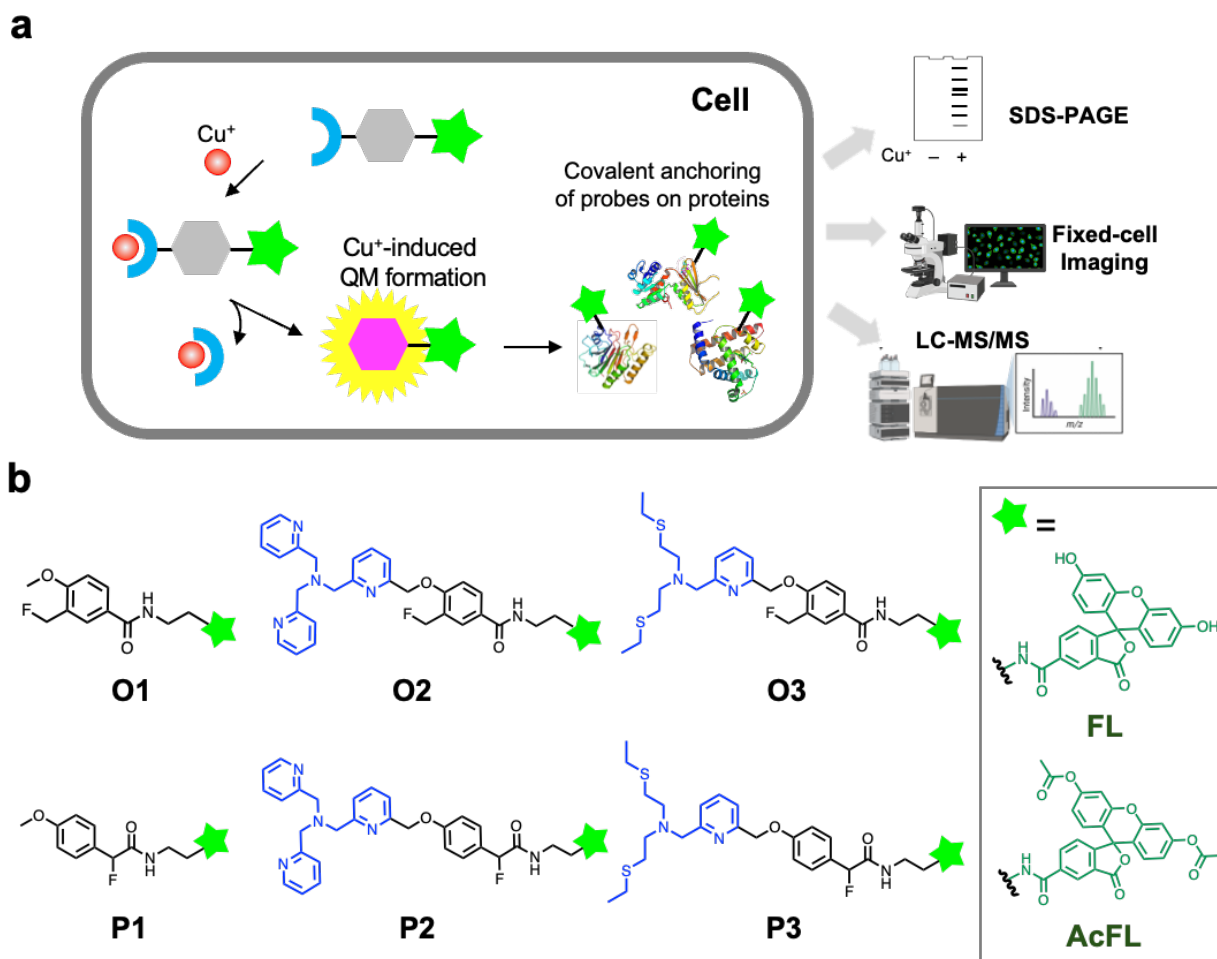


Figure 2.1 **Illustration of the strategy and the molecular design of the chemical tools.** (a) Schematic illustration of Cu^+ -responsive protein labeling in living cells. (b) Molecular structures of Cu^+ -responsive protein labeling reagents (CuRs) in this study. QM, quinone methide; FL, fluorescein; AcFL, diacetylated fluorescein; LC-MS/MS, liquid chromatography-tandem mass spectrometry. FL-appended CuRs are used for *in vitro* tests, while AcFL-appended CuRs are applied for in-live cell tests.

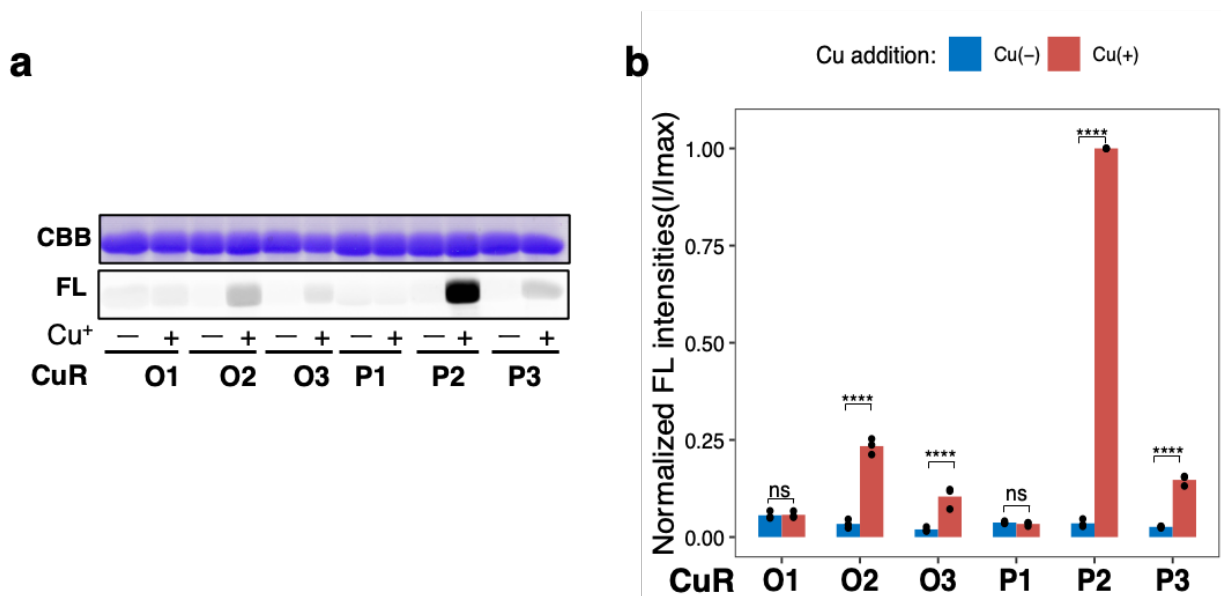


Figure 2.2 **Cu⁺-responsive protein labeling of CuRs *in vitro*.** (a) SDS-PAGE and in-gel fluorescence analysis of BSA labeling with fluorescein-tethered CuRs (FL-appended CuRs). The reagent (50 μ M) was added to 50 mM HEPES buffer (pH 7.2) containing BSA (10 μ M). The mixture was incubated at 37°C in the presence or absence of Cu⁺ (50 μ M) for 1 h. (b) Relative fluorescence intensity of proteins labeled by CuRs. $n = 3$ biological replicates. P -values in (b) were calculated using a two-way ANOVA and Tukey's test by comparing Cu⁺-treated and nontreated samples for each CuR. All values are expressed as independent dots. ns: $p > 0.05$, *: $0.01 < p \leq 0.05$, **: $0.001 < p \leq 0.01$, ***: $0.0001 < p \leq 0.001$, ****: $p \leq 0.0001$. FL, in-gel fluorescence; CBB, Coomassie brilliant blue; BSA, bovine serum albumin; CuRs, Cu⁺-responsive protein labeling reagents.

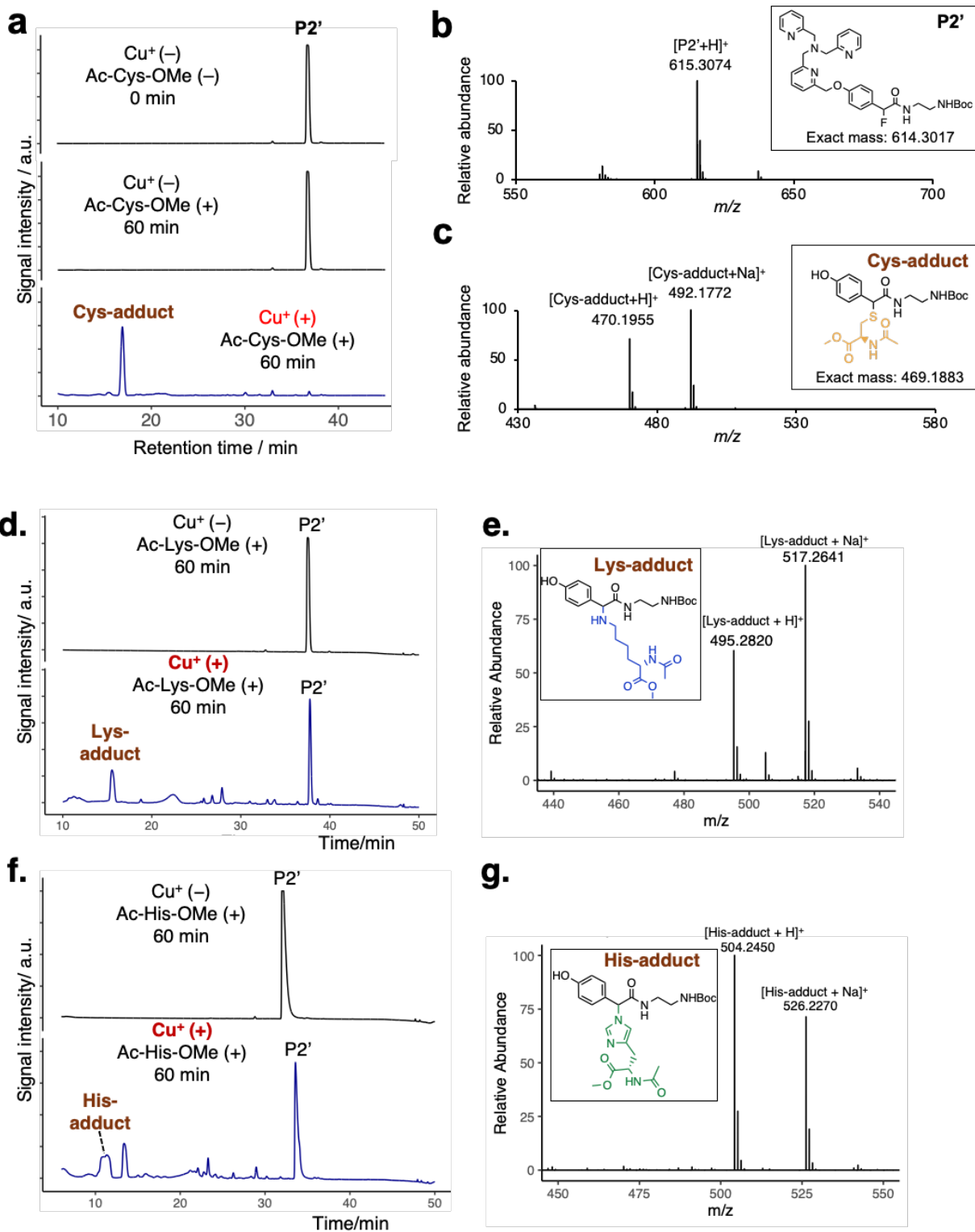


Figure 2.3 Confirmation of Cu^+ -dependent quinone methide formation and the reaction with amino acids. (a, d, f) High-performance liquid chromatography chromatograms of **P2'** (1 mM)

before (0 min) and after (60 min) treatment with Cu^+ (1 mM) and (a) Ac-Cys-OMe (5 mM), (d) Ac-Lys-OMe (5 mM), and (f) Ac-His-OMe (5 mM) in 50 mM HEPES buffer (pH 7.2)/acetonitrile 1:1 at 25°C. UV detection at 220 nm. (b, c) Mass spectra of the peaks at (b) 37 min and (c) 17 min in chromatogram (a). (e) Mass spectra of the peak at 16 min in the chromatogram (d), and (g) mass spectra of the peak at 10 min in the chromatogram (f).

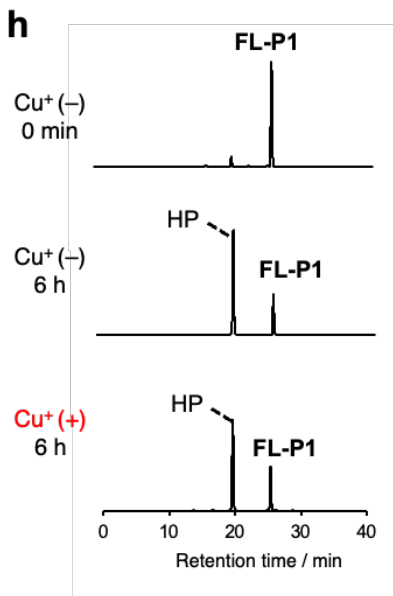
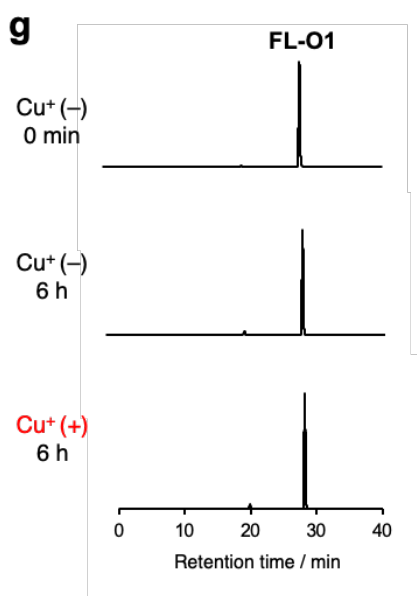
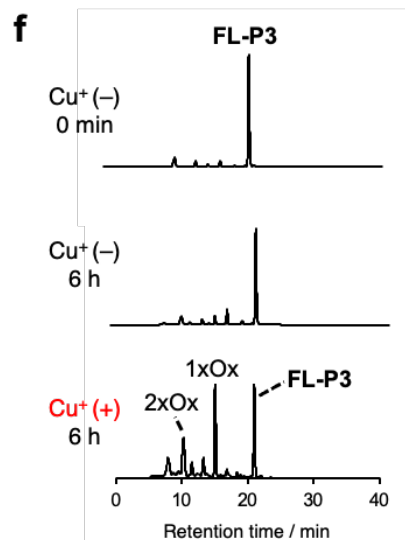
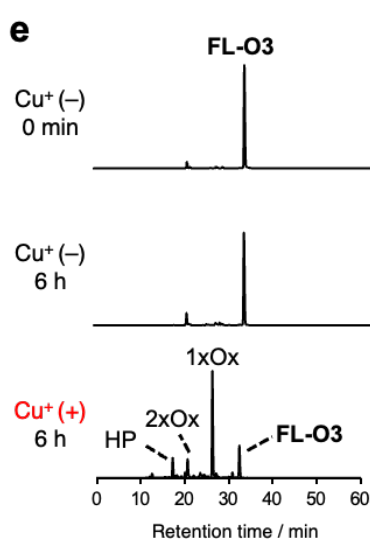
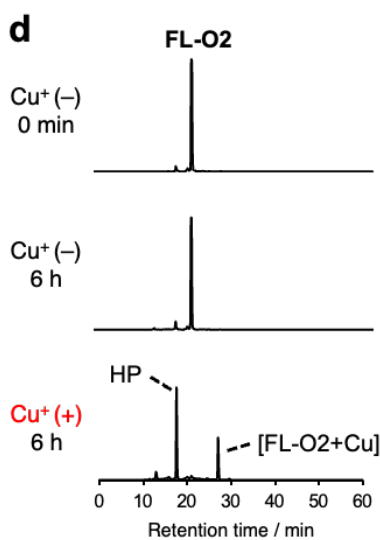
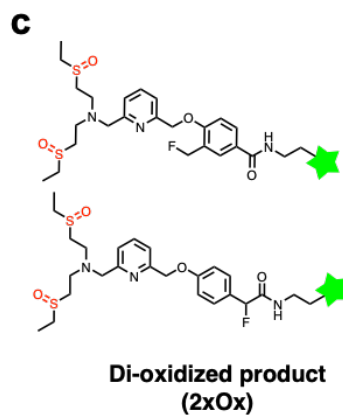
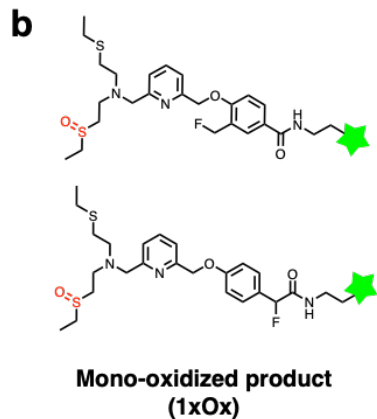
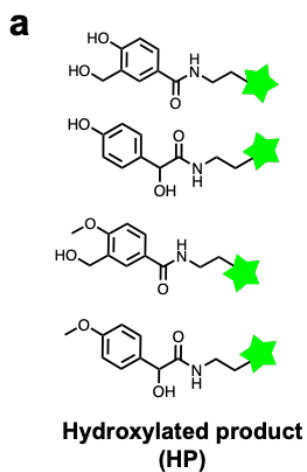


Figure 2.4 **Confirmation of Cu⁺-dependent quinone methide formation for fluorescein-appended O1, P1, O2, O3, and P3.** (a–c) Molecular structures of reaction products; (a) hydrolyzed products of *ortho*- and *para*-quinone methide or control compounds (O1 and P1). (b) Mono- and (c) di-oxidized products of O3 and P3. (d–h) HPLC analysis of reaction products of each reagent with and without the addition of Cu⁺. The reagent (50 μM) was incubated in sodium-*L*-ascorbate (100 μM)-containing 50 mM HEPES buffer (pH 7.2) in the presence or absence of Cu⁺ (50 μM) at 37 °C for 6 h. Fluorescence intensity was recorded (Ex: 490 nm/Em: 520 nm).

Evaluation of Cu⁺-responsive properties of the optimal CuR in vitro

I then investigated the selectivity of P2 (FL-appended P2) towards Cu⁺ over other biometals. As depicted in **Figure 2.5a**, P2 demonstrated the highest selectivity for Cu⁺ among all tested metal ions, including Cu²⁺, Zn²⁺, and redox-active Fe²⁺/Fe³⁺. Additionally, I verified that P2 is more effectively activated by Cu⁺ than a variety of ROS (**Figure 2.5b**). The reduced sensitivity towards ROS is crucial for the specific detection of Cu⁺ in cells, as intracellular copper accumulation often leads to generating various ROS. Notably, the Cu⁺-dependent protein labeling by P2 proceeded even in the presence of 5–10 mM glutathione, an abundant chelator of intracellular Cu⁺, indicating its applicability in a cellular context (**Figure 2.5e**). Furthermore, the Cu⁺-responsive protein labeling of P2 occurs rapidly in 10 min (**Figure 2.5c, 2.5d**) and exhibits a Cu⁺-concentration-dependent manner (**Figure 2.5f**).

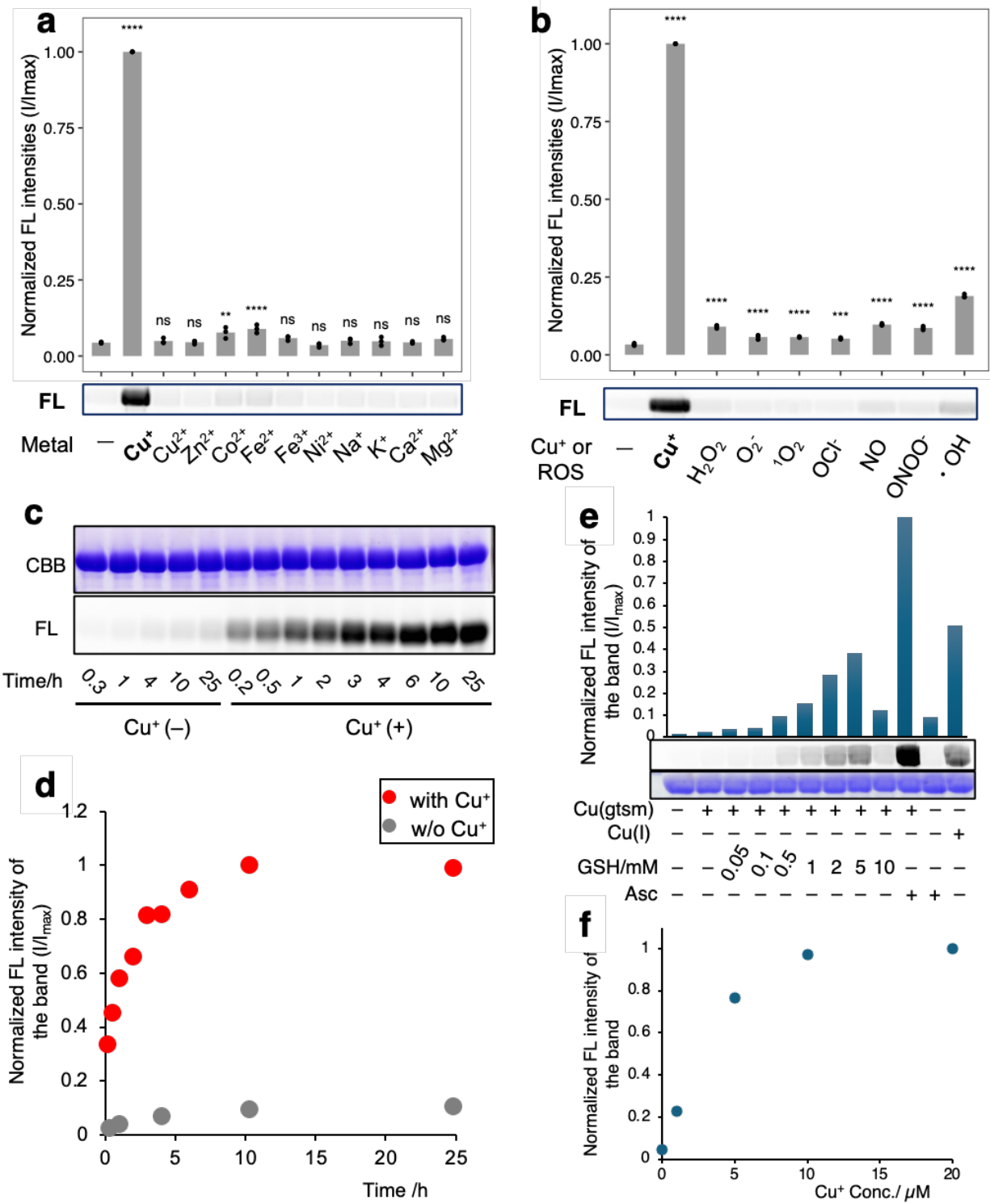


Figure 2.5 **Cu⁺-responsive protein labeling of P2 *in vitro*.** (a,b) Selectivity of P2 for several (a) metal ions and (b) ROS. A mixture of FL-appended P2 (50 μM) and BSA (10 μM) in 50 mM

HEPES buffer (pH 7.2) was incubated at 37°C for 1 h in the presence of various metal ions (50 μ M for Cu⁺, Cu²⁺, Zn²⁺, Co²⁺, Fe²⁺, Fe³⁺, and Ni²⁺, and 5 mM for Na⁺, K⁺, Ca²⁺, and Mg²⁺) or ROS/ROS generating reagent (50 μ M). $n = 3$ biological replicates. P -values in (a) and (b) were calculated using a one-way ANOVA and Dunnett's test by comparing metal or ROS-added samples to non-treated control. All values are expressed as independent dots. ns: $p > 0.05$, *: $0.01 < p \leq 0.05$, **: $0.001 < p \leq 0.01$, ***: $0.0001 < p \leq 0.001$, ****: $p \leq 0.0001$. (c) SDS-PAGE and in-gel fluorescence analysis and (d) quantitative analysis of the time course of BSA labeling with P2 in the presence or absence of Cu⁺. A mixture of P2 (50 μ M) and BSA (10 μ M) in 50 mM HEPES buffer (pH 7.2) was incubated at 37°C with and without Cu⁺ (50 μ M) for varying time. (e) Cu⁺-dependent BSA labeling with P2 in the presence of glutathione (GSH). A mixture of P2 (50 μ M) and BSA (10 μ M) in 50 mM HEPES buffer (pH 7.2) was incubated at 37°C with Cu(gtsm) or Cu(MeCN)₄PF₆ (50 μ M) and varying concentrations of GSH (0.05–10 mM) or Sodium-*L*-ascorbate (100 μ M) for 1 h. (f) Quantitative analysis of the Cu⁺-concentration dependencies of protein labeling by P2. A mixture of P2 (50 μ M) and BSA (10 μ M) in 50 mM HEPES buffer (pH 7.2) with varying concentrations of Cu⁺ in the presence of sodium-*L*-ascorbate (100 μ M) at 37°C for 1 h. Cu(gtsm), Glyoxal-bis(N(4)-methylthiosemicarbazonato)-copper(II).

Application of CuR in the living cells

Subsequently, I conducted experiments to determine whether the Cu⁺-responsive protein labeling reagent could effectively detect changes in labile Cu⁺ levels within cells. For applications involving live cells, I substituted the reporter moiety of FL-appended P2 with diacetyl fluorescein (AcFL) to enhance cell-membrane permeability (**Figure 2.1**; AcFL-appended P2). As anticipated, the reagent was promptly absorbed by living cells, emitted fluorescence upon the removal of the acetyl group by endogenous esterases, and was evenly distributed throughout the entire cell, thereby rendering it suitable for unbiased protein labeling and Cu⁺ detection in living cells (**Figure 2.6a**). To illustrate the responsiveness to Cu⁺, I employed HeLa cells that were transiently transfected with copper transporter 1 (CTR1)-expression plasmid and pretreated the cells with CuCl₂, followed by labeling with P2. In-gel fluorescence analysis revealed the labeling of numerous proteins in the CTR1-overexpressed cells treated with exogenous copper, while the corresponding bands were not observed in the gel when either CTR1-overexpression or copper supplementation was omitted (**Figure 2.6b**). Furthermore, treating the CTR1-overexpressed cells

with N-methylmaleimide (N-MEM), a thiol alkylation reagent,^{21,22,23,24} released copper ions that are bound to proteins or other intracellular Cu-buffering substances (**Figure 2.7**),^{25,26,27,28} resulting in a significant increase in protein labeling by P2 as indicated by western-blotting results (**Figure 2.6b**), suggesting that the majority of the copper ions transported by overexpressed CTR1 are bound to thiol groups of intracellular metal-buffering substances, such as glutathione and metallothionein. Confocal laser scanning microscopy (CLSM) demonstrated strong fluorescent signals derived from the fluorescein-labeled proteins in CTR1-overexpressing cells upon N-MEM treatment (**Figure 2.6c**). All these findings unequivocally establish that P2 is activated and modifies intracellular proteins in response to the accumulation of labile Cu⁺ transported into the cell by overexpressed CTR1. In contrast, the control compound P1 showed no Cu⁺ response (**Figure 2.8a**). The thioether ligand-appended P3 did not exhibit increased protein labeling in response to elevated intracellular Cu⁺ levels, whether due to increased Cu⁺-import by overexpressed CTR1 or increased labile Cu⁺ release upon N-MEM treatment (**Figure 2.8b**). This suggests that the application of P3 in live cells is ineffective. It is likely that intracellular oxidation of the thioether hindered the desired Cu⁺-catalyzed protein labeling, limiting its application in living cells. Additionally, P2 showed a higher intracellular Cu⁺ response than O2 (**Figure 2.8c**), consistent with the higher Cu⁺-responsive protein labeling efficacy of FL-appended P2 compared to FL-appended O2, as indicated by the *in vitro* test (**Figure 2.2**). Based on these results, P2 is the optimal Cu⁺-responsive protein labeling reagent among CuRs for live cell applications. It effectively responds to intracellular elevated labile Cu⁺ levels upon Cu treatment, increased Cu⁺-import by overexpressed CTR1, and released labile Cu⁺ from Cu-buffering substances.

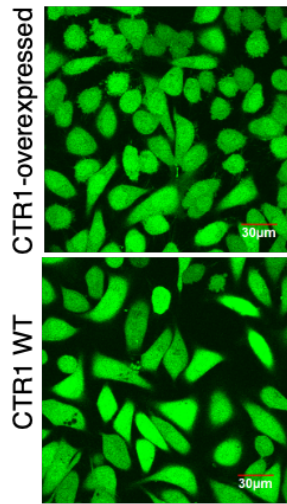
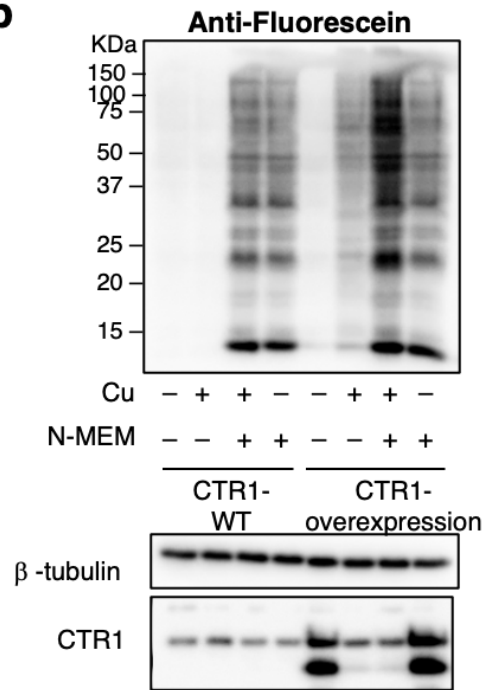
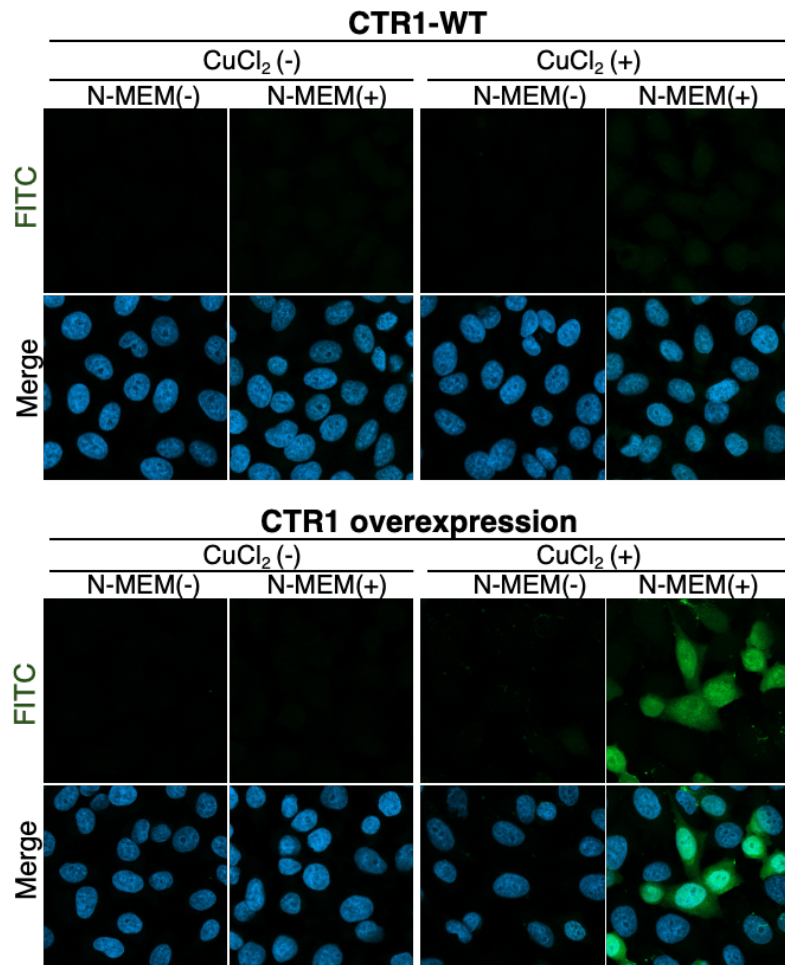
a**b****c**

Figure 2.6 Cu⁺-responsive protein labeling by P2 in live CTR1-overexpressed HeLa cells. (a) Fluorescence imaging showing the cell permeability and uniform distribution of AcFL-appended P2 in both CTR1-WT and CTR1-overexpressed live HeLa cells. (b) Western blotting analysis, and (c) CLSM imaging analysis of protein labeling by P2 in live CTR1-WT and CTR1-overexpressed HeLa cells. HeLa cells transfected with a CTR1-expression plasmid were pretreated with CuCl₂ (5 μM) for 8.5 h, then incubated with P2 (5 μM) for 25 min, followed by N-MEM treatment for 10 min. Note that the expression level of CTR1 in copper-treated transfected cells decreased due to the negative feedback of CTR1 in response to intracellular copper accumulation.²⁹ Also, note that the intensity of the excitation laser for CLSM in (c) was set low to avoid saturated fluorescent signals in the CTR1-overexpressed sample treated with both Cu and N-MEM and to ensure comparison of all samples under the same CLSM conditions. Consequently, the variances in fluorescent signals of the other seven samples were not distinguishable in (c). However, upon increasing the laser intensity, the variances of the fluorescent signals reflecting the changes in Cu⁺ levels, as indicated by Cu⁺-responsive protein labeling in these seven samples, became observable and consistent with the western blotting analyses (b) and Figure 2.7. The accompanying images were not shown. CTR1, copper transporter 1; WT, wild type; N-MEM, *N*-methylmaleimide; CLSM, confocal laser scanning microscopy; Nuclei are stained blue with DAPI solution; DAPI, 4',6-Diamidino-2-phenylindole Dihydrochloride Solution; Fluorescein fluorescence images (FITC, green); Merge: FITC images (green) were overlaid with DAPI images (blue) to give Merge images.

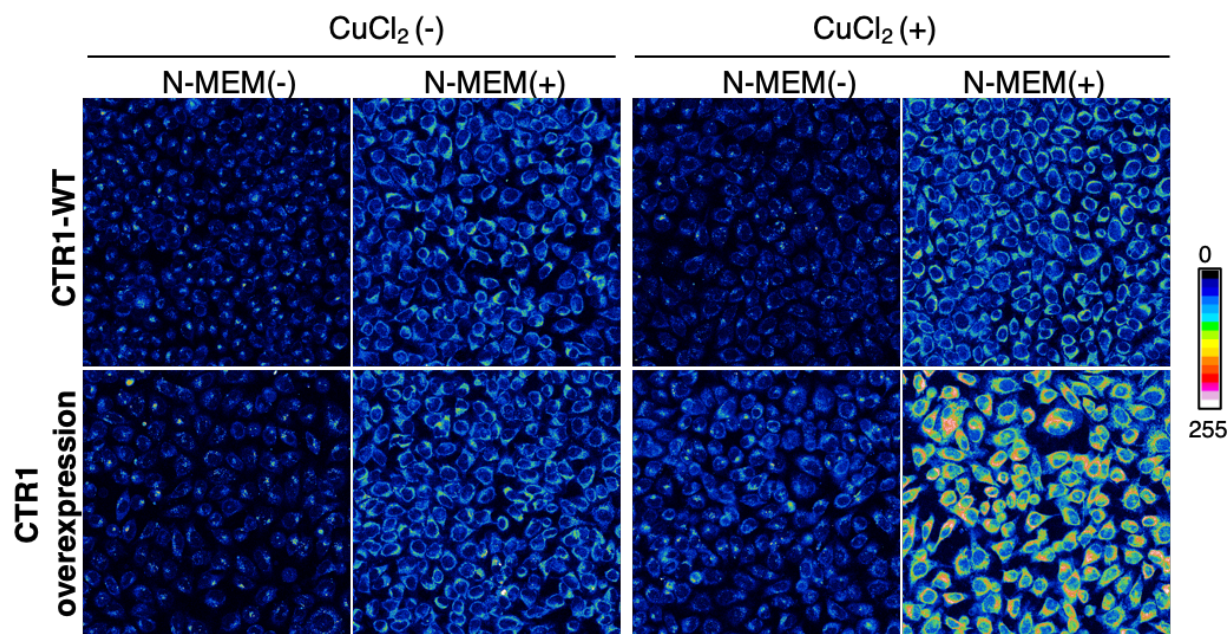


Figure 2.7 Pseudocolor imaging of fluorescent intensity of CTR1-WT and CTR1-overexpressed HeLa cells stained by CopperGREEN with and without treatment of N-MEM. The results demonstrated elevated intracellular labile Cu^+ levels following N-MEM treatment in both CTR1-WT and CTR1-overexpressed live HeLa cells. Additionally, the data indicated that Cu-supplementation and CTR1-overexpression resulted in increased intracellular labile Cu^+ in live cells. HeLa cells transfected with a CTR1-expression plasmid were pretreated with CuCl_2 ($5 \mu\text{M}$) for 8.5 h, incubated with CopperGREEN ($5 \mu\text{M}$) for 25 min, then treated with N-MEM for 10 min, followed by imaging.

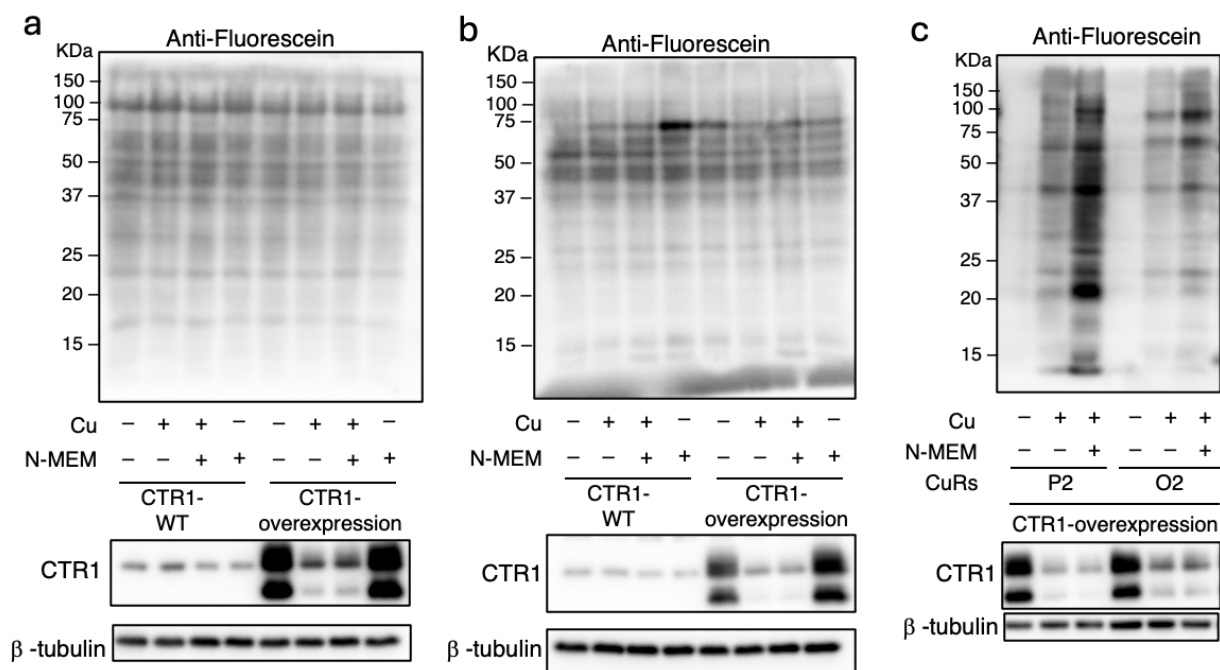


Figure 2.8 Protein labeling by P1, P3, and O2 in the CTR1-WT and CTR1-overexpressed HeLa cells. (a, b) Western blotting analysis of protein labeling by (a) AcFL-appended P1 and (b) AcFL-appended P3 in live CTR1-WT and CTR1-overexpressed HeLa cells. (c) Comparison of the protein labeling by AcFL-appended P2 and AcFL-appended O2 in live CTR1-WT and CTR1-overexpressed HeLa cells. Note that the expression level of CTR1 in copper-treated transfected cells decreased due to the negative feedback of CTR1 in response to intracellular copper accumulation.²⁹ HeLa cells transfected with a CTR1-expression plasmid were pretreated with CuCl_2 (5 μM) for 8.5 h, then incubated with 5 μM of P1, P2, P3, or O2 for 25 min, followed by N-MEM treatment for 10 min.

Conclusion

In this chapter, I have developed, synthesized, and tested multiple CuRs to investigate the most effective Cu⁺-responsive protein labeling reagent. These reagents, named O1, O2, O3, P1, P2, and P3, were designed and screened for their capabilities. All Cu⁺-ligand-appended CuRs (O2, O3, P2, and P3) demonstrated Cu⁺-responsive protein labeling abilities, while the control reagents (O1 and P1) did not exhibit any Cu⁺-responsive properties. Among these, P2 showed the most optimal Cu⁺-responsive efficacy based on both *in vitro* analysis and tests conducted in living cells. Furthermore, I confirmed that Cu⁺ catalyzes the C-O bond cleavage of P2, resulting in the formation of an active quinone methide. This active intermediate can react with multiple nucleophilic amino acids, such as Cys, Lys, and His. P2 displayed high selectivity for Cu⁺ compared to other biometal ions and reactive oxygen species (ROS). Additionally, the Cu⁺-responsive protein labeling reaction was compatible with the presence of physiological reducing agents. Moreover, P2 successfully detected intracellular elevated Cu⁺ levels in living cells when cells were Cu-supplemented, when Cu⁺ import was increased by genetic perturbation, and when there was increased labile Cu⁺ release from intracellular Cu-bound substances. In the following chapter, I focused on utilizing the optimal CuR, P2, in a genetic model of copper dysregulation induced by the knockout (KO) of ATP7A, a copper-translocating P-type ATPase that regulates copper export. This will probably allow us to explore the robustness of our tool and study Cu⁺ misregulation through imaging, protein profiling, and proteomics analysis.

Experimental section

General materials and methods for the biochemical/biological experiments

Unless otherwise noted, all proteins/enzymes and reagents were obtained from commercial suppliers (Sigma-Aldrich, Tokyo Chemical Industry (TCI), Fujifilm Wako Pure Chemical Corporation, Sasaki Chemical, Bio-Rad, Thermo Fisher Scientific, Dojindo, or Watanabe Chemical Industries) and used without further purification. SDS-polyacrylamide gel electrophoresis (SDS-PAGE) and western blotting were performed using a Bio-Rad Mini-Protean III electrophoresis apparatus. Fluorescence gel images and chemical luminescent signals using ECL Prime (Cytiva) were acquired with a FUSION FX (Vilber) equipped with a SPECTRA-Capsule BLUE (480) and a fluorescence filter (F535-Y2). Proteins were stained by Instant Blue Coomassie Protein Stain (Abcam) or Imperial Protein Stain (Thermo Fisher Scientific). Cell imaging was performed with a confocal laser scanning microscope (CLSM) (Carl Zeiss LSM800) equipped with a 20 × or a 63 × oil immersion objective lens. Reversed-phase HPLC (RP-HPLC) was carried out on a Hitachi Chromaster HPLC system equipped with a Chromaster 5410 UV detector (detection at 220 nm, 254nm, or 490 nm) and a Chromaster 5440 fluorescence detector (Ex: 490 nm/Em: 520 nm). All runs used linear gradients of acetonitrile containing 0.1% TFA (solvent A) and 0.1% aqueous TFA (solvent B) unless otherwise noted. High-resolution mass spectra were measured on an Exactive (Thermo Scientific) equipped with electron spray ionization (ESI).

HPLC tests of the Cu⁺-responsive reaction of P2'

1 mM compound 6 (P2') was dissolved in a mixing solvent of 50 mM HEPES (pH 7.2) and CH₃CN (1:1 v/v) containing 5 mM amino acid (Ac-Cys-OMe, Ac-Lys-OMe or Ac-His-OMe) and 2 mM sodium ascorbate, followed by addition of 1 mM Cu(MeCN)₄PF₆. The mixture was then vortexed at room temperature for 1 h. Then, 180 μL of the reaction mixture was mixed with 1 mL of quenching solution (CH₃CN: 200 mM EDTA aqueous solution = 2:8) to prepare the samples for HPLC loading. Then 1mL of the mixtures were subjected to RP-HPLC analyses (column; YMC-pack ODS-A or 5C₁₈-AR-II, 250 × 4.6 mm; mobile phase, CH₃CN /10 mM CH₃COONH₄ = 20/80 to 60/40 (linear gradient over 40 min); flow rate, 1.0 mL/min). The eluates were then collected and identified by HR-ESI MS.

HPLC test of the reactions of fluorescein-appended CuRs

50 μM CuR (FL-appended type) was dissolved in 50 mM HEPES (pH 7.2) buffer containing 100 μM sodium ascorbate, followed by the addition of 50 μM $\text{Cu}(\text{MeCN})_4\text{PF}_6$. The mixture was then incubated at 37°C. At each time point, 80 μL of the reacting mixture was taken and mixed with 1 mL of mobile solvents (CH_3CN (0.1 % TFA)/ H_2O (0.1 % TFA) = 20/80 or 30/70). Then 1 mL of the mixture was subjected to RP-HPLC (column; YMC-pack ODS-A, 250 \times 4.6 mm; CH_3CN (0.1 % TFA)/ H_2O (0.1 % TFA) = 20/80 to 50/50 (linear gradient over 30 min) or 30/70 to 60/40 (linear gradient over 30 min), flow rate, 1.0 mL/min). The eluates were then collected and identified by HR-ESI MS.

Cu^+ -responsive labeling of BSA with CuRs

10 μM purified bovine serum albumin (BSA) in 50 mM HEPES buffer (pH 7.2) was incubated with 50 μM CuR (FL-appended type) in the presence or absence of 50 μM $\text{Cu}(\text{MeCN})_4\text{PF}_6$ at 37°C for 1 h. For metal selectivity assay, various metal salts (5 mM of NaCl, KCl, MgCl_2 , CaCl_2 , or 50 μM of CuCl_2 , ZnCl_2 , FeCl_2 , FeCl_3 , CoSO_4 or CoCl_2 , NiCl_2) were used instead of $\text{Cu}(\text{MeCN})_4\text{PF}_6$. For evaluating responsiveness to ROS, 50 μM of H_2O_2 , O_2^- , $^1\text{O}_2$, OCl^- , $\cdot\text{NO}$, ONOO^- , or $\cdot\text{OH}$ was added. The ROS solutions were prepared freshly: KO_2 for O_2^- , 4-Methyl-1,4-etheno-2,3-benzodioxin-1(4H)-propanoic acid for $^1\text{O}_2$, Fenton reaction with FeCl_2 and H_2O_2 for $\cdot\text{OH}$, NaOCl for OCl^- , NOC-7 for $\cdot\text{NO}$, and SIN-1 (Cayman Chemical, 82220) for ONOO^- . To investigate the reaction under high GSH conditions, various concentrations of GSH (0–10 mM) with 50 μM $\text{Cu}(\text{gtsm})$ were added to a mixture of BSA and reagent. After the reaction, each sample was mixed with an equal volume of 2 \times SDS sample buffer (130 mM Tris-HCl, 6% SDS, 8% sucrose, 0.01% bromophenol blue) containing 10% 2-mercaptoethanol (2-ME) and 1 mM EDTA and boiled at 95°C for 5 min. The samples were then resolved by 12.5 % homemade polyacrylamide gel and analyzed by in-gel fluorescence imaging. The loaded protein was visualized by CBB stains. The fluorescence intensity of the labeled BSA band was quantitated by Image J.

Cell lines and culture conditions

HeLa cells were cultured in high glucose Dulbecco's Modified Eagle Medium (DMEM, 043-30085) supplemented with 10% fetal bovine serum (FBS; NICHIREI) and 1% Antibiotic-Antimycotic (Anti-Anti, Gibco) under a humidified atmosphere of 5% CO_2 in air at 37°C. The

cells were harvested from subconfluent cultures using a trypsin-EDTA solution (Gibco) or cell scraper and then resuspended in a fresh medium. Subculture was performed every 2–3 days.

Preparation of CTR1 expression plasmid

A cDNA encoding the full-length human copper transporter 1 (CTR1) and NheI/NotI sites was purchased from Eurofins. After digested with NheI and NotI, the fragment was inserted into the same digestion site of the pCAGGS2 plasmid to obtain the pCAGGS2-CTR1 plasmid.³⁰

Cu⁺-responsive protein labeling in CTR1-overexpressed HeLa cells

The HeLa cells (1.0×10^5 cells per well) were cultured on the 12-well plate in DMEM supplemented with 10 % v/v FBS and 1% anti-anti at 37 °C under 5% CO₂ for 24 h. The cells were transfected with pCAGGS2-CTR1 using Lipofectamine 2000 (Invitrogen) according to the manufacturer's instructions. After 18–24 h, the cells were cultured in the medium with and without CuCl₂ (5 μM) for 8.5 h. Subsequently, the cells were washed with growth medium twice and incubated in FBS-free DMEM-HEPES (Gibco, 1 % anti-anti) containing 5 μM AcFL-appended CuR at 37 °C under 5% CO₂ for 25 min. The cells were then washed once with DMEM-HEPES and added with fresh labeling medium with or without 100 μM N-methylmaleimide (N-MEM) and incubated for 10 min at 37 °C (5% CO₂). The cells were washed once with PBS containing 1mM EDTA, and then lysed with 100 μL of 1 × SDS-sample buffer (65 mM Tris-HCl, 3% SDS, 4% sucrose, 0.005% bromophenol blue) containing 1 mM EDTA and 100 mM dithiothreitol (DTT) on ice for 5 min. The lysate was collected into a 1.5 mL tube using a cell scraper and sonicated with Branson 450 Sonifier (Output control: 1; Duty cycle:10; Shots: 10). The obtained protein mixture was then vortexed for 10 min at room temperature and applied to 12.5 % homemade AA gels for protein electrophoresis. The proteins were then transferred to ImmunBlot PVDF membranes (Bio-Rad). After being blocked with 5% skim milk in TBST (Tris-buffered saline with 0.05% Tween 2036 (Sigma-Aldrich)) for 1 hour, membranes were incubated with primary antibodies diluted in 1 % skim milk in TBST at 4 °C overnight, followed by two rounds of 5 min wash with TBST and one round of 15 min wash with TBST. Membranes were then incubated with peroxidase (HRP)-conjugated secondary antibodies diluted in 1 % skim milk in TBST for 1 hour, followed by two rounds of 5 min wash with TBST and one round of 15 min wash with TBST. The membrane was immersed in ECL prime blotting substrate (Bio-Rad) for chemiluminescence

detection. Antibodies used in this study include rabbit anti-fluorescein (1:3000; ab19491, Abcam), rabbit anti-CTR1 (1:2000; ab129067, Abcam), and rabbit anti-beta tubulin (1:2000; ab15568, Abcam), and HRP-conjugated anti-rabbit IgG (CST, 7074s).

For imaging analysis, the cells, after labeling, were fixed with cold methanol (-20 °C) and placed at -20 °C for 15 min, followed by washing three times with 2 mL of PBS buffer. The fixed cells were then incubated with DAPI (Dojindo; 1/1000 dilution)-containing PBS buffer in the dark at room temperature for 30 min, then the DAPI-stained fixed cells were washed with PBS for three times to remove excessive DAPI, and the cells were immersed in PBS buffer. The fluorescent images were then obtained by excitation at 488 nm and 405 nm and simultaneous detection with FITC and DAPI emission filters.

Intracellular Cu⁺ observation by CopperGreen in the living CTR1-overexpressed HeLa cells

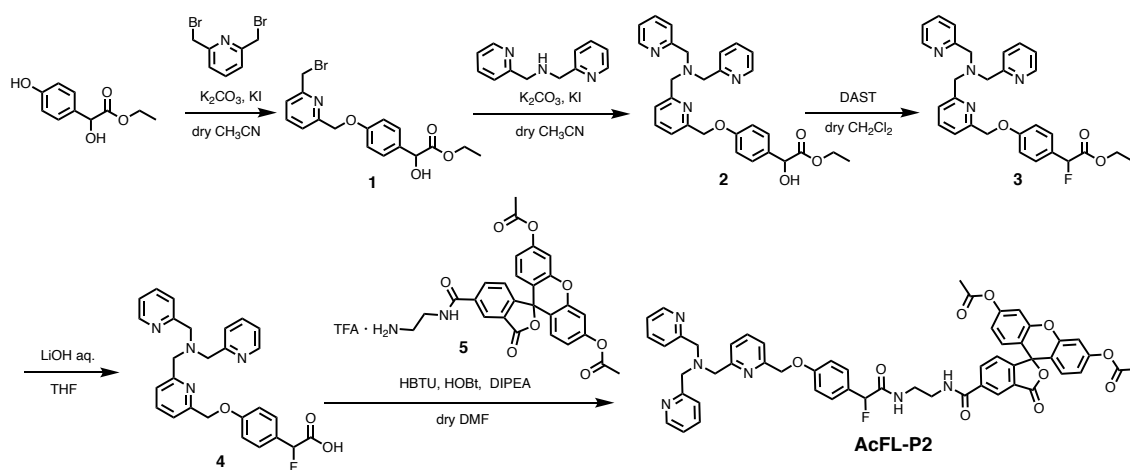
The HeLa cells (2.0×10^5 cells per 35 mm dish) were cultured on 35 mm dishes in DMEM supplemented with 10 % v/v FBS and 1% anti-anti at 37 °C under 5% CO₂ for 24 h. The cells were transfected with pCAGGS2-CTR1 using Lipofectamine 2000 (Invitrogen) according to the manufacturer's instructions. After 18–24 h, the cells were cultured in the medium with and without CuCl₂ (5 μM) for 8.5 h. Subsequently, the cells were washed with growth medium twice and incubated in FBS-free DMEM-HEPES (Gibco, 1 % anti-anti) containing 5 μM CopperGREEN at 37 °C under 5% CO₂ for 25 min. The cells were then washed once with DMEM-HEPES and added with fresh labeling medium with or without 100 μM N-methylmaleimide (N-MEM) and incubated for 10 min at 37 °C (5% CO₂). The fluorescent images were then obtained by excitation at 488 nm and simultaneous detection with a FITC emission filter (510-560 nm).

Synthetic schemes and processes

General Materials and methods for organic synthesis

All chemical reagents and solvents were obtained from commercial suppliers (Tokyo Chemical Industry (TCI), Sigma-Aldrich, Fujifilm-Wako Pure Chemical Corporation, Watanabe Chemical Industries, BLD Pharmatech Ltd., or Kanto Chemical Co., Inc.) and used without further purification. Thin layer chromatography (TLC) was performed on silica gel 60 F254 precoated aluminium sheets (Merck) and visualized by fluorescence quenching, fluorescence by 365 nm excitation, or staining with reagents (Ninhydrin, Bromocresol Green Stain, Phosphomolybdic Acid

(PMA). Chromatographic purification was accomplished using flash column chromatography on silica gel 60 N (neutral, 40–50 μm , Kanto Chemical) or Isolera Spektra One (Biotage) by using Sfar Silica HC Duo columns (Biotage) or on the manually packed silica gel 60 N (neutral, 40–50 μm , Kanto Chemical). $^1\text{H-NMR}$ spectra were recorded in deuterated solvents on a Varian Mercury 400 (400 MHz) spectrometer and calibrated to tetramethylsilane (= 0 ppm) or residual solvent peak. Multiplicities are abbreviated as follows: s = singlet, brs= broad singlet, d = doublet, t = triplet, td = triplet of doublets, q = quartet, dq = doublet of quartets, m = multiplet, dd = double doublets, and ddd = doublet of doublet of doublets. Matrix-assisted laser desorption/ionization time-of-flight mass spectrometry (MALDI-TOF MS) spectra were recorded on an Autoflex III instrument (Bruker Daltonics) using α -cyano-4-hydroxycinnamic acid (CHCA) as the matrix. High-resolution mass spectra were measured on an Exactive (Thermo Scientific) equipped with electron spray ionization (ESI). Unless otherwise noted, reversed-phase HPLC (RP-HPLC) was carried out on a Hitachi Chromaster HPLC system equipped with a Chromaster 5410 UV detector, and a YMC-Pack ODS-A column (5 μm , 250 \times 20 mm) at a flow rate of 9.9 mL/min. UV detection was at 220 nm and 254 nm. All runs used linear gradients of acetonitrile containing 0.1% TFA (solvent A) and 0.1% aqueous TFA (solvent B).



Scheme 1 Synthetic scheme of AcFL-P2.

Compound 1

To a solution of ethyl 4-hydroxymandelate (0.742 g, 3.78 mmol, 1.0 Eq) in super dehydrated CH_3CN (75 mL) was added 2,6-bis(bromomethyl)pyridine (2.01 g, 7.57 mmol, 2.0 Eq), dry

crushed potassium carbonate (K_2CO_3) (2.62 g, 18.9 mmol, 5.0 Eq) and potassium iodine (KI) (0.189 g, 1.14 mmol, 0.3 Eq). The mixture was refluxed for 4 h. After filtration, the solution was concentrated via a rotary evaporator and purified by Isolera (Sfar HC Duo 50 g, Hexane/EtOAc: 100/0 \rightarrow 60/40) to give compound **1** (0.744 g, 1.96 mmol, yield: 51.7 %) as light pink oil. **1H -NMR** (400 MHz, $CDCl_3$): δ /ppm 7.72 (t, $J = 7.8$ Hz, 1H), 7.44 (d, $J = 7.6$ Hz, 1H), 7.37 (d, $J = 8.0$ Hz, 1H), 7.34 (d, $J = 9.2$ Hz, 2H), 6.97 (d, $J = 8.8$ Hz, 2H), 5.19 (s, 2H), 5.10 (d, 1H, $J = 5.2$ Hz), 4.55 (s, 2H), 4.20–4.16 (m, 2H), 3.39 (d, $J = 5.6$ Hz, 1H), 1.23 (t, $J = 7.2$ Hz, 3H). **ESI-MS**: cald. For $[M+Na]^+$ as 402.0311, obsd. 402.0314.

Compound 2

A mixture of compound **1** (0.744 g, 1.96 mmol, 1.0 Eq), di-(2-picolyl)amine (0.391 g, 1.96 mmol, 1.0 Eq), dry crushed K_2CO_3 (1.35 g, 9.8 mmol, 5.0 Eq) and KI (9.8 mg, 0.59 mmol, 0.3 Eq) in super dehydrated CH_3CN (30 mL) was refluxed for 2 h. After cooling down to room temperature, the solution was filtered, concentrated, and purified by Isolera (Sfar HC Duo 25 g, $CHCl_3/MeOH(1\% NH_3 aq.)$: 100/0 \rightarrow 80/20) to give compound **2** (748 mg, 1.50 mmol, yield: 76.5 %) as orange oil. **1H -NMR** (400 MHz, $CDCl_3$): δ /ppm 8.52 (dq, $J = 4.9, 0.9$ Hz, 2H), 7.69–7.62 (m, 3H), 7.58 (d, $J = 7.9$ Hz, 2H), 7.51 (d, $J = 7.5$ Hz, 1H), 7.35 (d, $J = 7.5$ Hz, 1H), 7.31 (d, $J = 8.6$ Hz, 2H), 7.14 (ddd, $J = 7.3, 4.9, 1.3$ Hz, 2H), 6.95 (d, $J = 8.8$ Hz, 2H), 5.16 (s, 2H), 5.09 (s, 1H), 4.28–4.10 (m, 2H), 3.88 (s, 2H), 3.87 (s, 4H), 3.73 (s, 1H), 1.21 (t, $J = 7.1$ Hz, 3H). **ESI-MS**: cald. For $[M+Na]^+$ as 521.2159, obsd. 521.2156.

Compound 3

To a solution of compound **2** (474 mg, 0.95 mmol, 1.0 Eq) in super dehydrated CH_2Cl_2 (20 mL) was slowly added diethylaminosulfur trifluoride (459 mg, 2.85 mmol, 3.0 Eq) at 0 °C. The reaction mixture was stirred at 0 °C for 3 h, then warmed to room temperature and stirred overnight. The mixture was diluted with dd H_2O (60 mL) at 0 °C and extracted with CH_2Cl_2 (100 mL \times 2). The organic parts were collected, concentrated, and purified by Isolera (Sfar HC Duo 10 g, $CHCl_3/MeOH(1\% NH_3 \cdot H_2O)$: 100/0 \rightarrow 90/10) to give compound **3** (297 mg, 0.59 mol, yield: 62.1 %) as orange oil. **1H -NMR** (400 MHz, $CDCl_3$): δ /ppm 8.54 (dq, $J = 4.9, 0.9$ Hz, 2H), 7.70–7.61 (m, 3H), 7.58 (t, $J = 7.9$ Hz, 2H), 7.53 (d, $J = 7.7$ Hz, 1H), 7.38–7.34 (m, 3H), 7.15 (ddd, $J = 7.4, 4.9, 1.2$ Hz, 2H), 6.99 (d, $J = 8.2$ Hz, 2H), 5.69 (d, $J = 48.0$ Hz, 1H), 5.18 (s, 2H), 4.31–4.15

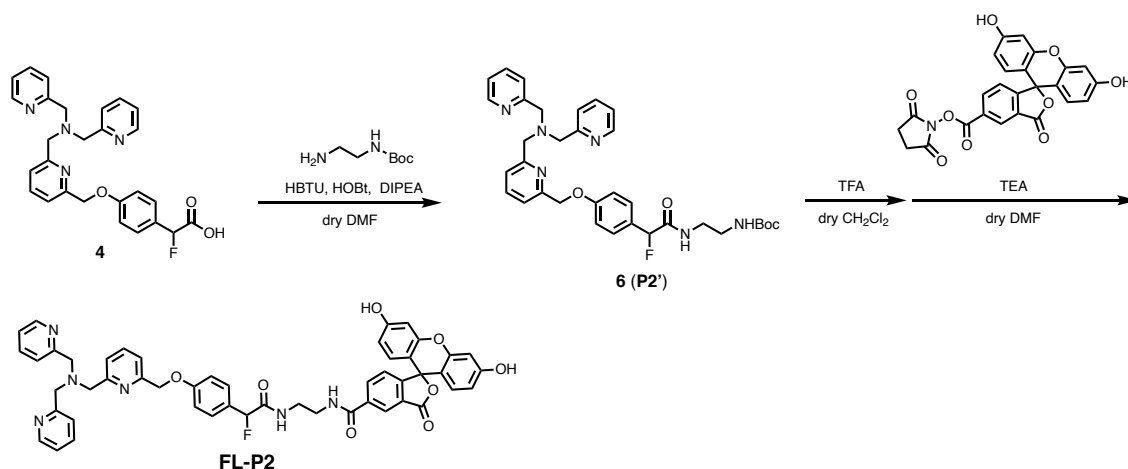
(m, 2H), 3.90 (s, 6H), 1.25 (t, $J = 7.1$ Hz, 3H). **ESI-MS**: cald. For $[M+Na]^+$ as 523.2116, obsd. 523.2119.

Compound 4

To a solution of compound **3** (297 mg, 0.59 mmol, 1.0 Eq) in THF (8 mL) and H₂O (0.5 mL) was added dropwise 1 M LiOH aq. (1.78 mL, 1.78 mmol, 3.0 Eq) at 0 °C. The reaction mixture was stirred at 0 °C for 1 h, then warmed to room temperature and stirred overnight. The mixture was diluted with water, neutralized with 0.1 M HCl until pH reached ~6, and extracted with CHCl₃ (60 mL × 3). The organic parts were collected and washed once with brine (20 mL), concentrated, and dried in vacuo to give compound **4** (115 mg, 0.243 mmol, yield: 41 %) as a brown oil. **¹H-NMR** (400 MHz, CDCl₃): δ /ppm 8.56 (d, $J = 4.9$ Hz, 2H), 7.66 (td, $J = 7.6, 1.8$ Hz, 2H), 7.58–7.52 (m, 3H), 7.42–7.36 (m, 3H), 7.31 (d, $J = 7.7$ Hz, 1H), 7.18 (ddd, $J = 7.3, 5.1, 1.0$ Hz, 2H), 6.90 (d, $J = 8.6$ Hz, 2H), 5.71 (d, $J = 48.7$ Hz, 1H), 5.11 (s, 2H), 3.87 (s, 4H), 3.86 (s, 2H). **ESI-MS**: cald. For $[M+H]^+$ as 473.1983, obsd. 473.1980.

AcFL-P2

To a solution of compound **4** (60.0 mg, 0.127 mol, 1.0 Eq) in super dehydrated DMF (1 mL) was added HBTU (72.8 mg, 0.192 mmol, 1.5 Eq), HOBT (25.6 mg, 0.189 mmol, 1.5 Eq), and compound **5**²⁰ (0.133 mmol, 1.0 Eq), and DIPEA (88.5 μ L, 0.508 mmol, 4.0 Eq). The mixture was stirred at room temperature overnight. After removing the solvent via evaporation, the residue was diluted with 4 mL of CH₃CN/H₂O (1/1; 0.1 % TFA), filtered with 0.45 μ m syringe filter, and purified by RP-HPLC (A: B = 30/70=> 55/45 (25 min)). A fraction that contains the target compound was collected and freeze-dried overnight to give **AcFL-P2** (11.93 mg, 12.5 μ mol, yield: 9.8 %) as a pale-yellow oil. **¹H-NMR** (400 MHz, CD₃OD): δ /ppm 8.65 (d, $J = 5.1$ Hz, 2H), 8.29 (s, 1H), 8.08 (dd, $J = 8.1, 1.5$ Hz, 1H), 7.98 (td, $J = 7.8, 1.6$ Hz, 2H), 7.75 (t, $J = 7.8$ Hz, 1H), 7.57–7.51 (m, 4H), 7.42 (d, $J = 7.7$ Hz, 1H), 7.38 (d, $J = 7.5$ Hz, 2H), 7.26 (t, $J = 8.0$ Hz, 2H), 7.17 (d, $J = 2.2$ Hz, 2H), 6.95 (d, $J = 8.6$ Hz, 2H), 6.87–6.75 (m, 4H), 5.73 (d, $J = 47.8$ Hz, 1H), 5.16 (s, 2H), 4.40 (s, 4H), 4.24 (s, 2H), 3.83–3.33 (m, 4H) *, 2.29 (s, 6H). *: the peaks overlapped with the solvent peak. **ESI-MS**: cald. For $[M+H]^+$ as 957.3254, obsd.957.3250., cald. For $[M+Na]^+$ as 979.3073, obsd. 979.3061.



Scheme 2 Synthetic scheme of **FL-P2**.

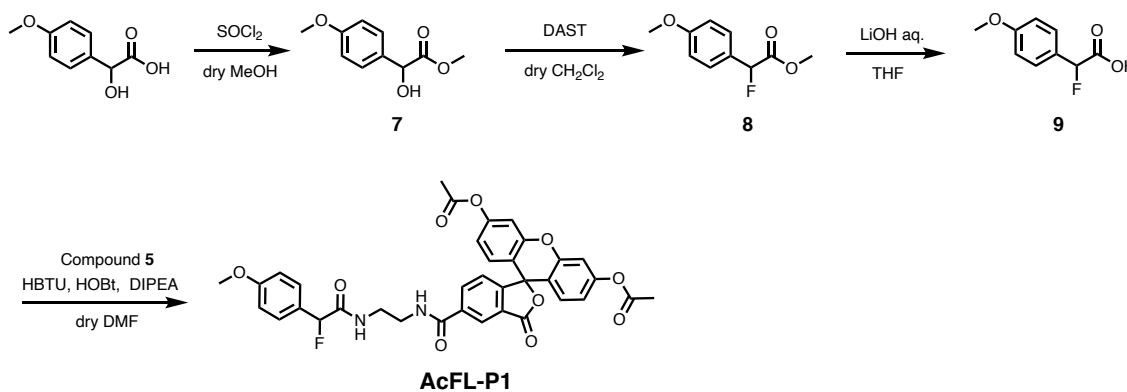
Compound 6 (P2')

To a solution of compound **4** (8.4 mg, 18.2 μmol , 1.0 Eq) in super dehydrated DMF (0.5 mL) was added HOBT (4.1 mg, 30.3 μmol , 1.7 Eq), HBTU (10.6 mg, 28.0 μmol , 1.5 Eq), and 2- (*N*-tert-butoxycarbonylamino) ethylamine (3.5 mg, 21.8 μmol , 1.2 Eq), and DIPEA (12.7 μL , 72.0 μmol , 4.0 Eq). The mixture was stirred at room temperature overnight. The solvent was removed by via rotary evaporation, and the residue was purified by column chromatography on silica gels ($\text{CHCl}_3/\text{MeOH}/\text{NH}_3 \text{ aq.} = 35/1/0.1 \Rightarrow 10/1/0.1$) to give compound **6** (5.7 mg, 9.3 μmol , yield: 51 %) as pale-yellow oil. **¹H-NMR** (400 MHz, CDCl_3): δ /ppm 8.52 (d, $J = 4.4$ Hz, 2H), 7.66–7.64 (m, 3H), 7.58 (d, $J = 7.6$ Hz, 2H), 7.50 (d, $J = 7.6$ Hz, 1H), 7.34 (d, $J = 8.4$ Hz, 3H), 7.15 (ddd, $J = 7.4$, 5.0, 1.2 Hz, 2H), 6.97 (d, $J = 8.4$ Hz, 2H), 5.68 (d, $J = 48.4$ Hz, 1H), 5.17 (s, 2H), 4.89 (s, 1H), 3.91 (s, 4H), 3.90 (s, 2H), 3.47–3.42 (m, 2H), 3.33–3.31 (m, 2H), 1.44 (s, 9H). **ESI-MS**: calcd. For $[\text{M}+\text{H}]^+$ as 615.3090, obsd. 615.3084.

FL-P2

To a solution of compound **6** (5.69 mg, 9.26 μmol , 1.0 Eq) in super dehydrated CH_2Cl_2 (0.5 mL) was added TFA (0.1 mL). The reaction mixture was stirred at room temperature for 1 h. The solvent was co-evaporated with toluene (2 mL \times 2) and dried in vacuo to give the deprotected product of **6** as pale yellow oil. The product was used for the next step without further purification. To a solution of the deprotected product of compound **6** (9.26 μmol , 1.0 Eq) in super dehydrated DMF (0.5 mL) was added 5-carboxyfluorescein *N*-succinimidyl ester (7.0 mg, 14.8 μmol , 1.6 Eq)

and triethylamine (TEA) (5.2 μL , 37 μmol , 4.0 Eq). The mixture was stirred at room temperature for 4 h. After removing the solvent via evaporation, the residue was diluted with 2 mL of $\text{CH}_3\text{CN}/\text{H}_2\text{O}$ (1/4; with 0.1 % TFA), filtered with 0.20 μm syringe filter, and then purified by RP-HPLC (A: B = 20/80 \Rightarrow 60/40 (40 min)). The fractions that contain the target compound were collected and freeze-dried overnight to give **FL-P2** (2.3 mg, 2.6 μmol , yield: 28 %) as yellow solids. $^1\text{H-NMR}$ (400 MHz, CD_3OD): δ/ppm 8.63 (d, $J = 5.2$ Hz, 2H), 8.28 (s, 1H), 8.07 (dd, $J = 8.0, 1.6$ Hz, 1H), 7.91 (td, $J = 7.7, 1.6$ Hz, 2H), 7.74 (t, $J = 7.7$ Hz, 1H), 7.48–7.44 (m, 4H), 7.41 (d, $J = 7.3$ Hz, 1H), 7.36 (d, $J = 7.2$ Hz, 2H), 7.23 (t, $J = 8.1$ Hz, 2H), 6.92 (d, $J = 8.6$ Hz, 2H), 6.64 (d, $J = 2.0$ Hz, 2H), 6.55–6.45 (m, 4H), 5.72 (d, $J = 48.0$ Hz, 1H), 5.12 (s, 2H), 4.42 (s, 4H), 4.31 (s, 2H), 3.77–3.38 (m, 4H). **ESI-MS**: cald. For $[\text{M}+\text{H}]^+$ as 873.3043, obsd. 873.3060., cald. For $[\text{M}+\text{Na}]^+$ as 895.2862, obsd. 895.2879.



Scheme 3 Synthetic scheme of **AcFL-P1**.

Compound 7

To a solution of DL-4-methoxymandelic acid (500 mg, 2.75 mmol, 1.0 Eq) in super dehydrated methanol (8 mL) in an ice/water bath was slowly added thionyl chloride (200 μL , 2.75 mmol, 1.0 Eq). The mixture was stirred at 0 $^\circ\text{C}$ for 20 min and then refluxed for 2 h. The reaction was quenched with H_2O (5 mL), and the solvent was removed via evaporation. The residue was dissolved in H_2O (10 mL) and extracted with EtOAc (20 mL \times 3). The organic parts were collected, washed with saturated NaHCO_3 (20 mL \times 1), and concentrated. The crude was purified by Isolera (Sfar HC Duo 25g, EtOAc/Hexane = 8 % \Rightarrow 40 %) to give compound **7** (347 mg, 1.77 mmol, yield: 64 %) as colorless oil. $^1\text{H-NMR}$ (400 MHz, CDCl_3): δ/ppm 7.32 (d, $J = 9.2$ Hz, 2H), 6.89

(d, $J = 8.8$ Hz, 2H), 5.12 (d, $J = 4.8$ Hz, 1H), 3.80 (s, 3H), 3.75 (s, 3H), 3.41 (d, $J = 5.2$ Hz, 1H). **ESI-MS**: calcd. For $[M+Na]^+$ as 219.0628, obsd. 219.0629.

Compound 8

To a solution of compound **7** (100 mg, 0.51 mmol, 1.0 Eq) in super dehydrated CH_2Cl_2 (8 mL) was slowly added diethylaminosulfur trifluoride (247 mg, 1.53 mmol, 3.0 Eq) at 0 °C. The reaction mixture was stirred at 0 °C for 1 h, then warmed to room temperature and stirred overnight. The reaction mixture was diluted with ddH₂O (15 mL) at 0 °C and extracted with CH_2Cl_2 (20 mL \times 2). The organic parts were collected, washed with brine (20 mL \times 1), dried over Na_2SO_4 , and filtrated. The filtrate was concentrated and dried in vacuo to give compound **8** (107 mg, 0.54 mmol, quant.) as orange oil. **¹H-NMR** (400 MHz, $CDCl_3$): δ /ppm 7.38 (dd, $J = 1.6, 8.8$ Hz, 2H), 6.93 (d, $J = 8.0$ Hz, 2H), 5.73 (d, $J = 48.0$ Hz, 1H), 3.82 (s, 3H), 3.78 (s, 3H). **ESI-MS**: calcd. For $[M+Na]^+$ as 221.0584, obsd. 221.0586.

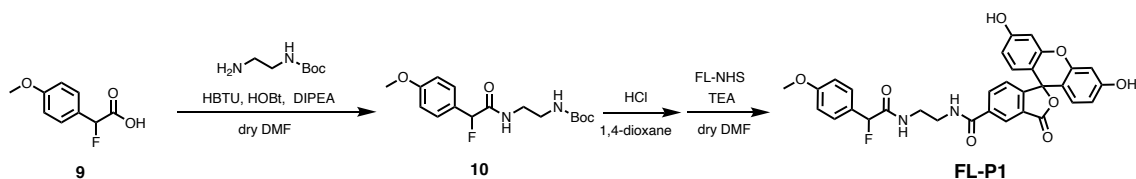
Compound 9

To a solution of compound **8** (80 mg, 403.6 μ mol, 1.0 Eq) in THF (4 mL) and H₂O (1 mL) was dropwise added 1 M LiOH aq. (1.21 mL, 1.21 mmol, 3.0 Eq) at 0 °C. The reaction mixture was stirred at 0 °C for 30 min, then warmed to room temperature and stirred overnight. After removing the solvent via evaporation, the residue was diluted with H₂O (5 mL) and neutralized with 0.1 M HCl until pH reached \sim 3. The solution was then extracted with EtOAc (25 mL \times 3). The organic parts were collected, washed once with brine (25 mL), dried over Na_2SO_4 and filtrated. The filtrate was concentrated and purified by Isolera (Sfar HC Duo 10 g, MeOH (10 % AcOH)/ $CHCl_3 = 5$ % \Rightarrow 10 %) to give compound **9** (21.2 mg, 115 μ mol, yield: 28.5 %) as pale-yellow oil. **¹H NMR** (400 MHz, $CDCl_3$): δ /ppm 7.41 (dd, $J = 1.2, 8.4$ Hz, 2H), 6.94 (d, $J = 8.4$ Hz, 2H), 5.76 (d, $J = 48.0$ Hz, 1H), 3.82 (s, 3H).

AcFL-P1

To a solution of compound **9** (1.9 mg, 10.3 μ mol, 1.0 Eq) in super dehydrated DMF (0.5 mL) was added HOBt (2.1 mg, 13.7 μ mol, 1.4 Eq), HBTU (5.2 mg, 13.7 μ mol, 1.4 Eq), and compound **5** (5.0 mg, 10.0 μ mol, 1.0 Eq), and DIPEA (6.3 μ L, 36.4 μ mol, 3.6 Eq). The mixture was stirred at room temperature overnight. After removing the solvent via evaporation, the residue was diluted

with 2 mL of CH₃CN/H₂O (1/1; 0.1 % TFA), filtered with 0.45 μm syringe filter, and purified by HPLC (Column: YMC-Triart-C18, 250 × 10.0 mm.L.D, A: B = 30/70 => 90/10 (60 min), flow rate: 3.0 mL/min). The target fraction was collected and freeze-dried overnight to give **AcFL-P1** (1.02 mg, 1.52 μmol, yield: 15.2 %) as white solids. **¹H-NMR** (400 MHz, CD₃OD): δ/ppm 8.33 (s, 1 H), 8.07 (d, *J* = 8.4 Hz, 1H), 7.33 (d, *J* = 8.4 Hz, 2H), 7.29 (d, *J* = 8.0 Hz, 1H), 7.20 (s, 2H), 6.91–6.87 (m, 4H), 6.81 (d, *J* = 8.0 Hz, 2H), 5.69 (d, *J* = 48.0 Hz, 1H), 3.70–3.63 (m, 5H), 3.54–3.47 (m, 2H), 2.29 (s, 6H). **ESI-MS**: cald. For [M+Na]⁺ as 691.1698, obsd. 691.1697.



Scheme 4 Synthetic scheme of **FL-P1**.

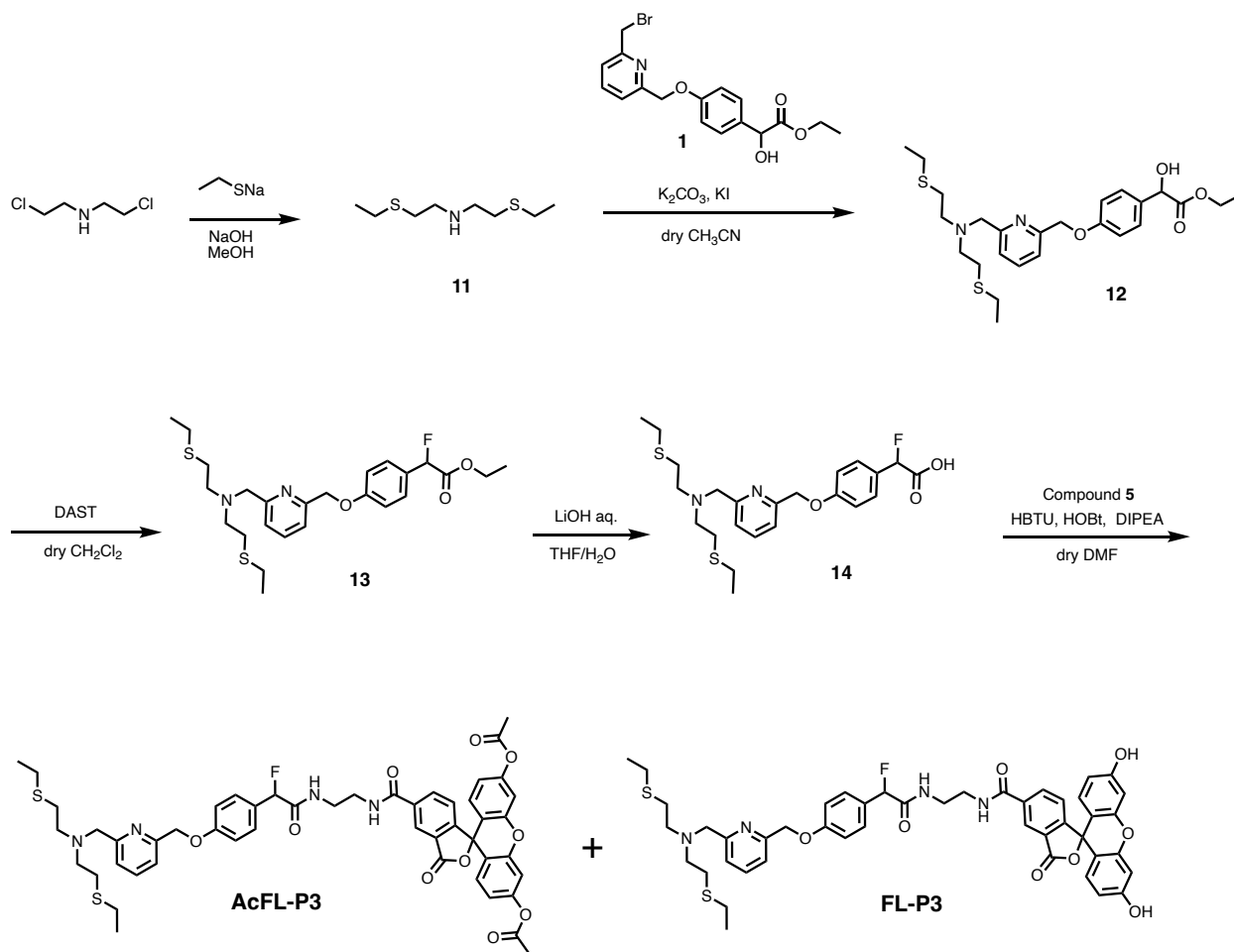
Compound 10

To a solution of compound **9** (41.6 mg, 0.226 mmol, 1.0 Eq), HOBt (45.8 mg, 0.339 mmol, 1.5 Eq) and HBTU (111.6 mg, 0.339 mmol, 1.5 Eq) in super dehydrated DMF (3 mL) was added 2-(*N*-tert-butoxycarbonylamino) ethylamine (36.2 mg, 0.226 mmol, 1.0 Eq) and DIPEA (157.5 μL, 0.904 mmol, 4.0 Eq). The mixture was stirred at room temperature overnight. The reaction mixture was diluted with EtOAc (30 mL), washed with saturated NaHCO₃ (15 mL), H₂O (15 mL), and brine (15 mL), dried over Na₂SO₄, and filtrated. The filtrate was concentrated and purified by Isolera (Sfar HC Duo 10 g, EtOAc/ Hexane: 0 % => 100 %) to give compound **10** (26.14 mg, 0.081 mmol, yield: 35.7 %) as pale-yellow oil. **¹H-NMR** (400 MHz, CD₃OD): δ/ppm 7.37 (dd, *J* = 8.7, 1.7 Hz, 2H), 6.94 (d, *J* = 8.4 Hz, 2H), 5.69 (d, *J* = 48.1 Hz, 1H), 3.80 (s, 3H), 3.38–3.30 (m, 2H) *, 3.20 (t, *J* = 5.9 Hz, 2H), 1.42 (s, 9H). *: the peaks overlapped with a peak of the solvent peak. **ESI-MS**: cald. For [M+Na]⁺ as 349.1534, obsd. 349.1534.

FL-P1

The solution of compound **10** (6.77 mg, 20.7 μmol, 1.0 Eq) in 4 mol/L HCl-1,4-dioxane (0.5 mL) was stirred on ice for 1 h and at room temperature for 0.5 h. The solvent was removed via rotary evaporation to give the deprotected product as white solids. The product was used for the next step without further purification. To a solution of the deprotected compound (1.30 mg, 4.95 μmol, 1.0

Eq) in super dehydrated DMF (0.2 mL) was added FL-NHS (2.81 mg, 5.94 μmol , 1.2 Eq) and triethylamine (TEA) (2.8 μL , 19.8 μmol , 4.0 Eq). The mixture was stirred at room temperature for 2 h. After removing the solvent via evaporation, the residue was diluted with 2 mL of CH_3CN , filtered with 0.20 μm syringe filter, and then purified by RP-HPLC (A/B: 20/80 \Rightarrow 70/30 (50 min)). The target fraction was collected and freeze-dried overnight to give **FL-P1** (1.47 mg, 2.51 μmol , yield: 50.7 %) as orange solids. $^1\text{H-NMR}$ (400 MHz, CD_3OD): δ/ppm 8.32 (s, 1H), 8.07 (dd, $J = 8.1, 1.6$ Hz, 1H), 7.34 (dd, $J = 8.7, 1.6$ Hz, 2H), 7.24 (d, $J = 7.9$ Hz, 1H), 6.82 (d, $J = 8.4$ Hz, 2H), 6.69 (d, $J = 2.2$ Hz, 2H), 6.60–6.52 (m, 4H), 5.70 (d, $J = 48.0$ Hz, 1H), 3.70 (s, 3H), 3.47–3.23 (m, 4H) *.*: the peaks overlapped with solvent peak. **ESI-MS**: calcd. For $[\text{M}+\text{H}]^+$ as 585.1668, obsd. 585.1666.



Scheme 5 Synthetic scheme of **AcFL-P3** and **FL-P3**.

Compound 11

To sodium enthamethiolate (592.0 mg, 7.04 mmol, 2.5 Eq) in super dehydrated MeOH (2 mL) was dropwise added NaOH (180.0 mg, 4.5 mmol, 1.6 Eq) in super dehydrated MeOH (2 mL) and bis(2-chloroethyl) amine·hydrochloride (504.2 mg, 2.82 mmol, 1.0 Eq) in super dehydrated MeOH (1 mL) under Ar protection. The mixture was stirred at room temperature for 18 h. Then the solvent was removed via rotary evaporation, and the crude was suspended in water (20 mL) and extracted twice with Hexane (35 mL). The organic part was collected, washed once with brine (20 mL), dried over Na₂SO₄, and filtrated. The filtrate was then concentrated and dried in vacuo to give compound **11** (344 mg, 1.78 mmol, yield: 63 %) as colorless oil. ¹H-NMR (400 MHz; CDCl₃): δ/ppm 2.83 (t, 4 H, *J* = 6.6 Hz), 2.69 (t, 4 H, *J* = 6.6 Hz), 2.55 (q, 4 H, *J* = 7.4 Hz), 1.72 (brs, 1 H), 1.26 (t, 6 H, *J* = 7.4 Hz). **ESI-MS**: cald. For [M+H]⁺ as 194.1032, obsd. 194.1034., cald. For [M+Na]⁺ as 216.0851, obsd. 216.0855.

Compound 12

To a solution of compound **1** (81 mg, 0.21 mmol, 1.0 Eq) in super dehydrated CH₃CN (5 mL) was added compound **11** (45 mg, 0.23 mmol, 1.1 Eq), dry crushed K₂CO₃ (146 mg, 1.06 mmol, 5.0 Eq) and KI (11 mg, 0.07 mmol, 0.3 Eq). The mixture was refluxed for 2 h. After cooling down to room temperature, the reaction solution was filtered and concentrated via a rotary evaporator. The crude was purified by Isolera (Sfar HC Duo 10 g, MeOH/ CHCl₃: 0 %→ 40 %) to give compound **12** (55 mg, 0.11 mmol, yield: 52 %) as pale-yellow oil. ¹H-NMR (400 MHz, CDCl₃): δ/ppm 7.69 (t, *J* = 7.8 Hz, 1H), 7.48 (d, *J* = 7.6 Hz, 1H), 7.37 (d, *J* = 7.6 Hz, 1H), 7.33 (d, *J* = 8.4 Hz, 2H), 6.96 (d, *J* = 9.2 Hz, 2H), 5.16 (s, 2H), 5.10 (s, 1H), 4.30–3.83 (m, 2H), 3.83 (s, 2H), 2.82–2.78 (m, 4H), 2.67–2.63 (m, 4H), 2.51 (q, *J* = 7.4 Hz, 4H), 1.22 (t, *J* = 7.4 Hz, 9H). **ESI-MS**: cald. For [M+H]⁺ as 493.2189, obsd.493.2197.

Compound 13

To a solution of compound **12** (21 mg, 43 μmol, 1.0 Eq) in super dehydrated CH₂Cl₂ (1 mL) was slowly added with diethylaminosulfur trifluoride (20.9 mg, 129.6 μmol, 3.0 Eq) at 0 °C. The reaction mixture was stirred at 0 °C for 1 h, then warmed to room temperature and stirred overnight. The mixture was diluted with ddH₂O (10 mL) and extracted with CH₂Cl₂ (15 mL× 2). The organic parts were collected, concentrated, and purified by Isolera (Sfar HC Duo 10 g, EtOAc/

Hexane:5 %→ 40 %) to give compound **13** (10.3 mg, 20.8 μmol , yield: 48.1 %) as pale-yellow oil. **$^1\text{H-NMR}$** (400 MHz, CDCl_3): δ/ppm 7.70 (t, $J = 8.0$ Hz, 1H), 7.49 (d, $J = 7.6$ Hz, 1H), 7.40–7.36 (m, 3H), 7.00 (dd, $J = 8.8, 0.8$ Hz, 2H), 5.70 (d, $J = 48.0$ Hz, 1H), 5.18 (s, 2H), 4.30–4.16 (m, 2H), 3.83 (s, 2H), 2.82–2.78 (m, 4H), 2.67–2.64 (m, 4H), 2.51 (q, $J = 7.4$ Hz, 4H), 1.26 (t, $J = 7.4$ Hz, 3H), 1.23 (t, $J = 7.4$ Hz, 6H). **ESI-MS**: calcd. For $[\text{M}+\text{H}]^+$ as 495.2146, obsd.495.2144.

Compound 14

To a solution of compound **13** (10 mg, 21 μmol , 1.0 Eq) in THF (0.5 mL) and H_2O (70 μL) was dropwise added 1 M LiOH solution (31.2 μL , 31.2 μmol , 1.5 Eq) at 0 °C. The reaction mixture was stirred at 0 °C for 30 min, then warmed to room temperature and stirred overnight. The mixture was diluted with H_2O (10 mL), neutralized with 0.1 M HCl until pH reached ~3, and extracted with CHCl_3 (15 mL \times 2). The organic parts were collected and dried over Na_2SO_4 and filtrated. Then the filtrate was concentrated and dried in vacuo to give compound **14** (6.7 mg, 14.3 μmol , yield: 68.8 %) as a pale-yellow oil. **$^1\text{H-NMR}$** (400 MHz, CDCl_3): δ/ppm 7.63 (t, $J = 7.8$ Hz, 1H), 7.43–7.39 (m, 4H), 6.87 (d, $J = 8.8$ Hz, 2H), 5.69 (d, $J = 49.2$ Hz, 1H), 5.06 (s, 2H), 4.06 (s, 2H), 2.99–2.95 (m, 4H), 2.74–2.70 (m, 4H), 2.49 (q, $J = 7.4$ Hz, 4H), 1.20 (t, $J = 7.4$ Hz, 6H).

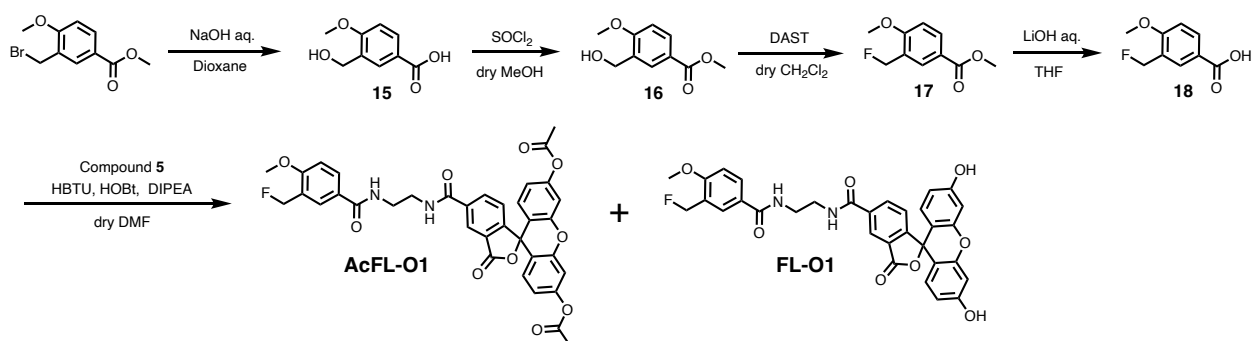
AcFL-P3 and FL-P3

To a solution of compound **14** (6.7 mg, 14 μmol , 1.0 Eq) in super dehydrated DMF (0.5 mL) was added HOBt (3.3 mg, 21 μmol , 1.5 Eq), HBTU (8.1 mg, 21 μmol , 1.5 Eq), compound **5** (8.6 mg, 17 μmol , 1.2 Eq), and DIPEA (9.9 μL , 57.2 μmol , 4.0 Eq). The mixture was stirred at room temperature overnight. After removing the solvent via evaporation, the residue was diluted with 2 mL of $\text{CH}_3\text{CN}/\text{H}_2\text{O}$ (1/1; 0.1 % TFA), filtered with 0.45 μm syringe filter, and purified by RP-HPLC (Column: YMC-Triart-C18, 250 \times 10.0 mm.I.D, A:B = 30/70 => 75/25 (45 min), flow rate: 3.0 mL/min). The fractions that contain the target compound were collected respectively and freeze-dried overnight to give **AcFL-P3** (1.46 mg, 1.5 μmol , yield: 10.5 %) as white solids and **FL-P3** (2.05 mg, 3.6 μmol , yield: 25.2 %) as yellow solids.

AcFL-P3: **$^1\text{H-NMR}$** (400 MHz, CD_3OD): δ/ppm 8.32 (s, 1H), 8.07 (d, $J = 7.6$ Hz, 1H), 7.89 (t, $J = 9.2$ Hz, 1H), 7.55 (d, $J = 7.6$ Hz, 1H), 7.42–7.36 (m, 3H), 7.29 (d, $J = 7.6$ Hz, 1H), 7.19 (s, 2H), 6.93 (d, $J = 8.0$ Hz, 2H), 6.88–6.80 (m, 4H), 5.71 (d, $J = 47.6$ Hz, 1H), 5.15 (s, 2H), 4.59 (s, 2H), 3.48 (t, $J = 7.2$ Hz, 4H), 3.34–3.30 (m, 4H)*, 2.92 (t, $J = 7.2$ Hz, 4H), 2.50 (q, $J = 7.4$ Hz, 4H),

2.29 (s, 6H), 1.18 (t, $J = 7.2$ Hz, 6H). *: the peaks overlapped with the solvent peak. **ESI-MS**: calcd. For $[M+H]^+$ as 951.3103, obsd. 951.3104.

FL-P3: $^1\text{H-NMR}$ (400 MHz, CD_3OD): δ/ppm 8.31 (s, 1H), 8.06 (d, $J = 8.0$ Hz, 1H), 7.88 (td, $J = 0.8, 8.0$ Hz, 1H), 7.54 (d, $J = 8.4$ Hz, 1H), 7.41–7.36 (m, 3H), 7.23 (d, $J = 7.6$ Hz, 1H), 6.92 (d, $J = 7.6$ Hz, 2H), 6.66 (s, 2H), 6.56–6.46 (m, 4H), 5.71 (d, $J = 47.2$ Hz, 1H), 5.14 (d, $J = 6.0$ Hz, 2H), 4.60 (s, 2H), 3.48 (t, $J = 7.4$ Hz, 4H), 3.34–3.30 (m, 4 H)*, 2.92 (t, $J = 7.0$ Hz, 4H), 2.50 (q, $J = 7.4$ Hz, 4H), 1.18 (t, $J = 7.4$ Hz, 6H). *: the peaks overlapped with the solvent peak. **ESI-MS**: calcd. for $[M+H]^+$ as 867.2892, obsd. 867.2895.



Scheme 6 Synthetic scheme of AcFL-O1 and FL-O1.

Compound 15

To a solution of methyl 4-(bromomethyl)-3-methoxybenzoate (2.59 g, 10.0 mmol, 1.0 Eq) in 1,4-dioxane (25 mL) and H_2O (8 mL) was added 1 M NaOH aq. (25 mL, 25 mmol, 2.5 Eq). The mixture was refluxed for 5 h. After cooling down to 0°C , the solution was neutralized with 1M HCl until pH reached ~ 3 and extracted with EtOAc (80 mL \times 3). The organic parts were collected, washed once with H_2O (70 mL), dried over MgSO_4 , and filtrated. The filtrate was concentrated and dried in vacuo to give compound **15** (1.96 g, 10.8 mmol, quant.) as pale-yellow solids. $^1\text{H-NMR}$ (400 MHz, CD_3OD): δ/ppm 7.64 (dd, $J = 7.8, 1.4$ Hz, 1H), 7.55 (d, $J = 1.6$ Hz, 1H), 7.48 (d, $J = 7.6$ Hz, 1H), 4.67 (s, 2H), 3.88 (s, 3H). **ESI-MS**: calcd. For $[M-H]^-$ as 181.0506, obsd. 181.0505.

Compound 16

To a solution of compound **15** (1.0 g, 5.5 mmol, 1.0 Eq) in super dehydrated MeOH (20 mL) was added dropwise thionyl chloride (399 μ L, 5.5 mmol, 1.0 Eq) at 0 °C. The mixture was stirred at 0 °C for 20 min and then refluxed for 2 h. The reaction was quenched with H₂O (10 mL) at 0 °C and concentrated. The residue was dissolved in H₂O (30 mL) and extracted with EtOAc (40 mL \times 3). The organic parts were collected, washed with saturated NaHCO₃ (35 mL \times 1), and concentrated. The crude was purified by Isolera (Sfar HC Duo 50g, EtOAc/Hexane = 0 % => 40 %) to give compound **16** (705 mg, 3.6 mmol, yield: 65 %) as white solids. **¹H-NMR** (400 MHz, CD₃OD): δ /ppm 7.63 (d, J = 7.7 Hz, 1H), 7.53 (s, 1H), 7.49 (d, J = 7.7 Hz, 1H), 4.66 (s, 2H), 3.88 (dd, J = 5.7, 1.8 Hz, 6H). **ESI-MS**: cald. For [M+H]⁺ as 197.0808, obsd.197.0807.

Compound 17

To a solution of compound **16** (298 mg, 1.52 mmol, 1.0 Eq) in super dehydrated CH₂Cl₂ (20 mL) was slowly added diethylaminosulfur trifluoride (602 μ L, 4.56 mmol, 3.0 Eq) at 0 °C. The reaction mixture was stirred at 0 °C for 1 h, then warmed to room temperature and stirred overnight. The mixture was added to H₂O (40 mL) at 0 °C and extracted with CH₂Cl₂ (60 mL \times 2). The organic parts were collected, concentrated, and purified by Isolera (Sfar HC Duo 25 g, EtOAc/Hexane = 0 % => 40 %) to give compound **17** (145 mg, 0.74 mmol, yield: 48.7%) as white solids. **¹H-NMR** (400 MHz, CD₃OD): δ /ppm 7.65 (d, J = 8.0 Hz, 1H), 7.59 (s, 1H), 7.46 (d, J = 8.0 Hz, 1H), 5.46 (d, J = 47.2 Hz, 2H), 3.91–3.90 (m, 6H). **ESI-MS**: cald. For [M+H]⁺ as 199.0765, obsd.199.0764.

Compound 18

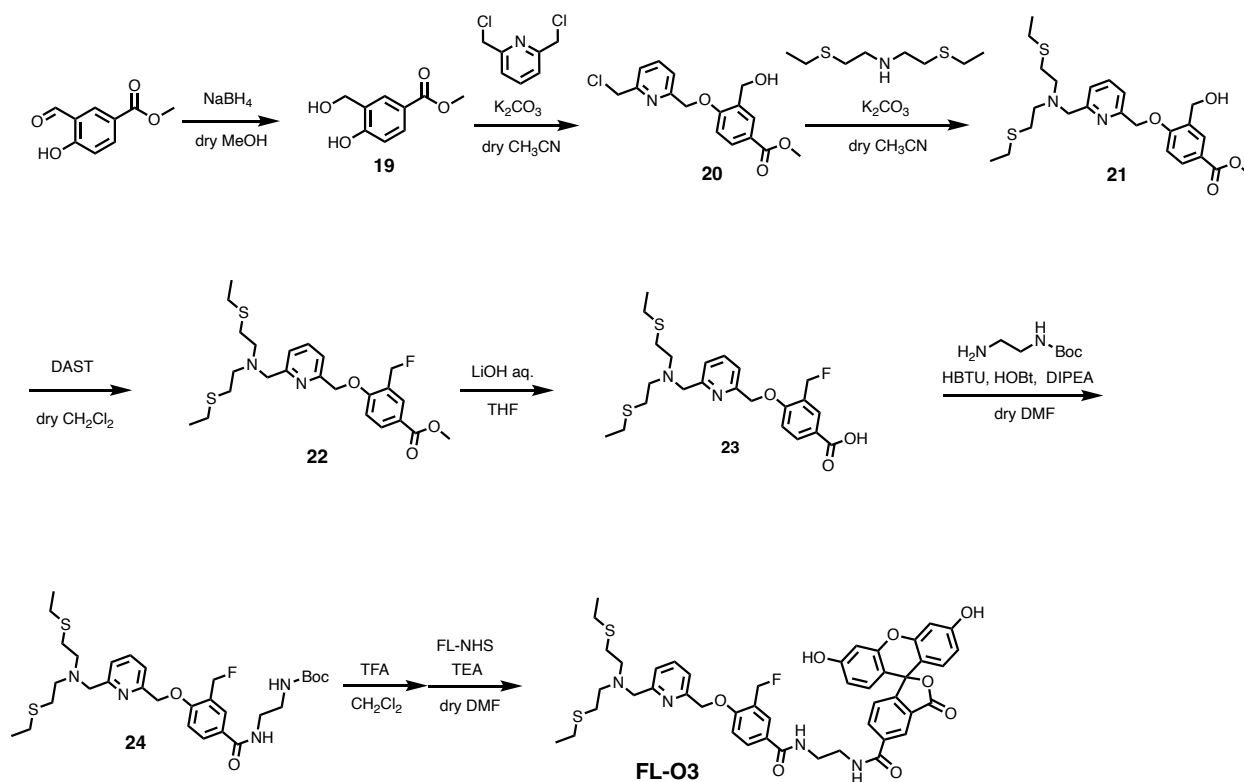
To a solution of compound **17** (72 mg, 0.39 mmol, 1.0 Eq) in THF (8 mL) and H₂O (1 mL) was added dropwise 1 M LiOH aq. (590 μ L, 0.59 mmol, 1.5 Eq) at 0 °C. The reaction mixture was stirred at 0 °C for 30 min, then warmed to room temperature and stirred overnight. The mixture was neutralized with 1 M HCl until pH reached ~3 and extracted with EtOAc (40 mL \times 2). The organic parts were collected and washed once with brine (30 mL), dried over Na₂SO₄ and filtrated. The filtrate was then concentrated and dried in vacuo to give compound **18** (68 mg, 0.37 mmol, yield: 95 %) as white solids. **¹H-NMR** (400 MHz; CD₃OD): δ /ppm 7.66 (d, J = 8.0 Hz, 1H), 7.60 (s, 1H), 7.45 (d, J = 7.6 Hz, 1H), 5.46 (d, J = 47.6 Hz, 2H), 3.90 (s, 3H). **ESI-MS**: cald. For [M-H]⁻ as 183.0463, obsd.183.0463.

AcFL-O1 and FL-O1

To a solution of compound **5** (17.8 μmol , 1.0 Eq) in super dehydrated DMF (1 mL) was added HOBt (4.1 mg, 26 μmol , 1.5 Eq), HBTU (10.0 mg, 26 μmol , 1.5 Eq), compound **18** (3.3 mg, 17.8 μmol , 1.0 Eq), and DIPEA (12.4 μL , 71.2 μmol , 4.0 Eq). The mixture was stirred at room temperature overnight. After removing the solvent via evaporation, the residue was dissolved in 4 mL of $\text{CH}_3\text{CN}/\text{H}_2\text{O}$ (1/1; 0.1 % TFA), filtered with 0.45 μm syringe filter, and purified by RP-HPLC (A: B = 30/70 \Rightarrow 80/20 (50 min)). The fractions that contain the target compound were collected respectively and freeze-dried overnight to give **AcFL-O1** (1.5 mg, 2.24 μmol , yield: 12.6 %) as white solids and **FL-O1** (1.6 mg, 2.74 μmol , yield: 15.4 %) as orange solids.

AcFL-O1: $^1\text{H-NMR}$ (400 MHz, CD_3OD): δ/ppm 8.46 (s, 1H), 8.20 (dd, $J = 8.2, 1.4$ Hz, 1H), 7.45–7.41 (m, 3H), 7.35 (d, $J = 8.0$ Hz, 1H), 7.20 (d, $J = 2.0$ Hz, 2H), 6.91–6.86 (m, 4H), 5.43 (d, $J = 47.6$ Hz, 2H), 3.89 (s, 3H), 3.67 (d, $J = 2.0$ Hz, 4H), 2.29 (s, 6H). **ESI-MS**: cald. For $[\text{M}+\text{H}]^+$ as 669.1879, obsd. 669.1886.

FL-O1: $^1\text{H-NMR}$ (400 MHz, CD_3OD): δ/ppm 8.43 (s, 1H), 8.19 (dd, $J = 7.8, 1.0$ Hz, 1H), 7.46–7.41 (m, 3H), 7.30 (d, $J = 8.4$ Hz, 1H), 6.71 (s, 2H), 6.62–6.54 (m, 4H), 5.44 (d, $J = 47.6$ Hz, 2H), 3.89 (s, 3H), 3.67 (s, 4H). **ESI-MS**: cald. For $[\text{M}+\text{H}]^+$ as 585.1668, obsd. 585.1677.



Scheme 7 Synthetic scheme of **FL-O3**.

Compound 19

To a solution of methyl 3-formyl-4-hydroxybenzoate (500 mg, 2.78 mmol, 1.0 Eq) in super dehydrated MeOH (10 mL) was added NaBH₄ (0.161 g, 4.24 mmol, 1.5 eq.) in several portions (portions over 3 min) at 0 °C under Ar atmosphere. The reaction mixture was stirred at room temperature for 1 h and concentrated. The residue was suspended in EtOAc (50 mL) and washed with a saturated aqueous solution of NH₄Cl (2 × 15 mL), water (15 mL), then brine (15 mL). Then the organic part was dried over Na₂SO₄, filtrated, and concentrated to give compound **19** (344 mg, 1.89 mmol, yield: 68%) as a white solid. ¹H-NMR (400 MHz, CD₃OD/CDCl₃): δ/ppm 7.93 (d, *J* = 2.0 Hz, 1H), 7.82 (dd, *J* = 8.4, 2.4 Hz, 1H), 6.82 (d, *J* = 8.0 Hz, 1H), 4.71 (s, 2H), 3.86 (s, 3H).

Compound 20

A mixture of compound **19** (202 mg, 1.11 mmol, 1.0 Eq), 2,6-bis(chloromethyl)pyridine (770 mg, 4.40 mmol, 4.0 Eq), and dry crushed K₂CO₃ (156 mg, 1.15 mmol, 1.0 Eq) in super dehydrated CH₃CN (25 mL) was heated to 50 °C for 4 h. After cooling down to room temperature, the reaction solution was filtered and concentrated via rotary evaporator. The crude was purified by Isolera

(Sfar HC Duo 25 g, MeOH/ CHCl₃: 2 % → 5 % → 10 % → 20 %) to give compound **20** (261.5 mg, 0.81 mmol, yield: 73 %) as white solids. **¹H-NMR** (400 MHz, CDCl₃): δ/ppm 8.03 (d, *J* = 2.0 Hz, 1H), 7.98 (d, *J* = 8.4 Hz, 1H), 7.78 (t, *J* = 7.8 Hz, 1H), 7.46 (d, *J* = 7.6 Hz, 1H), 7.37 (d, *J* = 8.0 Hz, 1H), 6.96 (d, *J* = 8.8 Hz, 1H), 5.32 (s, 2H), 4.80 (s, 2H), 4.68 (s, 2H), 3.89 (s, 3H). **ESI-MS**: cald. For [M+Na]⁺ as 344.0660, obsd. 344.0666.

Compound 21

To a solution of bis(2-(ethylthio)ethyl)amine (30.4 mg, 157 μmol, 1.0 Eq) in super dehydrated CH₃CN (5 mL) was added compound **20** (56.2 mg, 175 μmol, 1.1 Eq) and dry crushed K₂CO₃ (66.8 mg, 483 μmol, 3.1 Eq). The mixture was refluxed overnight. After cooling down to room temperature, the solution was filtered, concentrated, and purified by column chromatography on silica gels (Hexane/EtOAc: 1/1) to give compound **21** (44 mg, 92 μmol, yield: 59 %) as a pale-yellow oil. **¹H-NMR** (400 MHz, CDCl₃): δ/ppm 8.01–7.96 (m, 2H), 7.71 (t, *J* = 7.6 Hz, 1H), 7.56 (d, *J* = 7.6 Hz, 1H), 6.96 (d, *J* = 7.6 Hz, 1H), 5.28 (s, 2H), 4.78 (s, 2H), 3.88 (s, 3H), 3.83 (s, 2H), 2.80–2.76 (m, 4H), 2.66–2.62 (m, 4H), 2.50 (q, *J* = 7.4 Hz, 4H), 1.22 (t, *J* = 7.4 Hz, 6H). **ESI-MS**: cald. For [M+H]⁺ as 479.2033, obsd.479.2047.

Compound 22

To a solution of compound **21** (44 mg, 92 μmol, 1.0 Eq) in super dehydrated CH₂Cl₂ (2 mL) was slowly added with diethylaminosulfur trifluoride (36.5 μL, 276 μmol, 3.0 Eq) under Ar atmosphere at 0 °C. The reaction mixture was stirred at 0 °C for 10 min, then warmed to room temperature and stirred overnight. The reaction mixture was quenched by MeOH, concentrated, and purified by column chromatography on silica gel (Hexane/ EtOAc: 4/1→ 2/1) to give compound **22** (10 mg, 21 μmol, yield: 24 %) as a brown oil. **¹H-NMR** (400 MHz, CDCl₃): δ/ppm 8.10 (s, 1H), 8.02 (dt, *J* = 8.8, 1.6 Hz, 1H), 7.71 (t, *J* = 8.0 Hz, 1H), 7.50 (d, *J* = 8.0 Hz, 1H), 7.34 (d, *J* = 8.0 Hz, 1H), 6.96 (dd, *J* = 8.8, 1.0 Hz, 1H), 5.6 (d, *J* = 47.6 Hz, 2H), 5.27 (s, 2H), 3.89 (s, 3H), 3.83 (s, 2H), 2.82–2.78 (m, 4H), 2.68–2.64 (m, 4H), 2.52 (q, *J* = 7.4 Hz, 4H), 1.23 (t, *J* = 7.4 Hz, 6H). **ESI-MS**: cald. For [M+H]⁺ as 481.1989, obsd. 481.1993.

Compound 23

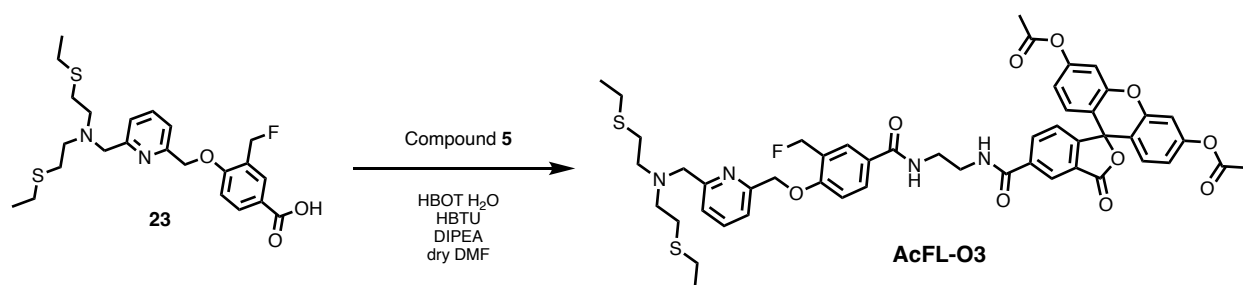
To compound **22** (32.6 mg, 67.8 μmol , 1.0 Eq) in THF (1.5 mL) on ice/water bath was dropwise added 1 M LiOH solution (101.7 μL , 101.7 μmol , 1.5 Eq). The reaction mixture was stirred at 0°C with an ice/water bath for 10 min, then the ice/water bath was removed to let the mixture stir at room temperature overnight. Since the reaction was not complete, an additional 1 M LiOH solution (101.7 μL , 101.7 μmol , 1.5 Eq) was added twice, and the reaction mixture was then stirred overnight at room temperature. After confirming the completion of the reaction by TLC, the mixture was added with 2 mL H₂O, then neutralized with 1 M HCl until pH reached ~5 in the ice/water bath. Then the mixture was added 10 mL H₂O and extracted with EtOAc (20 mL \times 2). The collected organic parts were washed once with Brine (20mL), then dried over Na₂SO₄ and filtrated. Then the filtrate was concentrated and dried in vacuo to give compound **23** (30.4 mg, 65.2 μmol , yield: 96.2 %) as pale-yellow oil. **¹H-NMR** (400 MHz, CDCl₃) δ 8.13 (s, 1H), 8.06 (d, J = 8.6 Hz, 1H), 7.73 (t, J = 7.7 Hz, 1H), 7.53 (d, J = 7.9 Hz, 1H), 7.37 (d, J = 7.5 Hz, 1H), 6.98 (d, J = 8.1 Hz, 1H), 5.56 (d, J = 47.6 Hz, 2H), 5.29 (s, 2H), 3.87 (s, 2H), 2.83-2.75 (m, 4H), 2.73-2.66 (m, 4H), 2.52 (q, J = 7.4 Hz, 4H), 1.23 (t, J = 7.4 Hz, 6H). **ESI-MS**: cald. For [M+H]⁺ as 461.1833, obsd.467.1840., cald. For [M+Na]⁺ as 489.1652, obsd. 489.1660.

Compound 24

To a solution of compound **23** (7.5 mg, 16.1 μmol , 1.0 Eq) in super dehydrated DMF (0.4 mL) was added HOBt (3.26 mg, 24.2 μmol , 1.5 Eq), HBTU (7.95 mg, 24.2 μmol , 1.5 Eq), 2- (*N*-tert-butoxycarbonylamino) ethylamine (6.20 mg, 38.6 μmol , 2.4 Eq), and DIPEA (11.2 μL , 64.4 μmol , 4.0 Eq). The mixture was stirred at room temperature overnight. The solvent was removed via rotary evaporation, and the residue was purified by Isolera (Sfar HC Duo 10 g, MeOH/ CHCl₃: 0 % =>20 %) to give compound **24** (8.19 mg, 13.4 μmol , yield: 83.2 %) as pale-yellow oil. **¹H-NMR** (400 MHz, CDCl₃): δ /ppm 7.88 (s, 1H), 7.82 (d, J = 8.6 Hz, 1H), 7.71 (t, J = 7.7 Hz, 1H), 7.51 (d, J = 7.7 Hz, 1H), 7.35 (d, J = 7.7 Hz, 1H), 6.95 (d, J = 7.9 Hz, 1H), 5.55 (d, J = 47.8 Hz, 2H), 5.25 (s, 2H), 3.83 (s, 2H), 3.55 (q, J = 5.3 Hz, 2H), 3.42–3.38 (m, 2H), 2.82–2.78 (m, 4H), 2.68–2.64 (m, 4H), 2.51 (q, J = 7.4 Hz, 4H), 1.43 (s, 9H), 1.23 (t, J = 7.4 Hz, 6H). **ESI-MS**: cald. For [M+H]⁺ as 609.2939, obsd. 609.2948.

FL-O3

To a solution of compound **24** (8.19 mg, 13.5 μmol , 1.0 Eq) in super dehydrated CH_2Cl_2 (0.2 mL) was added TFA (0.1 mL)-containing super dehydrated CH_2Cl_2 (0.3 mL) dropwise on ice. The reaction mixture was stirred on ice for 1 h. The solvent was co-evaporated with toluene (2 mL \times 2) and dried in vacuo to give the deprotected product as a pale yellow oil. The product was used for the next step without further purification. To a solution of the deprotected product in super dehydrated DMF (0.4 mL) was added FL-NHS (9.1 mg, 19.2 μmol , 1.4 Eq) and TEA (7.52 μL , 54.0 μmol , 4.0 Eq). The mixture was stirred at room temperature for 2 h. Then additional triethylamine (TEA) (3.0 μL , 21.5 μmol , 1.6 Eq) was added, and the mixture was stirred at room temperature for 1 h. After removing the solvent via evaporation, the residue was dissolved in 4 mL of $\text{CH}_3\text{CN}/\text{H}_2\text{O}$ (3/7; with 0.1 % TFA), filtered with 0.20 μm syringe filter, and then purified by RP-HPLC (A: B= 30/70= \Rightarrow 60/40 (30 min)). The fractions that contain the target compound were collected and freeze-dried overnight to give **FL-O3** (6.71 mg, 7.74 μmol , yield: 57.3 %) as orange solids. **$^1\text{H-NMR}$** (400 MHz, CD_3OD): δ /ppm 8.38 (s, 1H), 8.17 (dd, J = 8.1, 1.5 Hz, 1H), 7.98–7.93 (m, 2H), 7.88 (d, J = 8.8 Hz, 1H), 7.65 (d, J = 7.7 Hz, 1H), 7.47 (d, J = 7.5 Hz, 1H), 7.29 (d, J = 8.1 Hz, 1H), 7.13 (d, J = 8.8 Hz, 1H), 6.71 (d, J = 2.2 Hz, 2H), 6.60 (d, J = 8.8 Hz, 2H), 6.54 (dd, J = 8.8, 2.4 Hz, 2H), 5.54 (d, J = 47.8 Hz, 2H), 5.38 (s, 2H), 4.67 (s, 2H), 3.65 (s, 4H), 3.52 (t, J = 7.2 Hz, 4H), 2.95 (t, J = 7.1 Hz, 4H), 2.52 (q, J = 7.4 Hz, 4H), 1.19 (t, J = 7.4 Hz, 6H). **ESI-MS**: cald. For $[\text{M}+\text{H}]^+$ as 867.2892, obsd. 867.2894.



Scheme 8 Synthetic scheme of **AcFL-O3**.

AcFL-O3

To compound **23** (3.0 mg, 6.4 μmol , 1.0 Eq) in super dehydrated DMF (285 μL) was added with HOBt· H_2O (1.5 mg, 9.8 μmol , 1.5 Eq), HBTU (3.6 mg, 9.5 μmol , 1.5 Eq), and compound **5** (5.0 mg, 10.0 μmol , 1.5 Eq), and DIPEA (5.6.0 μL , 32 μmol , 5.0 Eq). The mixture was stirred at room

temperature overnight. The mixture was concentrated via evaporation and diluted with CH₃CN/H₂O/DMF (1/1/0.3; 0.1 % TFA), filtered via 0.45 μm filter, and loaded on RP-HPLC for purification (A : B: 20/80=> 80/20 (60 min) => 100/0 (5 min) => 20/80 (5 min)). The fractions that contained the target compound were collected and freeze-dried overnight to give **AcFL-O3** (0.86 mg, 0.91 μmol, yield: 14.1 %) as pale-white solids. **¹H-NMR for AcFL-O3** (400 MHz; CDCl₃): δ/ppm 8.42 (s, 1 H), 8.17 (d, 1 H, *J* = 8.4 Hz), 7.90 (s, 1 H), 7.84 (t, 1 H, *J* = 8.0 Hz), 7.75 (brs, 1 H), 7.56(d, 1 H, *J* = 8.4 Hz), 7.44 (d, 1 H, *J* = 8.0 Hz), 7.11 (d, 1 H, *J* = 2.0 Hz), 7.03 (brs, 1 H), 6.83-6.78 (m, 4 H), 5.56 (d, 2 H, *J* = 47.6 Hz), 5.30 (s, 2 H), 4.46 (s, 2 H), 3.76 (s, 4H), 3.40-3.36 (m, 4 H), 2.94-2.90 (m, 4 H), 2.53 (q, 4 H, *J* = 7.6 Hz), 2.32 (s, 6 H), 1.21 (t, 6 H, *J* = 7.6 Hz). **ESI-MS**: cald. For [M+H]⁺ as 951.3103, obsd. 951.3104; cald. For [M+Na]⁺ as 973.2923, obsd. 973.2923.;

Reference

- 1 Festa, R. A. & Thiele, D. J. Copper: an essential metal in biology. *Curr Biol* **21**, R877-883 (2011). <https://doi.org:10.1016/j.cub.2011.09.040>
- 2 Kim, B.-E. *et al.* Mechanisms for copper acquisition, distribution and regulation. *Nat Chem Biol* **4**, 176-185 (2008). <https://doi.org:10.1038/nchembio.72>
- 3 Tsang, T., Davis, C. I. & Brady, D. C. Copper biology. *Current Biology* **31**, R421-R427 (2021). <https://doi.org:10.1016/j.cub.2021.03.054>
- 4 Ackerman, C. M., Lee, S. & Chang, C. J. Analytical Methods for Imaging Metals in Biology: From Transition Metal Metabolism to Transition Metal Signaling. *Analytical Chemistry* **89**, 22-41 (2017). <https://doi.org:10.1021/acs.analchem.6b04631>
- 5 Banci, L. *et al.* Affinity gradients drive copper to cellular destinations. *Nature* **465**, 645-648 (2010). <https://doi.org:10.1038/nature09018>
- 6 Grubman, A. & White, A. R. Copper as a key regulator of cell signalling pathways. *Expert Rev Mol Med* **16**, e11 (2014). <https://doi.org:10.1017/erm.2014.11>
- 7 Falcone, E. *et al.* Extracellular Cu²⁺ pools and their detection: From current knowledge to next-generation probes. *Coordination Chemistry Reviews* **433** (2021). <https://doi.org:10.1016/j.ccr.2020.213727>
- 8 Cotruvo, J. A., Jr., Aron, A. T., Ramos-Torres, K. M. & Chang, C. J. Synthetic fluorescent probes for studying copper in biological systems. *Chem Soc Rev* **44**, 4400-4414 (2015). <https://doi.org:10.1039/c4cs00346b>
- 9 Zeng, L., Miller, E. W., Pralle, A., Isacoff, E. Y. & Chang, C. J. A selective turn-on fluorescent sensor for imaging copper in living cells. *Journal of the American Chemical Society* **128**, 10-11 (2006). <https://doi.org:10.1021/ja055064u>
- 10 Xiao, T. *et al.* Copper regulates rest-activity cycles through the locus coeruleus-norepinephrine system. *Nat Chem Biol* **14**, 655-663 (2018). <https://doi.org:10.1038/s41589-018-0062-z>
- 11 Chung, C. Y. *et al.* Activity-based ratiometric FRET probe reveals oncogene-driven changes in labile copper pools induced by altered glutathione metabolism. *Proc Natl Acad Sci U S A* **116**, 18285-18294 (2019). <https://doi.org:10.1073/pnas.1904610116>
- 12 Taki, M., Iyoshi, S., Ojida, A., Hamachi, I. & Yamamoto, Y. Development of highly sensitive fluorescent probes for detection of intracellular copper(I) in living systems. *J Am Chem Soc* **132**, 5938-5939 (2010). <https://doi.org:10.1021/ja100714p>
- 13 Lee, S. *et al.* Activity-Based Sensing with a Metal-Directed Acyl Imidazole Strategy Reveals Cell Type-Dependent Pools of Labile Brain Copper. *J Am Chem Soc* **142**, 14993-15003 (2020). <https://doi.org:10.1021/jacs.0c05727>
- 14 Pezacki, A. T. *et al.* Oxidation state-specific fluorescent copper sensors reveal oncogene-driven redox changes that regulate labile copper(II) pools. *Proc Natl Acad Sci U S A* **119**, e2202736119 (2022). <https://doi.org:10.1073/pnas.2202736119>
- 15 Miki, T. *et al.* A conditional proteomics approach to identify proteins involved in zinc homeostasis. *Nat Methods* **13**, 931-937 (2016). <https://doi.org:10.1038/nmeth.3998>
- 16 Ambundo, E. A. *et al.* Influence of coordination geometry upon copper(II/I) redox potentials. Physical parameters for twelve copper tripodal ligand complexes. *Inorganic Chemistry* **38**, 4233-4242 (1999). <https://doi.org:DOI 10.1021/ic990334t>
- 17 Toteva, M. M. & Richard, J. P. The Generation and Reactions of Quinone Methides. *Adv Phys Org Chem* **45**, 39-91 (2011). <https://doi.org:10.1016/B978-0-12-386047-7.00002-3>

- 18 Ali, K. *et al.* Reactivity vs. selectivity of quinone methides: synthesis of pharmaceutically important molecules, toxicity and biological applications. *Chem Commun (Camb)* **58**, 6160-6175 (2022). <https://doi.org:10.1039/d2cc00838f>
- 19 Yu, K. K., Li, K., Hou, J. T. & Yu, X. Q. Coumarin-TPA derivative: a reaction-based ratiometric fluorescent probe for Cu(I). *Tetrahedron Letters* **54**, 5771-5774 (2013). <https://doi.org:10.1016/j.tetlet.2013.08.046>
- 20 Zhu, H. *et al.* Imaging and Profiling of Proteins under Oxidative Conditions in Cells and Tissues by Hydrogen-Peroxide-Responsive Labeling. *Journal of the American Chemical Society* **142**, 15711-15721 (2020). <https://doi.org:10.1021/jacs.0c02547>
- 21 Menshikova, E. V., Cheong, E. & Salama, G. Low N-ethylmaleimide concentrations activate ryanodine receptors by a reversible interaction, not an alkylation of critical thiols. *J Biol Chem* **275**, 36775-36780 (2000). <https://doi.org:10.1074/jbc.C000367200>
- 22 Raycroft, M. A. R., Racine, K. E., Rowley, C. N. & Keillor, J. W. Mechanisms of Alkyl and Aryl Thiol Addition to N-Methylmaleimide. *J Org Chem* **83**, 11674-11685 (2018). <https://doi.org:10.1021/acs.joc.8b01638>
- 23 Inarrea, P. *et al.* Redox activation of mitochondrial intermembrane space Cu,Zn-superoxide dismutase. *Biochem J* **387**, 203-209 (2005). <https://doi.org:10.1042/BJ20041683>
- 24 Baldwin, A. D. & Kiick, K. L. Tunable degradation of maleimide-thiol adducts in reducing environments. *Bioconjug Chem* **22**, 1946-1953 (2011). <https://doi.org:10.1021/bc200148v>
- 25 Davis, A. V. & O'Halloran, T. V. A place for thioether chemistry in cellular copper ion recognition and trafficking. *Nat Chem Biol* **4**, 148-151 (2008). <https://doi.org:10.1038/nchembio0308-148>
- 26 Rosenzweig, A. C. Copper Delivery by Metallochaperone Proteins. *Accounts of Chemical Research* **34**, 119-128 (2001). <https://doi.org:10.1021/ar000012p>
- 27 Morgan, M. T., Nguyen, L. A. H., Hancock, H. L. & Fahrni, C. J. Glutathione limits aquacopper(I) to sub-femtomolar concentrations through cooperative assembly of a tetranuclear cluster. *J Biol Chem* **292**, 21558-21567 (2017). <https://doi.org:10.1074/jbc.M117.817452>
- 28 Hatori, Y., Inouye, S. & Akagi, R. Thiol-based copper handling by the copper chaperone Atox1. *IUBMB Life* **69**, 246-254 (2017). <https://doi.org:10.1002/iub.1620>
- 29 Petris, M. J., Smith, K., Lee, J. & Thiele, D. J. Copper-stimulated endocytosis and degradation of the human copper transporter, hCtr1. *J Biol Chem* **278**, 9639-9646 (2003). <https://doi.org:10.1074/jbc.M209455200>
- 30 Wakayama, S. *et al.* Chemical labelling for visualizing native AMPA receptors in live neurons. *Nat Commun* **8**, 14850 (2017). <https://doi.org:10.1038/ncomms14850>

Chapter 3

Imaging and profiling of proteome in response to intracellular cuprous ions in the living ATP7A knockout cells

Abstract

An optimal Cu⁺-responsive protein labeling reagent (CuR) has been developed to detect elevated intracellular Cu⁺ levels in live cells, as introduced in Chapter 2. This chapter explores the reagent's additional uses in different cell models to assess its reliability and investigate the intracellular regulation of labile Cu⁺. The ATP7A, a copper-transporting ATPase, plays a critical role in copper transport, and mutations in ATP7A can lead to the development of clinical syndromes. Utilizing live cell or *in vivo* models of ATP7A mutants and knockout (KO) is valuable in exploring the biological roles of ATP7A. The CuR tool, in combination with downstream analyses such as imaging and proteomics, can facilitate the study of proteins involved in copper misregulation in biological models with impaired ATP7A function. Cu(gtsm) is a copper complex that has the ability to penetrate cell membranes. Once inside a cell, it can be reduced to Cu⁺ and transferred to Cu⁺ sinks. I hypothesize that proteins labeled by CuR in Cu(gtsm)-supplemented ATP7A wild-type (WT) and ATP7A KO cells could provide insights into intracellular Cu⁺ regulation. Therefore, we prepared the ATP7A KO cell model and utilized the optimal CuR tool in the cells to assess its robustness in different cell models. I also conducted proteomics studies to identify and compare the labeled proteins in Cu-supplemented ATP7A WT and ATP7A KO cells to explore copper regulation changes. The results demonstrated the applicability of the CuR tool in different cell models. The CuR tool exhibited advantages over the ICP-Mass method and demonstrated specificity for Cu-concentrated cells. Additionally, the proteomics study suggested *in situ* interactions of cuproptosis proteins with Cu⁺ and highlighted the potential roles of the MXXXM motif in responding to toxic intracellular Cu⁺ levels, providing valuable insights into Cu⁺ regulation, trafficking, and export within living cells.

Introduction

In Chapter 2, an optimal Cu^+ -responsive protein labeling reagent (CuR) -P2- was developed and effectively utilized to detect elevated intracellular labile Cu^+ levels in live cells. This chapter focuses on further applications of the reagent in different cell models to assess its robustness and explore the intracellular regulation of accumulated labile Cu^+ .

The ATP7A, a P-type ATPase copper-transporting ATPase 1, is the primary copper exporter protein expressed ubiquitously across mammalian tissues.¹ It resides in the *trans*-Golgi network, transports copper into this compartment to integrate into secretory copper enzymes, and moves to the cytoplasmic membrane to eliminate excess copper, maintaining intracellular copper levels.^{2,3,4,5} Mutations in ATP7A lead to impaired copper transport and are associated with the development of three distinct clinical syndromes: Menke's disease, occipital horn syndrome (OHS), and isolated distal motor neuropathy.^{2,6,7} Although the fundamental pathway of copper ion transport and export via ATP7A has been reasonably well-established,^{2,5,8,9} the precise mechanisms governing the physiological and pathological roles of ATP7A remain insufficiently understood. Live cell or *in vivo* models of ATP7A mutants and knockout (KO) are valuable in exploring the biological roles of ATP7A using a combination of various biochemical methods and techniques. These models enable researchers to gain insights into ATP7A interactome and crosstalk with other proteins,^{10,11,12} changes in ATP7A localization,¹³ regulation of copper levels,^{2,14} and ATP7A trafficking,¹² as well as the organ-specific abundance of ATP7A,¹⁵ and its interaction with pathologies such as embryogenesis and redox balance change in mitochondria.^{16,17} However, these methods and techniques do not allow real-time, *in situ*, simultaneous detection of dynamic changes in copper levels and proteins at the site of significant changes in copper levels in living biological systems. Achieving this would likely enhance our understanding of the proteins involved in copper misregulation in live biological models with impaired ATP7A function. Therefore, the Cu^+ -responsive protein labeling tool (CuR) that I have developed, in conjunction with downstream analyses such as imaging and proteomics, can facilitate this endeavor.

Bis(thiosemicarbazones) complexes of copper belong to the typical class of Cu(II) complexes and have been utilized in copper supplementation to study biological copper roles, as well as in the treatment of copper-depletion-related diseases and copper overload for anti-cancer therapy.^{18,19,20,21,22,23,24} Glyoxal-bis(N(4)-methylthiosemicarbazonato)-copper(II) (i.e., $\text{Cu}^{\text{II}}(\text{gtsm})$ or $\text{Cu}(\text{gtsm})$) is part of the Cu(II) bis(thiosemicarbazones) class, and its ability to efficiently

penetrate cell membranes is attributed to the high lipid solubility of its bis(thiosemicarbazone) ligand.^{22,25,26} Once inside the cell, Cu^{II}(gtsm) can be reduced to Cu⁺ by cellular reductants, resulting in the formation of the less stable Cu^I(gtsm) due to its higher lability compared to Cu^{II}(gtsm).^{26,27} The resulting Cu⁺ can then be transferred to Cu⁺ sinks with a higher affinity for Cu⁺, such as cellular apo-Cu⁺-regulating proteins that can bind Cu⁺ more effectively (K_d 10⁻¹³ M ~ 10⁻¹⁹ M).^{27,28,29,30,31} It is worth noting that GSH (K_d = 9.1 × 10⁻¹² M)²⁹ exhibits less affinity for Cu⁺ compared to gtsmH₂, which makes the reductive transfer of Cu⁺ from Cu^I(gtsm) to Cu⁺ sinks more likely to occur. Additionally, the endogenous reductant GSH is inefficient at reducing Cu^{II}(gtsm) but can induce a faster reductive transfer of Cu⁺ to Cu⁺ sinks.^{27,32,33} *In vitro* kinetics studies have shown that the t_{1/2} of the reductive transfer of Cu⁺ from Cu^{II}(gtsm) to Zn7MT-1 (K_d of MTs 10⁻¹⁵ ~ 10⁻²⁰ M) and BCS (K_d ~ 10^{-19.8} M) is approximately 50 minutes and around 3 minutes, respectively.^{27,33} Furthermore, our CuR tool has the capability to compete with GSH for Cu⁺ and label the proteins, as proved in Chapter 2.

Based on the information above, I hypothesize that the proteins labeled by CuR in the Cu(gtsm)-supplemented cells could offer insights into proteins associated with intracellular Cu⁺ regulation. Furthermore, ATP7A KO cells provide a genetic model of copper misregulation, characterized by the lack of export of excessive Cu⁺ by ATP7A. It would be enlightening to compare the intracellular elevated labile Cu⁺-responsive labeled proteins by CuR in the Cu(gtsm)-supplemented ATP7A wild-type (WT) and ATP7A KO cells to explore how Cu⁺ regulation occurs with and without the roles of ATP7A. Additionally, in addition to comparing the labeled proteins in the ATP7A WT and ATP7A KO cells, I also investigated whether allowing cells time to export excessive Cu⁺ by inserting intervals between Cu supplementation and labeling may provide insightful information about Cu⁺ export in cells with and without genetic copper misregulation by comparing the profiled proteins.

In this chapter, an ATP7A KO cell model was prepared and Cu(gtsm) was used for Cu-supplementation in subsequent studies. Optimal CuR -P2- was applied to the cells to assess the tool's robustness in different cell models. Co-cultured ATP7A WT and ATP7A KO cells were also tested to determine whether the reagent could differentiate ATP7A KO cells with higher intracellular Cu⁺ levels from ATP7A WT cells with lower intracellular Cu⁺ levels. Furthermore, proteomics studies were conducted to identify and analyze the proteins labeled by the reagent in ATP7A KO and ATP7A WT cells.

Results and Discussion

Application of P2 in ATP7A KO cells

I utilized the optimal CuR, AcFL-appended P2, on a prepared genetic model of copper dysregulation induced by knockout (KO) of ATP7A, a copper-translocating P-type ATPase that regulates copper export.^{8,9} It is widely acknowledged that a loss of ATP7A function results in impaired extracellular copper secretion and subsequent intracellular copper accumulation, ultimately contributing to the pathogenesis of a few diseases.² As anticipated, the reagent was promptly taken up by living cells, fluoresced upon removal of the acetyl group by endogenous esterases, and was evenly distributed across the entire cell, making it suitable for unbiased protein labeling and Cu⁺ detection in these cell models (**Figure 3.1a**). The ATP7A KO³⁴ and ATP7A WT human melanoma Mewo cells were first treated with the cell-permeable Cu(gtsm) complex to raise intracellular copper levels in a short time (30 min). After that, they were incubated with P2 for labeling. The increased concentration of labile Cu⁺ in ATP7A-KO cells was confirmed through both SDS-PAGE and CLSM analysis, while ATP7A WT cells showed a weaker signal, indicating the involvement of ATP7A in the regulation of intracellular excess labile copper ions (**Figure 3.1b, 3.1c**). Quantitative imaging analysis revealed discernible differences in the naturally low basal labile Cu⁺ levels in the ATP7A KO and ATP7A WT cells (**Figure 3.2b, 3.2c**). Similar results were obtained using a well-established Cu⁺ chemosensor-CopperGREEN (**Figure 3.3**), confirming the responsiveness of P2 to intracellular elevated labile Cu⁺. We also conducted ICP-MS (Inductively coupled plasma mass spectrometry) analysis to investigate changes in the total copper levels, including bound and labile Cu⁺ and Cu²⁺, in ATP7A WT and ATP7A KO cells with and without Cu(gtsm) treatment. The findings revealed that ATP7A knockout increased total physiological copper levels compared to ATP7A WT cells, indicating enhanced Cu accumulation during cell subculture due to impaired copper export in genetically misregulated cells. Additionally, Cu(gtsm) treatment comparably increased intracellular total copper levels in both ATP7A KO and ATP7A WT cells, suggesting that Cu import primarily occurred during 30 minutes of Cu(gtsm) pretreatment while Cu export did not significantly contribute during this short timeframe (**Figure 3.2a**). These results demonstrate the responsive capability of P2 to labile Cu⁺ and underscore the advantages of using Cu⁺-responsive probes or protein labeling reagents over ICP-MS in their ability to detect labile Cu⁺. In summary, P2 can detect slightly elevated intracellular physiological labile Cu⁺ levels in cells with ATP7A misregulation, significantly increased labile Cu⁺ levels in

cells under Cu(gtsm) supplementation, and notably elevated labile Cu^+ levels under combined ATP7A misregulation and Cu supplementation conditions.

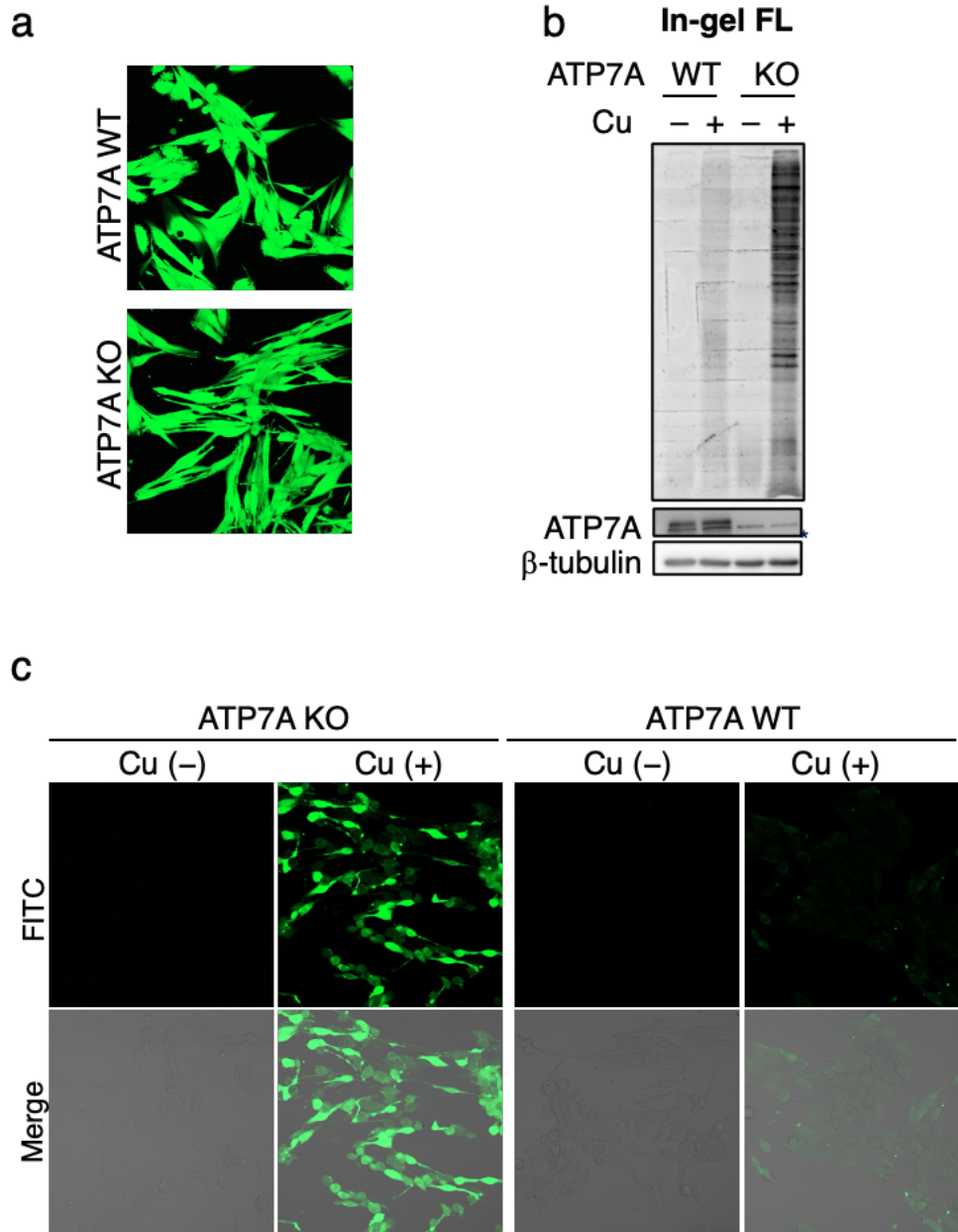


Figure 3.1 Cu^+ -responsive protein labeling with P2 in ATP7A WT and ATP7A KO cells. (a) Fluorescence imaging showing the cell permeability and uniform distribution of P2 in both ATP7A WT and ATP7A KO live Mewo cells. (b) SDS-PAGE and in-gel fluorescence analysis and (c) CLSM images of protein labeling with P2 in ATP7A WT and ATP7A KO Mewo cells. The cells were pretreated with Cu(gtsm) ($2 \mu\text{M}$) for 30 min, then washed with medium and further incubated with AcFL-appended P2 ($5 \mu\text{M}$) for 30 min. The band marked with an asterisk in (b) results from

the non-specific reactivity of the anti-ATP7A antibody. WT, wild type; KO, knockout; Cu(gtsm), glyoxal-bis(*N*(4)-methylthiosemicarbazonato)-copper(II); CLSM, confocal laser scanning microscopy; Fluorescein fluorescence images (FITC, green); Merge: FITC images were overlaid with differential interference contrast (DIC) images to give Merge images.

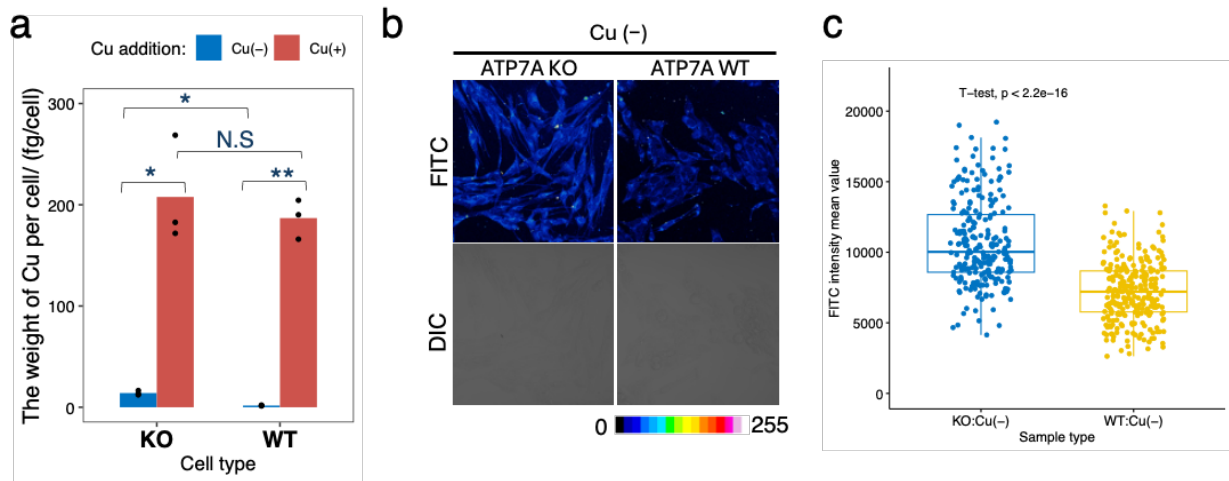


Figure 3.2 Quantitative analysis of intracellular Cu levels in the ATP7A KO and ATP7A WT cells. (a) Quantification of total copper content per ATP7A WT and ATP7A KO cells with and without Cu(gtsm)-pretreatment by inductively coupled plasma-mass spectrometry (ICP-MS). $n = 3$ biological replicates. P -values were calculated using the student t-test. N.S: $p > 0.05$, *: $0.01 < p \leq 0.05$, **: $0.001 < p \leq 0.01$. (b) Pseudocolor imaging of fluorescence intensity of AcFL-appended P2-stained ATP7A KO and ATP7A WT cells in the absence of Cu(gtsm) to give information about intracellular physiological labile Cu^+ levels. (c) Box plot of the fluorescent intensity of AcFL-appended P2-stained ATP7A KO and ATP7A WT cells in the absence of Cu(gtsm), measured using fluorescein channel ($n = 270$). The horizontal line within each box indicates the median. Boxes show interquartile range (IQR). Whiskers show $1.5 \times \text{IQR}$. The P -value was calculated by unpaired two-sided Student's t-test. Fluorescein fluorescence images (FITC channel; pseudocolor images); DIC, differential interference contrast images.

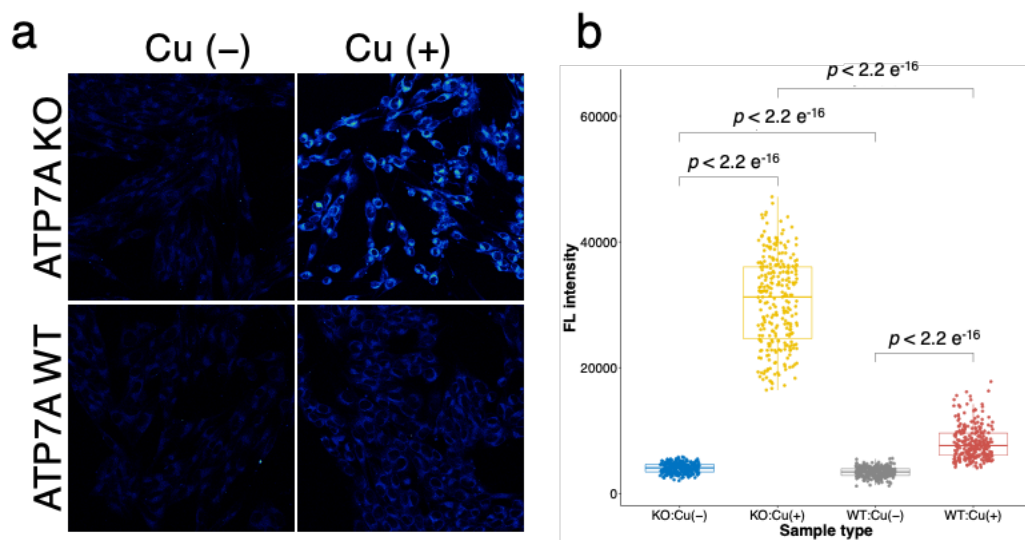


Figure 3.3 **Cu⁺-response by CopperGREEN in ATP7A WT and ATP7A KO cells.** (a) Pseudocolor imaging and (b) the quantitative analysis of the fluorescent intensity of CopperGREEN-stained by ATP7A KO and ATP7A WT Mewo cells with and without Cu(gtsm)-pretreatment. $n = 3$ biological replicates. P -values were calculated using the Student's t-test. All fluorescent intensity values are expressed as independent dots. The horizontal line within each box indicates the median. Boxes show interquartile range (IQR). Whiskers show $1.5 \times \text{IQR}$.

Application of P2 in co-cultured ATP7A KO and ATP7A WT cells

Due to the unique capability of P2 to covalently bind fluorescent tags to intracellular proteins when exposed to labile Cu⁺, it can serve as a valuable histochemical tool for distinguishing cells with relatively high labile Cu⁺ levels within a genetically diverse cell population. To illustrate this concept, I conducted a representative experiment using a mixed cell culture setup,^{35,36} wherein the cell surface of ATP7A WT cells was biotinylated and fluorescently tagged with an AlexaFluor647–streptavidin conjugate to differentiate them from non-biotinylated ATP7A KO cells (**Figure 3.4b**). Following Cu(gtsm) and P2 treatment, the mixed cell culture was examined using CLSM. As depicted in **Figures 3.4a and 3.4c**, ATP7A KO cells exhibited more intense fluorescence generated by the fluorescein-modified proteins compared to ATP7A WT cells. This observation highlights the selective labeling and fluorescent visualization of Cu⁺-accumulated cells by P2.

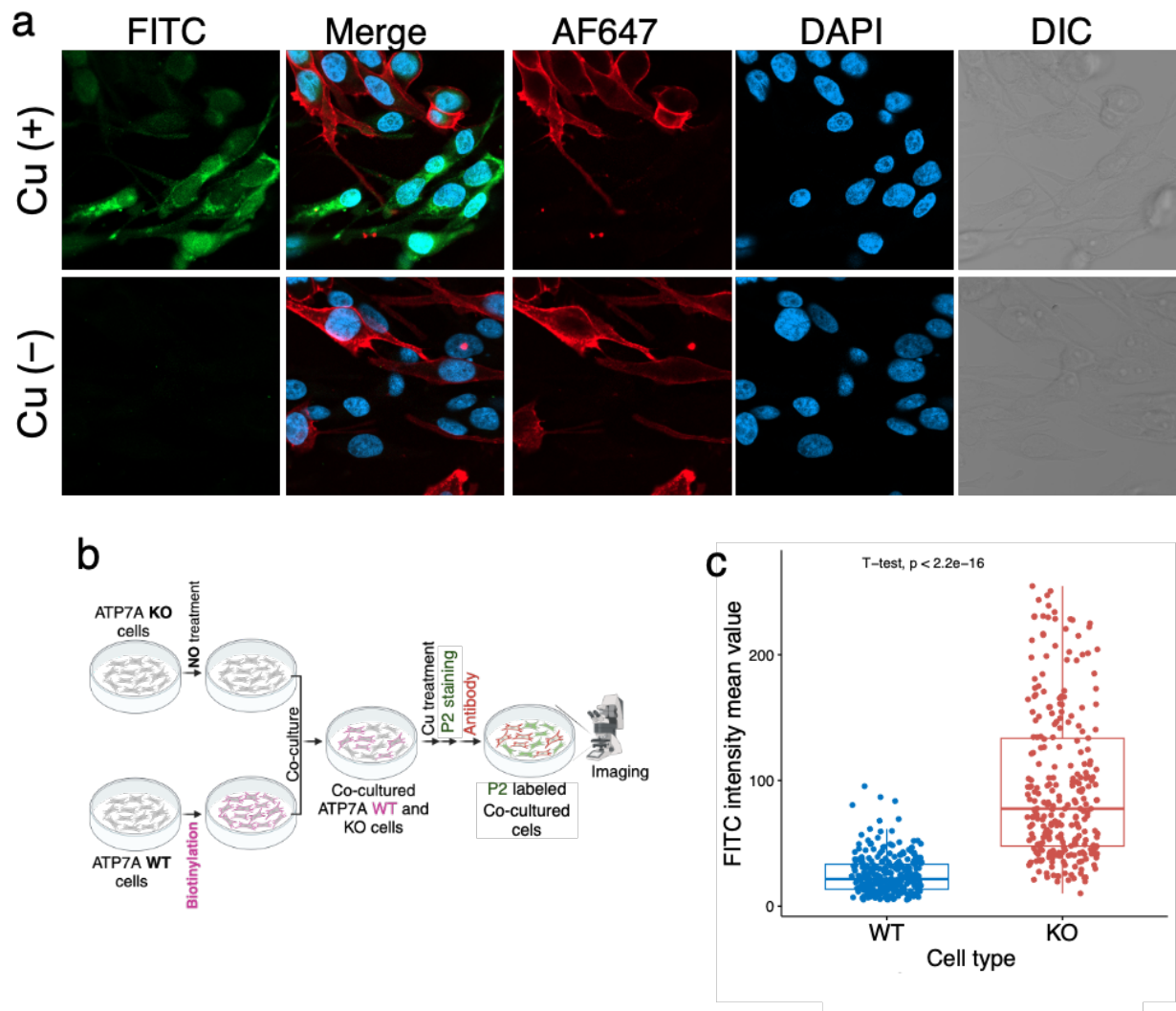


Figure 3.4 **Cu⁺-responsive protein labeling by P2 in a mixed culture system.** (a) CLSM analysis of Cu⁺-accumulated cell-specific labeling. A mixture of ATP7A-KO cells and surface-biotinylated ATP7A WT cells was treated with Cu(gtsm) (2 μ M) and subsequently incubated with AcFL-APPENDED P2 (5 μ M) for 30 min. After the reaction, the cells were fixed, treated with an AlexaFluor647–streptavidin conjugate (Av-647), and analyzed using CLSM. (b) Illustration of the workflow for Cu⁺-responsive protein labeling in a mixed culture system. (c) Box plot of the fluorescence intensity of cells, measured using a fluorescein channel ($n = 270$). The horizontal line within each box indicates the median. Boxes show interquartile range (IQR). Whiskers show $1.5 \times$ IQR. The p -value was calculated using an unpaired, two-sided Student t -test. CLSM, short for confocal laser scanning microscopy; Nuclei appear blue due to staining with DAPI solution; DAPI

stands for 4',6-Diamidino-2-phenylindole Dihydrochloride Solution; Fluorescein fluorescence images denoted with FITC are represented in green and indicate the labeling by P2; Images denoted with AF647 show AlexaFluor647 fluorescence in red, indicating cell surface-biotinylated ATP7A WT cells; Differential interference contrast images are represented as DIC; Merge images are created by overlaying FITC images (green) with DAPI images (blue) and AF647 images (red).

Proteomics study to identify labeled proteins in ATP7A KO and ATP7A WT cells

I proceeded to investigate the use of P2 for studying Cu⁺ trafficking or export in ATP7A KO cells by identifying the proteins tagged by P2. The approach involved introducing a specific time interval between Cu(gtsm) pretreatment and the labeling by P2. Subsequently, I conducted downstream analysis, including proteomics studies, to identify and compare the labeled proteins in both ATP7A WT and ATP7A KO cells with and without the inserted time interval.

I initially did the SDS-PAGE and imaging analysis to evaluate and compare the protein labeling efficiency in cells when interval time was added or not. Both PAGE and imaging results showed that the protein labeling intensity seemed to be not remarkably altered when interval time was inserted (**Figure 3.5**).

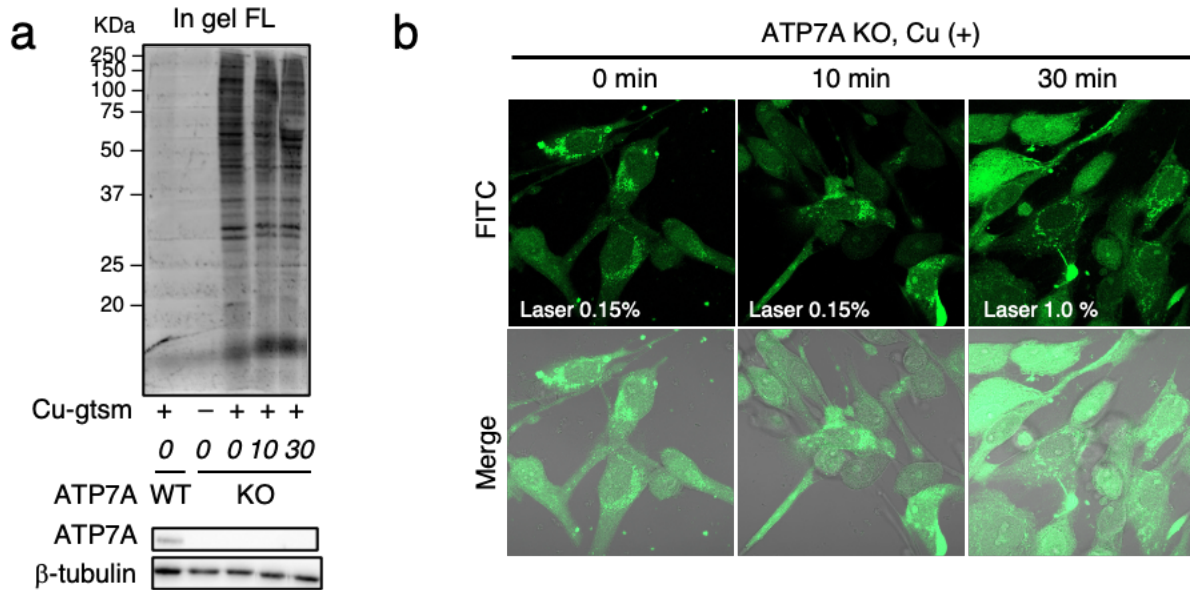


Figure 3.5 Cu⁺-responsive protein labeling by P2 in ATP7A WT and ATP7A KO live cells when the interval between Cu treatment and labeling was added. (a) SDS-PAGE and in-gel fluorescence analysis of labeled proteins in the ATP7A WT and ATP7A KO cells when inserting the varying interval time (0- 30 min) between Cu(gtsm)-treatment and labeling. (b) CLSM images

of Cu(gtsm)-pretreated ATP7A KO cells after labeling when the varying interval time (0- 30 min) between Cu(gtsm)-treatment and labeling was applied. CLSM, confocal laser scanning microscopy; FITC, Fluorescein fluorescence images (green); Merge: FITC images were overlaid with differential interference contrast images (DIC) to give Merge images.

I then performed proteomics analysis to identify and compare the labeled proteins in Cu-treated ATP7A WT and ATP7A KO cells when inserting 0-minute and 30-minute interval times between Cu(gtsm) treatment and labeling. The investigations aimed to shed light on the proteins potentially involved in the trafficking or regulation of excess intracellular labile Cu^+ . The labeled proteins were enriched via immunoprecipitation using an anti-fluorescein antibody, digested with trypsin, and then subjected to analysis using liquid chromatography-tandem mass spectrometry (LC-MS/MS) (**Figure 3.6a**). Label-free quantification was employed in the mass spectrometry analysis to observe the dynamic changes in protein labeling induced by exogenous copper in comparison to the basal (non-copper-treated) condition (**Figure 3.6a**).

I conducted an analysis on three independent biological replicates for each sample, resulting in four proteomics datasets: WT_0min, WT_30min, KO_0min, and KO_30min. Initially, I compared the distribution of abundance ratios of proteins in each dataset (**Figure 3.6b**) and then identified significantly labeled proteins using cutoff criteria (number of identified peptides ≥ 2 , fold change ($\text{Cu}(+)/\text{Cu}(-)$) ≥ 2 , and p -value < 0.05). The size of each proteomics dataset of the significantly labeled proteins was compared (**Figure 3.6c**) and used for subsequent analysis. With this approach, I identified a total of 60 and 547 proteins in ATP7A WT and ATP7A KO cells, respectively, when a 0-minute interval was applied between Cu treatment and labeling (**Figure 3.6c**). Similarly, 293 and 325 proteins were identified in ATP7A WT and ATP7A KO cells, respectively, when a 30-minute interval was applied (**Figure 3.6c**). The larger number of proteins detected in ATP7A KO cells than in ATP7A WT cells aligns with the gel- and imaging-based analyses (**Figure 3.1b, 3.5a**). Interestingly, the number of labeled proteins detected in the ATP7A WT cells when a 30-minute interval was applied was significantly larger than when a 0-minute interval was used, which was not observed in the gel-based analysis (**Figure 3.6c**; the in-gel FL result of the labeling in Cu-treated ATP7A WT cells when a 30 min interval was added is not shown). This indicates that high-sensitivity LC-MS/MS may detect small amounts of significantly labeled proteins compared to low-resolution gel-based analysis.

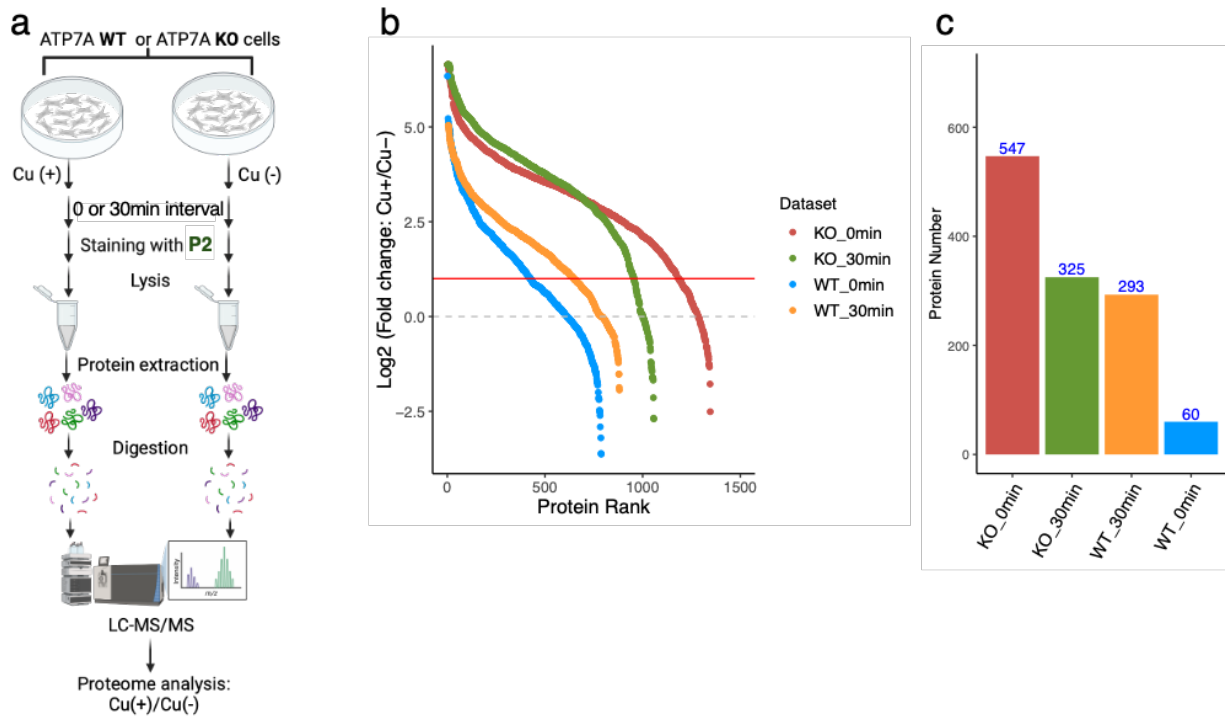


Figure 3.6 Proteomics study of the proteins labeled by P2 in the Cu(gtsm)-pretreated ATP7A WT and ATP7A KO cells for obtaining CuR proteomics dataset. (a) Illustration of the workflow for label-free quantitative analysis of the proteins labeled by AcFL-appended P2 using LC-MS/MS. $n = 3$ biological replicates. (b) The distribution of the fold change of all the labeled proteins (number of identified peptides ≥ 2) detected by LC-MS/MS in each obtained proteomics dataset. (c) The number of the significantly labeled proteins in each proteomics dataset. The criteria set for the significantly labeled proteins is fold change (Cu(+)/Cu(-)) ≥ 2 , number of identified peptides ≥ 2 , and $p < 0.05$. CuR, Cu⁺-responsive protein labeling reagents; CuR proteomics dataset, the proteomics dataset of the labeled proteins by P2 obtained by proteomics study illustrated in (a); KO_0min, one CuR proteomics dataset that represents the labeled proteins detected in Cu(gtsm)-treated ATP7A KO cells when 0 min-interval was inserted between Cu-treatment and labeling; KO_30min, one CuR proteomics dataset that represents the labeled proteins detected in Cu(gtsm)-treated ATP7A KO cells when 30 min-interval was inserted between Cu-treatment and labeling; WT_0min, one CuR proteomics dataset that represents the labeled proteins detected in Cu(gtsm)-treated ATP7A WT cells when 0 min-interval was inserted between Cu-treatment and labeling; WT_30min, one CuR proteomics dataset that represents the labeled proteins detected in

Cu(gtsm)-treated ATP7A WT cells when 30 min-interval was inserted between Cu-treatment and labeling.

I thoroughly examined the proteins labeled in the two datasets obtained from ATP7A WT cells: WT_0min and WT_30 min datasets (**Figure 3.7**). The volcano plots illustrated the distribution of proteins based on the abundance ratio and *p*-value in each dataset (**Figure 3.7a, 3.7b**). The WT_0min dataset showed that more background proteins were eliminated by the cutoff criteria than in the WT_30min dataset. This explains why more significantly labeled proteins were detected in the WT_30min than in the WT_0min dataset. The overlapping proteins above the threshold in the two datasets indicated that many proteins in WT_0min are also common in the WT_30min dataset (**Figure 3.7c**). The correlation plot demonstrated that most common proteins have similar fold change values, while a few proteins, exhibited higher fold change in the WT_0min dataset, suggesting their association with the regulation of excessive Cu⁺ (**Figure 3.7d**). Additionally, I performed a Gene Ontology (GO) enrichment analysis of the cellular components of the significantly labeled proteins in the two datasets (**Figure 3.7e**). This analysis provided insights into intracellular Cu⁺ metabolism. For instance, proteins in extracellular exosome, vesicle, rough ER, and mitochondria were more enriched in the WT_30min dataset compared to the WT_0min dataset, indicating the sequestration and concentration of copper in these intracellular compartments for subsequent excretion. Proteins in the nucleus and ribonucleoprotein complex were more enriched in the WT_30min dataset compared to the WT_0min dataset, suggesting that the export of excessive copper may be regulated by the interaction of proteins in these cellular components with excessive Cu⁺. Furthermore, cytosolic proteins were more enriched in the WT_30min dataset, indicating that the efflux of excessive copper leads to increased labile copper in the cytosol in a time-dependent manner.

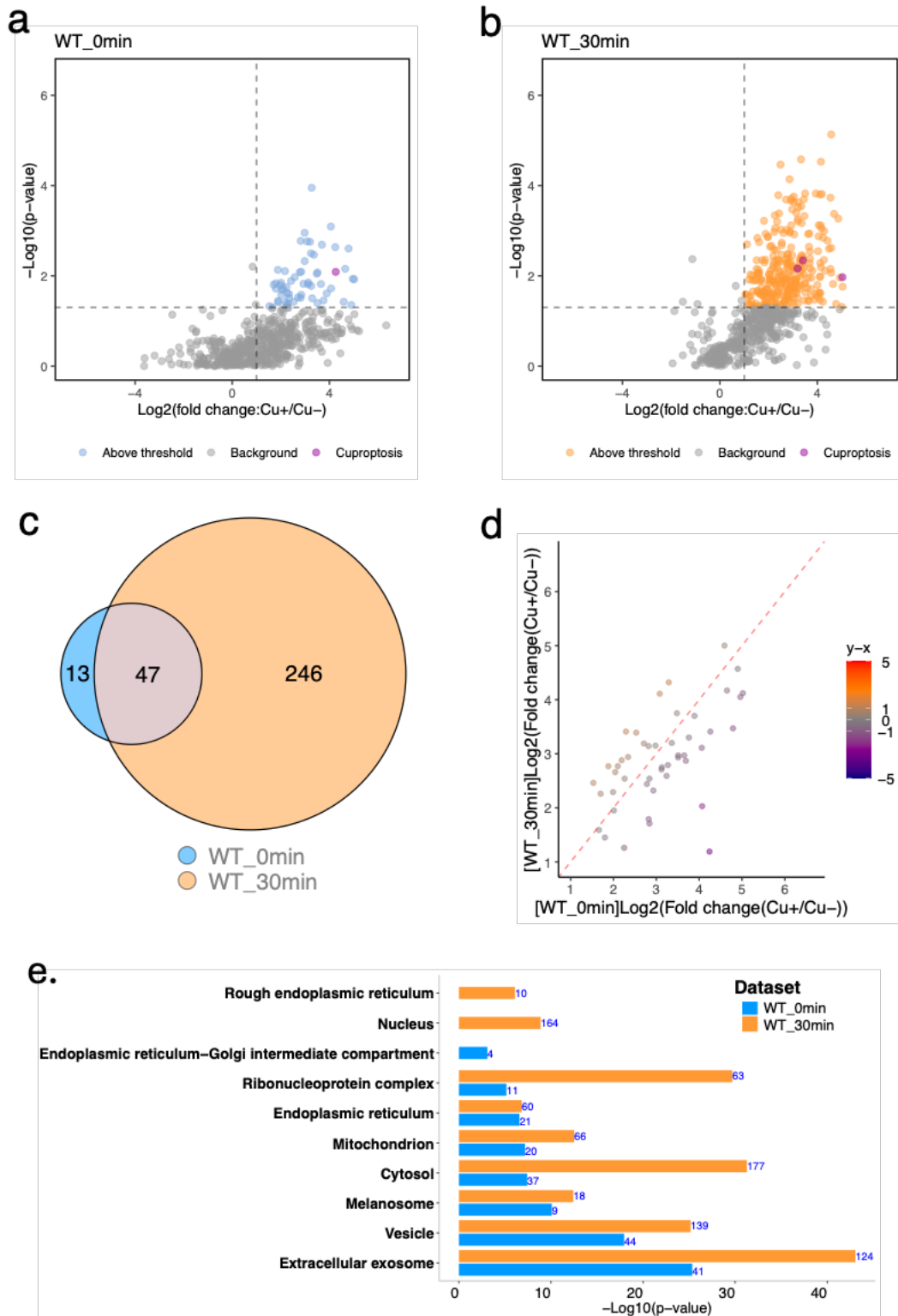


Figure 3.7 Compare the significantly labeled proteins in the Cu-pretreated ATP7A WT cells when adding 0 min-interval (WT_0min dataset) and 30 min-interval time (WT_30min

dataset) between Cu-treatment and labeling. (a, b) Volcano plots of (a) WT_0min and (b) WT_30min proteomics dataset. The horizontal dashed line indicates p -value = 0.05, and the vertical dashed lines denote fold-change = 2. The cuproptosis-associated proteins above the threshold are shown in magenta color. The threshold, the so-called criteria of the significantly labeled proteins, is set as the number of identified peptides ≥ 2 , fold change ≥ 2 , and p -value < 0.05 . (c) Venn diagram of the significantly labeled proteins in the two proteomic datasets. (d) Scatter plots of $\text{Log}_2(\text{fold change (Cu}^+/\text{Cu}^-))$ of the common significantly labeled proteins in the two proteomic datasets. (e) The GO enrichment analysis of the cellular components of the significantly labeled proteins in two proteomics datasets. The number of the significantly labeled proteins enriched in each cellular component in the corresponding dataset is displayed at the top of the bar.

I proceeded to analyze the significantly labeled proteins identified in the two datasets from ATP7A KO cells: KO_0min and KO_30min datasets (**Figure 3.8**). The distribution of proteins based on abundance ratio and p -value in each dataset was visualized in volcano plots, revealing that more proteins exhibited higher fold change values in KO_30min compared to KO_0min (**Figure 3.8a, 3.8b**). Additionally, most proteins in the KO_30min dataset were also present in the KO_0min dataset (**Figure 3.8c**), and the fold change analysis of the common proteins showed that more of them displayed higher fold change in the KO_30min dataset compared to the KO_0min dataset (**Figure 3.8d**). This may indicate time-dependent changes in Cu^+ regulation or trafficking. Furthermore, I conducted a Gene Ontology (GO) enrichment analysis of the cellular components of the significantly labeled proteins in the two datasets to acquire insights into intracellular Cu^+ metabolism in ATP7A KO cells (**Figure 3.8e**). Notably, I found that proteins in the KO_0min dataset were more enriched in mitochondria but less enriched in melanosome compared to proteins in the KO_30min dataset, suggesting a time-dependent shift in Cu^+ regulation from mitochondria to melanosome.

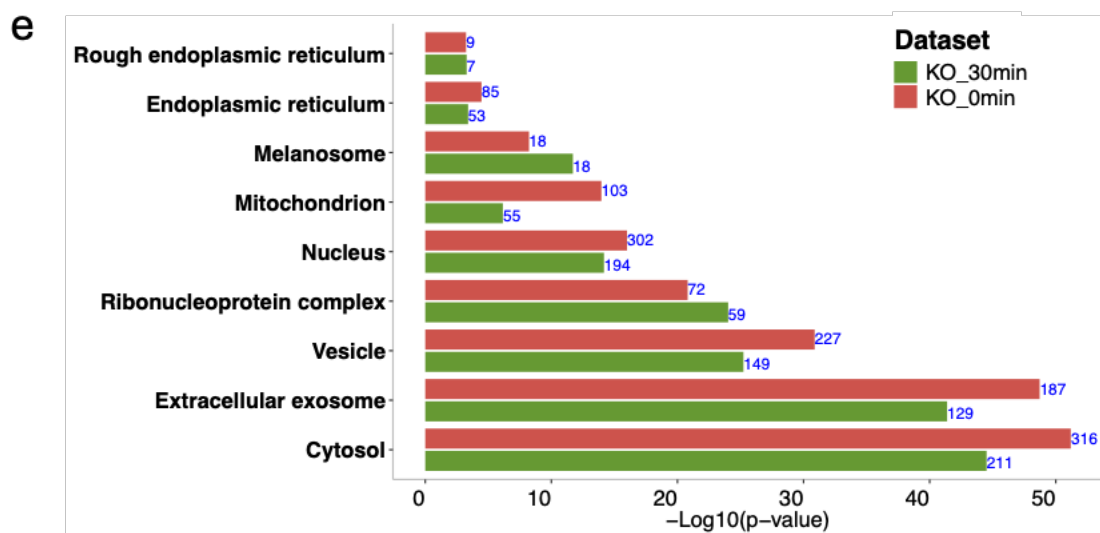
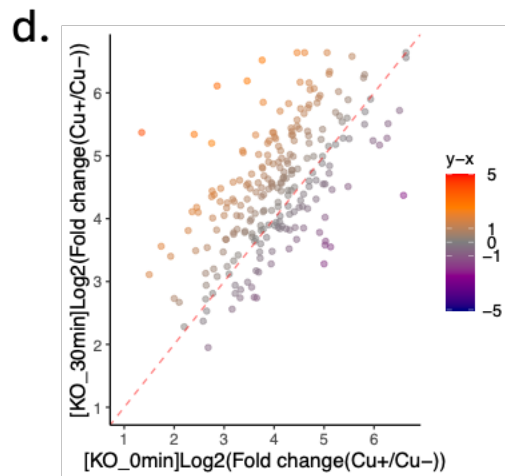
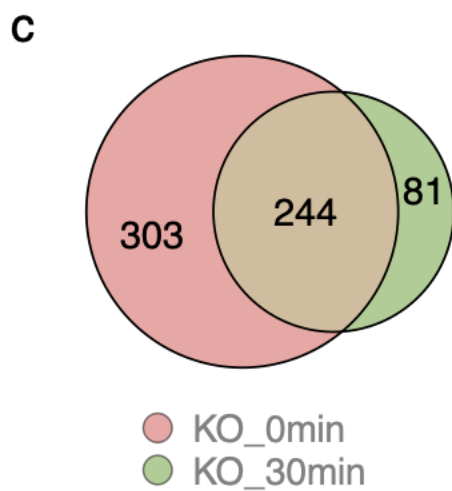
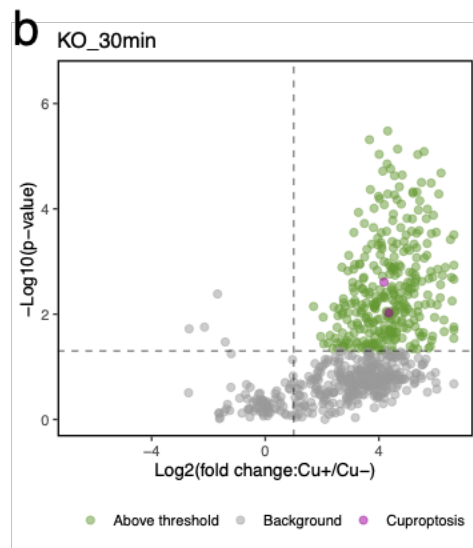
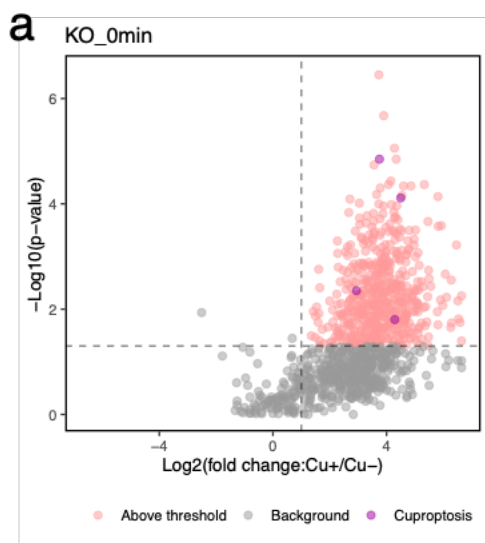


Figure 3.8 Compare the significantly labeled proteins in the Cu-pretreated ATP7A KO cells when adding 0 min-interval (KO_0min dataset) and 30 min-interval time (KO_30min dataset) between Cu-treatment and labeling. (a, b) Volcano plots of (a) KO_0min and (b) KO_30min proteomics dataset. The horizontal dashed line indicates p -value = 0.05, and the vertical dashed lines denote fold-change = 2. The cuproptosis-associated proteins above the threshold are shown in magenta color. The threshold, so-called the criteria of the significantly labeled proteins, is set as the number of identified peptides ≥ 2 , fold change ≥ 2 , and p -value < 0.05 . (c) Venn diagram of the significantly labeled proteins in the two proteomic datasets. (d) Scatter plots of $\text{Log}_2(\text{fold change (Cu}^+/\text{Cu}^-))$ of the common significantly labeled proteins in the two proteomic datasets. (e) The GO enrichment analysis of the cellular components of the significantly labeled proteins in two proteomics datasets. The number of the significantly labeled proteins enriched in each cellular component in the corresponding dataset is displayed at the top of the bar.

The proteins associated with cuproptosis, such as DLAT (dihydrolipoamide acetyltransferase), DLST (dihydrolipoamide S-succinyltransferase), PDHA1 (pyruvate dehydrogenase E1 component subunit alpha 1), and DLD (dihydrolipoamide dehydrogenase), play a crucial role in regulating entry into the TCA cycle (tricarboxylic acid cycle). Studies have reported misregulation of TCA cycle-associated metabolites in cuproptosis, indicating a potential link between the TCA cycle and cuproptosis.³⁷ Volcano plots have shown the presence of cuproptosis-related proteins in the proteomics datasets (**Fig. 3.7a, 3.7b, 3.8a, 3.8b**). While it is reported that Cu^+ can accelerate the aggregation of lipoylated DLAT, impacting the TCA cycle, the importance of other PDH complex components and the direct effects of Cu^+ on TCA cycle proteins remain unclear, and the binding between Cu^+ and lipoylated DLAT and DLST was not proved in living cells.³⁷ To identify and investigate the changes in the labeling of cuproptosis-regulatory proteins, I compared the fold change of the labeled cuproptosis-associated proteins and TCA cycle proteins (**Figure 3.9**). The key cuproptosis-related protein DLAT, which binds Cu^+ in its lipoylated form and is a key mediator of cuproptosis, was found to be labeled in Cu(gtsm)-treated ATP7A WT and ATP7A KO cells under 0 min- and 30 min- interval conditions, suggesting its significant role in responding to toxic intracellular copper levels. Furthermore, it was observed that more cuproptosis-related and TCA cycle proteins are enriched in the KO_0 min dataset

compared to the KO_30min dataset, while more are enriched in the WT_30min dataset compared to the WT_0min dataset (**Figure 3.9**). This suggests that cuproptosis initiation and processing may differ in Cu-treated ATP7A WT and ATP7A KO cells due to variations in the labile Cu^+ levels in the two cell lines.

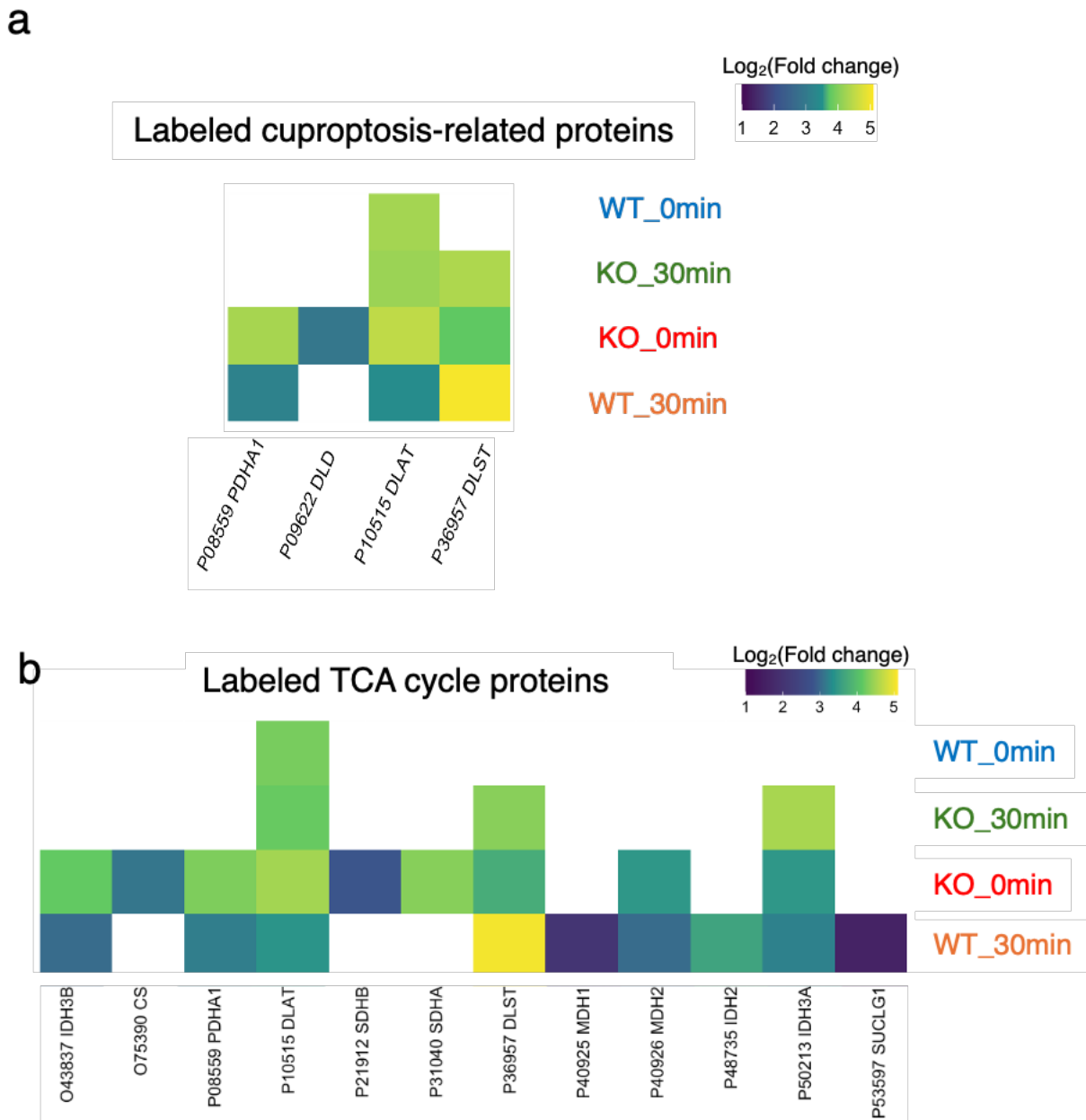


Figure 3.9 Compare the significantly labeled Cuproptosis-associated and TCA cycle proteins in the four CuR proteomics datasets. (a, b) Heatmap of the Log₂(fold change (Cu⁺/Cu⁻)) of the significantly labeled (a) Cuproptosis-associated and (b) TCA cycle proteins in the four CuR

proteomics datasets. All Cuproptosis proteins were referred to the report ³⁷. The TCA cycle proteins are the reviewed TCA cycle proteins in Homo sapiens in the Uniprot database (Keyword: KW-0816; retrieved in May 2023). Each protein is accompanied by its name and Uniport ID.

I also analyzed the ratios of potential Cu⁺-regulatory proteins in the CuR's Cu-treated proteomics datasets (KO_0min, KO_30min, WT_0min, WT_30min) to investigate the potential of CuR in profiling the Cu⁺-regulatory proteins or distinguishing the relevant Cu-regulatory proteins in living cells. Given the limited size of the currently known copper-binding proteins dataset (only 73 reviewed proteins in Uniprot: KW_0186; retrieved in July 2023), I then focused on the potential Cu⁺-binding proteins that have conserved Cu⁺-binding motifs in the CuR's proteomics datasets. The predominant Cu⁺-binding residues in cells are cysteine and methionine, found in specific motifs ³⁸ such as CC,^{39,40} CXC,^{41,42} CXXC,^{43,44,45,46} CXXXC,^{47,48,49} and MXXXM.^{50,51} I compared the occurrence of motif-containing proteins in the entire Homo sapiens proteome and in proteomics datasets of proteins labeled by CuR in Cu-treated cells (CuR datasets). My goal was to investigate whether the labeled proteins in CuR datasets are more likely to be associated with Cu⁺-regulation. I found a significant increase in the ratio of MXXXM-motif-containing proteins in CuR datasets compared to control datasets (p -value < 0.01), suggesting a potential role of the MXXXM motif in regulating intracellular excessive Cu⁺ (**Figure 3.10**). Additionally, the ratio of proteins containing at least one cysteine-containing motif (CC, CXC, CXXC, CXXXC) significantly increased (p -value < 0.05) in the CuR datasets compared to the control datasets (**Figure 3.10**). Moreover, the ratio of proteins containing at least one of the potential Cu⁺-binding motifs (CC, CXC, CXXC, CXXXC, MXXXM) showed a highly significant increase in the CuR datasets (p -value < 0.01) (**Figure 3.10**). These results indicate the potential of CuR in identifying proteins associated with statistically regulating labile Cu⁺.

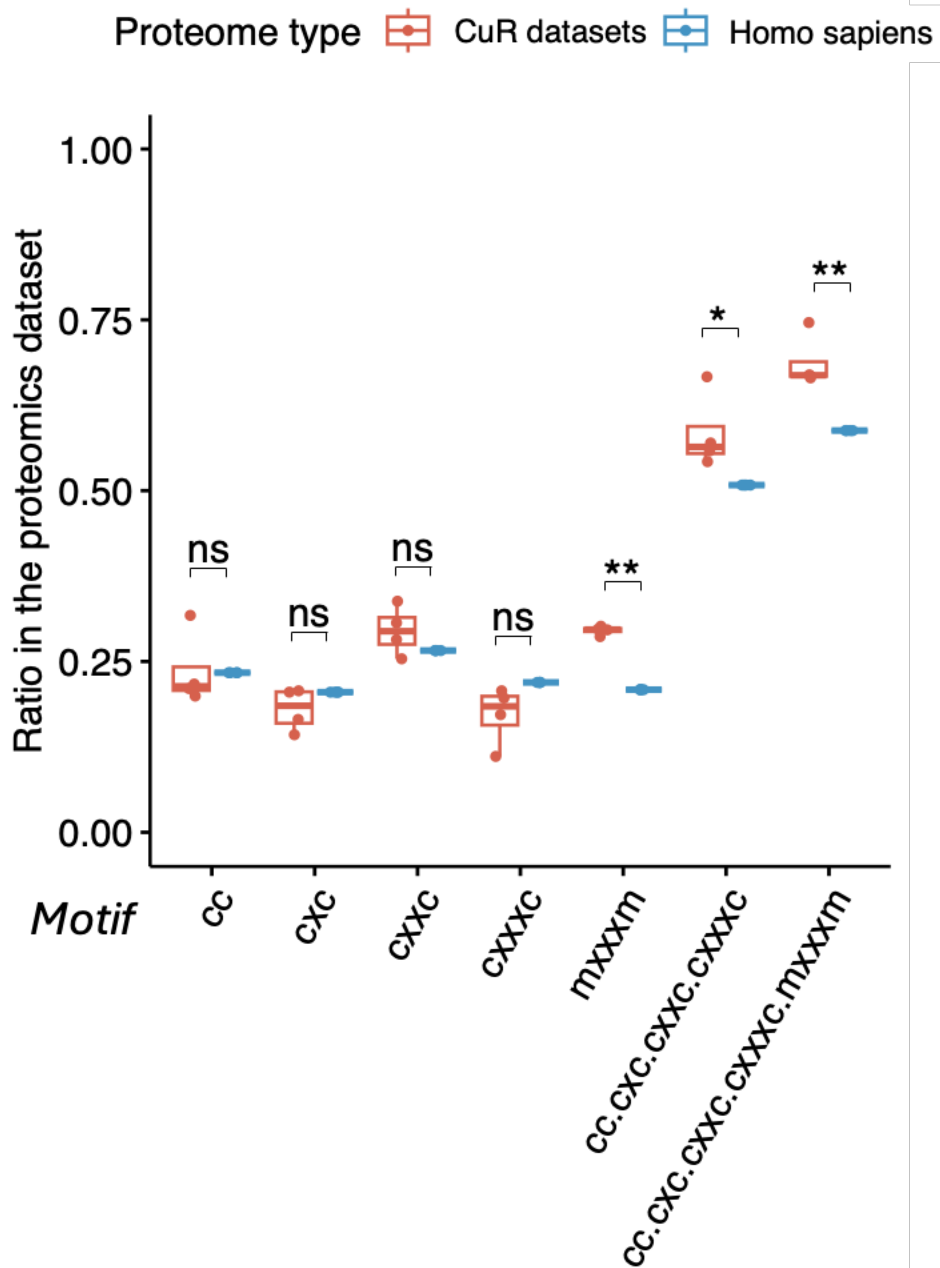


Figure 3.10 **Compare the ratio of the potential Cu⁺-binding motif-containing significantly labeled proteins in the four CuR proteomics datasets and Homo sapiens proteome dataset.** The box plot for comparing the ratio of the proteins that contain at least one CC, CXC, CXXC, CXXXC, or MXXXM motif, and that contain at least one of the following Cys-containing motifs: CC, CXC, CXXC, and CXXXC-motifs, and that have at least one of the following motifs: CC, CXC, CXXC, CXXXC, and MXXXM motifs in the significantly labeled proteins in the CuR datasets and in the control Homo sapiens proteomic dataset. The CuR proteomics datasets consist

of WT_0min, WT_30min, KO_0min, and KO_30min proteomics datasets. The control Homo sapiens proteomics dataset was retrieved from Uniport (taxonomy id: 9606). The p -values were calculated using two ANOVA and Tukey tests to compare the ratio of the motif-of-interest-containing proteins in CuR proteomics datasets and control Homo sapiens proteomics dataset. All values are expressed as independent dots. ns: $p > 0.05$, *: $0.01 < p \leq 0.05$, **: $0.001 < p \leq 0.01$.

In addition, I analyzed the variations in protein expression in both Cu(gtsm)-treated ATP7A WT and ATP7A KO cells. The results show that Cu(gtsm)- treatment did not lead to noticeable expression changes in most proteins labeled by P2 in either ATP7A WT or ATP7A KO cells (**Figure 3.11**). This confirms that the significantly labeled proteins identified in the CuR datasets mentioned above stem from Cu⁺-responsive protein labeling rather than increased protein expression levels.

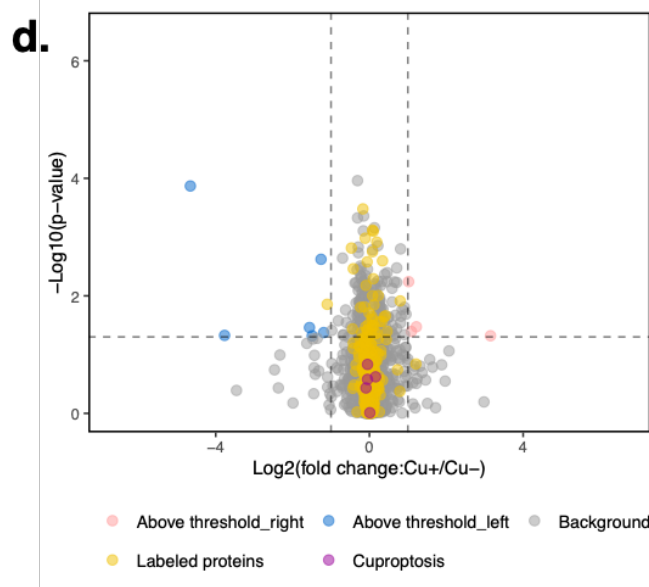
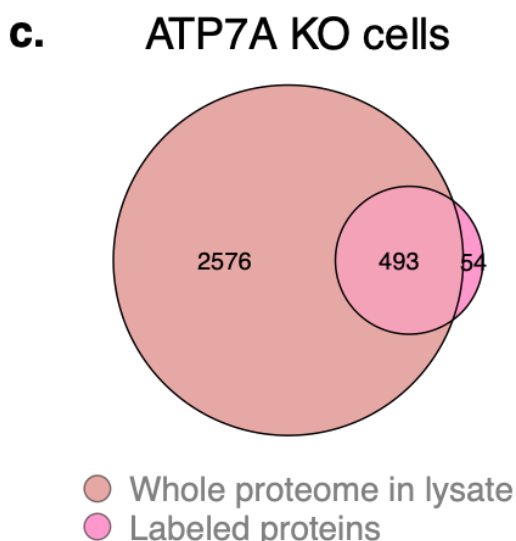
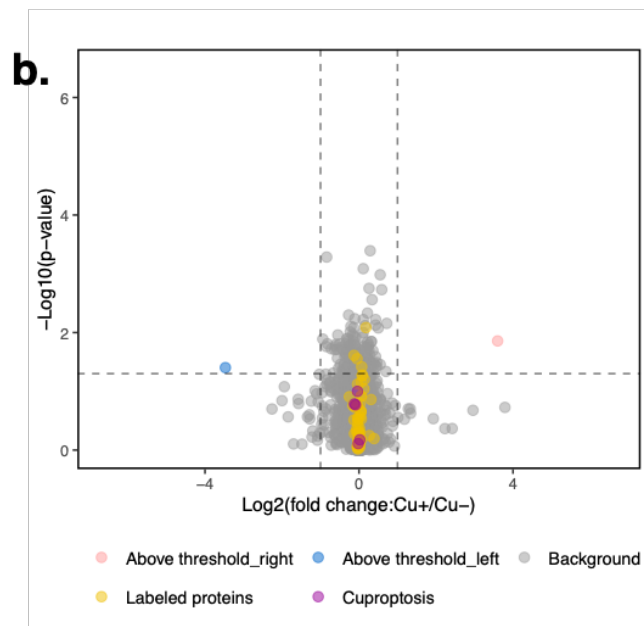
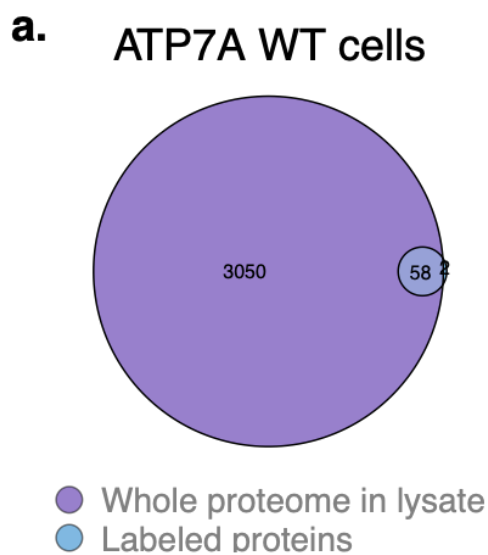


Figure 3.11 **Changes in protein expression in the Mewo cells with and without Cu(gtsm) treatment** (n = 3 biological replicates). (a, c) Venn diagram shows that the proteins identified in (a) ATP7A WT and (c) ATP7A KO cell lysate cover most of the proteins identified by AcFL- appended P2 (Figure 3.7a and 3.8a). (b, d) Volcano plot of the proteins identified from the lysate of (b) ATP7A WT and (d) ATP7A KO cells.

Conclusion

In this chapter, I utilized P2 in ATP7A WT and ATP7A KO cell models and verified its ability to detect slightly but significantly elevated intracellular labile Cu^+ levels in cells with misregulated ATP7A, highly increased labile Cu^+ levels in cells supplemented with Cu(gtsm), and markedly increased labile Cu^+ levels in cells with both ATP7A misregulation and Cu supplementation. I also observed that P2 possibly offers advantages over the ICP-MS method by detecting changes in labile Cu^+ levels that the ICP-MS method cannot. Furthermore, I successfully applied P2 in more complex co-cultured cell systems and demonstrated its specificity for Cu^+ -concentrated cells. Additionally, the proteomics study identified significantly labeled proteins in ATP7A KO and ATP7A WT cells. The alterations in size and composition of the proteome dataset, fold change of proteins, and enriched cellular components in the proteomics datasets under different cell types or treatment conditions provide insights into the diverse Cu^+ -regulation, trafficking, and export within living cells. Notably, the identification of labeled cuproptosis-associated proteins in Cu-supplemented cells also implies *in situ* interactions of cuproptosis proteins with Cu^+ . Variations in the labeling and labeling efficiency of cuproptosis-related and TCA cycle proteins in ATP7A WT and ATP7A KO cells under different conditions also likely indicate changes in the regulation of excessive Cu^+ through interactions with these proteins. Additionally, the higher ratio of potential Cu^+ -binding motif-containing proteins in the labeled proteome datasets suggests that P2 can statistically identify proteins associated with regulating labile Cu^+ .

Experimental section

General materials and methods for the biochemical/biological experiments

Unless otherwise noted, all proteins/enzymes and reagents were obtained from commercial suppliers (Sigma-Aldrich, Tokyo Chemical Industry (TCI), Fujifilm Wako Pure Chemical Corporation, Sasaki Chemical, Bio-Rad, Thermo Fisher Scientific, Dojindo, or Watanabe Chemical Industries) and used without further purification. SDS-polyacrylamide gel electrophoresis (SDS-PAGE) and western blotting were carried out using a Bio-Rad Mini-Protean III electrophoresis apparatus. Fluorescence gel images and chemical luminescent signals using ECL Prime (Cytiva) were acquired with a FUSION FX (Vilber) equipped with a SPECTRA-Capsule BLUE (480) and a fluorescence filter (F535-Y2). Cell imaging was performed with a confocal laser scanning microscope (CLSM) (Carl Zeiss LSM800) equipped with a 20 × or a 63 × oil immersion objective lens.

Cell lines and culture conditions

Mewo cells were cultured in E-MEM (Fujifilm Wako, 051-07615) supplemented with 10 % v/v heat-inactivated FBS and 1% anti-anti under 5% CO₂ in air at 37 °C. These cells were harvested from subconfluent cultures using a trypsin-EDTA solution (Gibco) or cell scraper and then resuspended in fresh medium. Subculture was performed every 2–3 days.

Generation of ATP7A-knockout Mewo cells

ATP7A gene was disrupted using CRISPR/Cas9-mediated genome editing as described previously.³⁴ Oligonucleotides for generating sgRNA expression plasmids were annealed and cloned into the BsaI site of the PX-330-B/B vector. The following oligonucleotides were used for guide RNA (gRNA) for ATP7A: ATP7A-F: 5'- CACCGGTGAAGAGTTGCAAAGTGG-3', ATP7A-R: 5'-AAACCCACTTTGCAACTCTTCACC-3' (gRNA sequences are underlined). The constructed plasmid and one-tenth quantity of pA-puro (which contains the puromycin resistance gene) were cotransfected into 80% confluent Mewo cells using Lipofectamine 2000 reagent in Opti-MEM medium (Invitrogen). The cells were cultured for 1 day and transferred to a 10 cm cell culture dish containing the culture medium with 0.75 µg/mL puromycin (Sigma) to establish stable clones. Two-bp insertion in the exon 8 of *ATP7A* gene was confirmed in ATP7A-KO cells by

direct sequencing of the fragments amplified using genomic DNA PCR. The primers used are described previously.³⁴

Preparation of ICP-MS sample

The ATP7A WT or ATP7A KO Mewo cells (1.0×10^6 cells per 10 cm dish) were cultured on 10 cm dish in growth medium at 37 °C under 5% CO₂ for three days. The cells were washed once with 10 mL of phosphate buffer saline (PBS) buffer, then incubated in 10 mL of solvent vehicle (DMSO) or 2 μM Cu(gtsm)-containing growth medium at 37 °C (5% CO₂) for 30 min. After removing the medium, the cells were washed with once with 10 mL of PBS buffer. Then, the cells were detached with 1 mL of 1× trypsin-EDTA (Gibco) by incubation at 37°C (5% CO₂) for 2 min; the detached cells were suspended in 10 mL of growth medium. After that, the cell suspension was centrifuged at 800 rpm for 3 min, and the cell pellet was washed with 10 mL PBS buffer for three times. In each washing, the PBS was removed after centrifugation (800 rpm, 3 min). Then the supernatant was carefully removed. The remained cell pellets were immediately frozen in liquid nitrogen and kept at -80 °C until the ICP-MS measurement.

ICP-MS measurement

Concentrated nitric acid (60%, FUJIFILM Wako Pure Chemicals, Osaka, Japan) was added to the cell pellet, and the resulting solutions were transferred to glass test tubes. Organic components were decomposed by heating on a hotplate. After acid digestion, samples were diluted with Milli-Q water and subjected to solution nebulization ICP-MS analysis. The contents of Cu were determined by standard calibration method with an internal standard of yttrium (Y) using an ICP-MS (Agilent 8800 ICP-MS/MS, Agilent Technologies, Tokyo, Japan). Based on the number of the cells subjected to acid digestion, we calculated the Cu contents per single cell. Details of the instrument and the operation parameters were as follows; ICP incident power: 1600 W, Ar carrier gas flow rate: 1.0 L/min, Ar make-up gas flow: 0.23 L/min, H₂ collision gas flow rate: 5.5 mL/min, monitored isotopes: ⁶⁵Cu, ⁸⁹Y.

Intracellular Cu⁺ observation by CopperGreen in the ATP7A KO and ATP7A WT cells

ATP7A WT and KO cells (2.0×10^5 cells per 35 mm dish) were cultured on 35 mm dishes in the growth medium at 37 °C under 5% CO₂ for three days. The cells were washed twice with 2 mL of

PBS buffer, followed by incubation in the 2 mL of solvent vehicle (DMSO) or 2 μ M Cu(gtsm)-containing growth medium at 37 °C for 30 min. The cells were washed with 2 mL of growth medium once and 2 mL of PBS once. The cells were then incubated in 180 μ L of 5 μ M CopperGREEN (Goryochemical)-containing DMEM-HEPES medium at 37 °C under 5% CO₂ for 30 min. The fluorescent images were then obtained by excitation at 488 nm and simultaneous detection with a FITC emission filter (510–560 nm).

Cu⁺-responsive labeling in the ATP7A KO and ATP7A WT cells

ATP7A WT and ATP7A KO Mewo cells (2.0×10^5 cells per 35 mm dish) were cultured on 35 mm dishes in the growth medium at 37 °C under 5% CO₂ for three days. The cells were washed twice with 2 mL of PBS buffer, followed by incubation in the 2 mL of solvent vehicle (DMSO) or 2 μ M Cu(gtsm)-containing growth medium at 37 °C (5% CO₂) for 30 min. If the interval time (10 min or 30 min) is inserted between Cu-treatment and labeling, the Cu(gtsm)-containing growth medium was removed, and the cells were then incubated in 2 mL of growth medium for 10 min or 30 min. The cells were washed with 2 mL of growth medium once and 2 mL of PBS once. The cells were then incubated in 180 μ L of 5 μ M AcFL-appended P2-containing DMEM-HEPES medium at 37 °C under 5% CO₂ for 30 min. The cells were washed once with PBS containing 1mM EDTA, and then lysed with 100 μ L of 1 \times SDS-sample buffer (65 mM Tris-HCl, 3% SDS, 4% sucrose, 0.005% bromophenol blue) containing 1 mM EDTA and 100 mM dithiothreitol (DTT) on ice for 5 min. The lysate was collected into a 1.5 mL tube using a cell scraper and sonicated with Branson 450 Sonifier (Output control: 1; Duty cycle:10; Shots: 10). The obtained protein mixture was then vortexed for 10 min at room temperature and applied to 12.5 % homemade AA gels for protein electrophoresis and analyzed by in-gel fluorescence imaging.

For the western blotting analysis, the proteins were then transferred to ImmunBlot PVDF membranes (Bio-Rad). After being blocked with 5% skim milk in TBST (Tris-buffered saline with 0.05% Tween 2036 (Sigma-Aldrich)) for 1 hour, membranes were incubated with primary antibodies diluted in 1 % skim milk in TBST at 4 °C overnight, followed by two rounds of 5 min wash with TBST and one round of 15 min wash with TBST. Membranes were then incubated with peroxidase (HRP)-conjugated secondary antibodies diluted in 1 % skim milk in TBST for 1 hour, followed by two rounds of 5 min wash with TBST and one round of 15 min wash with TBST. The membrane was immersed in ECL prime blotting substrate (Bio-Rad) for chemiluminescence

detection. Antibodies used in this study include mouse anti-ATP7A (1:500, sc-376467, Santa Cruz Biotechnology), chicken anti-ATP7A (1:2000, ab13995, Abcam), rabbit anti-beta tubulin (1:2000; ab15568, Abcam), HRP-conjugated anti-rabbit IgG (CST, 7074s), HRP-conjugated anti-mouse IgG (CST, 7076s), and HRP-conjugated anti-chicken IgY (Abcam, ab97135).

For imaging analysis, the cells, after the labeling, were fixed with cold methanol (-20 °C) and placed at -20 °C for 15 min, followed by washing twice with PBS buffer. The fluorescent images were obtained by excitation at 488 nm and simultaneous detection with a FITC emission filter (510-560 nm).

Cu⁺-responsive labeling in the cocultured ATP7A WT and ATP7A KO cells

ATP7A WT Mewo cells were suspended in PBS (pH 8.0) containing 2 mM Biotin-AC5 Sulfo-OSu (Dojindo) and 1000 mg/L D-glucose and incubated at room temperature for 30 min to biotinylate the cell surface. The medium was then removed after centrifugation (800 rpm, 3 min), and the cell pellets were quenched and washed with 10 mL of PBS (pH 8.0) containing 100 mM glycine. The biotinylated ATP7A WT cells (2.0×10^5 cells) were then suspended in 10 mL of growth medium and added to dishes seeded ATP7A KO Mewo cells (5.0×10^4 cells) two days earlier. The mixed cells were cultured at 37 °C for an additional two days. The cells were washed twice with 2 mL of PBS buffer, followed by incubation in the 2 mL of solvent vehicle (DMSO) or 2 μ M Cu(gtsm)-containing growth medium at 37 °C for 30 min. The cells were washed with 2 mL of growth medium once and 2 mL of PBS once. The cells were then incubated in 180 μ L of 5 μ M P2-containing DMEM-HEPES medium at 37 °C under 5% CO₂ for 30 min. After washing cells with 2 mL of PBS twice, the cells were incubated in serum-free DMEM-HEPES medium containing 5 μ g/mL Streptavidin-Alexa Fluor™ 647 conjugate (Invitrogen) at room temperature for 5 min. The cells were then washed with PBS buffer once, then fixed with cold methanol (-20 °C), and placed at -20 °C for 15 min, followed by washing three times with 2 mL of PBS buffer. The fixed cells were then incubated with DAPI (Dojindo; 1/1000 dilution)-containing PBS buffer in the dark at room temperature for 30 min, then the DAPI-stained fixed cells were washed with PBS for three times to remove excessive DAPI, and the cells were immersed in PBS buffer. The fluorescent images were then obtained by excitation at 488 nm, 640 nm, and 405 nm and simultaneous detection with FITC, Alexa 647, and DAPI emission filters.

Image analysis and quantification

The fluorescent intensities of the images were quantified using Zen 2.5 software. Each sample was prepared with three biologically independent replicates, each with three images taken from different fields as technical replicates. In each technical replicate, three regions of interest (ROI) were delineated using the freehand selection tool to capture the highest fluorescence intensities within the cell. These ROIs were placed within the cytosol of the cells, and the average pixel fluorescence intensity value within the ROI was measured for 10 randomly selected cells to minimize bias. The ROI was set as a circle, with a constant area for each technical replicate and limited to an area of $5 \mu\text{m}^2$ - $8 \mu\text{m}^2$ for different technical or biological replicates. Therefore, 270 data points were collected for each sample, representing the mean fluorescent intensity value, and used for quantitative and statistical analysis. Statistical analysis was performed using a non-paired Student's t-test (R software). For the co-cultured ATP7A WT and ATP7A KO Mewo cells analysis, each sample was analyzed in the same way with 10 cells of each technique replicate of each cell line (ATP7A WT or ATP7A KO) in one technical replicate. This resulted in the collection of 270 data points for ATP7A WT and ATP7A KO cells in one co-cultured sample, which were used for quantitative and statistical analysis.

Enrichment of the proteins labeled by P2

ATP7A WT and KO cells (1×10^6 cells) were separately cultured on 10 cm-dish in growth medium at 37°C under 5% CO_2 for three days. The cells were washed once with 10 mL of PBS buffer followed by incubation in the 10 mL of solvent vehicle (DMSO) or $2 \mu\text{M}$ Cu(gtsm)-containing growth medium at 37°C (5% CO_2) for 30 min. The cells were washed with 10 mL of growth medium once and 10 mL of PBS once. The cells were then incubated in 5 mL of $5 \mu\text{M}$ AcFL-P2-containing DMEM-HEPES medium at 37°C under 5% CO_2 for 30 min. The cells were then washed once with 10 mL of 1mM EDTA-containing PBS buffer, and lysed with 500 μL of modified-RIPA buffer (pH 7.4, 25 mM Tris-HCl, 150 mM NaCl, 1% SDS, 1% Nonidet P-40, 0.25% deoxycholic acid, 1 mM EDTA, 100 mM DTT, 1% PI) on ice for 10 min. The lysate was further homogenized by sonication with Branson 450 Sonifier (Output control: 1; Duty cycle:10; Shots: 20). The resulting solution was then mixed with 5 mL of cold acetone and kept in the -80°C freezer overnight for protein precipitation. The precipitated proteins were then centrifuged (4°C , 3980 g, 10 min) and washed with 5 mL of cold acetone again. The precipitated proteins were then

resolubilized by 500 μ L of solubilizing buffer (pH 7.4, 25 mM Tris-HCl, 150 mM NaCl, 1% SDS, 1% Nonidet P-40, 0.25% deoxycholic acid, 1% PI) and sonication. The resolubilized protein solution was then gently boiled at 65 °C for 10 min and centrifuged to remove insoluble fraction. The protein concentration of the supernatant was determined by BCA assay and uniformed to 0.724 mg/mL with the solubilizing buffer. The protein solution (666 μ L) was diluted with the same volume of normal RIPA buffer (pH 7.4, 25 mM Tris-HCl, 150 mM NaCl, 0.1% SDS, 1% Nonidet P-40, 0.25% deoxycholic acid, 1% PI) and incubated with anti-FITC (MBL, M228-3) antibody at 4 °C overnight and then mixed with 50 μ L of Protein G sepharose 4 fast flow beads (Cytiva, 17061801). After 2 h rotation at 4 °C, the beads were washed with 1 mL of normal RIPA buffer ten times. The beads were then mixed with 50 μ L of 5 \times laemmli buffer (325 mM Tris-HCl, 15% SDS, 20% sucrose, 0.025% bromophenol blue) containing 500 mM DTT, vortexed at room temperature for 10 min, and boiled at 95 °C for 5 min. The supernatant was then used for the sample preparation for nanoLC-MS/MS.

Extraction of whole proteome in cell lysate

ATP7A WT and KO cells (1×10^6 cells) were separately cultured on 10 cm dishes in a growth medium at 37 °C under 5% CO₂ for three days. The cells were washed once with 10 mL of PBS buffer followed by incubation in the 10 mL of solvent vehicle (DMSO) or 2 μ M Cu(gtsm)-containing growth medium at 37 °C (5% CO₂) for 30 min. The cells were then washed once with 10 mL of 1mM EDTA-containing PBS buffer, and lysed with 300 μ L - 350 μ L of modified-RIPA buffer (pH 7.4, 25 mM Tris-HCl, 150 mM NaCl, 1% SDS, 1% Nonidet P-40, 0.25% deoxycholic acid, 1 mM EDTA, 100 mM DTT, 1% PI) on ice for 10 min. The lysate was further homogenized by sonication with Branson 450 Sonifier (Output control: 1; Duty cycle:10; Shots: 20). The protein concentration was determined by BCA assay and uniformed to 1.178 mg/mL with the solubilizing buffer (pH 7.4, 25 mM Tris-HCl, 150 mM NaCl, 1% SDS, 1% Nonidet P-40, 0.25% deoxycholic acid, 1% PI). The protein solution was then mixed with 5 \times laemmli buffer (325 mM Tris-HCl, 15% SDS, 20% sucrose, 0.025% bromophenol blue) containing 500 mM DTT, vortexed at room temperature for 10 min and boiled at 95 °C for 5 min.

Sample preparation for nanoLC-MS/MS

The protein solutions were loaded to a BioRad precast gel (10 % AA) and resolved 10 mm by the running gel. The gel containing protein samples was manually cut into gel slices, fixed with 47.5% methanol/water containing 5% acetic acid for 20 min, and rinsed with 50% methanol and pure water. After dehydration in acetonitrile, the gels were swelled with 200 μ L of 10 mM DTT in 100 mM TEAB (triethylamine bicarbonate) buffer (Sigma-Aldrich) and heated at 56°C for 30 min. The DTT solutions were replaced with 55 mM iodoacetamide in 100 mM TEAB buffer and allowed to react for 30 min in the dark. The gel fractions were washed with 100 mM TEAB buffer, dehydrated in acetonitrile, rehydrated in 100 mM TEAB buffer, and dehydrated in acetonitrile again. The gels were swelled in 100 mM TEAB buffer containing 10 ng/ μ L Sequence Grade Trypsin (Promega) and incubated overnight at 37°C. After the digestion, the supernatants were transferred to a new tube, and the remaining gel pieces were sonicated in a water bath with 50 μ L of 50% acetonitrile (0.1% TFA) to extract peptide fragments. Extracted peptides were concentrated by the centrifugal concentrator and purified by GL-Tip SDB (GL Sciences).

NanoLC–MS/MS analyses

NanoLC–MS/MS analyses were performed on a Q-Exactive mass spectrometer (Thermo Fisher Scientific) and an Ultimate 3000 nanoLC pump (AMR) as described previously.⁵² Samples were automatically injected using the PAL system (CTC analytics, Zwingen, Switzerland) into a peptide L-trap column OSD (5 μ m) attached to an injector valve for desalinating and concentrating peptides. After washing the trap with MS-grade water containing 0.1% TFA and 2% acetonitrile, the peptide solution (0.1% TFA, 5% acetonitrile) was loaded into a nano HPLC capillary column (C18 packed with the gel particle size of 3 μ m, 0.1 \times 125 mm, Nikkyo Technos, Tokyo Japan) by switching the valve. The injection volume was 10 μ L and the flow rate was 500 nL/min. The mobile phases consisted of (A) 0.5% acetic acid and (B) 0.5% acetic acid and 80% acetonitrile. A two-step linear gradient of 5–45% B in 60 min, 45–95% B in 1 min, and 95% B for 20 min was employed. Spray voltages of 2,000 V were applied. The mass scan ranges were m/z 350–1,800, and the top ten precursor ions were selected in each MS scan for subsequent MS/MS scans. The normalized collision energy was set to be 30. The raw MS data files were analyzed by Proteome Discoverer 3.0 (Thermo Fisher Scientific) to create peak lists based on the recorded fragmentation spectra. Peptides and proteins were identified using automated database searching using Sequest HT (Thermo Fisher Scientific) against human proteome (UniprotKB/Swiss-Prot, release 2020-07-

08) with a precursor mass tolerance of 10 p.p.m., a fragment ion mass tolerance of 0.02 Da, and trypsin specificity that allows for up to two missed cleavages. Methionine oxidation was allowed as a variable modification. A reversed decoy database search was conducted to set false discovery rates (FDRs) of less than 1% both at peptide and protein levels. Three independent biological replicates were used in label-free quantitative analysis, and the high confidence proteins (fold change (Cu(+)/Cu(-)) ≥ 2 , identified peptide ≥ 2 , and p -value < 0.05) were considered as the identified proteins, in which several keratins (contaminants) were excluded. The proteomics data were then analyzed and visualized using R.

Reference

- 1 Linz, R. & Lutsenko, S. Copper-transporting ATPases ATP7A and ATP7B: cousins, not twins. *J Bioenerg Biomembr* **39**, 403-407 (2007). <https://doi.org:10.1007/s10863-007-9101-2>
- 2 Kaler, S. G. ATP7A-related copper transport diseases-emerging concepts and future trends. *Nat Rev Neurol* **7**, 15-29 (2011). <https://doi.org:10.1038/nrneurol.2010.180>
- 3 Migocka, M. Copper-transporting ATPases: The evolutionarily conserved machineries for balancing copper in living systems. *IUBMB Life* **67**, 737-745 (2015). <https://doi.org:10.1002/iub.1437>
- 4 Pase, L., Voskoboinik, I., Greenough, M. & Camakaris, J. Copper stimulates trafficking of a distinct pool of the Menkes copper ATPase (ATP7A) to the plasma membrane and diverts it into a rapid recycling pool. *Biochem. J.* **378**, 1031-1037 (2004). <https://doi.org:10.1042/bj20031181>
- 5 Lutsenko, S., Barnes, N. L., Bartee, M. Y. & Dmitriev, O. Y. Function and regulation of human copper-transporting ATPases. *Physiol. Rev.* **87**, 1011-1046 (2007). <https://doi.org:10.1152/physrev.00004.2006>
- 6 De Feyter, S., Beyens, A. & Callewaert, B. ATP7A-related copper transport disorders: A systematic review and definition of the clinical subtypes. *Journal of Inherited Metabolic Disease* **46**, 163-173 (2023). <https://doi.org:10.1002/jimd.12590>
- 7 Petris, M. J. *et al.* Copper-regulated trafficking of the Menkes disease copper ATPase is associated with formation of a phosphorylated catalytic intermediate. *Journal of Biological Chemistry* **277**, 46736-46742 (2002). <https://doi.org:10.1074/jbc.M208864200>
- 8 Chen, J. *et al.* The molecular mechanisms of copper metabolism and its roles in human diseases. *Pflugers Arch* **472**, 1415-1429 (2020). <https://doi.org:10.1007/s00424-020-02412-2>
- 9 Hartwig, C. *et al.* Trafficking mechanisms of P-type ATPase copper transporters. *Current Opinion in Cell Biology* **59**, 24-33 (2019). <https://doi.org:10.1016/j.ceb.2019.02.009>
- 10 Comstra, H. S. *et al.* The interactome of the copper transporter ATP7A belongs to a network of neurodevelopmental and neurodegeneration factors. *eLife* **6**, 28 (2017). <https://doi.org:10.7554/eLife.24722>

- 11 Ash, D. *et al.* The P-type ATPase transporter ATP7A promotes angiogenesis by limiting autophagic degradation of VEGFR2. *Nat Commun* **12**, 3091 (2021). <https://doi.org:10.1038/s41467-021-23408-1>
- 12 Gudekar, N. *et al.* Metallothioneins regulate ATP7A trafficking and control cell viability during copper deficiency and excess. *Sci Rep* **10**, 11 (2020). <https://doi.org:10.1038/s41598-020-64521-3>
- 13 Mercer, S. W., Wang, J. B. & Burke, R. In Vivo Modeling of the Pathogenic Effect of Copper Transporter Mutations That Cause Menkes and Wilson Diseases, Motor Neuropathy, and Susceptibility to Alzheimer's Disease. *Journal of Biological Chemistry* **292**, 4113-4122 (2017). <https://doi.org:10.1074/jbc.M116.756163>
- 14 Linz, R. *et al.* Intracellular targeting of copper-transporting ATPase ATP7A in a normal and Atp7b^{-/-} kidney. *Am J Physiol Renal Physiol* **294**, F53-61 (2008). <https://doi.org:10.1152/ajprenal.00314.2007>
- 15 Chun, H., Catterton, T., Kim, H., Lee, J. & Kim, B. E. Organ-specific regulation of ATP7A abundance is coordinated with systemic copper homeostasis. *Sci Rep* **7**, 12001 (2017). <https://doi.org:10.1038/s41598-017-11961-z>
- 16 Wang, Y., Zhu, S., Weisman, G. A., Gitlin, J. D. & Petris, M. J. Conditional knockout of the Menkes disease copper transporter demonstrates its critical role in embryogenesis. *PLoS One* **7**, e43039 (2012). <https://doi.org:10.1371/journal.pone.0043039>
- 17 Bhattacharjee, A. *et al.* The Activity of Menkes Disease Protein ATP7A Is Essential for Redox Balance in Mitochondria. *J Biol Chem* **291**, 16644-16658 (2016). <https://doi.org:10.1074/jbc.M116.727248>
- 18 Babak, M. V. & Ahn, D. Modulation of Intracellular Copper Levels as the Mechanism of Action of Anticancer Copper Complexes: Clinical Relevance. *Biomedicines* **9**, 852 (2021). <https://doi.org:10.3390/biomedicines9080852>
- 19 Zhong, W. *et al.* Activation of the MAPK11/12/13/14 (p38 MAPK) pathway regulates the transcription of autophagy genes in response to oxidative stress induced by a novel copper complex in HeLa cells. *Autophagy* **10**, 1285-1300 (2014). <https://doi.org:10.4161/auto.28789>
- 20 Marzano, C., Pellei, M., Tisato, F. & Santini, C. Copper Complexes as Anticancer Agents. *Anti-Cancer Agents Med. Chem.* **9**, 185-211 (2009). <https://doi.org:10.2174/187152009787313837>
- 21 Cater, M. A. *et al.* Increasing intracellular bioavailable copper selectively targets prostate cancer cells. *Acs Chem Biol* **8**, 1621-1631 (2013). <https://doi.org:10.1021/cb400198p>
- 22 Munakata, M. *et al.* Menkes disease: Oral administration of glyoxal-bis(N(4)-methylthiosemicarbazone)-copper(II) rescues the macular mouse. *Pediatric Research* **84**, 770-777 (2018). <https://doi.org:10.1038/s41390-018-0116-7>
- 23 Su, T. A. *et al.* A Modular Ionophore Platform for Liver-Directed Copper Supplementation in Cells and Animals. *Journal of the American Chemical Society* **140**, 13764-13774 (2018). <https://doi.org:10.1021/jacs.8b08014>
- 24 Ashraf, J. & Riaz, M. A. Biological potential of copper complexes: a review. *Turk J Chem* **46**, 595-623 (2022). <https://doi.org:10.55730/1300-0527.3356>
- 25 Booth, B. A. & Sartorelli, A. C. Synergistic Interaction of Kethoxal bis(Thiosemicarbazone) and Cupric Ions in Sarcoma 180. *Nature* **210**, 104-105 (1966). <https://doi.org:10.1038/210104b0>

- 26 Crouch, P. J. *et al.* Increasing Cu bioavailability inhibits A β oligomers and tau phosphorylation. *Proceedings of the National Academy of Sciences* **106**, 381-386 (2009). <https://doi.org:10.1073/pnas.0809057106>
- 27 Xiao, Z., Donnelly, P. S., Zimmermann, M. & Wedd, A. G. Transfer of Copper between Bis(thiosemicarbazone) Ligands and Intracellular Copper-Binding Proteins. Insights into Mechanisms of Copper Uptake and Hypoxia Selectivity. *Inorganic Chemistry* **47**, 4338-4347 (2008). <https://doi.org:10.1021/ic702440e>
- 28 Petering, D. H. Concerning the role of zinc in the antitumor activity of 3-ethoxy-2-oxobutyraldehyde bis(thiosemicarbazone) zinc(II) and related chelates. *Biochem Pharmacol* **23**, 567-576 (1974). [https://doi.org:10.1016/0006-2952\(74\)90621-2](https://doi.org:10.1016/0006-2952(74)90621-2)
- 29 Banci, L. *et al.* Affinity gradients drive copper to cellular destinations. *Nature* **465**, 645-648 (2010). <https://doi.org:10.1038/nature09018>
- 30 Xiao, Z. G. *et al.* Unification of the Copper(I) Binding Affinities of the Metallo-chaperones Atx1, Atox1, and Related Proteins DETECTION PROBES AND AFFINITY STANDARDS. *Journal of Biological Chemistry* **286**, 11047-11055 (2011). <https://doi.org:10.1074/jbc.M110.213074>
- 31 Xiao, Z., Loughlin, F., George, G. N., Howlett, G. J. & Wedd, A. G. C-Terminal Domain of the Membrane Copper Transporter Ctr1 from *Saccharomyces cerevisiae* Binds Four Cu(I) Ions as a Cuprous-Thiolate Polynuclear Cluster: Sub-femtomolar Cu(I) Affinity of Three Proteins Involved in Copper Trafficking. *Journal of the American Chemical Society* **126**, 3081-3090 (2004). <https://doi.org:10.1021/ja0390350>
- 32 Foyer, C. H. & Noctor, G. Stress-triggered redox signalling: what's in pROSpect? *Plant, Cell & Environment* **39**, 951-964 (2016). <https://doi.org:10.1111/pce.12621>
- 33 Santoro, A. *et al.* The Glutathione/Metallothionein System Challenges the Design of Efficient O(2) -Activating Copper Complexes. *Angew Chem Int Ed Engl* **59**, 7830-7835 (2020). <https://doi.org:10.1002/anie.201916316>
- 34 Wagatsuma, T. *et al.* Pigmentation and TYRP1 expression are mediated by zinc through the early secretory pathway-resident ZNT proteins. *Commun Biol* **6**, 403 (2023). <https://doi.org:10.1038/s42003-023-04640-5>
- 35 Nishikawa, Y. *et al.* Development of a Nitric Oxide-Responsive Labeling Reagent for Proteome Analysis of Live Cells. *Acs Chem Biol* **14**, 397-404 (2019). <https://doi.org:10.1021/acscchembio.8b01021>
- 36 Thimaradka, V., Utsunomiya, H., Tamura, T. & Hamachi, I. Endogenous Cell-Surface Receptor Modification by Metal Chelation-Assisted Pyridinium Oxime Catalyst. *Organic Letters* **25**, 2118-2122 (2023). <https://doi.org:10.1021/acs.orglett.3c00541>
- 37 Tsvetkov, P. *et al.* Copper induces cell death by targeting lipoylated TCA cycle proteins. *Science* **375**, 1254-1261 (2022). <https://doi.org:10.1126/science.abf0529>
- 38 Boal, A. K. & Rosenzweig, A. C. Structural biology of copper trafficking. *Chem Rev* **109**, 4760-4779 (2009). <https://doi.org:10.1021/cr900104z>
- 39 Horng, Y.-C., Cobine, P. A., Maxfield, A. B., Carr, H. S. & Winge, D. R. Specific Copper Transfer from the Cox17 Metallochaperone to Both Sco1 and Cox11 in the Assembly of Yeast Cytochrome c Oxidase. *Journal of Biological Chemistry* **279**, 35334-35340 (2004). <https://doi.org:10.1074/jbc.m404747200>
- 40 Arnesano, F., Balatri, E., Banci, L., Bertini, I. & Winge, D. R. Folding Studies of Cox17 Reveal an Important Interplay of Cysteine Oxidation and Copper Binding. *Structure* **13**, 713-722 (2005). <https://doi.org:10.1016/j.str.2005.02.015>

- 41 Schmidt, P. J. *et al.* Multiple Protein Domains Contribute to the Action of the Copper Chaperone for Superoxide Dismutase. *Journal of Biological Chemistry* **274**, 23719-23725 (1999). <https://doi.org:10.1074/jbc.274.34.23719>
- 42 Banci, L. *et al.* Solution Structure of Cox11, a Novel Type of β -Immunoglobulin-like Fold Involved in CuB Site Formation of Cytochrome c Oxidase. *Journal of Biological Chemistry* **279**, 34833-34839 (2004). <https://doi.org:10.1074/jbc.m403655200>
- 43 Wernimont, A. K., Yatsunyk, L. A. & Rosenzweig, A. C. Binding of Copper(I) by the Wilson Disease Protein and Its Copper Chaperone. *Journal of Biological Chemistry* **279**, 12269-12276 (2004). <https://doi.org:10.1074/jbc.m311213200>
- 44 Wernimont, A. K., Huffman, D. L., Lamb, A. L., O'Halloran, T. V. & Rosenzweig, A. C. Structural basis for copper transfer by the metallochaperone for the Menkes/Wilson disease proteins. *Nat Struct Biol* **7**, 766-771 (2000). <https://doi.org:10.1038/78999>
- 45 DiDonato, M., Hsu, H. F., Narindrasorasak, S., Que, L. & Sarkar, B. Copper-induced conformational changes in the N-terminal domain of the Wilson disease copper-transporting ATPase. *Biochemistry* **39**, 1890-1896 (2000). <https://doi.org:10.1021/bi992222j>
- 46 Gitschier, J., Moffat, B., Reilly, D., Wood, W. I. & Fairbrother, W. J. Solution structure of the fourth metal-binding domain from the Menkes copper-transporting ATPase. *Nature Structural Biology* **5**, 47-54 (1998). <https://doi.org:10.1038/nsb0198-47>
- 47 Nittis, T., George, G. N. & Winge, D. R. Yeast Sco1, a Protein Essential for Cytochrome cOxidase Function Is a Cu(I)-binding Protein. *Journal of Biological Chemistry* **276**, 42520-42526 (2001). <https://doi.org:10.1074/jbc.m107077200>
- 48 Banci, L. *et al.* A hint for the function of human Sco1 from different structures. *Proceedings of the National Academy of Sciences* **103**, 8595-8600 (2006). <https://doi.org:10.1073/pnas.0601375103>
- 49 Banci, L. *et al.* A Structural Characterization of Human SCO2. *Structure* **15**, 1132-1140 (2007). <https://doi.org:10.1016/j.str.2007.07.011>
- 50 Puig, S., Lee, J., Lau, M. & Thiele, D. J. Biochemical and Genetic Analyses of Yeast and Human High Affinity Copper Transporters Suggest a Conserved Mechanism for Copper Uptake. *Journal of Biological Chemistry* **277**, 26021-26030 (2002). <https://doi.org:10.1074/jbc.m202547200>
- 51 Eisses, J. F. & Kaplan, J. H. The Mechanism of Copper Uptake Mediated by Human CTR1. *Journal of Biological Chemistry* **280**, 37159-37168 (2005). <https://doi.org:10.1074/jbc.m508822200>
- 52 Tamura, T. *et al.* Rapid labelling and covalent inhibition of intracellular native proteins using ligand-directed N-acyl-N-alkyl sulfonamide. *Nature Communications* **9** (2018). <https://doi.org:10.1038/s41467-018-04343-0>

List of Publications and presentations

Publications

1. **Rong Cheng**, Yuki Nishikawa, Takumi Wagatsuma, Taiho Kambe, Yu-ki Tanaka, Yasumitsu Ogra, Tomonori Tamura, Itaru Hamachi. Protein-Labeling Reagents Selectively Activated by Copper(I). *ACS Chem. Biol.*, **2024**, *19* (6), 1222-1228.

Other Publications

1. Hao Zhu, Tomonori Tamura, Alma Fujisawa, Yuki Nishikawa, **Rong Cheng**, Mikiko Takato, Itaru Hamachi. Imaging and Profiling of Proteins under Oxidative Conditions in Cells and Tissues by Hydrogen-Peroxide-Responsive Labeling. *J. Am. Chem. Soc.* **2020**, *142*, 15711-15721.

Review

1. Kazuki Shiraiwa, **Rong Cheng**(共同筆頭著者), Nonaka Hiroshi, Tomonori Tamura, Itaru Hamachi. Chemical tools for endogenous protein labeling and profiling. *Cell Chem. Biol.*, **2020**, *27*, 970–985.

国内学会発表

Rong Cheng, Tomonori Tamura, Hao Zhu, Itaru Hamachi 「Conditional プロテオミクスを指向した銅イオン応答ラベル化剤の開発」第14回バイオ関連化学シンポジウム（オンライン開催）, 2p-17, 2020年9月7日.

Rong Cheng, Tomonori Tamura, Yuki Nishikawa, Itaru Hamachi,

「新規銅イオン応答性タンパク質修飾試薬の開発」新学術領域「生命金属科学」夏の合宿（オンライン開催）, p-17, 2021年9月4日.

受賞歴

2017年 7月 中国薬科大学 優秀卒業生賞

2021年 9月 若手優秀研究発表賞 (新学術領域「生命金属科学」夏の合宿)